UNIVERSITÀ DEGLI STUDI DI SIENA

DIPARTIMENTO DI INGEGNERIA DELL'INFORMAZIONE E SCIENZE MATEMATICHE

UNIVERSITÀ
DI SIENA
1240

Novel Devices for Haptics Repurposing

From Metaverses Towards a Mechanobiological Cancer Treatment

Villani Alberto

PhD in Information Engineering and Science

Supervisor
Prof. Domenico Prattichizzo

Examination Commitee
Prof. Chiara Mocenni
Prof. Arianna Menciassi
Prof. Manuel Ferre

Thesis reviewers
Prof. Arianna Menciassi
Prof. Manuel Ferre

SIENA, 18/06/2024

To my family, lover
and friends

Abstract

I n the pharmaceutics and drug research fields, the term *"repurposing "* refers to the practice of testing the effects of an already assessed drug and its molecules on pathologies different from the one for which the medicine was created. Sometimes, repurposing allows researchers to discover new ways to treat serious pathologies and diseases. For example, thalidomide, initially marketed as a sedative, was later found to be effective in treating multiple myeloma, a type of cancer. Similarly, AZT (Zidovudine), originally developed as a cancer drug, became the first approved treatment for HIV/AIDS.

Additionally, technologies can also be repurposed. Extended Realities and their graphic engines, typically used for producing video games, are now being utilized in medicine to visualize 3D models of organs, in factories for training and instructing workers, and in communication to render the body language of companions through avatars, among other applications.

In this thesis, the repurposing of haptic technologies will be discussed, drawing from a study of state-of-the-art haptics and notable examples of reusing tactile displays for various applications. Devices for rendering the sense of touch provided by interaction with virtual objects will be presented for their potential applications in enhancing the user experience of metaverses. Tactile displays for kinesthetic and cutaneous stimulation are designed and redesigned to tailor rehabilitation and manual treatment of trauma and chronic pain in human extremities. Finally, a completely innovative use of haptic methods and technologies is proposed as a tool to investigate new therapies for cancer inhibition based on mechanobiology theories. Here, the role of ad-hoc soft haptic technologies as instruments to dissect the relationship between the low recurrence of cancer in the cardiac muscle and the mechanical load of a heartbeat is investigated.

All these new application fields will be presented and categorized based on their level of novelty, progressing from haptic technologies enriching metaverse-mediated dialogs with humans and surroundings to the exploration of new treatments for superficial tumors, such as melanoma or breast cancer, based on mimicking the heart pulse on the skin. This work aims to expand the application fields of haptics toward new frontiers of digitality and reality.

Contents

Part I

Introduction to Haptics

Introduction to Haptics

Touch was never meant to be a luxury. It is a basic human need. It is an action that validates life and gives hope to both the receiver and the giver

Anais Nin

H aptics, derived from the Greek word "haptesthai," meaning "to touch," is a multidisciplinary field that explores the sense of touch and its interaction with technology. Unlike common user interfaces that exploit visual and auditory sensory channels, haptics focuses on enhancing human-computer interaction through the sense of touch. This study field a wide range of technologies and applications that enable users to perceive and manipulate virtual or remote objects as if they were physically present.

Haptic technology leverages tactile sensations to provide users with a more immersive and realistic experience for various applications, including virtual reality, gaming, medicine, robotics, and communication devices. The aim of this research field consists of augmenting human perception of the remote and digital world and creating a sense of presence and engagement by delivering feedback through the sense of touch, allowing users to feel textures, forces, vibrations, and other tactile cues. In recent years, haptics has seen significant advancements, driven by innovations in sensor technologies, actuators, complaints materials, and haptic algorithms. The integration of haptic feedback in consumer electronics, such as smartphones and game controllers, has become increasingly prevalent, contributing to a more intuitive and engaging user experience. This introduction sets the stage for discussing the human perception of tactile cues (Chapter 1), technological solutions to provide haptic stimuli (Chapter 2), and their usage (Chapter 3). While these chapters do not aim to present an exhaustive review of all the subjects explored in this thesis, they offer a brief overview of the current state of technologies, approaches, and concepts that will be further examined in the subsequent parts.

Chapter 1

Sense of Touch

The sense of touch empowers us with the ability to discern various properties of objects, such as temperature, texture, shape, mass distribution, friction, hardness, viscoelasticity, and many more. This perception is facilitated through physical contact between human skin and the object under consideration. Without the sense of touch, our understanding and interaction with the physical world would be greatly limited. It plays a crucial role in our daily activities, allowing us to navigate our environment, manipulate objects, and communicate with others through gestures. Furthermore, our sense of touch extends beyond the static properties of objects. It allows us to comprehend not only their dynamic aspects but also interactions with them, such as inertia or gravitational effects [1]. Hence, the sense of touch serves as a vital interface with our surroundings.

Figure 1.1: Touch consists of perceiving the environment using skin-provided sensations.

Individuals deprived of this sense find it challenging to perform manipulative tasks, even something as simple as picking up and placing objects. The sense of touch is also closely linked to our emotional well-being. Studies have shown that touch can elicit strong emotional responses and have a profound impact on our feelings of connection, trust, and affection. For example, a comforting hug can provide solace during times of distress, while a gentle touch on the arm can communicate support and empathy. An outline of the sense of touch, our perception of tactile stimuli, and the involved body parts in haptic sensation are presented in the following chapter.

1.1 Haptic Sensing

Distinct from the other four human senses, touch does not rely on a localized sensory organ; instead, it functions as a distributed phenomenon processed by the skin, the body's largest organ, which constitutes about 15% of the total body weight in adult humans [2].
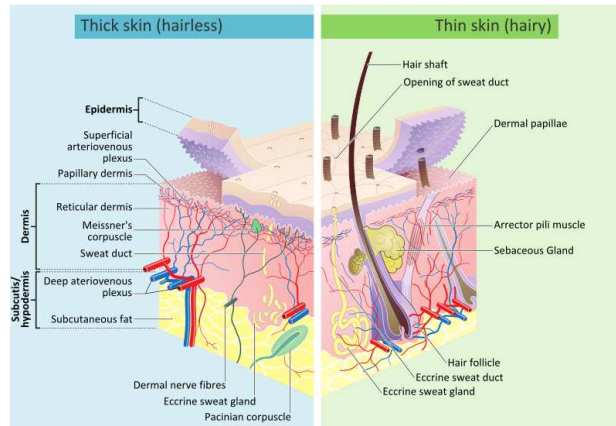
Figure 1.2: Anatomy of human skin both glabrous and hairy. The most superficial layer of the skin is the epidermis, followed by the dermis, and then the hypodermis. Also depicted in this figure is a specialized skin structure: the hair follicle.

The skin covers the entire external surface, with an approximate area of 1.5-2.0 square meters and a thickness of 2-3 millimeters. Due to its widespread distribution and the complexity of its nature, treating a tactile signal as a well-defined quantity, similar to visual and auditory signals, proves challenging. The intricate functioning of touch makes it difficult to replicate accurately in scientific or engineering tasks [3]. Any active or passive contact between the skin and an object or the environment results in a collection of information, including temperature, pain, and pressure, which allows the brain to explore and understand the world around us.

As shown in Fig. 1.2, skin is organized in three layers, from top to bottom:

Epidermis, made of dead skin cells, which provides a waterproof barrier and creates human skin tone;

Dermis, containing nerve endings, hair follicles, sweat glands, sebaceous glands, and touch receptors with the function to sustain and support the epidermis by diffusing nutrients to it and replacing the skin cells that are shed off the upper layer of the epidermis;

Hypodermis, consisting of adipose and connective tissue. It mainly acts as an insulator and helps regulate body temperature. It also acts as a cushion to protect underlying tissue from damage.

The sense of touch is based on a vast network of nerve endings and touch receptors in the skin, responsible for all the sensations felt by humans (cold, hot, smooth, rough, pressure, tickle, itch, pain, vibrations). This complex system is known as the somatosensory system. However, the cells that make up the skin tissues are also involved in haptic sensing. The cells are equipped with mechano-, thermo-, and piezo-sensors on their membrane, capable of acquiring and interpreting tactile information from the extracellular medium and other cells. A practical example of haptic sensation mediated by skin cells is the cold sensation perceived when a menthol-based ointment is applied to the skin: in this case, the cold perception is triggered by the cells, whose thermo-sensor, namely

transient receptor potential ion channel subfamily M (melastatin) member 8 (TRPM8), is affected by the menthol molecule contained in the ointment, which acts as an antagonist to that cellular sensor.

1.1.1   Somatosensory System Receptors

The somatosensory system comprises four main types of receptors:

Mechanoreceptors which respond to various mechanical stimuli, including light brush, stretch, vibration, and noxious pressure; **thermoreceptors**, responsible for perceiving sensations related to the temperature of objects; **Nociceptors**, that detect pain caused by mechanical stimuli (cut or scrape), thermal stimuli (burn), or chemical stimuli (poison from an insect sting) that may damage the skin and other tissues; and **proprioceptors** that return the sense the relative position between different parts of the body and the surrounding environment.

However, the distribution of these receptors in the body is not uniform, with the most sensitive areas being the face, the back of the neck, the chest, the upper arm, the fingers, the soles of the feet, and the legs. In addition, the deep of somatotopic sensors depends also on the type of these, in fact, the mechanoreceptors are distributed in different levels of the skin, while the thermal ones are most distributed in the dermis with higher concentration in the face and ears.

Over three million pain receptors are distributed throughout the body completely differently the proprioceptors are located in strategic positions such as tendons, muscles, and joint capsules, detecting changes in muscle length and skin tension. In Fig. 1.3 the inequality among the proportions of touch sensors represented in the brain is visually depicted using the representation of cortical homunculus.

In accordance with the scope of this thesis, a brief focus will be given to mechanoreceptors.

Mechanoreceptors

Mechanoreceptors transmit signals in the form of a stream of voltage pulses, with the amplitude represented as pulse density [3]. When stimulated, a mechanoreceptor triggers action potentials at an elevated frequency, with higher stimulus strength resulting in a higher frequency. As the cell adapts to the stimulus, the pulse frequency subsides to its normal rate [4]. Traditionally distinguished based on the types of stimulation to which they respond, the size of their receptive fields, and their rates of adaptation [5], each mechanoreceptor comprises a primary afferent neuron and its sensory endings. Somatosensory neurons are grouped into low-threshold mechanoreceptors (LTMRs), which respond to benign pressure, and high-threshold mechanoreceptors (HTMRs), which respond to harmful mechanical stimulation. Associated nerve fibers are classified as $A\beta$, $A\delta$, or C fibers based on their action potential conduction velocities. C fibers are unmyelinated with the slowest conduction velocities (about 2 m/s), while $A\delta$ and $A\beta$ fibers are lightly and heavily myelinated, exhibiting intermediate (about 12 m/s) and rapid (about 20 m/s) conduction velocities, respectively [6]. HTMRs and LTMRs are further classified as slowly or rapidly adapting based on their rates of adaptation to sustained mechanical
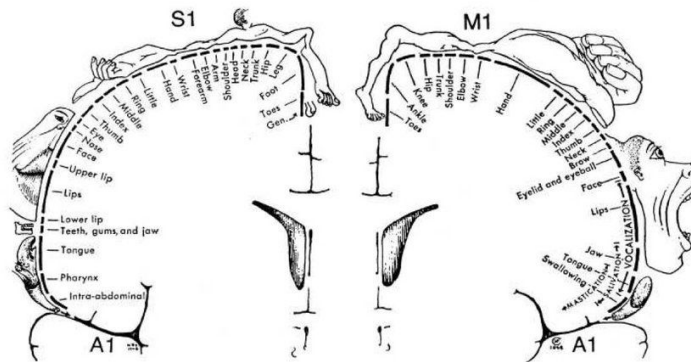
Figure 1.3: The Cortical Homunculus presents a distorted representation of the human body, originating from a neurological "map" that illustrates the distribution and proportions of brain regions responsible for motor and sensory functions related to various body parts. Nerve fibers transmitting somatosensory data from across the body converge in different regions of the parietal lobe within the cerebral cortex, forming a map that represents the body's sensory input.

indentation. Rapidly adapting (RA) receptors sense the initiation and cessation of contact with an object but not the continuation and duration of skin indentation. Slowly adapting (SA) receptors continue firing during constant mechanical stimuli.

Moreover, based on their receptive field structure, mechanoreceptors are further classified into type I (small) with a receptive field diameter of about 2-8 mm and distinct borders, type II (medium) with a larger receptive field and diffuse borders, and also type III and IV, with the largest and smallest receptive fields, respectively [7]. Four sensory endings in glabrous skin specifically perceive indentations and vibrations: Meissner's corpuscles, Merkel cells, Ruffini endings, and Pacinian corpuscles.

Morphological observations, including receptive field characteristics, adaptive properties to stepwise indentation, and frequency response to sinusoidal vibration, have associated different sensing characteristics with these receptors:

Meissner's corpuscles are ovoid structures in the dermis of glabrous skin, most sensitive to vibrations in the 20-40 Hz range. Found on the fingertips, they are typically associated with rapidly adapting type I receptors [8].

Merkel cells are located in the deepest layer of the epidermis of glabrous skin, and they register pressure. Associated with slowly adapting type I afferent fibers, their density is estimated at 80 mm^2 [9].

Ruffini endings have a spindle-like shape, these are located in the deepest part of the dermis of both hairy and glabrous skin, responding to pressure and sensitive to pressure variations. Typically, they are associated with rapidly adapting type II receptors [10].
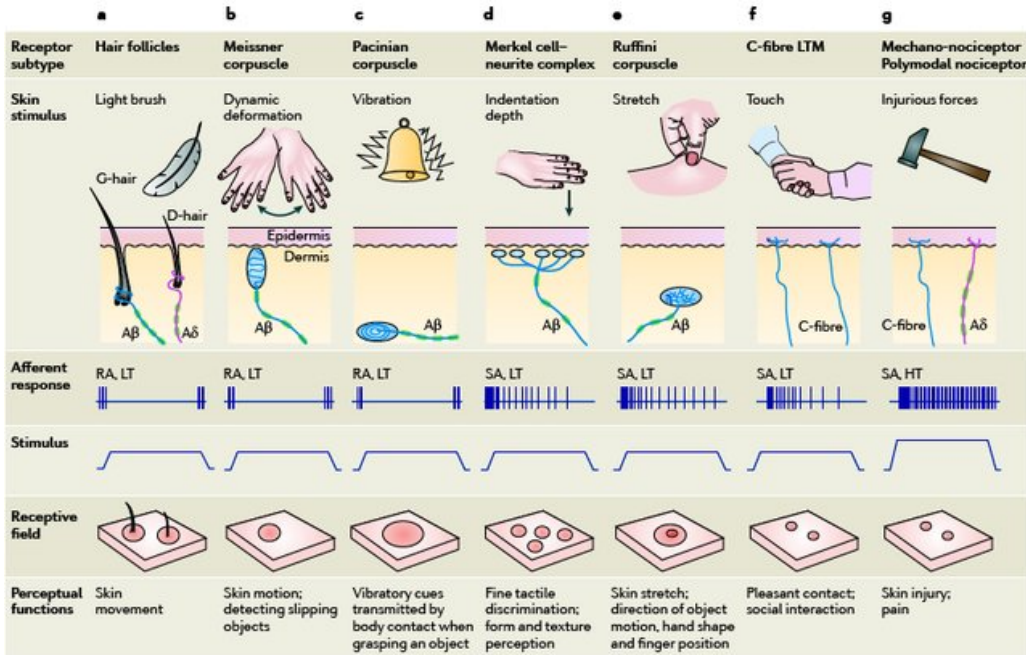
Figure 1.4: Mechanoreceptors comprise a diverse class of nervous endings capable of collecting a wide range of sensory inputs. Different sensations are registered by distinct receptor types, which vary in anatomy, position within the skin, and other physical features.

> **Pacinian corpuscles** are multi-layered structures, onion-shaped, deep within the dermis and subcutaneous fat layer of both hairy and glabrous skin. Most sensitive to vibrations in the 200-550 Hz range and associated with slowly adapting type II receptors [11].

More details about corpuscles and endings is visually reported in Fig. 1.4.

1.1.2 Cellular Receptors

As aforementioned, haptic sensing is also powered by the direct interaction of human cells with the environment. In fact, human cells exploit specialized mechanosensors, including proteins and protein complexes, to discern external mechanical signals. These mechanosensors are typically situated on the membrane interfaces between cells and between the cell and its environment. Upon detection of mechanical stimuli, a mechanosensor triggers mechanotransduction pathways, converting mechanical signals into biochemical cues that affect and alter various cellular processes, such as gene expression [12, 13, 14], signaling cascades [15, 16, 17], cytoskeletal rearrangement [18, 19], or apoptosis [20, 21]. Several cell organelles and proteins play the role of mechanosensor: the **ion channels** detect mechanical stimuli that force the opening of membrane gates, the **adhesion complexes** perceive external forces because they mediate the mechanical connections between cells
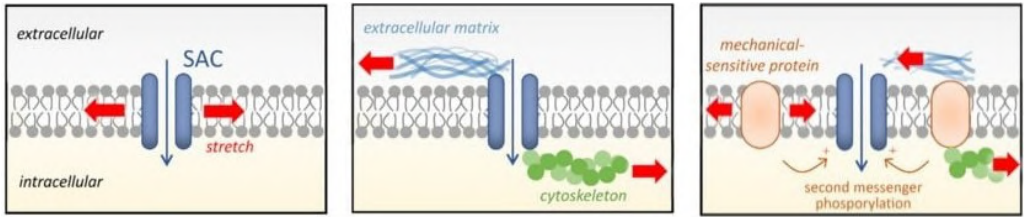
Figure 1.5: Three general models of SAC enabling are proposed: (a) In the "bilayer model," the tension applied (red arrow) in the lipid bilayer itself is directly responsible for channel gating; (b) In the "tether model," the force is transmitted to the channel via proteins located in the extracellular matrix, the cytoskeleton, or both. Tensions are conveyed by these accessory proteins to induce the channel opening. (c) In the "secondary signal model," the channel activation depends on a distant mechanical-sensitive protein generating a diffusible second messenger.

and the extracellular matrix (ECM), and the **cilia proteins** and **microtubules** sense mechanical cues and fluid flow due to their flexible structure.

Ion Channel

Ion channels are proteins that allow the preferential passage of ions through the cell membrane. The opening or closing of an ion channel gate is related to a signal measured between the inside and outside of the cell, which varies over time. This signal is the so-called action potential, which is generated precisely thanks to the entry and escape of ions like sodium (Na^+), potassium (K^+), calcium (Ca^{2+}) and magnesium (Mg^{2+})[22, 23]. One relevant class of mechanosensitive ion channels consists of piezo-channels, particularly Piezo1 and Piezo2, which play a central role in translating mechanical forces into electrical and biochemical signals. These large transmembrane proteins have a complex, trimeric structure with multiple transmembrane domains and a central pore region[24]. Mechanically induced deformations in the cell membrane activate Piezo channels, leading to changes in membrane potential and intracellular calcium levels [25].

Similarly, stretch-activated channels (SAC) respond to mechanical stretching of the cell membrane. Deformation of the membrane causes these channels to change conformation, allowing ions to pass through and triggering the mechanotransduction pathway. SACs are capable of measuring three different models of interaction: *i)* the bilateral interaction, which occurs when both gates of an ion channel are directly subjected to a force, the *ii)* tethered interaction when the ion channel gate is open due the combined effect of a mono-directional force and the inertial response of the cytoskeletal structure, *iii)* the secondary signal model, in which to be triggered are near mechanoreceptors that trigger the ion channel to open. All of these are visually depicted in Fig. 1.5.
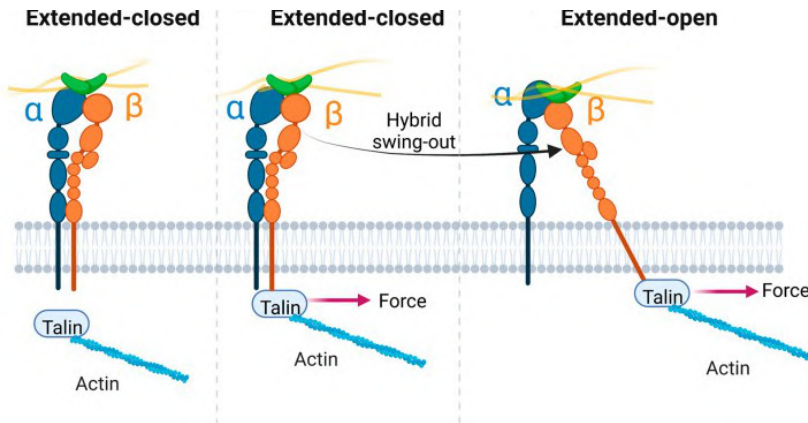
Figure 1.6: Example of catch-bonding on integrin conformations: The schematics of ECM-bound integrin in extended-closed conformation. Once the extended-closed conformation of integrin attaches to intracellular talin, a membrane-parallel force is exerted on the β tail, providing a lateral pulling of the β tail, the transmembrane β helix change orientation with respect to the α helix.
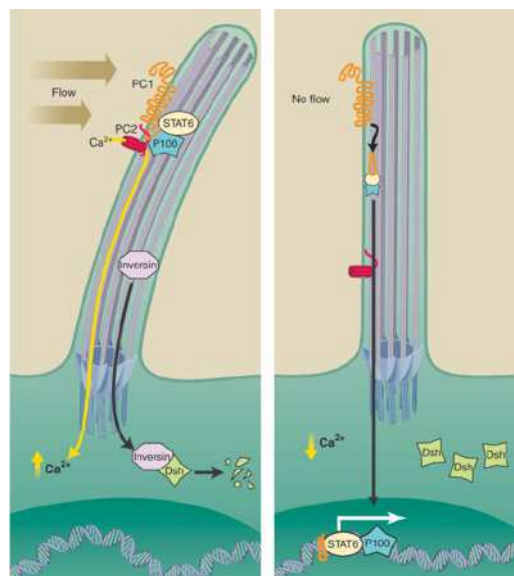
Figure 1.7: Primary cilia cells sense flow and control cell proliferation. The deflection of the primary cilium caused by flow within the nephron tubule is detected by PC1 (orange) and PC2 (red), two trans-membrane proteins. Flow induces Ca^{2+} flow. In the absence of flow, Ca^{2+} influx is reduced and the tail of PC1 is cleaved, triggering a bio-transcription.

Adhesion Complexes

Adhesion Complexes or Cell Adhesion Molecules (CAMs) consist of proteins like integrins, cadherins, selectins, and immunoglobulin that mediate cell adhesion, i.e., the ability of

cells to stick to one another or to various surfaces, such as ECM, or foreign particles[26]. Integrins and cadherins filaments are capable of measuring external mechanical cues being subjective to a *catch bond mechanism*[27, 28] that strengthen them when a force is directly applied: mechanical tension induces detectable structural changes in these molecules triggering a mechanotransduction pathway, as represented in Fig. 1.6.

Cilia, and Microtubules

Cilia are slender, hair-like protrusions found on the surface of many cell types, while microtubules are structural components of the cytoskeleton. Both are involved in the cell's mechanosensing process:

> **Cilia:** When mechanical stimuli, such as fluid flow or touch, exert force on cilia, it induces bending or deflection. This mechanical deformation is detected by specialized proteins located at the ciliary base, including polycystins (PC) and other mechanosensitive transient ion channels [29]. Its functioning is visually depicted in Fig. 1.7.

> **Microtubules:** CeCertain microtubule-associated proteins (MAPs) can undergo conformational changes or alterations in their interactions with other cellular components in response to mechanical stimuli. For example, the motor protein dynein, which moves along microtubules, can be activated by mechanical forces, leading to changes in microtubule dynamics or cellular movement [30, 31, 32].

Additionally, microtubules themselves can deform or buckle in response to mechanical stress, transmitting mechanical signals to the cell interior.

1.2 Haptics Perception

All information provided by cutaneous mechanoreceptors, muscles, articulation, and skin consisting cells is successively interpreted, selected, and organized thanks to a process called haptic perception [33, 34].

The sense of touch is commonly defined as a multidimensional system consisting of two main kinds of perception: the **cutaneous** and **kinesthetic** ones[35]. Cutaneous perception elaborates the stimuli sensed by the skin's mechanoreceptors, and vice versa kinesthetic perception relates to understanding the position and movement of limbs through proprioceptor sense, where "proprioception" denotes awareness of movement originating from the body itself (muscles, tendons, and articulations)[36]. In accordance with the proprioception definition given by physiologist Sherrington in the early 19th century [37], this is distinguished from exteroception (data from outside the body) and interoception (information from internal organs). Although "kinesthesia" is often used interchangeably with "proprioception", the former places a greater emphasis on motion. More recently, the term "kinesthesia" has been broadly defined to include the perception of force as well [38]. It is noticeable that kinesthetic and cutaneous perception are not entirely independent. For instance, the cutaneous skin stretching receptors play a crucial role in collecting

information about changes in limb position and movement of some body parts like the hands. Edin and Johansson in [39] revealed that joint and/or cutaneous anesthesia can impact the ability to detect finger movements and perceive their position. Conversely, for more proximal joints like the knee, receptors in the joint or skin have minimal influence on perceived joint angles, contributing only marginally to sensory inflow [40].

Moreover, haptic perception is affected by the modality through which touch is experienced [41, 42, 43]. Typically, the touch involving exploratory movements aimed at perceiving haptic cues is defined "**active**", while "**passive**" touch entails the decoupling of the subject's movements from the stimuli display.

In the last decades, researchers have employed various psychophysical methods to investigate human haptic perception and its limitations lighting the boundaries of our sensory capabilities [44, 45]. A pioneer of this research field was Weber, whose systematic investigations led to the establishment of Weber's law, asserting that the just noticeable difference (JND) between two stimuli, indicating the minimum change in a stimulus's magnitude that can be detected, is proportional to its magnitude [46]. Starting from the Weber law assertion several studies has been conducted about discrimination or identification of material properties (roughness, compliance, viscosity, friction, coldness) [47, 48, 49, 50], spatial properties (shape, curvature, size, orientation)[51, 52, 53], limb positions, and numerosity of items [54, 55], in case both of active and passive touch.

Most recent investigations are focused on perceptual illusions (namely "*psuedo-haptics*") within the haptic system for providing insights into the cognitive processes of haptic perception and serving as a manipulation tool to enhance information display [56].

Chapter 2

Haptics Interfaces

The term "haptic interface" refers to a robotic device that mediates user interaction with virtual environments or teleoperated remote systems. Typically, a distinction is done according to the level of wearability (see Fig. 2.1) [1] of the haptic interfaces, distinguishing two main categories of devices: the **grounded** haptic interfaces and the **wearable** ones.

A grounded interface, as suggested by the name, is typically a robotic device fixed or mounted to a surface. Commonly this kind of interface is capable of exerting kinesthetic cues to the user, providing the human hand with forces and torques through handles. Commercial haptic interfaces, such as Phantom (3D Systems, SC, USA) and Omega (Force Dimension, CH), are two noticeable examples of desktop robots capable of accurately generating a wide range of forces, primarily offering kinesthetic feedback. While ensuring realistic interaction with virtual objects, these interfaces are not portable due to their bulky form factor. Despite these technologies being widely used for single-point interaction [57, 58, 59, 60], a multi-contact interaction is extremely challenging to exert. The ground-based systems HIRO III [61] is ad-hoc designed to exert three-dimensional forces to all five users' fingertips, bi-contact interaction frameworks were powered by synergistic actions of two Omega interfaces [62, 63].
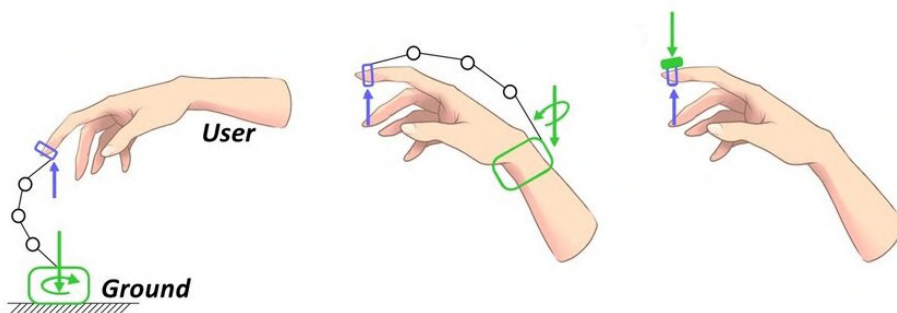
Figure 2.1: From left to the right schematic representation of haptic interfaces sorted by wearability levels: grounded haptic interfaces (on the left), an exoskeleton (in the middle), and high wearable device (on the right)

---

[1]Oxford University Press defines "wearable" as *"denoting or relating to a computer or other electronic device that is small or light enough to be worn or carried on one's body".*

2.1 Wearable Haptic Interfaces

Portability, weight, dimensions, form factors, encumbrance, softness, and type of connectivity are all proprieties that define the level of wearability of haptic interfaces [64]. To provide a comprehensive overview, the following briefly explores the most relevant devices known today, presented in ascending order based on their level of wearability and portability according to their form factor.

2.1.1 Exoskeletons

Exoskeletons represent a category of external structural mechanisms resembling human body joints and links. These consist of wearable haptic interfaces capable of monitoring and tracking the hand or limb's position and providing them with kinesthetic stimuli by transmitting torques to human joints [65, 66, 67]. Hand exoskeletons can also integrate cutaneous feedback. For instance, in [68], a 3-degree-of-freedom (3-DoF) fingertip cutaneous device and a 1-DoF finger kinesthetic exoskeleton are combined to render both kinesthetic and cutaneous cues to the finger pulp of a user. Exoskeletons are typically portable, lighter, and smaller than grounded interfaces; however, they remain bulky and cumbersome.

2.1.2 Bands

Moving beyond exoskeletons, current technologies are aimed to minimize their interference with the wearer's motion and consequently maximize their wearability. The highly wearable interface's base is as close as feasible to the force application point. Typically, this collocation shift reduces haptic interaction expressiveness, losing the capability to render the kinesthetic cues, fostering the cutaneous ones [69], including skin indentation and vibrotactile stimuli. The state-of-the-art highly wearable haptic interfaces are populated with several devices like arm and hand bands for skin stimulation, such as those presented in [70]. These consist of wearable devices for forearm guidance, generating independent skin stretch stimuli at the palmar and dorsal hand sides and ulnar and radial arm sides. In [71], the haptic expressiveness resembles integrating a 4-degrees-of-freedom (4-DoF) hand wearable haptic device for Virtual Reality (VR) with exchangeable end-effectors to provide a wide range of haptic sensations. Bimbo *et al.* in [72] exploit vibrotactile channels of human haptic sensing to enhance the user performance of teleoperating a robot in a cluttered environment, while, in [73] and in [74] vibrating cues are used to make more intuitive the control of robotic extra fingers or mobile robots, respectively.

2.1.3 Thimbles

Among highly wearable devices, interfaces for the fingertip, namely haptic thimbles, have received significant attention. Examples include wearable interfaces for skin indentation having one or more degree of freedom (e.g. , [75, 76, 77] and [78, 79], respectively), for vibrotactile display, as [80, 81, 82, 83], and thermal rendering [84, 85]. Moreover,

commercially available devices, such as the TouchDIVER (WeArt, IT), offer a combination of forces, vibrations, and thermal cues.

2.2 Soft Haptic Technologies

Another way to enhance the wearability of a haptic device is to exploit the usage of soft matters (e.g., fabric, polyester, or silicone rubber) in its design. Pneumatic pumps, new kinds of motors, like dielectric or fluid elastomeric actuators or shape memory alloys, deformable structures, and tendon-driven transmission systems may be used to enhance the softness of a haptic device and consequently its wearability. Combining these technologies with compliant materials allows to creation of highly wearable devices that are lightweight and minimally intrusive to the wearer.

For an exhaustive overview of the state of the art of soft haptics, refer to [86]. In what follows, some examples of soft haptic interfaces are summarized. These are organized in three clusters according with their form factor: *i)* whole hand device (gloves), *ii)* limb-worn bands and *iii)* finger-oriented interfaces (ring and thimbles).

2.2.1 Gloves

Recent advancements, including the usage of soft materials, have powered research on exoskeletons for haptic, promoting the design of haptic gloves. Unlike conventional exoskeletons, gloves do not interfere with natural human movements. The research proposed in [87] and [88] focuses on the design of wearable soft haptic gloves for force feedback using hydraulic and shape memory alloy-based actuation, respectively. In [89] and [90], the authors design and optimize an under-actuated exoskeleton called FLEXotendon Glove-III, combining soft materials and tendon-driven actuation.

For example, cable-driven exoskeletons allow the delocalization of the actuation mechanism and control unit to remote areas of the wearer's body. In a TSA-based (twisted string actuation) wearable haptic glove presented in [91], two independent twisted string actuators with integrated force sensors and small-size DC motors were used. The resulting device, named the "ExoTen-Glove", is capable of providing a kinematic cue of at least 80N intensity while weighing under 400g. Conversely, [92] introduces a lightweight and compliant haptic glove that employs tendon-drive actuation and a compliant robotic mechanism capable of exerting high forces, with a total weight of 230g.

Inflatable structures and pneumatic actuators can be employed to control joint posture and simulate the hardness of virtual objects. Soft clutches, for example, can be used to simulate highly stiff tactile interactions. Hinchet *et al.* presented an electrostatic clutch with high force density integrated into a kinesthetic glove to immobilize finger motion upon contact with a virtual solid object [93]. Starting from a comparative study about silicone- and fabric-based inflatable actuators, Suulker *et al.* in [94], demonstrated that both can exert high forces, are lightweight, and have an extensive flexion angle potential, however, materials like cotton makes the exoskeleton more comfortable and user-friendly, consequently increasing wearability. In [95], the FlowGlove device is presented, this consists of haptic devices that can render a variety of tactile sensations like

pressure, vibration, and temperature enabling virtual reality haptic interactions by water flowing in the liquid bladder. For a comprehensive understanding of the state-of-the-art in soft exoskeletons (not only for haptic applications), referring to literature review articles presented in [96, 97, 98] is recommended.

2.2.2   Bands

Soft matter could be also used, to create haptic bands. These devices are typically made of flexible materials such as fabric or silicone rubber and contain small vibration motors or pneumatic actuators arranged to deliver sensations to specific body parts, such as wrists, arms, forearms, and ankles. Pneumatic actuators are used to enable the inflations of air chambers pressing on the user's skin. Bellowband [99] is a noticeable example of this kind of technology. It consists of a wristband with eight equally spaced pneumatic air chambers that extend into the wrist, providing local pressure and vibrations. The exploitation of polyester thermoplastic polyurethane (TPU), a printable soft elastic material reduced drastically the weight of the device (11 g) and ensured the low encumbrance of its form factor. Agharese *et al.* , in [100] proposed HapWRAP, growing wearable haptic bracelets that grow out of a compact housing unit and provide a combination of directional and force feedback to a user. Pneumatic actuators are also used to realize wearable haptic sleeves. In [101], the authors exploited a linear array of air chambers to provide the illusion of the stroking gesture, while, in [102], a soft sleeve is designed to render a wide range of haptic sensations, including compression, skin stretch, and vibration.

Regarding textile bands and tendon-driven bracelets, works as [103, 104, 105] and [104], exploits the length reduction and the synchronous movements of the fabric end to induce squeezing and shearing cues on the wearer's skin.

Shape memory alloys were involved in the design of the squeezing band, as the "Haptic-Clench", a haptic band presented in [106]. This provides several levels of pressure feedback exploiting Flexinol, a commercially available Nickel-Titanium SMA with a low span that contracts like muscles when electrically driven.

2.2.3   Thimbles and Rings

Similarly for the bands presented above, fabrics and tendons are widely exploited in the design of finger-oriented devices. The hRing [107] is a noticeable result of this field of research. The ring consists of a textile haptic ring designed to provide normal and shear stimuli to the proximal phalanx of the user's finger by means of moments and length reduction of fabric bands. An analog design is proposed in [108] where a tendon-driven device is realized to provide normal mechanical cues on the finger pulp of wearing users, while, in the device proposed in [109], a silicone rubber platform indents three-dimensionally the wearer skin. For what concern other technologies, in[110], dielectric elastomer actuators were involved to enable a soft, thin, light and flexible haptic display to wear on the finger pulp, while Talhan *et al.* in [111] and in [112] exploited pneumatic actuation to trigger squeezing sensation on the wearer's digits. In addition, shape memory alloy actuators can power miniature haptic ring fingerpads such as the one presented in [113] allowing the display of touch/pressure and shearing force fingerpads.

Chapter 3

Haptic Application

In the last decades, haptic technologies, including those previously introduced, have been exploited in a wide range of applications: tactile interfaces have been used to enhance the immersion of a virtual experience or to increase the realism of training simulators for industrial and medical purposes, as well as to increase student engagement in class attendance through multimedia and multi-sensory lessons. The applications of haptic technologies span from the gaming and virtual reality fields to those for medical simulation and training, but also this extends to the telecommunications, robotics, and automotive industries, offering new tools for triggering unconventional sensory channels for transmitting awareness or notification signals.

Figure 3.1: Haptics rings can be exploited to remotize the sense of touch and transmit it like a audio trace.

Furthermore, since the target of haptic technologies consists of activating the sense of touch by cutaneous and kinesthetic stimulation, they can be leveraged as a valuable supplementary, compensatory, or augmentative instrument for all patients affected by sensory disabilities.

3.1 State of the Art

Before coming into the contribution of the present thesis, a brief overview of the most common application fields of haptic technologies is reported here.

Gaming and Extended Reality

Maybe the most notable application of haptic technology consists of gaming. In commercial gaming platforms, haptic feedback is integrated to enhance the gaming experience by providing users with tactile sensations that correspond to in-game events. From the subtle vibration for simulating footsteps, [114] to the force feedback replicating the resistance of a virtual world object making them tangible [115, 116, 117], haptic feedback amplifies immersion [118, 119], making the gaming experience more realistic and engaging. Over the years, haptic research has provided several novel interfaces integrating
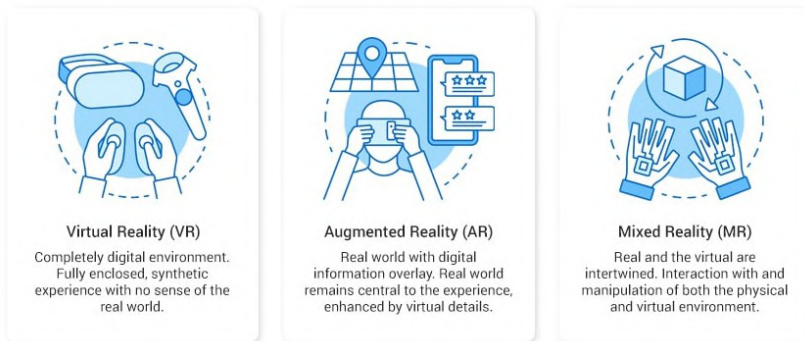
Figure 3.2: Representation and details of types of Extended Reality according with the Reality-Virtuality continuum.

tactile cues with commonly used controllers. For instance, Aziz *et al.* , in [120], proposed a handheld multimodal haptic feedback controller integrating whole hand and finger pulp stimulation cores with tracker systems, or also in [121, 122] proposed the design of laptop mouses haptic-enabled by electromagnet and vibromotors, respectively. Wu *et al.* in [123] presented a laptop keyboard with realistic haptic feedback to provide users with a fully immersive virtual experience.

However, gaming is only a sub-field of Extended Reality (XR) that comprises augmented reality (AR), virtual reality (VR), and mixed reality (MR) (see Fig. 3.2). In the XR domain, the physical world and its consisting objects are digitalized and mirrored employing "digital twin world" and "digital twin objects", respectively.

Haptic gloves [124, 125] and suits [126, 127, 128] take the VR experience a step further by enabling users to feel the virtual environment. As users interact with digital objects or navigate through virtual spaces, the haptic feedback transmits the sense of touch, adding a new sensory layer to the immersive experience. A wearable haptic thimble for virtual reality experiences is presented in [129], it conveys the sensation of touching objects made of different materials, rendering pressure and texture stimuli through a moving platform and a vibromotor. In [130], haptic devices with variable stiffness actuators are presented for bimanual interaction with digital twins populating virtual realities. For a comprehensive overview of haptic technologies tailored for virtual realities, refer to [131, 132]. On the other hand, with regards to AR, several investigations about the haptic role and tactile display design were conducted: Normand *et al.* , in [133], investigated the effect of the visual-haptic rendering devices to address the lack of mutual visual occlusion between virtual and real content as well as the lack of haptic sensations; in[134] a comparison between devices differing for wearability is conducted to assess the best form factor for AR haptic interfaces; In [135] 2-D haptic rings and 3-D thimbles are tested in a user evaluation about haptic interface integrability with external cameras and head-mounted display. In [136], an overview of haptic interfaces for virtual and augmented reality is provided, introducing an identification of applicative opportunities specifically for soft haptic devices.

Robotics

Wearable and grounded haptic interfaces are usually involved in the bilateral force-position teleoperation of a robot, fostering the force feedback from the robot to the user. The operator directs and guides the robot in task completion while receiving feedback regarding interactions with objects and the surrounding environment [137, 138, 139]. Kinesthetic feedback plays a crucial role in enhancing the transparency of the teleoperation system and amplifying users' sense of telepresence. However, it can adversely affect system passivity and stability. To address this issue, two alternative frameworks are proposed in [140] and [141], wherein kinesthetic feedback is replaced with cutaneous cues or combined with energy-aware control mechanisms, respectively. These frameworks aim to ensure system stability while avoiding transparency lack.

Furthermore, haptic feedback can be leveraged for robotic awareness, wherein 'awareness"encompasses the machine's ability to perceive, interpret, and respond to its surroundings akin to human awareness. It involves transmitting changes in the robot's status to a human operator. Haptic cues facilitate this dialog between humans and machines [142]. According to findings presented in [143], incorporating awareness haptic feedback enhances human performance during cooperative tasks with robots, particularly for non-skilled individuals. In such scenarios, awareness of the robot's state is fostered by equipping the human with a vibrotactile ring that transmits acknowledgment signals during critical phases of the task. Moreover, the transmission of awareness signals can be extended to mobile robots and drones. For instance, [144] tackles the challenge of relieving the visual channel's burden by utilizing the tactile sense channel to provide multimodal feedback in Unmanned Ground Vehicle teleoperation. Similarly, [145] proposes a haptic-based framework for teleoperation and awareness for rescue robots operating in noisy environments with low visibility.

Medicine and surgery

Usually, surgeons and medical professionals can leverage tactile technologies to practice complex procedures in a risk-free virtual environment using haptic-enabled simulators. The outcome of the study presented in [146] demonstrates an enhancement of performance for an orthopedic surgical task when using a VR-based simulation model incorporating haptic feedback, compared to one without haptic feedback supporting the pursuit and implementation of haptics in surgical training simulation models to enhance their educational value. In [147], Basdogan *et al.* integrated commercially available haptic devices into a training system designed to simulate minimally invasive procedures, while in [148, 149, 150] are presented the ad-hoc design of a user interfaces capable of providing force feedback in all the degrees of freedom (DOFs) available during endoscopic surgery. A compressive overview of haptic-enabled simulators for medical training is presented in [151]. All these interfaces provide realistic tactile feedback, allowing practitioners to develop and hone their skills in a controlled setting before performing surgeries on actual patients, both supporting expert surgeons during their mansions. Haptics in teleoperated medical interventions enables measurement and rendering of force information to the operator during tool-body interaction as stated in [152]. Gaudeni *et al.* in [153] presented

a pneumatic sensing case and a haptic interface to render the forces that surgical drills apply on the patient's cranium. In [154], commercially available haptic interfaces are exploited to correct anxious movements by transmitting tactile cues to the surgeon. In [155] and [156], haptic-based controls using virtual fixtures are developed to guide the surgeon during tasks like cutting or suturing. Moreover, tactile interfaces and the haptic feedback provided by them are commonly leveraged to set a force-position teleoperation framework, enhancing the experience transparency of the surgeons and increasing their engagement concerning the task [157, 158, 159]. Finally, haptics technologies are also involved in setting ad-hoc immersive virtual environments for rehabilitation, such as those presented in [160].

Communication and Lifestyle

Smartphones and tablets utilize tactile feedback to simulate the sensation of pressing physical buttons on the touchscreen, providing users with a more tactile and responsive interface [161]. This technology also extends to wearable devices, such as smartwatches, where haptic feedback enhances the user's awareness of notifications and alerts without the need for visual or auditory cues.

Furthermore, haptic communication has applications beyond personal devices. Remote communication tools, like video conferencing platforms, can incorporate haptic feedback to enhance the sense of presence, transmitting gestures like head nodding [162]. This can be particularly valuable in professional settings, enabling users to feel more connected and engaged during virtual meetings. Additionally, in [163], the authors present a pair of soft wearable anklets to enable people to have a 'remote social walk'. The streaming of the gait cadence between two persons walking in different places induces the synchronization of the footsteps and increases the sense of mutual presence. Moreover, haptic technologies can be used to communicate emotions or control stress levels, as proposed in [164, 165, 166] and [167].

Accessibility and Inclusiveness

Haptic technology plays a crucial role in creating more accessible and inclusive digital and real experiences. For individuals with visual or auditory impairments, haptic feedback provides an additional sensory layer for interacting with environments, objects, and other persons. Haptic displays can convey information for users affected by visual impairments, exploiting the Braille tactile writing system [168, 169], or render graphical representations of data [170]. In [171] and [172], haptic gloves are proposed to foster communication between users using the Lorm alphabet and to improve computer usage for blind persons in a VR setting, respectively.

Haptics may also enhance the sense of direction [173, 174] and guidance [175, 176] for blind people in structured and unstructured environments. Moreover, vibrotactile technologies, such as those presented in [177, 178, 179], are suitable for overcoming freezing of gait (FOG) and balancing issues in Parkinsonian patients.

Education

The educational sector has embraced haptic technology to enrich learning experiences by providing multi-sensory content. Biology classes, chemical studies [180], and architectural simulations in design courses [181] have become more interesting and captivating through the use of haptic interfaces. Students can engage with digital content in a more hands-on manner, bridging the gap between theoretical knowledge and practical application [182].

Furthermore, haptic stimuli can be exploited to correct bad habits in daily activities, such as continuous face-touching [183] or lifting heavy objects with unergonomic postures [184, 185].

Automotive

The automotive industry has integrated haptic technology to enhance safety and improve the driving experience by incorporating haptic feedback into steering wheels or seats to alert drivers to potential dangers [186, 187, 188, 189] or ensure the safety of pedestrians [190]. Lane departure warnings, collision alerts, and parking assistance systems utilize haptic technologies to communicate with drivers, as presented in [191], [192], and [193], respectively. Moreover, advancements in haptic technology contribute to the development of autonomous vehicles. Haptic feedback assists in creating a seamless transition between manual and autonomous driving modes, ensuring that drivers remain aware and engaged when necessary [194, 195].

3.2 Haptic Repurposing

In the field of medicine and pharmacology, "'describes the method of identifying novel medical applications for existing drugs or compounds initially devised for other medical indications. This approach utilizes the established data and safety profiles of current molecules to explore their effectiveness in combating various health conditions or diseases, taking precedence over creating new drug molecules [196]. A renowned instance of this strategy is found in the application of Aspirin. Originally utilized for pain relief, Aspirin is now also prescribed to diminish the risk of heart attacks and strokes.

Similarly, the concept of "'is witnessed in the field of haptic technology. For instance, a vibrating anklet, initially conceived for enhancing the social aspect of running [163], has since been adapted for diverse uses. These applications range from facilitating rendezvous for pedestrians [197] to directing groups of people in various environments, impacting significantly on crowd management [163].

This thesis encapsulates three years of investigation into discovering new applications for tactile technology. It documents the process of repeatedly refining tactile interfaces and haptic methodologies to extend their utility across multiple fields, analogous to the repurposing seen in pharmaceuticals. Haptic technology, initially designed for specific uses—such as gaming, surgical assistance, or communication—has been reconceived for groundbreaking environments like metaverses, hands-on medical therapies, and cancer research.

Subsequent sections of this thesis will introduce a series of studies in this realm, organized by the degree of innovation in their application. We will explore a spectrum of haptic technology repurposing, progressing from the conventional to the most pioneering.

- In the first part entitled "**Haptics for Metaverse Experiences**" will be presented several technologies designed for virtual and extended realities but suitable also to enhance the tactile experience of life in metaverses, summarizing technologies for human-human physical dialog, both active and passive virtual object interaction leveraging haptic stimuli and pseudo-haptics illusions.

- The second part of this work, namely "**Haptics for Medical Treatments**" is focused on the innovative application of haptic to investigate the effects of robot-exerted manual treatments of end-limb affected by trauma and chronic illness.

- The third part,"**Haptics for Mechanobiological Research on Cancer**" consists of an overview of preliminary technologies designed to foster the biotechnology research *in-vitro* and *in-vivo* about cancer proliferation in order to dissect the hypothesis of mechanical inhibition of cancer proliferation.

Finally, a conclusive part collects the perspective of conducted activities and the planned future works for each research field.

Part II

Haptics for Metaverse Experiences

Haptics for Metaverse Experiences

The metaverse is here, and it's not only transforming how we see the world but how we participate in it – from the factory floor to the meeting room.

Satya Nadella

M etaverse word is a portmanteau of the words "meta," which means beyond, and "universe," which refers to everything that surrounds us in the most general sense. In its simplest definition, the metaverse is a three-dimensional virtual world where social, cultural, and recreational activities take place as in the *real* world. A more complex definition incorporates the use of Extended Reality (XR) technologies, i.e. Augmented, Mixed and Virtual Reality, to either fully immerse or superimpose the user in a digital environment that enhances or replaces the physical reality of its body and its surroundings [198]. Started as a game-oriented application, today its popularity is rapidly growing thanks to a pool of users who are getting ever more familiar with the "digital lifestyle", laying fertile ground for its commercialization as a broader application for work and life [199]. The main difference between a massive life simulator video game and a metaverse consists of the persistence of the latter, in fact, at any time users can reset their avatar history or the whole game, while it is not allowed in a metaverse.

Thanks to the metaverse, people may share the environment and interact with each other even if physically located in remote places, being engaged in a more immersive experience than the one offered by standard teleconferencing tools. Indeed, video calls can stream audiovisual content, but fail to convey the sense of presence as they lack the transmission of in-person interaction components, including body language and physical cooperation. In this regard, researchers are tackling the challenge of integrating the haptic channel with the audio and video streams [200, 201, 162, 202, 203]. Their results offer great potential also for metaverses where the user can interact with:

- **Virtual objects**, manipulating them and sifting their digitally-assigned physical and geometrical proprieties, such as shape, stiffness, or viscosity;
- **Other users**, dialoguing and exchanging social gestures to show complicity or greeting;

- **The whole surrounding environment**, inspecting it using all digitalized senses as view, hear, and in that case touch.

It has been demonstrated that collaborating with shared objects improves the quality and the efficacy of the communication [204, 205, 206, 207] and increases the sense of presence [1], co-presence [2] and social presence [3] intensifying the emotions felt in the virtual environments [212, 213, 214]. Moreover, adding the tactile layer is beneficial for increasing the realism of the interaction, as enabling users to manipulate objects in the shared environment shifts the participant's role from observer to actor. In what follows novel haptic interfaces and new methodologies tailored for virtual object discrimination (Chapter 4) and manipulation (Chapter 5), human-human non-verbal communication (Chapter 6) and virtual environment exploration (Chapter 7) will be presented. Each of them is thought to foster the expressiveness of remote communication and to improve the realism of virtual worlds, and then, all of these are efficacious tools to enhance the user experience immersed in digital environments consisting of a metaverse.

---

[1] According to [208] and [209], it is the perceptual illusion of non-mediation in the communicative environment and it can be considered an index of success of the metaverse

[2] According to Youngblut [210], this is defined as "the subjective experience of being together with others in a computer-generated environment, even when participants are physically situated in different sites"

[3] In line with Biocca [211], the "social presence occurs when users feel that a form, behavior, or sensory experience indicates the presence of another individual. The amount of social presence is the degree to which a user feels access to the intelligence, intentions, and sensory impressions of another.

Chapter 4

Object Passive Interaction
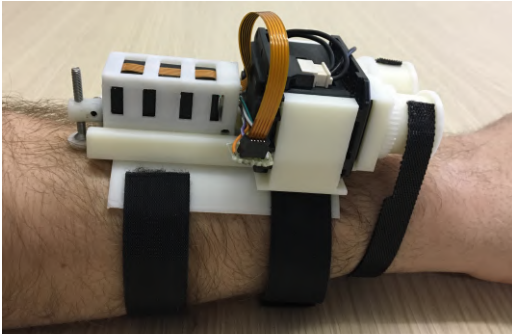
Figure 4.1: The wearable haptic device developed to recreate the dynamics of the interaction with compliant objects. It is able to display two different cues: force (through squeezing effect) and displacement (through skin-stroking effect).

The ability to estimate compliance is an important human skill related to the tactile sense. When the perception of compliance is mediated by haptic devices, the interaction with objects usually takes place through active exploration from the subject. In this paper, we present a wearable haptic device for transmitting information about object compliance through passive touch, meaning that stimuli are generated by an external agent rather than by user motion. More precisely, the dynamics describing the object indentation is reproduced on the user's forearm in the form of decoupled cues representing applied force and surface displacement. The development of such a device has a twofold purpose. Firstly, it allows the study of the human capacity for processing decoupled information to deduce object compliance. Secondly, it makes possible to convey object compliance to someone who is not performing the object indentation. This is especially important in contexts like telemedicine and human-robot collaboration. Users' perception of stiffness, force, and displacement were estimated. Then, a two-phase experiment was carried out to compare the proposed approach with the state of the art.

4.1 Motivation

Object compliance can be defined as the amount of object deformation under a given applied force.

When a tool or a finger indents a compliant object, the force applied and the displacement generated on the object are related to the extension of the contact area. This implies that compliance has not an absolute value, but depends on the way the object is touched [215]. Besides, humans perceive compliance through tactile interaction and in terms of *softness* and *hardness*, which are subjective rather than physical measures of compliance [216]. Such indeterminacy justifies the large number of published stud-

ies on human compliance perception, most of which concern the case of active touch, i.e. with voluntary movement on the part of the subject [217]. In [218], subjects were asked to squeeze a series of specimens between finger and thumb. Subjective hardness was found to follow the psycho-physical power law and to grow as the physical hardness raised to a power. In [219], authors found that the stiffness perception varies on an individual level for different exploration velocities. In [220], an electro-mechanical system was used to measure the compliance Just Noticeable Difference and to investigate the roles of force and mechanical-work (i.e., force integrated over displacement) cues in compliance discrimination.

Results suggested that people tend to use mechanical work cues for compliance discrimination whenever such cues are available. Compliance JNDs appeared to be considerably larger than force JNDs, and their values depended upon the particular experiment used for testing. As regards the case of passive touch, i.e. when the stimuli are generated by an external agent rather than by the user motion, few studies have been done. Despite that, it is generally agreed that there is a difference in compliance perception between active and passive exploration. In [216], authors report that kinesthetic information alone is insufficient to judge the relative softness of objects with deformable surfaces in case of active touch. Differently, the lack of kinesthetic feedback in case of passive touch deteriorates only slightly the discriminability compared with active touch performance gained where both tactile and kinesthetic information are available. In [221], a neuronal spiking model emulating the firing activity of human mechanoreceptors was adopted to deliver haptic information about objects stiffness (i.e., the inverse of compliance) on thumb and index fingers of a remote subject. To indent each rubber sample, the experimental protocol provided for random force and duration, while the indentation velocity was constant. This approach enabled the remote discrimination of most of the proposed pairs of samples, with an overall average of $74 \pm 7\%$ of correct answers.

Within this context, this paper explores the use of a wearable haptic device (see Fig. 5.1) worn on the forearm for conveying information about objects compliance through passive touch. More precisely, the device is meant to *i)* reproduce the dynamics describing the object indentation in the form of decoupled cues regarding applied force and surface displacement, *ii)* act as a sensory substitution system [222] in charge of presenting information to be processed by the intrinsic sensory body system for the compliance estimation, and *iii)* enable the real-time representation of tactile information coming from a remote operation context, without preventing the wearer from using the hand. The development of such a device has a twofold purpose. On the one hand, it allows us to investigate the human capacity for processing information provided in a very different way from how the person would actively acquire it. In particular, we are interested in understanding whether it is possible to deduce the compliance of an object starting from decoupled information on force and displacement, without establishing a constant speed of the indenter. This contributes to the body of knowledge in the human augmentation field [223] by providing a method to convey additional information without interfering with the main receptive channels of the human sensory system (in this case, the hand). On the other hand, our device is a haptic interface that can be adopted in teleoperation contexts where the person who has experience in the matter is not the operator. Explanatory examples are

telemedicine activities [224], where the physical exam assessment through palpation still represents a limit. In fact, typically the patient is not able to evaluate tissues according to their compliance, which however is fundamental in order to localize tumours and lesions [225]. Another paradigmatic context is the industrial robotics field, where collaborative solutions in which human workers and robots share their skills are becoming the new frontier [226]. Supply human operators with intuitive tactile feedback can enhance their comprehension of the current system status and facilitate intervention in dynamic and unforeseen situations.

As a final remark, complying with wearability requirements is relevant to develop haptic systems capable of communicating in a natural and private way with the user [64]. Specifically, we designed a device to be worn on the forearm, leaving the hands free to interact with the surrounding. This requirement is crucial for exploiting the potential of passive touch, i.e. the possibility of perceiving information through haptic cues regardless of our actions.

4.2 System Overview

As introduced in the previous section, this work presents a novel approach to convey object compliance through passive touch, based on the concept of sensory decoupling. To recreate the dynamics of the interaction with compliant objects, two haptic cues are needed: squeezing (displaying the force applied on the object) and skin-stroke (emulating the indentation of the object surface).

4.2.1 Device

A novel wearable haptic interface (depicted in Fig. 4.2) was designed to implement the envisaged sensory decoupling technique. The device is composed of two parts, one thought to convey *skin-stroking* cues (Fig. 4.2), i.e. to stimulate the skin by means of a contact point that moves linearly, and the other intended to apply *squeezing* cues, i.e. to exert a force on the normal (radial) direction of the forearm (Fig. 4.2). The skin-stroking effect is realized through a Micro Linear Actuator PQ12-30-12-P (Actuonix, Canada), characterized by a maximum speed of 28mm/s, a stall current of 0.21A-12V, a stroke length of 20mm, a positional repeatability of ±0.1mm, and a weight of 15g. This actuator was selected because it satisfied the requirements of being reliable, fast, and small enough to be embedded in a wearable device. The actuator is controlled with a linear actuator control (LAC) board (Actuonix Motion Devices Inc., USA), which receives a digital signal d_{LAC} from a PC.

The linear actuator position d_{la} is computed according to the duty cycle of the input signal $d_{LAC} \in [0, 1]$ as $d_{la} = d_{LAC} M_{la}$, where $M_{la} = 2^{10} = 1023$ is the maximum actuator position. This results in a theoretical control resolution of $20mm/1023 \approx 0.02mm$, which is however subordinated to the resolution imposed by the mechanical characteristics of the actuator. A length-adjustable tip with an ABS end-effector is attached at the end of the stroke (as visible in Fig. 4.2), with a contact surface of 2cm^2.

(a)   (b)
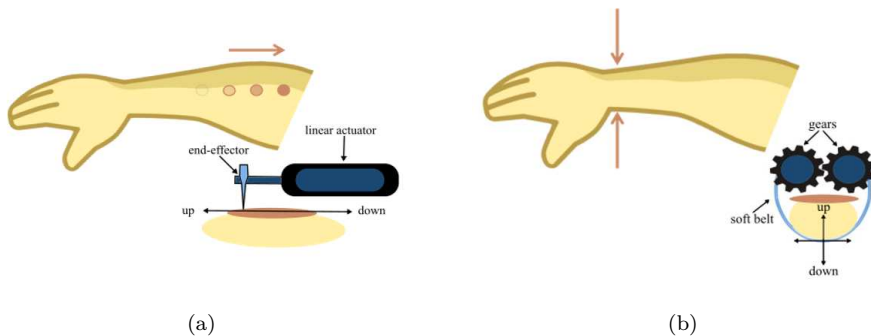
Figure 4.2: Lateral and front views of the haptic device are in (a) and (b), respectively.

This size was sufficient to stimulate the receptive field of a C-Tactile (CT) fibres unit, whose dimension ranges from 1 to 35 mm^2 [227]. CT afferents are known to respond to tactile stimuli with the specific characteristics of a gentle caress [228]. Although there is currently no accurate method to assess the innervation density of CT afferents in human body, there is scientific evidence that these fibres are present in the skin of the human forearm [229]. For this reason, we designed the device with the linear actuator stimulating the hairy skin of the user's forearm.

The squeezing effect is obtained by means of a 5mm^2 wide fabric belt, whose tension is controlled with a Dynamixel MX-28AT actuator (Robotis Inc., USA) with a stall torque of 2.5Nm (stall current 1.4A-12V) and a weight of 72g. An USB2Dynamixel controller (Robotis Inc., USA) mediates the communication between the PC and the actuator through serial communication and TTL protocol, respectively. The ends of the belt are attached to two pulleys, which in turn are housed on two mechanically coupled gears. Both pairs of pulleys and gears have the same radius, which corresponds to 1.0cm and 1.2cm, respectively. When the motor drives the master gear, the torque applied on the latter is transmitted on the slave gear, which assumes an opposite spinning direction. As a consequence, the belt moves along the vertical axis (as depicted in Fig. 4.2) applying a normal force on the user's forearm. We decided to display the force in the lower part of the forearm because of the wide distribution of Merkel nerve endings (mechanoreceptors that provide information on mechanical pressure) in the basal layer of glabrous skin [230].

Furthermore, we applied the two stimuli at the opposite sides of the device for ensuring that, from a mechanical point of view, the motion of one motor does not affect the action of the other (a force applied to the base of the linear motor could unbalance the device and prevent the contact between the arm and the end-effector). To cope with the uncertainties due to the non-ideality of the mechanical system, an ATI Gamma sensor (SI-130-10, maximum torque 10Nm, resolution 1/800Nm) was used in a preparatory experiment to find the relationship mapping the digital motor torque input $d_{dyn} \in [0, 1023]$

into generated torque values τ. This relationship can be described by a linear model as:

$$\tau = -0.04012 + 0.00158 \cdot d_{dyn} \tag{4.1}$$

with a negligible error in the range $[0, 0.1]$Nm (mean RMSE = 0.0013 Nm). It follows that digital values $d_{dyn} \leq 25$ are not sufficient to actuate the motor and move the mechanism. In addition, preparatory experiments revealed that a force greater than 7N is perceived as uncomfortable by the users, therefore we decided to limit the maximum force exerted by the Dynamixel actuator to $F_{max} = 7N$. Thus, the torque range exploited by the device is $[0, \tau_{max}]$, with $\tau_{max} = r_p \cdot F_{max} = 0.07Nm$, being $r_p = 10mm$ the radius of the servo motor pulley. Following the relationship identified in Eq. (4.1), [25, 69] is the range of d_{dyn} that generates $[0, 0.07]$ Nm, which implies a resolution of $0.07Nm/44 = 0.0016$ Nm. Equivalently, the smallest force variation exerted by the device is 0.16 N, a quantity which is lower than the average force JND (see Section 4.2.2).

To reproduce the required forces, the squeezing mechanism needs an initial calibration procedure that brings the belt into contact with the user's arm. This is done by winding up the belt with a torque of 0.001Nm (i.e., $d_{dyn} = 26$) until the contact between the arm and the belt is detected by the motor. When this occurs, the motor is stopped and the current motor position is saved as starting position. It is worth noticing that this value of torque guarantees a contact between the belt and the forearm with a negligible pre-charge effect. Controller boards and related electronic circuitry are enclosed in a external 3D printed box and supplied by an external power source. The total weight of the device is 170g.

4.2.2 Perceptual Psychophysical Study

In order to evaluate the practical working range of the device, we performed a preliminary campaign investigating about users' perception of stiffness, force and displacement in terms of JNDs. In psychophysics, a stimulus JND is the amount of change on a primary stimulus which is just sufficient to produce a change of one sensation JND upward at that point [231].

In particular, we assessed the JND for *i)* stiffness perceived during active exploration of virtual objects, *ii)* squeezing force applied on the lower part of the forearm, and *iii)* skin-stroking displayed on the higher part of the forearm. In the first case, the goal was to evaluate the users' ability in discriminating object stiffness in the most natural condition, that is with active exploration. This result was considered as the best achievable result for the purpose of evaluating users' performance in perceiving device-mediated stiffness. The second and the third cases were instead needed to characterize the range of stiffness representable with the device, which can be expressed as

$$[k_{min}, k_{max}] = \left[\frac{F_{min}}{x_{max}}, \frac{F_{max}}{x_{min}} \right]$$

where F_{min} and x_{min} are the force and displacement JND, respectively, while F_{max} and x_{max} are limits imposed by the device mechanical structure.

Ten subjects (6 males and 4 females, age 22-40) took part to the preliminary campaign, and all of them were involved in the three experiments. The experimental evaluation

protocols followed the declaration of Helsinki. Participants were blindfolded and asked to wear a headset providing white noise to avoid visual-audio bias in the stimuli evaluation.

Stiffness JND   An Omega.3 (Force Dimension, CH) was used to render pairs of virtual objects with different stiffness. The reference object was displayed in the left part of the workspace with a constant stiffness k_{ref} which was maintained throughout the experiment, whereas the compared object was displayed in the right part of the workspace and its stiffness k_{com} was changed at each step.

Participants were asked whether there was a difference in stiffness between the two proposed objects. In order to perceive the stiffness, they were allowed to freely touch the virtual objects using their index fingertip as long as they needed and with the force they preferred. An ad-hoc thimble was mounted as end-effector on the haptic interface to facilitate the exploration. At each step, depending on the user's answer, the stiffness variation Δ computed with respect to k_{ref} was changed according to the one-up one-down single descending staircase procedure[232]. More precisely,

$$k_{com}(n) = k_{ref} + \Delta(n)$$

with

$$\Delta(n)|_{n=0} = 0.75 k_{ref}$$
$$\Delta(n)|_{n\neq0} = \Delta(n-1) \pm \delta k_{ref}$$

where $n = 1, 2, ..., 30$ was the current step, and $\delta = 0.05$ until the first reversal point of the participant's perception, after which the value was halved ($\delta = 0.025$). The same procedure was repeated four times, and for each trial a different value of $k_{ref} \in \{50, 150, 250, 350\}$ N/m was selected. These values were chosen in accordance with the range of stiffness of the human skin within the limits considered in [233]. For each participant, the stiffness JND was evaluated as the average of the Δ values at the reversal points. The experiment revealed a linear dependence between stimulus and perception with an average stiffness JND of $(0.10 \pm 0.04) k_{ref}$.

The same comparative analysis was further repeated to evaluate the minimum stiffness that could be perceived with the proposed setup, in order to provide a lower bound for the validity range of the previous result. On average, the minimum perceptible stiffness was equal to $k_{min} = 14.8 \pm 2.3$ N/m.

Force and Displacement JNDs   The minimum force and displacement perceived with the device were evaluated with a procedure similar to the one used in the previous experiment. Depending on the JND of interest, the device was controlled to actuate only the squeezing effect or the skin-stroking one. Participants were asked to wear the device on the forearm of the dominant hand (one left-handed and nine right-handed) and to evaluate if there was a difference between the pair of proposed stimuli, i.e. F_{ref} and F_{com} in the first case, and x_{ref} and x_{com} in the second one. The reference value was always the first stimulus proposed and each test lasted $n = 30$ steps. At each step, depending on the user's answer, the stimulus variation Δ computed with respect to the reference value was

changed according to the one-up one-down single descending staircase procedure[232]. We defined $F_{ref} = 0$ N, $\Delta(n)|_{n=0} = 5$ N and $\delta = 0.3$ N for the force case, and $x_{ref} = 0$mm, $\Delta(n)|_{n=0} = 20$mm and $\delta = 1$ mm for the displacement case, respectively. The value of δ was halved after the first reversal point and the stimulus JNDs were computed as the average Δ values provided at the reversal points. Results reported mean force JND of 0.87 ± 0.41 N and an average displacement JND of 1.51 ± 0.45 mm.

Device Characterization   Considering the boundaries identified in the previous experiments and the mechanical characteristics of the actuators, we computed the practical working range of the device. The theoretical range of stiffness representable with the device is $[45, 7000]$ N/m.

4.3   Experimental Validation

The aim of the experimental validation was to test the effectiveness of decoupling cues representing applied force and surface displacement to convey information about the objects compliance.

A two-phase experiment was carried out, with each phase lasting 24 trials. A software developed in LabVIEW (National Instruments, Texas) was used in both phases to simulate the indentation of virtual objects, modelled as ideal springs with a control rate of 10Hz. In each trial, participants perceived the indentation of three virtual objects through the wearable haptic interface presented in Section 5.2, and were asked to rearrange them according to ascending order of stiffness. At each indentation, the maximum force to apply on the virtual spring was pseudo-randomly selected from the set $\{2.5, 4, 5.5, 7\}$N in order to have six repetitions per value across 24 trials. These values were selected to span the entire device force range and to comply with the average force JND (see Section 4.2.2). As regards the stiffness values, we considered $k_1 = 350$ N/m, $k_2 = 420$ N/m, $k_3 = 525$ N/m, and $k_4 = 683$ N/m, being

$$k_1 = \frac{F_{max}}{x_{max}},$$
$$k_{i+1} = k_i + round((0.2 + 0.05(i-1))k_i), i = 1, 2, 3. \qquad (4.2)$$

Notice that k_1 was chosen to make feasible all possible pairs of force and stiffness in terms of displacement, while the other values were chosen with increasing percentage increments. Despite the preliminary campaign revealed that the average stiffness JND is $(0.10 \pm 0.04)k_{ref}$ (see Section 4.2.2), we decided to set greater percentage increments to account for the fact that passive touch is in general more challenging than active touch [216, 221]. For each trial, the three indentations were presented one after the other with a 2s pause in between, and participants could ask to repeat the entire set a second time. To ensure that each stiffness value was presented an equal number of times and reduce order-effects, each participant tested all the combination resulting from simple dispositions of 3 elements out of 4, for a total of 24 trials per subject per phase. This experimental protocol had a twofold aim: not to increase users' memory load asking to memorize a
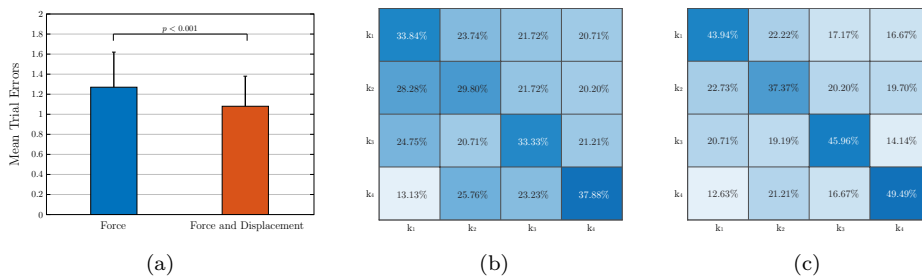
Figure 4.3: Experimental validation results. In (a), the average number of not correctly sorted objects stiffness is reported for the two experimental conditions. The p-value is detailed on top of the bars. The confusion matrices for the first and second phase of the experimental validation are depicted in (b) and (c), respectively.

hight number of objects, and to limit the probability of guessing by chance the correct objects arrangement. A 5 minutes break was given between the twelfth and thirteenth trial to enhance concentration and avoid distress. The order of the experiment phases was randomized for each participant.

The perceived order of stiffness was communicated verbally to the experimenter by indicating with *A*, *B* and *C*, the first, second and third displayed stimulus, respectively. The error committed in arranging the stimuli was considered as a metric. This was computed for each trial as half of the sum of the distances between the virtual object position assigned by the subject and the correct one. For example, if the correct sequence was *'BCA'* and the subject declared *'ABC'*, the error associated to the trial was 2.

Eleven subjects (7 males and 4 females, age 22-50) took part to the experiment. Each participant was asked to wear the haptic interface on the forearm of the dominant hand (two left-handed and nine right-handed). To avoid visual-audio evaluation of the stimuli, participants were asked to place the arm in a box with the palm facing down and to wear a headset providing white noise to mask the sound from the activation of the motors. The experimental evaluation protocol followed the declaration of Helsinki, and there was no risk of harmful effects on subjects' health. Each participant gave written informed consent and was able to discontinue participation at any time during experiments. The first experimental condition was in line with the state of the art and served as benchmark test, while the second one was focused on the approach proposed within this work.

4.3.1 Phase 1: Force (F)

In this phase, a single haptic cue was displayed to the user, i.e. the force applied on the virtual object, therefore subjects were not informed about the surface displacement. The indention velocity was fixed at $v = 1.25$cm/s. This experimental condition was shaped to be representative of the state of the art and was instrumental for the second phase. Indeed, most devices developed for conveying stiffness make use of constant indentation speed, inducing users to evaluate stiffness on the basis of the integral of the force over time, i.e. the impulse [234, 221, 235]. In other words, the greater the perceived impulse,

the greater the stiffness of the indented object. While functional, this approach imposes limits on how the object has to be indented, for example with constant speed.

Before the starting of the experiment, every participant was presented with a training session consisting of three trials that were not counted for the purposes of the analysis. In these trials, the stiffness values were pseduo-randomly selected from those exploited for the stiffness JND evaluation, while the force applied was pseudo-randomly generated in the range $[1, 7]$ N.

4.3.2   Phase 2: Force and Displacement (FD)

In the second phase, both the force applied on the virtual objects and the surface displacements were displayed through the wearable haptic interface. For guaranteeing a very challenging task, the indention velocity was pseudo-randomly selected from the set $\{1, 1.25, 1.5\}$ cm/s in order to have eight repetitions per value across 24 trials. Similarly to the first phase, each participant was presented with a training session consisting of three trials that were not counted for the purposes of the analysis. In these trials, the stiffness values were pseduo-randomly selected from those exploited for the stiffness JND evalutation, while the force applied and the indentation velocity were pseudo-randomly generated in the ranges $[1, 7]$N and $[0.5, 1.5]$ cm/s, respectively.

4.3.3   Results Analysis and Discussion

A statistical analysis was conducted to assess users performance in perceiving stiffness with the proposed sensor decoupling technique. The set of virtual objects combinations was the same across the two phases, thus a comparison of users capacity for discriminating stiffness using different approaches was obtained exploiting a paired sample t-test. The average of errors committed in sorting each triplet was compared considering the two feedback methodologies. No outliers were detected. The assumption of normality was not violated, as assessed by Shapiro-Wilk's test ($p > 0.05$). The t-test revealed that users better distinguished object compliance when both applied force and surface displacement were displayed (mean error per trial $= 1.087 \pm 0.300$) as opposed to the single stimulus case (mean error per trial $= 1.276 \pm 0.355$). A statistically significant mean decrease of 0.189 errors per triplet was observed, $t(23) = 4.509$, $p < 0.001$. Results are visually depicted in Fig. **??**. For the sake of clarity and completeness, users' answers versus correct stiffness order for the two phases are reported in confusion matrix structures in Fig. **??** and Fig. **??**.

A confusion matrix, also known as an error matrix, is a specific table layout that allows for performance visualization. Rows of the matrix represent the right objects positions with respect to a scale ordered by ascending stiffness, while columns represent the ones guessed by the users. Each element of the matrix contains the occurrences of each assignment. For instance, the value in the first row and third column reports the amount of times that users identified k_3 as k_1. As a consequence, the diagonal outlines the number of correct compliance recognitions, whereas upper and lower triangular portions of the matrices indicate the errors. For an easier comprehension, we reported the results expressed as the percentage among all the users. As noticeable and supported by the

statistical analysis, the percentage of correct matches is higher in the FD case than in the F one, i.e. users performed better when they could perceive the compliance with both squeezing and skin-stroking cues (case FD, Fig. **??**). These results are in line with the expectations and confirm the effectiveness of the proposed approach. In both cases, users found easier to discriminate higher stiffness rather than smaller ones, as it can be seen from the values reported in the main diagonals. It should also be emphasized that, moving away from the main diagonal, the extent of the errors depends on the stiffness that have been confused. As an example, to arrange k_4 in the place of k_1 is more serious than confusing k_2 and k_3 considering that $k_4 = k_1 + 0.95k_1$ while $k_3 = k_2 + 0.25k_2$ (see Eq. (**??**)). Both matrices report a percentage error that is higher in case of pairs made of similar stiffness than in case of pairs in which the stiffness difference was more relevant. This outcome confirms that perception through passive touch is in general more challenging than perception by means of active exploration. Besides, providing an enriched information on the object indentation dynamics contributes to reduce the error even in the most challenging cases.

4.4   Conclusions

This work presents a novel wearable haptic device for object compliance discrimination through passive touch. To date, most of the haptic devices for transmitting stiffness exploit constant speed for object indentation, inducing users to evaluate stiffness on the basis of the integral of the force over time. Even if functional, this strategy imposes limits on how the object has to be indented to let the system work. Conversely, the proposed device implements a sensory decoupling approach with the aim of recreating the dynamics of the interaction with compliant objects. The combination of squeezing and skin-stroking cues provides the user with information about applied force and surface displacement, enabling the perception of objects stiffness. We described the mechanical structure, the working principle, the sensory decoupling approach, and the control of the proposed device. In order to evaluate users' capacity for discriminating object compliance through the proposed device, we conducted an experimental campaign where users wore the haptic interface to sort different objects by their stiffness. The results show that the envisaged sensory decoupling technique is effective to identify and sort different stiffness. In future work, we plan to run a more extensive evaluation to assess the perceived cognitive load and the ease of learning, as well as the implication of creating the sensation on the arm, when it would usually be felt by the finger. Moreover, we aim to improve the wearability and ergonomics of the device by reducing the size of actuators, or by selecting more compact form-factor ones. Finally, further psychophysical studies will be crucial to generate more informative tactile signals in order to improve the perception of object compliance. This work represents the first attempt to recreate the interaction with compliant objects displaying at the same time both the force applied and the surface indentation. The device here presented paves the way for novel design choices and improvements in this direction.

Chapter 5

Kinestetic Interaction by Self Contact

Figure 5.1: The user wears a head mounted display and interacts with a virtual object exploiting Self Contact. The virtual fingers are in contact with the virtual object when the user's fingertips are in contact with each other. The hand is tracked through a Leap Motion placed on the table. The virtual scene is repeated on the monitor for explanatory purposes only.

Despite the considerable technological progress of haptic technology in recent years, to date there are still no wearable systems capable of providing both kinesthetic and cutaneous feedback that are universally recognized and adopted outside the research contexts. This is particularly evident when dealing with virtual reality, where the lack of truthful tactile feedback has often been addressed by exploiting Pseudo-Haptics methods. Being designed to indirectly stimulate the somatosensory system, these methods are not meant to be integrated with haptic devices. With the idea of providing a meeting point between the haptic and pseudo-haptic fields, this work proposes Self Contact: exploiting the pseudo-haptic principles to lead the user in generating a real kinesthetic feedback through the contact between his/her fingers. Self Contact can be implemented alone or in combination with haptic thimbles, allowing to complete the set of tactile stimuli that is necessary for a realistic interaction with virtual objects in pick and place operations. A step-wise validation demonstrated that the proposed approach is suitable for recovering the kinesthetic feedback into virtual reality, towards the development of increasingly immersive environments.

5.1 Motivation

The impressive research carried out over the last years has led virtual reality to be recognized nowadays as a powerful tool for a large variety of applications. The possibility of creating simulated environments modelled on specific requirements has opened new opportunities for both academic and industrial research. Anyway, despite the field of application, the development of convincing environments faces the challenge of providing

users with consistent sensory inputs.

Indeed, when immersed in the real world, our senses are continuously exposed to multiple stimuli that allow us to acquire information about the environment. However, inducing the same stimulation in virtual reality is still an open issue due to technological limitations. While it is reasonable to assume that users have available audio-visual displays, the same assumption cannot be extended to tactile and olfactory displays. Although there exist in literature systems able to provide this kind of stimuli [236, 129], this branch of technology is not yet mature enough for guaranteeing its interfacing with common virtual reality systems in an effective way. Especially for what concerns the haptic field, there are examples of technologies ranging from fully grounded [63] to fully wearable [124], but the only form of haptic feedback that is actually exploited outside the laboratory settings is the vibratory cue embedded in videogame controllers, which typically fails in rendering complex contact interactions.

To overcome this limitation, alternative methods to stimulate tactile perception without directly stimulating the somatosensory system have been studied. These methods fall under the concept of *Pseudo-Haptic Feedback* [237], i.e. the use of visual feedback and properties of human visuo-haptic perception to simulate tactile sensations in virtual environments. Following the characterization proposed in [238], the pseudo-haptic feedback capitalizes on four factors: *i)* the presence of one or more visuo-haptic sensory conflicts, *ii)* the dominance of visual displacement over actual physical sensorimotor displacement when perceiving spatial properties, *iii)* the combination of haptic and visual information resulting in a new and coherent representation of the environment, and *iv)* the possibility of creating haptic illusions, that is, to alter the perception of a haptic property present in the real environment. Pseudo-haptics has been exploited in literature to simulate numerous virtual objects haptic properties such as physical shape [239], friction [237], stiffness [240], mass [241], and texture [242].

As previously stated, what these examples have in common is the manipulation of the users' perception through indirect stimulation of the somatosensory system. In other words, the physical haptic stimulation presented to the users in the virtual environment is different from the one they would perceive through physical contact with objects, but a proper visual stimulation is able to circumvent this dissimilarity. Following this consideration, it is interesting to speculate on how the user experience would change if the visual feedback was made for triggering a real kinesthetic feedback. This approach would allow to exploit the visual displacement to guide the user towards making and breaking contact with real surfaces, with a consequent direct stimulation of the somatosensory system.

In this context, this work proposes the *Self Contact* paradigm: exploiting the Control/Display (C/D) ratio for the virtual hand joint-angle velocity, i.e. the ratio between the human hand velocity and the virtual hand velocity, to let the user make contact between fingers during grasping tasks (Fig. 5.1). Indeed, the underlying concept is enabling users to feel a real kinesthetic feedback during pick and place tasks, instead of a simulated version of it. Furthermore, being a software-based approach, Self Contact can be combined with additional cutaneous feedback thanks to the integration with haptic thimbles. As a result, this novel approach offers a twofold advantage. On the one hand, it simplifies the implementation of the kinesthetic feedback in virtual reality, towards

more and more realistic experiences. On the other hand, it allows researchers to reduce the encumbrance of wearable haptic technology by embedding in the devices only the hardware needed for providing the cutaneous feedback. On the whole, this work exploits the pseudo-haptic principles to override the user's kinematic proprioception, while at the same time it provides a real haptic feedback without the need of additional devices. To the best of our knowledge, Self Contact represents the first attempt to create a joining link between the pseudo-haptic and the haptic fields.

5.2 Self Contact paradigm

To make the user perceive a real hand kinesthetic feedback during a grasping operation, the *Self Contact* paradigm exploits the C/D ratio to slow down the velocity of the virtual hand. Then, the virtual fingers result in contact with the virtual object when the user's fingertips are in contact with each other, thus, the kinesthetic sensation of grabbing an object is restored by the "self contact". In what follows, we present the Self Contact algorithm, while the step-wise validation that led to its implementation is provided in Section 5.3.

As basic building block, the algorithm takes advantage of the postural synergies introduced in [243].

Synergies represent a set of linear dependencies between the joint variables of the whole hand, therefore they allow to define the hand posture through a lower number of degrees of freedom. We exploit the synergy definition detailed in [244]. Let $q(t) \in \mathbb{R}^{20 \times 1}$ be the vector of the hand joint-angle values at time instant t as $q(t) = Sz(t) + q_m$,

where $q_m \in \mathbb{R}^{20 \times 1}$ is the average hand posture over all datasets of joint positions q, $z \in \mathbb{R}^{n_z \times 1}$ is the vector of synergy variables, with $n_z \leq 15$ being the exploited number of synergies, and $S \in \mathbb{R}^{20 \times n_z}$ is the matrix of coefficients evaluated in [243].

As formalized in [245], the hand joint velocities vector $\dot{q}$ is defined by the linear mapping

$$\dot{q}(t) = S\dot{z}(t). \tag{5.1}$$

Starting from the joint-angle velocity $\dot{q}$ estimated by a hand tracking system, such a relationship allows to reconstruct the current synergy value $\dot{z}$. Indeed, (5.1) can be rewritten as

$$\dot{z} = S^\dagger \dot{q} \tag{5.2}$$

where $S^\dagger$ is the pseudoinverse of the matrix S. This set of equations can be exploited to map the user's hand movements in a virtual hand avatar. For the sake of simplicity and without lack of generality, in this work the virtual hand is moved along the first postural synergy and the user hand velocity is referred to the index PIP (Proximal InterPhalangeal) joint-angle velocity[1]. The first synergy is commonly used for replicating grasp actions [246]. In terms of formulas, this translates to choose $n_z = 1$ and extract from S the first column, i.e. $\tilde{S} \in \mathbb{R}^{20 \times 1}$, thus (5.2) can be rewritten as

$$\dot{z}(t) = \frac{\dot{q}_{PIP}(t)}{\tilde{S}_{PIP}}.$$

---

[1]Hand-closure motions are associated to positive velocities.

where $\dot{\hat{q}}_{PIP}(t)$ represents the tracked joint-angle velocity, and $\tilde{S}_{PIP}$ is the first synergy coefficient corresponding to the index PIP joint-angle. Once the value of $\dot{\hat{z}}(t)$ has been estimated, the joint-angle velocity of the virtual hand $\dot{q}_v(t) \in \mathbb{R}^{20 \times 1}$ is given by

$$\dot{q}_v(t) = \tilde{S}\dot{\hat{z}}(t). \tag{5.3}$$

At this point, it is possible to manipulate $\dot{q}_v(t)$ by introducing in (5.3) a scaling factor $k(t) \in \mathbb{R}$, that is

$$\dot{q}_v(t) = \tilde{S}\dot{\hat{z}}(t)k(t).$$

This term is used to evaluate the C/D ratio. Indeed, considering as $\dot{q}_{v_{PIP}}(t)$ the index PIP joint-angle of the virtual hand computed at time instant t, the C/D ratio can be expressed as

$$C/D_{ratio} = \frac{\dot{\hat{q}}_{PIP}(t)}{\dot{q}_{v_{PIP}}(t)} = \frac{\tilde{S}_{PIP}\dot{\hat{z}}(t)}{\tilde{S}_{PIP}\dot{\hat{z}}(t)k(t)} = \frac{1}{k(t)}.$$

Depending on whether the virtual object is graspable or not, i.e. if the object is between the virtual fingers, a different $k(t)$ is applied to the virtual hand. In the latter case, virtual and real hand joint-angle velocities coincide, that is $k(t) = 1$, while in the former case

$$k(t) = k_{des}(t)m(t) + \hat{k}(|\dot{\hat{q}}_{PIP}(t)|)(1 - m(t))$$

with

$$k_{des}(t) = \begin{cases} 0 & \text{if } d_v(t) > d_r(t) \text{ and } \dot{\hat{q}}_{PIP}(t) \leq 0 \\ \frac{d_v(t)}{d_r(t)} & \text{if } d_v(t) \leq d_r(t) \text{ and } \dot{\hat{q}}_{PIP}(t) \leq 0 \\ \frac{d_v(t) - l_{obj}(t)}{d_r(t)} & \text{if } \dot{\hat{q}}_{PIP}(t) > 0 \end{cases}$$

$$m(t) = \begin{cases} 1 & \text{if } k_{des}(t) > \hat{k}(|\dot{\hat{q}}_{PIP}(t)|) + \sqrt{\vartheta} \\ \alpha(t) & \text{if } \hat{k}(|\dot{\hat{q}}_{PIP}(t)|) < k_{des}(t) < \hat{k}(|\dot{\hat{q}}_{PIP}(t)|) + \sqrt{\vartheta} \\ 0 & \text{if } k_{des}(t) < \hat{k}(|\dot{\hat{q}}_{PIP}(t)|) \end{cases}$$

$$\alpha(t) = \frac{k_{des}(t) - \hat{k}(|\dot{\hat{q}}_{PIP}(t)|)}{\sqrt{\vartheta}}$$

where $d_r(t) = \|\hat{p}_t(t) - \hat{p}_i(t)\|$ is the distance between thumb ($\hat{p}_t(t)$) and index ($\hat{p}_i(t)$) fingertips of the real hand, $d_v(t) = \|p_{v_t}(t) - p_{v_i}(t)\|$ is the distance between thumb ($p_{v_t}(t)$) and index ($p_{v_i}(t)$) fingertips of the virtual hand, l_{obj} is the size of the object computed along the direction of thumb and index fingertips, $\hat{k}(t) = f(|\dot{\hat{q}}_{PIP}(t)|)$ is the minimum admissible value for $k(t)$ given $\dot{\hat{q}}_{PIP}(t)$, and ϑ is the accepted mean square error. A detailed description of the function and its selection is provided in Section 5.3.1. The desired scaling factor $k_{des}(t)$ is thought to exploit the hand-closure motion (i.e., $\dot{\hat{q}}_{PIP}(t) > 0$) for obtaining Self Contact, and to remove the misalignment between the virtual and the real hand during the opening phase (i.e., $\dot{\hat{q}}_{PIP}(t) \leq 0$). The term $m(t) \in [0, 1]$ smooths the variation of $k(t)$ when $k_{des}(t)$ is at distance less than $\sqrt{\vartheta}$ from $\hat{k}(|\dot{\hat{q}}_{PIP}(t)|)$, avoiding abrupt changes of the C/D ratio.
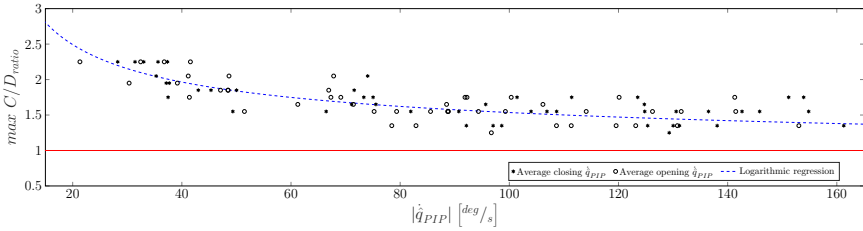
Figure 5.2: Maximum accepted C/D_{ratio} are reported for each subject. Average closing $\dot{q}_{PIP}$ are reported with an asterisk, whereas average opening $\dot{q}_{PIP}$ are indicated with circles. The blue dashed curve depicts the interpolation function, while the red line highlights the C/D_{ratio} lower bound.

5.3 Experimental validation

To assess the feasibility and the benefits of Self Contact, we conducted a step-wise validation by means of two research questions that have been asked and answered within this work. In this Section, we retrace the progression of the experimental process describing experimental protocol, setup, and results per each step. Each subject gave her/his written informed consent to participate and was able to discontinue participation at any time during experiments. The experimental evaluation protocols followed the declaration of Helsinki, and there was no risk of harmful effects on subjects' health.

A virtual environment was developed in C# for the purposes of the experimental campaign. The user hand was tracked by means of a Leap Motion, while the virtual scene was rendered using an Oculus Rift DK2 and Unity game engine (v. 2019.4.26).

5.3.1 Maximum acceptable C/D ratio

As a first step, we evaluated the ability of humans in discriminating slowed down movements of the hand. We define as *maximum acceptable C/D ratio* the maximum scaling factor applicable to the virtual hand joint-angle velocity without affecting the users' perception. The first research question is:

Does the maximum acceptable C/D ratio change according to the hand velocity assumed by the user?

In accordance with the study undertaken in [247], during active free movements the JND of PIP joint-angle position is about 2.5 deg, which corresponds to a displacement JND of about 2.2mm at the fingertip of the index finger considering a standard hand[248]. As a further step, it is reasonable to assume that these values are not constant, but that they depend on the PIP joint-angle velocity. Indeed, a small C/D ratio could be perceptible during rapid grasping actions, while it could be considered negligible in slow movements. This hypothesis has been verified through the following JND experiment, which was aimed at finding the relationship between joint-angle velocity and maximum acceptable C/D ratio. Ten subjects (7 males, 3 females, age 22-50) took part to the experiment. Each trial consisted in three main phases, that were repeated cyclically 50 times:

evaluation: the participant is tasked to rhythmically open and close his/her hand five times at constant speed following the first synergy. The rhythm is suggested by a small indicator bar placed in the top left corner of the screen. A constant C/D_{ratio} is used to scale the hand motion speed;

interview: the participant is asked about the realism of the virtual hand, i.e. "Could you feel a difference in speed between your physical and virtual hand?" "Yes/No";

update: the C/D_{ratio} is updated based on the user's response, following the staircase progression [249] with a step size of 0.05.

For each trial, the initial C/D_{ratio} value was pseudo-randomly selected from the set $\{1, 2\}$. Once a trial was completed, the last C/D_{ratio} was taken as JND value and a new trial with a different motion rhythm was proposed to the user after 5 minutes of rest. The tested range was from 0.4Hz to 1.2Hz, with an increment of 0.2Hz, for a total of 5 trials. The indicated frequency refers to a complete opening and closing movement of the hand. Lower and higher motion rhythms were discarded after a preparatory investigation because it is considered unnatural to follow during grasping actions. Index PIP joint-angle velocity $\dot{q}_{PIP}$ and JND of C/D_{ratio} were recorded for each trial.

Results and discussion Results of the experiment are graphically reported in Fig. 5.2 We decided to calculate the average opening and closing $\dot{q}_{PIP}$ separately and then interpolate their absolute value. Several mathematical models interpolating the outcomes of the C/D_{ratio} JND were tested. Finally, the logarithmic model was chosen as the most descriptive one for its lower mean square error, which is equal to $\vartheta = 0.004$. As a consequence, the *max* C/D_{ratio} can be described as

$$max \ C/D_{ratio} = \frac{1}{\hat{k}(|\dot{q}_{PIP}|)} \qquad (5.4)$$

where

$$\hat{k}(|\dot{q}_{PIP}|) = \beta_1 ln(|\dot{q}_{PIP}|) + \beta_2$$

with $\beta_1 = 0.1314$ and $\beta_2 = 0.0290$. The experimental results on the regression model are consistent with the Weber–Fechner law [250], which describes the relationship between perception and stimulus. Outcomes demonstrate that there always exists a $C/D_{ratio} > 1$ that can be used to scale down the virtual hand velocity without affecting the users' perception.

Moreover, as noticeable in Fig. 5.2 and in line with the hypothesis, the maximum acceptable C/D_{ratio} decreases as the joint-angle velocity increases.

Anyway, to have *max* $C/D_{ratio} > 1$ for all the considered $\dot{q}_{PIP}$ values is not enough for guaranteeing the algorithm feasibility. It is in fact necessary to evaluate if the values of C/D_{ratio} that lie within this boundary are suitable to truly achieve Self Contact or if the *max* C/D_{ratio} values are too strict for that purpose. To this end, an analysis of the worst-case was performed, looking for the case in which the difference between $d_v(t)$ and $d_r(t)$ is the smallest obtainable and it is applied during the whole grasping operation. Starting from the real hand opened, i.e. $\hat{q}_{PIP} \simeq 4$ deg corresponding to an index-thumb

fingertips distance of about 80mm, it was experimentally assessed that the worst-case corresponds to making a closing movement at constant joint-angle velocity $\dot{q}_{PIP} = 20$ deg/s (identified as a reasonable lower bound in the preparatory phase), which implies to get $d_v(t) - d_r(t) \simeq 5.19$cm. This measure can be associated to the worst-case maximum width of the virtual object, meaning that in all the other cases users can exploit Self Contact while interacting with bigger objects.

5.3.2 Self Contact evaluation

As a further step towards a complete evaluation of Self Contact, the second question is:

Is Self Contact a valid method for providing a kinesthetic feedback during the interaction with virtual objects?

Ten subjects (6 males, 4 females, age 23-59) were asked to perform two-fingers (i.e., thumb and index) pick and place grasps of a virtual cylinder with radius 1.5cm for 3 times, exploiting 4 different feedback policies aimed at informing the user about the grasping action:

- *i)* No Feedback (N), any type of feedback is provided to the user.

- *ii)* Visual feedback (V), a color change of the cylinder informs the user that the object is grasped.

- *iii)* Haptic feedback (H), the user interacts with the object exploiting Self Contact.

- *iv)* Visual and Haptics (VH), both visual and haptic feedback are enabled.

. Each user was involved in four trials, i.e. one per feedback modality, presented in a pseudo-random order, for a total of 12 pick and place operations. Participants wore 3D-printed ABS thimbles on thumb and index fingertips to reduce the cutaneous feedback component deriving from Self Contact. Task completion time and number of failures were used as metrics for comparing users' performance as the type of feedback modality changes. A failure consisted in a drop of the grasped object while moving it, while the time counter started the first time the object was touched and ended when the object was placed at the goal position. The object was considered grasped when both virtual index and thumb fingertips simultaneously penetrated the surface of the cylinder by no more than 30% of its radius, i.e. 0.45cm.

Results and discussion Results on number of failures and task completion times are reported in Fig. 5.3.(a) and Fig. 5.3.(b), respectively.

As far as it concerns the number of failures, a preliminary analysis revealed that the assumption of normality was violated for all the four conditions (as stated by the Shapiro-Wilk test, $p < 0.001$ for all the cases). A Friedman test revealed statistically significant differences among the four different feedback strategies. Pairwise comparisons performed with a Bonferroni correction assessed that number of failures significantly depends on the feedback modalities, $\chi^2(3) = 48.497, p < 0.001$. Post hoc analysis revealed statistically significant differences in number of failures from N to V ($p = 0.03$), H ($p < 0.001$), and
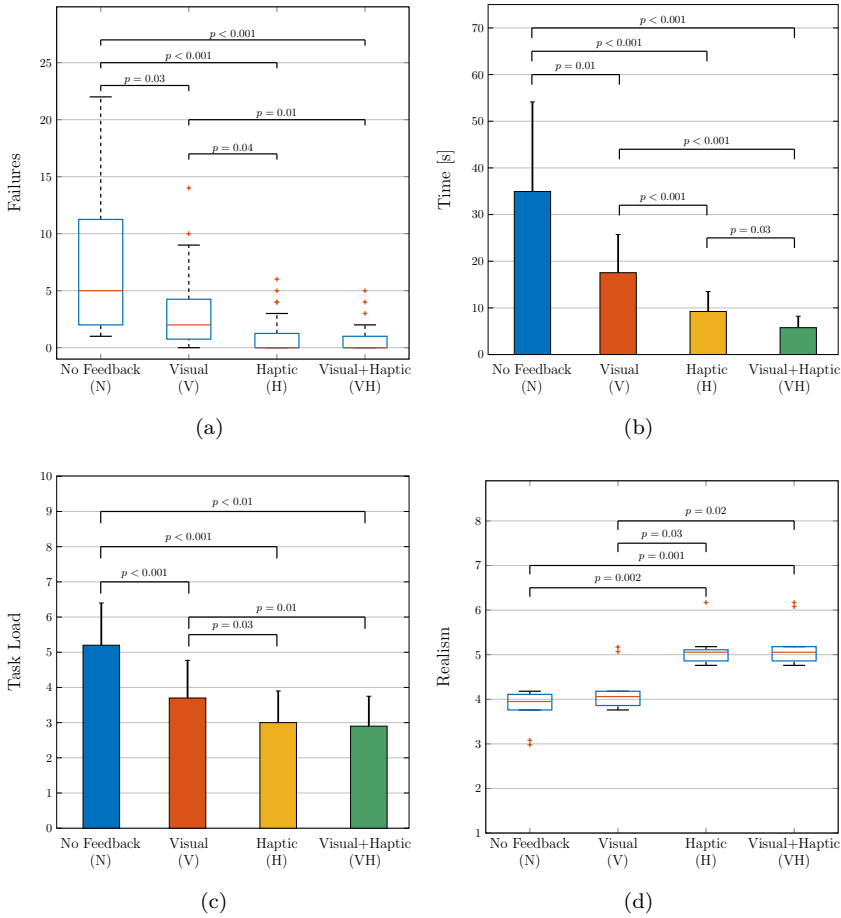
Figure 5.3: Experimental validation results for the four feedback modalities. The number of failures and the task completion time are reported in (a) and (b), respectively. Results of the users' opinion questionnaire are in (c) for the task load and in (d) for the realism. The p-values are reported on top of the bars.

VH ($p < 0.001$). Similarly, statistically significant differences were found between V and VH ($p = 0.014$), and V compared to H ($p = 0.039$). No statistical difference was assessed between H and VH ($p = 1$).

From the statistical analysis, it is evident that it is easier to correctly grasp an object when a feedback is given rather than without feedback. What is interesting is that users found easier to maintain the grasp when the fingertips were in contact. Indeed, the visual feedback only informs the users about the grasp, but does not help them in maintaining the object grasped. Conversely, having the fingertips in contact almost avoids failures in performing the task.

A one-way repeated measures ANOVA was conducted to determine whether there were statistically significant differences on the time in accomplishing the task over the

four modalities. There was an outlier in the N modality that was removed without affecting the dataset. Data were transformed using the squareroot transformation and passed the Shapiro-Wilk normality test ($p > 0.05$). Mauchly's test of sphericity indicated that the assumption of sphericity had been violated, $\chi^2(5) = 29.31, p < 0.001$. Therefore, a Greenhouse-Geisser correction was applied ($\epsilon = 0.584$). The results of the test assessed that the feedback modality elicited statistically significant changes in completion time, $F(3.87) = 63.024, p < 0.001$. Post hoc analysis with a Bonferroni adjustment revealed that the reduction of time elapsed for completing the pick and place task was statistically significant for all the feedback modalities.

Outcomes of the statistical analysis performed on task completion times are in line with those discussed for the number of failures. This was an expected result considering that the number of failures is directly related to the time taken to complete the task. Anyway, especially for the H and VH cases, we observed that users spent most of the time in trying to grab the object (the number of failures is very low). This is a common bias among the cases because generally users need time to acquaint with the first-person perspective in virtual environments. As a matter of fact, if the user receives a notification from the environment when the grasp has taken place (i.e., the visual feedback), he/she is faster in grasping the object compared to the case in which the visual feedback relies only to the perspective. As in real situations, the kinesthetic feedback is meant to inform the user of being in contact with something, which can be the virtual object or the virtual fingertips themselves in the case of an ungraspable object.

5.3.3 Users' feedback

At the end of each trial of the experiment detailed in Section 5.3.2, participants were requested to fill an online questionnaire which was based on the NASA Task Load Index (NASA-TLX) [251] and extended with a question about the realism of the interaction[2]. The resulting questionnaire assesses Mental Demand (MD), Physical Demand (PD), Frustration Level (FR), and Realism (RE) on a 7-point Likert scale,

considering 1 as *"very low"* and 7 as *"very high"*. Results of the survey are reported in Tab. 5.1.

Results and discussion

Firstly, the three answers about the task load (MD, PD, FL) were analysed together. A one-way repeated measures ANOVA was conducted to determine whether there were statistically significant differences in users' feedback considering different feedback strategies. There were no outliers and the data were normally distributed, as assessed by Shapiro-Wilk test ($p > 0.05$). The assumption of sphericity was violated, as assessed by Mauchly's test of sphericity ($p < 0.001$). Therefore, a Greenhouse-Geisser correction was applied ($\epsilon = 0.661$). Different feedback strategies elicited statistically significant changes in users' rate, $F(1.98, 57.53) = 65.24, p < 0.001$, with average decreasing from N (5.1 ± 1.4) to V (3.7 ± 1.2), H (3.0 ± 0.8), and VH (2.9 ± 0.9). Post hoc analysis with a Bonferroni adjustment revealed that the users' rate decrease was statistically significant from N to all the

---

[2]The survey is available at `https://www3.diism.unisi.it/~lisini/questionnaires/NASARE.html`

	N	V	H	VH
	mean $\pm$ std	mean $\pm$ std	mean $\pm$ std	mean $\pm$ std
MD	5.1 ± 1.2	3.6 ± 1.3	3.3 ± 0.7	3.2 ± 0.7
PD	4.5 ± 0.8	3.5 ± 0.9	2.7 ± 0.6	2.5 ± 0.6
FR	5.8 ± 1.0	3.9 ± 0.9	3.0 ± 0.5	2.9 ± 0.9
Task Load	$\mathbf{5.1 \pm 1.4}$	$\mathbf{3.7 \pm 1.2}$	$\mathbf{3.0 \pm 0.8}$	$\mathbf{2.9 \pm 0.9}$
Realism	$\mathbf{3.8 \pm 1.4}$	$\mathbf{4.2 \pm 1.6}$	$\mathbf{5.1 \pm 0.8}$	$\mathbf{5.2 \pm 0.9}$

Table 5.1: Mean and standard deviation (std) for the users' opinion questionnaire.

other feedback strategies, and from V to H and VH, but not from H to VH. Results are visually reported in Fig. 5.3.(c).

Further investigation about users' opinion was carried out by analysing each answer individually.

A one-way repeated measures ANOVA was used to determine differences in the MD scores among different feedback strategies. There were no outliers and the data were normally distributed (assessed using Shapiro-Wilk test, $p > 0.05$). The assumption of sphericity was verified by Mauchly's test, $p = 0.36$. The test revealed a statistically significant differences between the four feedback conditions, $F(3, 27) = 7.8, p < 0.001$. Post hoc analysis with Bonferroni adjustments revealed a significant reduction in the perceived MD for conditions providing visual and/or haptic feedbacks (N vs V, $p = 0.002$; N vs H, $p = 0.003$; N vs VH, $p = 0.002$).

The same approach was adopted to analyse the PD dimension. Data were normally distributed (Shapiro-Wilk test, $p > 0.05$) and without outliers. The assumption of sphericity was not violated, as assessed by Mauchly's test, $p = 0.186$. The test revealed statistically significant difference between the feedback conditions, $F(3, 27) = 31.0, p < 0.001$. Post hoc analysis with Bonferroni adjustments revealed a significant PD reduction depending on whether feedback is given or not (N vs V, $p = 0.006$; N vs H, $p < 0.001$; N vs VH, $p = 0.001$). A statistically significant PD reduction was observed also between V and H, and VH (V vs H, $p = 0.019$; V vs VH, $p = 0.023$), whereas there was not significant difference in scores having V or VH.

The FR dimension was also analysed by means of a one-way repeated measures ANOVA. Data were without outliers and passed Shapiro-Wilk test ($p > 0.05$). The assumption of sphericity was not violated (Mauchly's test, $p = 0.281$). The test assessed statistically significant variation, $F(3, 27) = 31.34, p < 0.001$. Post hoc analysis with Bonferroni adjustments revealed that the FR reduction was significant only in giving feedback or not, regardless its typology (N vs V, $p = 0.004$; N vs H, $p < 0.001$; N vs VH, $p < 0.001$).

Finally, the last evaluation was made on users' feedback about the realism of the pick and place task with the four different approaches. Results are graphically reported in Fig. 5.3.(d). Data were not normally distributed, thus a Friedman test was run to determine if there were differences in the perceived realism. Users' opinions were statistically different using different feedback, $\chi^2(3) = 27.36, p < 0.001$. Post hoc analysis was performed with a Bonferroni correction. Statistically significant differences were found between N ($Median = 3.95$) and H ($Median = 5.0$), $p = 0.002$; between H and VH ($Median = 5.05$), $p = 0.001$. Additionally, the test assessed an increase of realism between V ($Median = 4.05$) and H, $p = 0.034$, and between V and VH, $p < 0.019$.

Statistical analyses on the users' feedback support our hypotheses and confirm the quantitative results obtained in the second experiment. The kinesthetic feedback increases the realism of the interaction, giving the user the perception of grasping something. Such realism is not influenced by the presence of the visual feedback, which remarks that the added value is given by the haptic feedback. Similarly, for what concerns the task load, results demonstrate that receiving a feedback when grasping an object reduces the mental demand and the frustration level, which are the lowest if haptic and visual feedback are combined. Finally, Self Contact reduces the physical demand, which is a reasonable result considering that the contact between fingers helps the user in preserving the position, thus maintaining the grasping becomes easier.

5.4 Conclusion and future work

Self Contact is a novel approach that exploits pseudo-haptic principles for recovering kinesthetic feedback in virtual reality. The benefits of this method are twofold: on the one hand Self Contact allows to provide real kinesthetic feedback without the need for haptic devices, on the other hand it promotes the development and the subsequent integration of cutaneous devices, usually less bulky and more suitable for being adopted in combination with common audio-visual displays. In addition, developing devices that leverage Self Contact to provide kinesthetic feedback paves the way for new scientific investigations, whose interest ranges from the mechanical design to the evaluation of the set of stimuli to be generated to make the interaction with virtual objects as realistic as possible. The hypotheses presented in this paper have been validated by means of a careful step-by-step procedure, which demonstrated the feasibility of the approach and the added value which comes with that. In conclusion, we believe that this work contributes to both the development of haptic technologies and the understanding of the human perception, towards an increasingly stable inclusion of the tactile layer in virtual reality applications.

50

Chapter 6

Human-Human Interaction

Handshake is a gesture used worldwide for greeting and communication purposes that is impossible in remote and forced distance contexts. In this paper, we exploited recent results in wearable haptics for designing HANS, a novel haptic system developed for reproducing a remote handshake between two users. It consists of two modules: the sensing part composed of three rings developed for recording the handshake force and the actuation part a bracelet worn on user's palm, able to apply a pressure distribution that simulates the handshake action. Once a couple of devices are worn by two users, each of them has to grasp an everyday life object simulating the force that she/he would apply to their partner's hand, the force is recorded by the sensing rings and transmitted to the partner's actuation bracelet. The paper shows HANS 's main design and integration features, and a set of preliminary evaluation tests. Users involved in the tests found the handshake perception reasonably realistic and their feedback on device usefulness, quality and ease of use was overall positive.

(a)   (b)

Figure 6.1: HANS concept. In (a), a real handshake. In (b), a remote handshake realised with HANS.

6.1 Motivation

Handshake is one of the most common human gestures, used in many social contexts, with a long history [252, 253]. Born as a way of conveying peaceful intentions, nowadays it is still the most ubiquitous greeting around the world. It is used to introduce each other and make agreements both in private and official contexts.Handshake and holding hands are social and affective interactions that are very important in our interpersonal

relationships, and were profoundly impacted by COVID-19 disruption [254, 255]. This affective communication interruption is even more impactful in critical patients, that are isolated and constrained to stay alone on a hospital bed, with no interaction with their dearest. The other critical aspect to be considered is the risk of contagion of doctors, nurses, and all the hospital operators when interacting with patients, so that any interaction and contact should be limited to the very fundamental operations [256]. Besides the physical pain due to the disease, heavy psychological and emotional pains affect both hospital patients and operators [257, 258]. At least a part of the non-physical pain can be relief if some contacts with families and friends can be restored. Some solutions for allowing patients to video-call their families, realised by means of autonomous mobile robots bringing tablets over hospital wards, have been recently proposed [259].

With this work, we want to add another perception channel to such communication, transmitting the tactile feeling of holding hands between distanced people. We propose the realization of a haptic system able to both feel and apply the tactile pressure generated when two people hold their hands. The system is designed to be flexible and light so that it can be easily worn by the user and does not limit their movements.

It is therefore a bilateral haptic system for remote transmission of a cutaneous perception on hand palm, generated when another hand is holding it. The system behaviour is twofold: on one side, it works as a sensor that measures the squeezing force that one hand applies to the other, on the other side, it can apply a pressure distribution on the hand that wears it, reproducing the contact with another hand.

6.1.1 Related works

The human-robot handshaking has been exploited in the literature from different points of view. The purpose of these researches was to provide to robots, for instance to humanoids, the capability of realizing a handshake that is perceived as human-like and can convey an affective and emotional content. A comprehensive review on the state of the art has been recently presented in [260]. In [261], experiments with humanoid robots were conducted to investigate how haptic interaction and facial expression convey emotions in a handshake interaction. In [262], Beadoin et al. proposed a haptic device for reproducing a realistic human-robot handshake. The hardware structure had an anthropomorphic structure and its elements, in particular those of the palm, were designed to replicate human hand compliance. The problem analysed by Vigni et al. in [263] was the role of feedback in handshaking behaviour: open-loop and closed-loop handshake force controllers were compared, in order to determine the importance of haptic feedback and closed-loop control in handshaking. For the experiments, a soft underactuated anthropomorphic robot hand, instrumented with pressure sensors, was used.

6.1.2 work contribution

Notwithstanding the researches briefly introduced herein presented fundamental results for understanding the handshaking task both from the physical, psychological and emotional points of view, the main limit of the aforementioned studies was that the devices that were used to perceive and realize the artificial handshakes were grounded and not
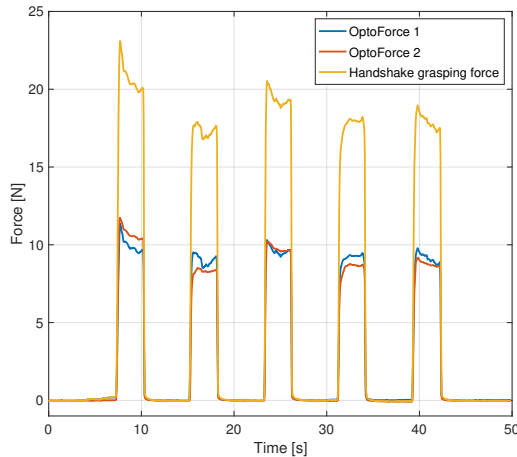
Figure 6.2: Preliminary experiment for handshake grasping force measurement: The results of a representative trial. Blue and red lines report force measurements along the z-axis of each sensor, while the total grasping force is depicted in yellow.

wearable. Such systems are complex and expensive to be provided to several users in out-of-the-lab contexts. Contextually, interesting studies and solutions are spreading in the wearable haptics field [64]. Compact and light devices have been developed not only to render forces [69] and contacts with slanted surfaces [68] to the fingertips and to the palm [264], but also to provide haptic feedback as a communicative social cue in a remote conversation [162].

In this work we propose HANS, a wearable haptic system for both perceiving and reproducing the contact between hands in a human-to-human remote handshake. The sensing part consists in a series of rings equipped with force sensors that provide an estimation of the squeezing force. The actuation part is realized by an active band that is worn on the hand palm, and it is actuated through a motorized tendon-driven mechanism that reduces the length of the band simulating the squeezing force on the palm, with a principle similar to the h-bracelet presented in [265]. The system concept is visually summarized in Fig. 6.1.

6.2   Design Requirements

Handshake is a task in which the hand at the same time perceives and applies a grasping force. Therefore, a haptic system for replicating this type of stimulus has to include both these aspects. In this study, furthermore, both these elements are designed to be rendered in devices worn by the user. Another important aspect related to the handshake is that the whole hand is involved both actively, i.e. as an actuator, and passively, i.e. as a sensing system. Designing a device that in the same place contains both these elements is technologically challenging. Moreover, to make the system as versatile as possible to a variety of use case scenarios, sensing and actuation modules are thought as two

independent devices, an actuation bracelet and a set of sensing rings, to let the user free to decide whether to wear one of them or both.

As first step towards the development of HANS, we exploited the results reported in [266] to identify the contact areas mostly involved during such gesture, that is the concave area between the thumb and the index, the lateral part close to the little finger, the hand palm and the inner part of proximal and intermediate phalanges. In particular, the fingers are the elements of the hand that are in charge of applying the handshake force with their closure, while the hand palm is mostly in charge of feeling the handshake force. On the basis of these preliminary considerations, for the sensing part of the device, a set of rings equipped with force sensors and worn on the proximal phalanges of the thumb, index and middle rings were designed and developed to measure the handshake force. The number of rings (three) was defined as a trade-off between the reliability of the measure and the system wearability, the overall complexity and the weight.

Concerning the actuation part, a bracelet was designed to apply forces on the hand palm. A preliminary literature review was performed to identify proper force values. The available data are quite heterogeneous, ranging from a maximum value of 6N in [267], to a maximum of 40N in [262], to a mean value of 67N in [266]. Besides, handshake force is the result of a complex non-homogeneous pressure distribution and its quantification clearly depends on the measuring setup. For this reason, to quantify the force exerted during the interaction, we realized an *ad hoc* measuring setup consisting in a dummy hand, 3D-printed in Acrylonitrile Butadiene Styrene (ABS), covered with a glove, and sensorized with two OptoForce 3D force sensors OMD-20-SE-40N (OptoForce Ltd., Budapest). These sensors are able to measure a three dimensional force with a maximum value of 40N along the principal axis (indicated with z) with a resolution of 2.5mmN, and 20N in the secondary directions (indicated with x and y) with 2mmN of resolution. Since we were interested in measuring the force normal to the contact point, sensors were mounted with the z-axis orthogonal to the surface, and only data along this axis were acquired.

Twelve subjects (8 males and 4 females, aged 27-54, all right-handed) were involved in a preliminary experiment. Each session consisted of three trials, each of which included five squeezes at five seconds time intervals. Subjects were asked to shake the dummy hand as naturally as possible for 3 seconds. During the trial, a beep signal was used to inform the user when to squeeze and release the handshake. Each grasping force was computed as the sum of the forces applied on each sensor, and the mean grasping force among subjects (calculated as the mean grasping force of fifteen squeezes for twelve subjects) resulted to be 17.37 ± 5.08 N. A representative trial is reported in Fig. 6.2.

6.3 The haptic system

HANS is composed of two independent modules: *i)* the sensing rings, which acquire the contact forces to be transmitted during the remote handshake, and *ii)* the actuation bracelet, which applies the handshake force to the user. In the following, more details on the sensing rings (Sec. 6.3.1), on the actuation bracelet (Sec. 6.3.2), on the communication protocol (Sec. 6.3.3), and on the system calibration and validation (Sec. 6.3.4) are
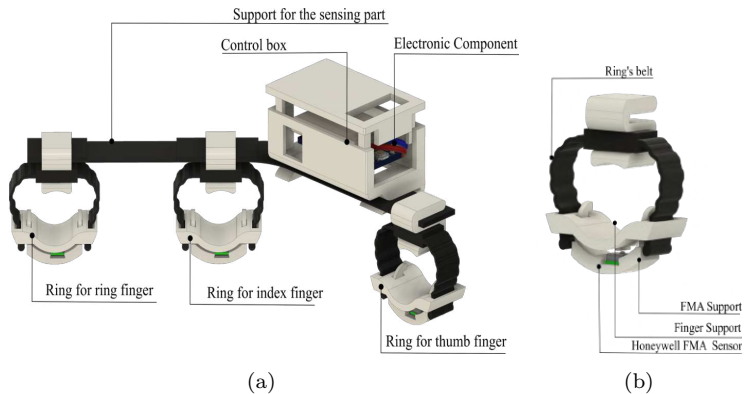
Figure 6.3: HANS sensing rings. In a), the complete CAD model of the sensing device is reported. It consists of three rings, a flexible support connecting them, and a control box containing electronic circuitry and battery. In b), the CAD model of a single sensing ring is detailed.
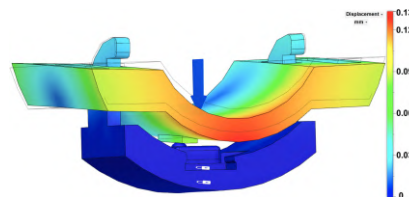
Figure 6.4: The results of the FEM structural analysis performed on a single ring simulating the force applied by the finger during the handshake. The padlocks indicate the parts of the model in which constraints are set in the simulation, while the blue arrow indicates the force applied with a magnitude of 10N. The transparent wireframe CAD model is the reference model, while the coloured surface corresponds to a 1X deformation.

reported.

6.3.1   Feeling the handshake: the sensing rings

The device in charge of measuring the handshake force consists of three rings, a flexible support connecting them, and a control box, as depicted in Fig. 6.3.

The three rings are designed to be worn on ring finger, index finger, and thumb. They share the same design, whose CAD model is shown in Fig. 6.3. In particular, each ring consists of four parts: a support holding the force sensor, a support for the finger, a flexible belt, and a support for attaching the ring to the sensing device. Force sensor support, finger support and attaching support were realized in ABS using Fused Deposition Modeling technique. To better adapt the device to the user's specific anthropometric characteristics and to improve user's comfort, the flexible belt was realised using NinjaFlex Material, a flexible thermoplastic polyurethane. This flexible material enables the user to wear the ring easily and provides a stable grip on the proximal phalanx.

Each ring includes an FMA MicroForce Sensor FMAMSDXX025WCSC3 (Honeywell, North Carolina), a piezoresistive based force sensor providing a digital output proportional to the force applied on it. This type of sensor is well known for its small size and high accuracy. On the basis of the results obtained with the handshake force measurement introduced in Sec. 8.2, the FMA version having a force range of 25N and an accuracy of 0.5N was chosen. Sensors are interfaced using SPI protocol with a maximum digital clock frequency of 800kHz, and are powered with an operating voltage of 3.3V.

The finger support was designed with the specific aim of enabling the user to press effectively on top of the force sensor. Static structural mechanics FEM (Finite Element Method) analyses were performed in the design phase to verify that, during finger closure in a grasping task, the sensor is properly pressed (see Fig. 6.4). The control box holds all the electronics circuitry and the battery for standalone operation. An Arduino Pro Mini (5V,16MHz version) is used as main control unit for receiving the force measures from the three rings, processing them and sending the corresponding handshake force value to the actuation bracelet. A Bluetooth RN42-i/rm module is embedded in the control box for communication purposes, and the complete sensing device is powered up using a single cell 3.7V Li-Ion battery.

When the sensing device is worn and turned on, the user is asked to keep the hand open and the three rings acquire force samples at a frequency of 1kHz for 5 seconds. This procedure is needed for calibration purposes. Indeed, the average value of these samples is used to compute the digital value corresponding to zero force applied, i.e. to remove a possible force bias δ due to the ring positioning on the finger. After calibration, each force value is computed as:

$$FMA_i = \beta_i \left(\frac{1}{20} \sum_j^{20} \gamma_{j,i} - \delta_i \right) \ \forall i \in \{1, 2, 3\}, \forall j \in [1, 20]$$

where δ_i is the offset of the *i-th* FMA force sensor, $\gamma_{j,i}$ is the *j-th* sample acquired by the *i-th* force sensor, and β_i is the gain associated to the *i-th* FMA force sensor, calculated as reported in Sec. 6.3.4. The force value is averaged each 20 samples to remove possible unwanted noise. As soon as a new force value is available for all the three sensors, data are packed and sent to the actuation bracelet.

6.3.2   Applying the handshake: the actuation bracelet

The proposed actuation bracelet consists of a flexible structure designed to wrap the palm of the hand, and a box containing the electronics and the motors, placed on the back of the hand (see Fig. 6.5). The hand band is composed of two parts, i.e. one reproducing four fingers close together, and one simulating the thumb.

The external layer of the hand band is made with flexible material, namely the Flex-45 thermoplastic co-polyurethane,

while the internal layer is a combination of silicone rubbers. To reproduce on the user's hand the handshake contact area reported in [266], we increased the stiffness of specific hand band parts realizing thicker finger pads.
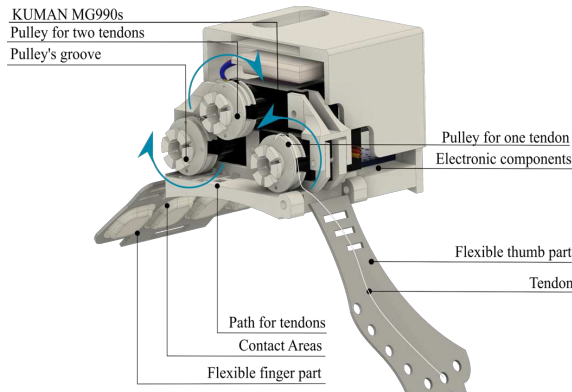
Figure 6.5: CAD model of HANS actuation bracelet. It consists of a flexible structure designed to wrap the palm of the hand, and a box placed on the hand back containing the electronics and the motors. The hand band is composed of two parts, i.e. one reproducing four fingers close together, and one simulating the thumb.

Then, to let the contact realized by the device be more human-like, the finger pads were covered with silicone rubber and ethylene-vinyl acetate foam. A velcro band between the two parts is used to fix the actuation bracelet to the user's hand. The box on the back of the hand was made in ABS material, and contains the hardware components of the actuation bracelet: an Arduino Pro Mini (5V, 16MHz version), a Bluetooth RN42-i/rm module, and three Kuman MG90S servo motors (Kuman Trade Shenzhen Co., Ltd., US). Each servo motor has a stall torque of 25Ncm at 6V, which is sufficient for reproducing the forces involved in a real handshake according to our initial requirements.

Furthermore, in order to transform the torque of the motor into force applied on the hand palm, a tendon-actuated system was realized.

A tendon was connected to each contact area of the palm: the four finger pads on one side and the flexible thumb on the opposite side. The fingers tendons were arranged in two couples, that is index/middle and ring/little, and each couple was then connected to one motor. The thumb tendon was directly connected to the corresponding motor.

Internal paths were designed inside the support in order to route the tendons from the motors to the contact areas. Each motor was equipped with a pulley with radius $r = 5mm$ to transform the rotation θ of the motor in displacement d of the tendon, following the relation $d = r\theta$.

Two types of pulleys were realized, one with a single groove to pull the tendon connected to the thumb, and two pulleys with double grooves to pull simultaneously each couple of tendons connected to the fingerpads.

The actuation bracelet is powered using a single cell 3.7V Li-Ion battery, and a step up booster is used to provide 6V to the servo motors.

Both the tightening velcro band and the length of the tendons are adjustable to let the actuation bracelet adapts to the specific anthropometric characteristics of the user. In particular, once the device is worn and turned on, the three motors return to their rest position, and the length of the traction tendons can be adjusted using the additional

grooves in the pulleys.

Each motor is in charge of applying the force measured by the associated sensing ring, that is thumb motor with thumb ring, index/middle motor with index finger ring, and finally ring/little motor with the remaining ring. To map the force measurements received by the sensing rings in a coherent squeezing force, we exploited the values of human hand stiffness reported in [268]. In particular, we extrapolate from the latter work the results regarding the hand's regions involved in the handshake, that is *'medial and proximal palm'*, and *'rest of distal palm'*, respectively. Considering that hand stiffness varies at different force intervals, hand stiffness and applied force values were interpolated to find the set of parameters that would best approximate the elastic response of the human hand under squeezing force. Data were fitted to a power law distribution with an adjusted R-square of 0.79, and the displacement d of the tendon was computed as $d = \frac{F}{k(F)}$, where $k(F) = aF^b$ is the stiffness of the hand at a given force F, and $a = 0.76$ and $b = 0.43$ are the parameters resulting from the interpolation. Taking into account that the FMA force sensors full-scale output is 25N, the maximum tendon displacement that can be required following the aforementioned law is $d_{max} = 8.2mm$, which in turn corresponds to $\theta_{max} = \frac{d_{max}}{r} \approx 100deg$, i.e. a value inside the range of the servo motors.

6.3.3 Communication protocol

Data transmission system of HANS is based on Bluetooth communication for a dual purpose. On one side, the latter represents a fair compromise between accelerating system prototyping and developing wireless devices. Indeed, once the system functioning is assessed, having a Bluetooth interface already embedded in the devices allows for a further easy integration with widespread technologies (e.g., smartphones, computers) that can enable long distance connection by means of web-based applications. On the other side, the aim of our system is not only to transmit the handshake between people who are in different places, but also between people who are physically close but cannot touch each other (for instance because of hygiene rules, social distance, physical impairments). The sensing and actuation modules communicate with each other through two Bluetooth RN42-i/rm modules, which are suitable for sending and receiving information at a frequency of 50Hz. Once the two devices are powered, the initialization phase is performed (i.e., calibration of sensing rings, and setting the motors of the actuation bracelet in the rest position). Then, the two Bluetooth modules pair and begin to exchange information. During the handshake, the sensing device processes the information collected from the three sensing rings and transmits it to the actuation bracelet. These data are used by the actuation bracelet to control the handshake force. In particular, the communication protocol provides that the actuation device constantly requests information from the sensing device. The latter processes data coming from the three FMA force sensors and creates the data packet adding to the measurement a start and an end marker. The actuation bracelet receives the data and maps them in digital values to drive the three servo motors in such a way to apply the force read by the sensors, as described in Sec. 6.3.2.

Fig. 6.6 shows the communication scheme of the wearable haptic system for remote handshake.
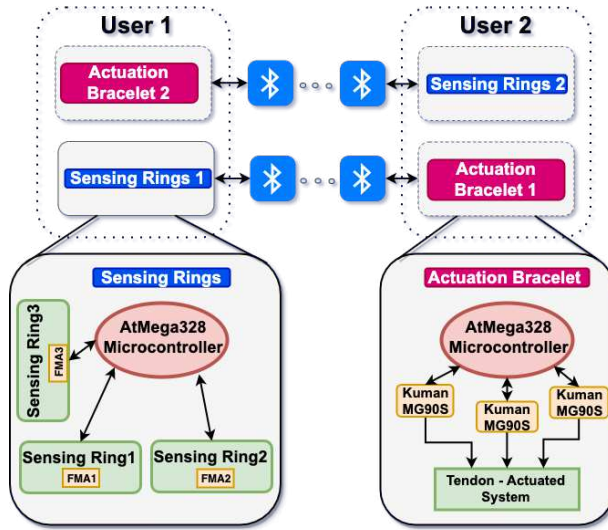
Figure 6.6: Block diagram representing HANS 's functioning.

6.3.4   System calibration and validation

A preliminary stationary structural FEM analysis on the CAD model of one of the rings
was used to verify the overall stress/deformation distribution when the force is applied by
the finger proximal phalanx during the handshake. In Fig. 6.4, the results obtained with
an applied force of 10N are reported. The analyses highlighted how the force is transmitted
through the two different elements of the ring, i.e. the finger support and the sensor
support. More in details, results show how the force is concentrated on the sensor thanks
to the designed finger support. We exploited this result to calibrate the sensing device
after the fabrication of each ring. In particular, each ring underwent three repetitions of a
calibration procedure that consisted in the application of an orthogonal decreasing force in
a range from 20N to 0N. The applied and measured forces were sampled simultaneously
at 400Hz by a dual-range Vernier dynamometer (Vernier Software & Technology, US)
with accuracy of 0.05N, and by the sensor, respectively. The dynamometer was routed
normally to the sensor through a specially designed 3D-printed guide. A systematic
error between force exerted and force measured was detected for each ring. Therefore,
the calibration consisted in the evaluation and subsequent application of a multiplicative
gain β computed as the mean of the ratio between force applied and measured value, with
the aim to minimize the measurement error for each sensor. After calibration, the root
mean squared error between the two force profiles was 0.54N, 0.75N, and 0.45N for the
three rings, respectively. These values were found to be in line with the sensors' accuracy.
A representative trial of the calibration procedure is shown in Fig. **??**.

As regards the actuation bracelet, both for safety reasons and for device force ana-
lysis, the device was placed on the sensorized dummy hand exploited in the preliminary
experiments (see Sec. 8.2) to measure the maximum force that can be actually exerted
by the motors. In fact, despite the maximum torque applicable by each motor is 25Ncm,
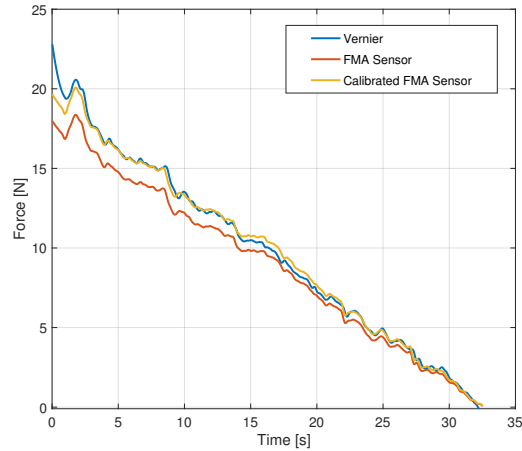
Figure 6.7: A representative trial of the sensing ring calibration. In blue, the force acquired by the Vernier dynamometer, in red the force values read by the FMA force sensor, while in yellow the FMA force sensor measurement corrected with the gain factor.
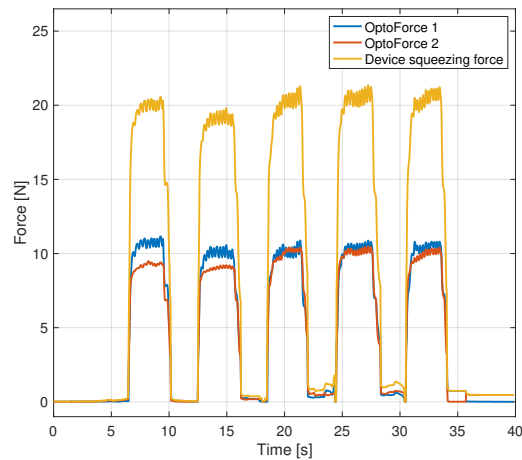
Figure 6.8: HANS actuation bracelet validation: the grasping force acquired in a representative trial. Blue and red lines report force measurements along the z-axis of each dummy hand's sensor, while the total grasping force is depicted in yellow. Each motor is driven until the stall is reached, as it can be seen looking at the distinctive noisy profile presented by the sensors measurements at10N.

a non-ideal mechanical coupling and the presence of friction between device components can lead to an ineffective force application. A profile covering the range of motion of the servo motors was simulated with Matlab and sent to the actuation bracelet via Bluetooth communication, with a sample rate of 50Hz. The device was temporarily programmed to drive the motors to rotate as required by the simulated profile, with the aim of reaching

the motors stall. The experiment consisted of a total of fifteen squeezes held for three seconds at 5 seconds time intervals. The mean force among the squeezes was 20.11N with a standard deviation of 0.57N, i.e. a reasonable value considering the average grasping squeeze computed in Sec. 8.2. The grasping force acquired in a representative trial is reported in Fig. 6.7.

6.4   User studies

In this section, an investigation about users' opinion of the wearable haptic system for remote handshake is presented.

Twelve participants (6 males and 6 females, aged 24-59, all right-handed) took part in the experimental campaign. Each subject gave her/his written informed consent to participate and was able to discontinue participation at any time during experiments. The experimental evaluation protocol followed the declaration of Helsinki, and there was no risk of harmful effects on subjects' health.

Each participant was asked to shake hands with one of the two investigators of their choice. The designated investigator showed the participant how to wear the actuation bracelet and the sensing rings by wearing them himself, and then asked the participant to do the same. The participant, then, wore the complete haptic system for remote hand-shaking. Each user performed three remote handshakes with the experimenter exploiting the wearable haptic system, with a rest period of 2 minutes in between. For each of the three handshakes, the experimenter grabbed a different object randomly chosen between the 3D-printed model of the human hand exploited for the preliminary experiments (see Sec. 8.2), a tennis ball, and a bottle. These three objects were chosen because of their increasing level of abstraction from the human hand and their diffusion in domestic and office environments, to verify the feasibility of transmitting an handshake by grabbing common and different objects. Therefore,each participant was asked whether he/she perceived differences between the three handshakes, and then was asked to complete a survey. The evaluation questionnaire developed to collect users' opinions and feedback was defined by elaborating the Technology Assessment Model [269, 270]. In particular, the survey was divided into three topics: *i)* perceived usefulness (Us), *ii)* characteristics of the equipment (Eq), and *iii)* perceived ease of use (Ea). Each topic consisted of four to six sentences for a total of 15 statements, reported in Tab. 6.1. The judgements were expressed in the form of a Mean Opinion Score (MOS), a standardize policy to evaluate the Quality of Experience according to [271]. The user opinion scale ranged from 0 to 5, where 0 indicates *"Strongly Disagree"*, and 5 means *"Strongly Agree"*. We denote with $s_{i.j|k}$ the score assigned to the *j-th* sentence of the *i-th* topic ($i \in \{Us, Eq, Ea\}$) by the *k-th* participant.

6.4.1   Results

The first result obtained is that no user found differences between the handshakes performed by the experimenter grabbing the three different objects. All the handshakes were perceived similar to the previous and/or to the subsequent ones.

Table 6.1: Survey statements arranged by topic of investigation.

	Perceived usefulness
Us.1	*I think using the device is an effective way to feel the handshake with a distant friend/relative.*
Us.2	*I would feel embarrassed to wear the device in my everyday life.*
Us.3	*I find that the tactile information provided by the handshake device are insightful.*
Us.4	*I find human-like the handshake perception.*
Us.5	*I find pleasant the handshake perception provided by the device.*
Us.6	*I found that the device is useful.*
	Quality of equipment
Eq.1	*I feel safe while wearing the device.*
Eq.2	*I was concerned that the device is not securely attached to me.*
Eq.3	*I would be able to perform my daily tasks as usual while wearing the device.*
Eq.4	*I find the device comfortable.*
	Ease of use
Ea.1	*I find the device easy to use.*
Ea.2	*I was able to wear the device easily without help from another person.*
Ea.3	*I was able to remove the device easily without help from another person.*
Ea.4	*I was able to put the device on in a reasonable amount of time.*
Ea.5	*I have the knowledge necessary to use the device.*

The results collected by means of the survey qualitatively demonstrated a widespread favourable opinion in every field of investigation. For the purposes of quantification and mathematical analysis of the results, the complement to 5-value of the score assigned by each participant to the declarations Us.2 and Eq.2 was executed, i.e. $s_{Us.2|k} = 5 - s_{Us.2|k}$ and $s_{Eq.2|k} = 5 - s_{Eq.2|k} \ \forall k \in [1, 12]$. The reason is that Us.2 and Eq.2 are the only ones among all sentences with a negative meaning.

The scores assigned by each user to each sentence are graphically shown in Fig. 6.8 for each survey section, while the histograms of the scores assigned for each question and grouped by topic have been reported in Fig. 6.9 for the sake of clarity and completeness. The average user's opinion per topic of investigation was defined as the average of the
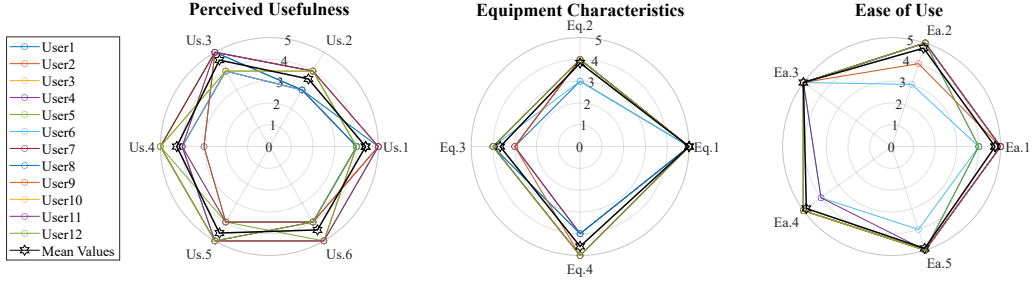
Figure 6.9: The scores equivalent to the users' opinions about each sentence are reported from right to left for perceived usefulness, equipment characteristics, and ease of use, respectively. The user opinion scale ranges from 0 to 5, where 0 indicates *"Strongly Disagree"*, and 5 means *"Strongly Agree"*. The users' average score is depicted in black for each topic.

scores assigned to each statement of the same topic, that is

$$\overline{s}_{j|k} = \frac{1}{N_j} \sum_{i}^{N_j} s_{i.j|k} \ \forall j \in \{Us, Eq, Ea\} \text{ and } \forall k \in [1, 12]$$

where N_j is the number of sentences used to investigate the topic j. Accordingly, we defined a general opinion score (GOS) $\overline{\overline{s}}_j$ for the *i-th* topic as the average on the users of the $\overline{s}_{j|k}$ values, i.e.

$$\overline{\overline{s}}_j = \frac{1}{12} \sum_{k}^{12} \overline{s}_{j|k} \ \forall j \in \{Us, Eq, Ea\}$$

The general opinion score regarding the perceived utility was $\overline{\overline{s}}_{Us} = 4.31 \pm 0.31$, while the characteristics of equipments have achieved a GOS equal to $\overline{\overline{s}}_{Eq} = 4.27 \pm 0.22$. Finally, the results of the survey have reported that users were extremely satisfied about the ease of use, with a value of GOS equal to $\overline{\overline{s}}_{Ea} = 4.87 \pm 0.29$.

A further investigation into the symmetry of the distribution of the scores assigned to the statements showed that average $\overline{s}_{Eq|k}$ and $\overline{s}_{Ea|k}$ were usually less than their median and mode. The skewness values μ_i were equal to $\mu_{Eq} = -0.55$, and $\mu_{Ea} = -2.39$ for equipment characteristics and ease of use, respectively. For the sake of completeness, we report also the skewness value of perceived usefulness equal to $\mu_{Us} = 0.006 (\approx 0)$. In other words, it is possible to assert that a sample of the population considered system usefulness, equipment characteristics and simplicity of the device in a range between "Good" and "Excellent", with a slight tendency towards a more positive opinion.

6.5   Conclusion and future work

This work presented HANS, a novel wearable haptic system for exchanging remote human-to-human handshakes. Despite handshakes are commonly recognized as an important social behaviour between two people [272], to date there are still no wearable devices
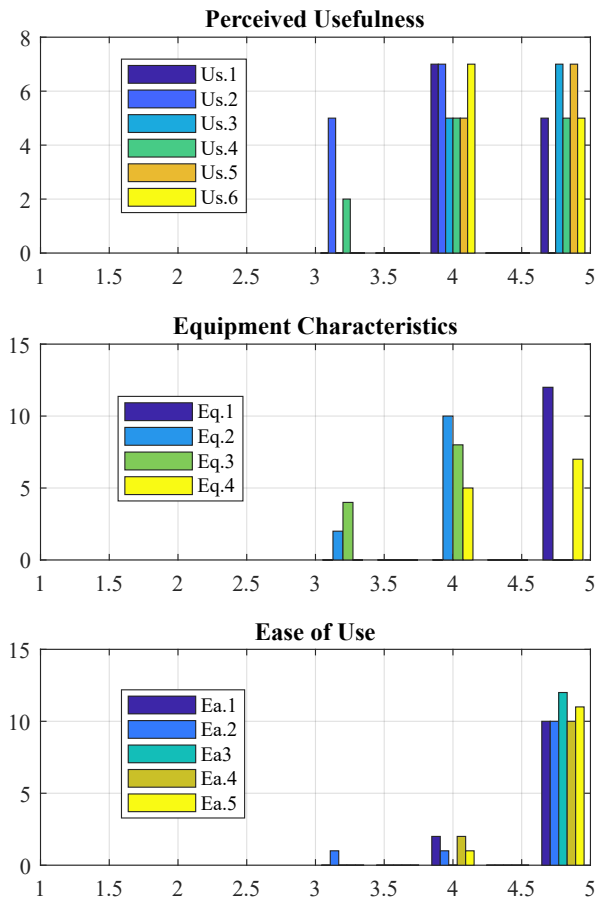
Figure 6.10: The occurrence of the same opinions expressed as a numerical score are reported from top to bottom in the form of histograms for each sentence for the three survey topics.

able to measure and convey this body language at a distance. Here we introduced a pair of wearable devices, namely the sensing and actuation part of HANS, whose design was defined following requirements based on specific handshake properties, such as contact area and contact force. We described the system mechanical structure, the system functioning, and the overall validation process. An experimental campaign was conducted to assess users' opinions about the system. Results show that HANS allows to perceive and transmit a human-like handshake using common daily-life objects. All users asserted that the device is easy to use and to wear. Furthermore, a user with reduced mobility of the upper limbs was invited to try HANS after the experimental campaign. He was enthusiastic about the device, since HANS allowed him to perform the social protocol of the handshake without experiencing strain and feeling uncomfortable.

To conclude, this work represents the first attempt to introduce in people's life a

wearable device for exchanging handshakes at a distance. In future work, we plan to extend the usage of our system by integrating HANS with common social platforms for combining tactile interaction with visual and auditory cues. In addition, we will investigate about psychological and emotive impact of HANS on life of people with arm diseases.

Chapter 7

Open Hand Interaction

(a)   (b)

Figure 7.1: HapticPalm prototype worn by a user. (a) Lateral view showing the end effector. (b) Top view showing the actuators and electronic components on the hand back.

This Chapter describes the design, prototyping steps, and validation of a novel haptic device for cutaneous stimulus of hand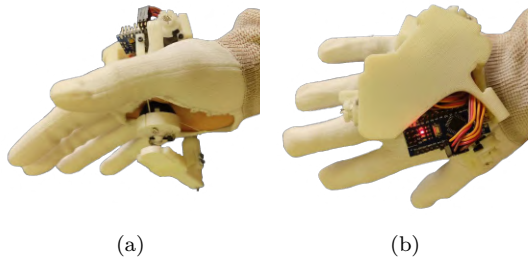 palm. This part of the hand is fundamental in several grasping and manipulation tasks, but is still less exploited in haptics applications than other parts of the hand, as for instance the fingertips. The proposed device has a parallel tendon-based mechanical structure and is actuated by three motors positioned on the hand back. The device is able to apply both normal and tangential forces and to render the contact with surfaces with different slopes. The end-effector can be easily changed to simulate the contact with different surface curvatures. The design is inspired by a smaller device previously developed for the fingertips, however, in the device presented in this paper, there are significant differences due to the wider size, the different form-factor and structure of hand palm. The hand palm represents the support for the fingers and is connected to the arm through the wrist. The device has to be developed taking into account fingers' and wrist's motions, and this requirement constrains the number of actuators and the features of the transmission system. The larger size of the palm and the higher forces challenge the device from the structural point of view. Since tendons can apply only tensile forces, a spring-based support has been developed to keep the end-effector separated from the palm when the device is not actuated or when the force to be rendered is null. The work presents the main design guidelines and the main features of the proposed device. A prototype has been realized for the preliminary tests and an application scenario with a VR environment is introduced.

7.1 Motivations

Nowadays technology is increasingly present in our everyday lives, and among the emerging technologies those oriented to the reproduction of tactile, kinesthetic and skin sensations are getting interest in several application fields. These technologies allow enriching

the sensory experience of humans, for instance in virtual environments, in augmented or mixed-reality applications and/or during teleoperation tasks. Recent studies available in literature confirm that the use of tactile technologies not only increases the involvement of users in teleoperation tasks but also increases their accuracy and performance, [273, 274]. Interesting applications of haptic technologies are also present in telemedicine and in tele-rehabilitation, these applications have become particularly significant in since the beginning of the past year, when the pandemic situation required solutions for guaranteeing social distance and human/human physical contacts.

The hand is one of the primary interfaces connecting humans and the surrounding environment, and it is also one of the main targets of haptics technology development. Most of the haptic devices for tactile stimuli are located on the fingers or on the wrist, while fewer are developed specifically for the palm [64], although Klatzky and Lederman's studies demonstrated that the hand-closing task depends on haptic information in the palm [275]. Haptic devices developed for the hand palm can be broadly divided in two types: the grounded ones, having a base external to the user's body and connected to a fixed base and the wearable ones. Concerning grounded devices, for instance, in [276] the authors presented a device that can change the shape of the surface in contact with the hand using vertical motions of some pistons, while in [277] an array of actuators returns vibrotactile stimuli on users' palm. In [278] a grounded planar device returns haptic stimuli and several sensations on users' palms, the ultrasound technology allows to provide stimuli on hand that is detached from the surface of the device, so that the hand is free to move in a wider workspace.

The research in this topic is increasingly oriented towards wearable devices to free completely the users and their workspace. To date, wearability is a fundamental requirement for haptic devices, and in this context the trade-off between the extension of the area of the palm that can be stimulated, and the number of actuators used is almost inevitable [279].

In this work we present a haptic wearable device for rendering forces in the palm that attempt to find a trade-off between the aforementioned requirements. The state-of-the-art devices are mostly based on localized and fixed contact points on the palm. Among these, there are two main typologies of devices: devices based on vibrotactile actuations, and devices using mechanical actuation. The last ones usually employ tightening bands reproducing only a normal pressure on the palm, as presented in [280]. However, this kind of technology allows the user to feel a limited and predetermined type of sensations.

Similarly in [281] Minamizawa et al. present a band with mobile contact surface on the palm, while Achibet et al. in [282] show a passive device composed by an elastic band to return distance hand/body by haptic feedback.

In [283] and in [284] two haptics gloves with several mechanical active points are designed and developed: the first uses small rigid links, while the second is tendon actuated. The limit of these devices is the high number of actuators needed to reproduce haptic stimuli in an extended area as the human palm, for this reason the authors of [171, 285, 286] choose vibrotactile matrices in contact with the palm to reduce the cluttered of mechanical actuators, reducing, however, the similarity between the desired stimulus and the transmitted one. A combination of mechanical stimuli and vibrotactile stimuli is shown

Name	Type of actuation	Contact area	Electronics
Ghostglove [280, 281]	sqeezing band	fixed and extended	on board
Achibet et al [282]	passive elastic band	fixed and pont-like	–
Son et al. [283]	4 pressure points	fixed and point-like	on arm
Son et al. [284]	10 pressure points tendon drive	fixed and point-like	delocalized
Gollner et al. [171]	35 vibrating motors	fixed and point-like	on arm
Martınez et al. [285]	6 vibrating motors	fixed and point-like	delocalized
Borja et al. [286]	5 vibrating motors	fixed and point-like	on arm
Haptic pivot [287]	mobile vibrating mass	fixed and extended	on arm
Zubrycki et al. [289]	10 pneumatic pad	fixed and extended	delocalized
Weatavix [290]	mobile mass	fixed and extended	on arm
Deltatouch [291, 292]	3D Mobile platform	mobile and point-like	delocalized
HapticPalm –	**3D Mobile platform tendon drive**	**mobile** and interchangable	**on board**

Table 7.1: Comparison between the proposed haptic device (indicated as HaptiPalm, last row) and other solutions available in the literature.

by Kovacs et al. in [287] where a mobile mass comes in touch with palm in case of collision between a hand avatar and the surrounding environment in virtual reality, while pneumatic solutions are presented by Kajimoto et al. in [288] and by Zubrycki and by Grzegorz in [289].

The authors in [290] present a wearable haptic interface for natural manipulation of tangible objects in Virtual Reality that render contact force using a sensorized mobile mass grounded on wrist. Haptic devices with mobile and orientable contact area such as those presented by Trinitatova et al. in [291] and in [292] are closer to what we propose in this work for what concerns the design, however in this work we want to investigate the possibility of reducing the footprint in the palm and the overall mechanical load on the hand through the use of cables for the transmission of forces.

In order to summarize and clarify the solutions available in the literature, Table 7.1 shows the details of the implementation and electronics of the devices mentioned above and of the device presented in this work.

The device presented in this work is able to stimulate a large area of the palm with a limited number of actuators (three), therefore assuring a good wearability. In order to achieve these objectives a parallel mechanism has been designed in which the mobile platform (end-effector) has interchangeable contact interfaces. The various contact interfaces, having different shapes, can be easily connected and disconnected to/from the device to reproduce a tactile sensation more similar to the desired stimulus in different tasks. Inspired from a family of wearable devices that we developed for fingertip stimulation [293, 68], the mobile platform has a "Y" shape and it is actuated by three servomotors positioned on the back of the hand by means of tendons, allowing the transmission motion. Notwithstanding the kinematic structure of the device presents some similarities with the
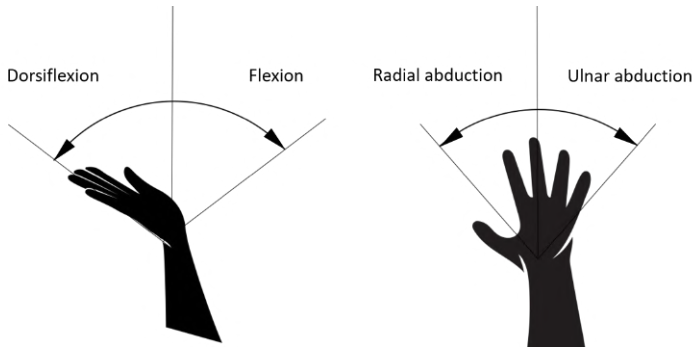
Figure 7.2: Primary hand movements due to the biomechanical structure of the carpus: palmarflexion/dorsiflexion (left) and radial abduction/ulnar adduction (right).

devices previously presented for the fingertips, the solicitation of hand palm presents several different challenges, due to the different size, kinematic structure, form factor, force level. In order to provide to the user the possibility to easily wear the device and avoid the continuous contact with the palm, we added an elastic element at the base of the platform. The tendons and the springs allow us to reproduce the cutaneous stimulus both in static and dynamic conditions. The use of three actuators furthermore allows reproducing both normal and tangential components of the contact force (necessary for simulating shear forces), and the contact with virtual/remote surfaces with different orientations (that can be used for instance for reproducing the contact with variable curvature surfaces).

The wearable haptic device for hand palm stimulation is shown in Figure 7.1. In particular in this work we will: *i*) describe the haptic device for hand palm stimulation based on tendons, designed taking into account the physical/anatomical features of the palm; *ii*) present the design of interchangeable modules for simulations of different types of contact; *iii*) detail the mechanical, mechatronics and manufacturing aspects of the device, including finite element method (FEM) analysis, hardware and control description; *iv*) present a working prototype of the device with some preliminary applications.

7.2   Biomechanics and perceptive receptor of palm

The design of the wearable haptic device started from the analysis of the hand palm: its biomechanical structure and the features of the stimuli to be rendered define the requirements and the constraints. From an anatomical point of view, the palm of the hand is the ventral (or anterior) region of the hand, the one to which the fingers converge when punching. The back of the hand, on the other side, is the posterior region of the hand, located from the opposite side of the palm. The bones of the palm can be divided into carp bones and metacarpal bones. The metacarpus is the set of five long bones that connect the carpus to the phalanges, they are numbered from 1 to 5 starting from the thumb to the little finger. The carpus consists of eight short bones spread over two rows, the proximal and the distal row, and connects the radio with the metacarpus.

The proximal row is composed by scaphoid, lunate, triquetrum and pisiform bones,

while the distal row is defined by trapezium, trapezoid capitate and hamate bones. The biomechanical structure of palm bones, muscles and ligaments allows the radial abduction, the ulnar adduction, the palmar flexion/dorsiflexion and combined movement, all depicted in Figure 7.2. According to [294] the *palmar flexion* is the flexion of the wrist towards the palm and ventral side of forearm, while the *dorsiflexion* is the hyperextension of the wrist joint, towards the dorsal side of forearm, radial abduction is a motion that pulls a structure or part away from the midline of wrist and ulnar adduction is a motion that pulls the hand structure toward the midline of wrist. Other two principal motions are provided by the biomechanical structure of palm: the opposition and apposition of thumb. In apposition the side part of thumb is in touch with other fingers, while the pulp side of thumb distal is in contact with fingertips of other digits during opposition [295]. The contact surface of the developed haptic device has been dimensioned and placed according with biomechanics of palm, avoiding cluttering of palm and the reduction of carpus mobility. The mobile platform should not constrain and limit any motion described above, it should be placed under metacarpal bone situ and extended from upper bound of first row of carpal bone to transverse metacarpal ligament. The articulation of the bones of the carpus constitutes on the handheld side a cavity called the carpal tunnel. The carpal tunnel develops flywheel on the wrist and is crossed by the superficial and deep flexor muscles of the fingers and the long flexor of the thumb. The median nerve also runs through the carpal tunnel, its palmar branches, called digital cutaneous branches or cutaneous digital nerves, are distributed to the palmar skin up to the first three fingers (thumb, index finger and middle). The palm, like the fingertips, is one of the densest regions of the human body of mechanoreceptors. Then channel of haptic stimulus transmission is the same for fingertips and palm. However biomechanics of palm is more complex than finger one, the geometry, anatomic constrains and mechanical compliance [296] are different, the increased extension of the device is the cause of greater structural fragility, while the forces to render on palm are higher and, consequently, the structural stress on device is greater, too.

7.3 Haptic stimulus of hand palm: design principles and modeling

The proposed device is able to both push the end-effector towards the palm and to differentiate applied force direction and contact location and orientation, ensuring robustness, ergonomics and low weight. To achieve these requirements, the end-effector is passively supported by a spring connected to a C-shape structure fixed on one side on hand back. The end-effector is then moved by three tendons actuated by three motors positioned on hand back.

Both the part fixed on hand back and the active end-effector have a Y-shape, whose vertices are connected by three tendons actuated by three motors. This structure allows to apply a wide set of movements to the end-effector and to interact with most of the palm surface.

In the following we will introduce a simplified mathematical model that relates the force applied to hand palm to the forces applied by the motors to the tendons.
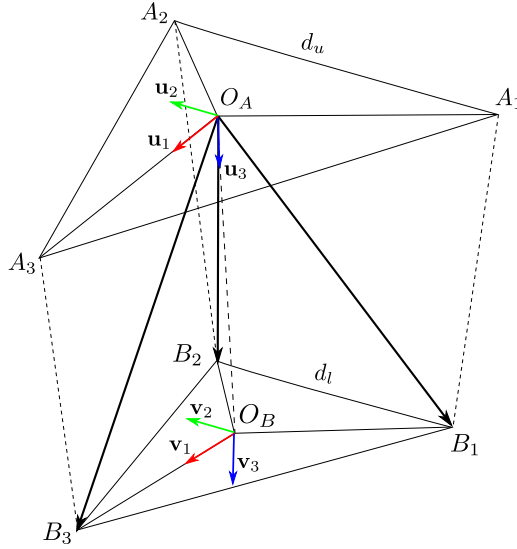
Figure 7.3: Main points and coordinate frames for the analysis of the wearable haptic device.

The problem of cable driven parallel mechanisms is an interesting topic studied by several researchers in robotics context. Using cables and tendons to transmit movements allows designers and engineers to obtain compact and small-size devices, reducing the weight and inertial effects of mechanical components.

The solution of the direct geometric-static problem of three cable-driven parallel robots by interval analysis is presented in [297], while the case of direct geometric-static analysis of an underconstrained 4-cables parallel robot is presented in [298]. In [299] the differential kinematics is studied for calibration, system investigation, and force based forward kinematics. Moreover, the dynamic modeling of cable driven parallel robots for a fully-constrained planner case is investigated in [300] and for an underconstrained spatial case is presented in [301].

Solving the forward kinematics problem means finding the relationship between lengths of the cables and posture of the moving platform, this information is important for the device control, but it is not easy to be solved in parallel mechanisms. On the other hand, the inverse kinematics problem evaluates the lengths of the cables corresponding to a given platform posture.

Static analysis defines the relationship between cable tensions and wrench exchanged with the palm.

To describe the device as a cable driven parallel robot, two coordinate frames are defined. The first one $A = \{O_A, \mathbf{u}_1, \mathbf{u}_2, \mathbf{u}_3\}$ is fixed on the device body on the hand back, while the second one $B = \{O_B, \mathbf{v}_1, \mathbf{v}_2, \mathbf{v}_3\}$ is fixed on the mobile platform in contact with hand palm, as shown in Fig. 7.3.

In the following, to simplify the notation, if quantities are expressed in A frame, superscript A is omitted.

On the device body we define three connection points A_1, A_2, A_3, representing the points where the tendons pass through in the device fixed part; assuming they define an equilateral triangle, their coordinates are:

$$\mathbf{a}_1 = \left[\frac{\sqrt{3}d_u}{-6}, \frac{d_u}{-2}, 0\right]^{\mathrm{T}} \mathbf{a}_2 = \left[\frac{\sqrt{3}d_u}{-6}, \frac{d_u}{2}, 0\right]^{\mathrm{T}} \mathbf{a}_3 = \left[\frac{\sqrt{3}d_u}{3}, 0, 0\right]^{\mathrm{T}} \tag{7.1}$$

where d_u is the upper triangle side length. The wires are connected to the mobile platform in three points B_1, B_2, B_3, defining an equilateral triangle with center O_B, their coordinates in B frame are:

$$\mathbf{b}_1^B = \left[\frac{\sqrt{3}d_l}{-6}, \frac{d_l}{-2}, 0\right]^{\mathrm{T}} \mathbf{b}_2^B = \left[\frac{\sqrt{3}d_l}{-6}, \frac{d_l}{2}, 0\right]^{\mathrm{T}} \mathbf{b}_3^B = \left[\frac{\sqrt{3}d_l}{3}, 0, 0\right]^{\mathrm{T}} \tag{7.2}$$

where, d_l is the length side of lower triangular plate, while their coordinates in A reference frame are indicated as:

$$\mathbf{b}_1 = [x_1, y_1, z_1]^{\mathrm{T}}, \mathbf{b}_2 = [x_2, y_2, z_2]^{\mathrm{T}}, \mathbf{b}_3 = [x_3, y_3, z_3]^{\mathrm{T}},$$

and vary according to the platform motion. The coordinates of O_B point, expressed in A frame, are defined by the vector $\mathbf{o}_B = [x, y, z]^{\mathrm{T}}$.

Let us define a rotation matrix $\mathbf{R}(\boldsymbol{\eta}) = \mathbf{R}_z(\phi)\mathbf{R}_y(\theta)\mathbf{R}_x(\psi)$ representing the orientation of B frame w.r.t. A frame. We indicate with $\boldsymbol{\eta} = \left[\psi, \theta, \phi\right]^{\mathrm{T}}$ a vector containing roll, pitch, and yaw angles, respectively.

7.3.1 Inverse Kinematics

The inverse kinematic problem consists in finding the values of cable lengths l_i for a given position $\mathbf{o}_B$ and orientation $\mathbf{R}$.

The geometric constraints of the parallel structure relates the length of the cables to the norm of the geometric vectors connecting B_i to A_i, i.e.,

$$\|\mathbf{b}_i - \mathbf{a}_i\| = l_i \quad i = 1, 2, 3 \tag{7.3}$$

where l_i is the length of cable i, that can be controlled by the motors. The coordinates of the mobile platform connection points can be evaluated as

$$\mathbf{b}_i = \mathbf{o}_B + \mathbf{R}\mathbf{b}_i^B \quad i = 1, 2, 3 \tag{7.4}$$

By substituting (7.4) in the cable constraint relationship (7.3), we can easily evaluate l_i as a function of $\mathbf{o}_B$ and $\mathbf{R}$.

7.3.2 Statics

In stationary conditions, the sum of the forces and torques (wrench) applied to the platform through the wires is balanced by the forces and torques (wrench) due to the physical contact with the finger pad as follows:

$$\sum_{i=1}^{3} \mathbf{f}_i + \mathbf{f}_{\mathbf{o}_B} + \mathbf{f}_{\mathbf{s}} = 0 \tag{7.5a}$$

$$\sum_{i=1}^{3} \boldsymbol{\tau}_i + \boldsymbol{\tau}_{\mathbf{o}_B} + \boldsymbol{\tau}_{\boldsymbol{s}} = 0 \tag{7.5b}$$

we indicate with $\mathbf{f}_i \in \mathbb{R}^3$ the forces applied by the cables, with $\boldsymbol{\tau}_i \in \mathbb{R}^3$ the corresponding momentum, with $\mathbf{f_{O_B}} \in \mathbb{R}^3$ the reaction force applied by the hand palm to the platform, with $\mathbf{f_s} \in \mathbb{R}^3$ the force due to spring deformation, with $\boldsymbol{\tau}_{O_B} \in \mathbb{R}^3$ the reaction torque and with $\boldsymbol{\tau_s} \in \mathbb{R}^3$ the torque due to spring deformation, both expressed w.r.t. O_B point. Expanding the equilibrium equations (7.5) we get:

$$\sum_{i=1}^{3} \rho_i \mathbf{u_{f_i}} + \mathbf{f_{o_B}} + \mathbf{f_s} = 0 \tag{7.6a}$$

$$\sum_{i=1}^{3} \rho_i \mathbf{b}_i \times \mathbf{u_{f_i}} + \boldsymbol{\tau_{o_B}} + \boldsymbol{\tau_s} = 0 \tag{7.6b}$$

where ρ_i is the tension cable i, and $\mathbf{u_{f_i}}$ is the unit vector representing the cable direction, and can be evaluated as:

$$\mathbf{u_{f_i}} = \frac{\mathbf{b}_i - \mathbf{a}_i}{l_i} \tag{7.7}$$

From (7.6), and (7.7), we can express (7.5) in the matrix form:

$$\begin{bmatrix} \mathbf{u_{f_1}} & \mathbf{u_{f_2}} & \mathbf{u_{f_3}} \\ \mathbf{b}_1 \times \mathbf{u_{f_1}} & \mathbf{b}_2 \times \mathbf{u_{f_2}} & \mathbf{b}_3 \times \mathbf{u_{f_3}} \end{bmatrix} \begin{bmatrix} \rho_1 \\ \rho_2 \\ \rho_3 \end{bmatrix} + \begin{bmatrix} \mathbf{f_{o_B}} + \mathbf{f}_s \\ \boldsymbol{\tau_{o_B}} + \boldsymbol{\tau}_s \end{bmatrix} = 0 \tag{7.8}$$

(a well-known as geometric-statics equation of cable driven parallel robots [297]).

7.4   Design and Analysis

The device presented in this work is the result of a trade-off between wearability, weight and resistance to mechanical stress. The symmetrical geometry of the supports on the back of the hand back and under the palm allows a homogeneous distribution of the forces applied by the motors and transmitted through tendons. One of the drawbacks of tendon actuated devices is that the end-effector has to be always in contact with the hand and the tendons have to be stretched. To overcome this issue and allow the device to activate and deactivate the contact with the palm, the end-effector is connected to a C-shape, fixed element by means of an elastic element.

In the following we describe with more details the device from the design point of view, the interchangeable end-effector's modules that are in contact with the palm, and we show some results of a structural mechanical analysis.

7.4.1   HapticPalm

The device has a parallel structure and consists of two main parts, one on the back of the hand, and the other below the palm defined as the end-effector of the device.

The part on the hand back consists of a mechanical support for the force actuation/transmission system, the microcontroller and the power supply (indicated with A in Figure 7.4). Three tendons are routed in three paths extruded from the support, arranged at 120 deg from each other in order to achieve an equilateral "Y-shape". The
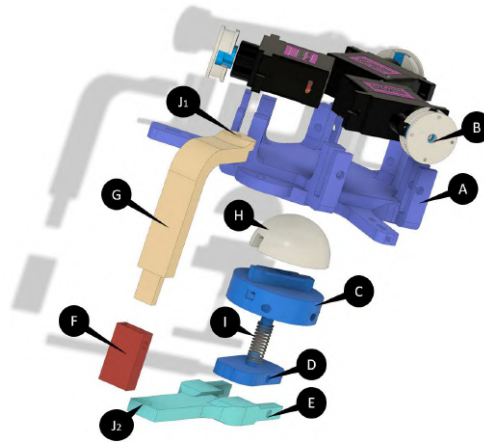
Figure 7.4: Exploded CAD view of the device. The end-effector of the device is composed of the components indicated with (C), (I), (D). (H) indicates the end-effector's module while the "Y-shape" platform is indicated with (A) and the pulleys are indicated with (B). (E), (F) and (G) are the elements that realize the link between the two platforms. (J$_1$) and (J$_2$) are the two joints that allow to rotate the end-effector.

tendons transmit the forces applied by the motors, through the pulleys, from the back of the hand to the device's end-effector (B) and therefore to the hand palm. This type of actuation has an easy wearability and avoids the problems present in parallel mechanisms based on rigid links, that have higher weight, and lower flexibility/adaptability and requires suitable procedures to be adapted to different users and needs [302].

The end-effector is composed of two platforms (D) and (C). The first is connected to the actuation system through the tendons, the second is connected directly to the part on the back by means of a "C" shaped rigid link (E). The two platforms are connected by an elastic element (a spring, I) that allows the tip-palm disconnection when no contacts and forces have to be applied. The connection points between tendons and the platform have a "Y-shape" structure similar to the support on the back of the hand. A magnetic "T-shape" interlocking is designed on the first platform, allowing to easy interchange the different end-effectors' modules (H) realized to reproduce different types of cutaneous stimuli.

The rigid link connecting the two main parts (G, F, E) has an adjustable telescopic height to adapt the device dimension to the needs of users with different anthropometric dimension of the hand, and can be rotated through two revolute joints (J1, J2), with the aim to ensure the ergonomics for several users and allow them to temporary move away the end-effector from the palm without remove the device.

7.4.2 Modules

As mentioned before the end-effector modules of the device are manually interchangeable. They are fixed to the device by means of a "T-shape" interlocking system. The modules
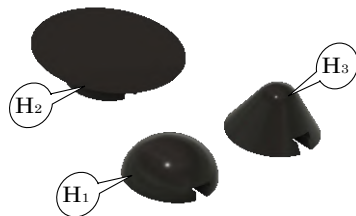
Figure 7.5: CAD models of the end-effector' modules. H_1 indicate the spherical modules with different radii of curvature while H_2 and H_3 are respectively the dot-shaped module and the plane-shaped module.

can be connected/ disconnected easily to the end-effector platform thanks to the "T-shape" path and are fixed by a magnet inserted in each module. The magnets allow the modules to position themselves exactly in the center of the "Y-Shape" platform and to keep them fixed during the force rendering. In order to transmit the sensation of touching objects and surfaces that are interesting in haptics applications. three different end-effector modules have been created. The basic idea is to let the user feeling common shapes such as spheres, corners, edges and flat surface. In this work we have created a spherical modul with the aim to reproduce the curved surfaces (H1, in Figure 7.5), a dot-shaped module and a plane-shaped module in order to reproduce the contact with edges and flat shapes respectively (H2, H3).

7.4.3   FEM Analysis

Even if the basic structure of the device is similar to the one developed for the fingertip for instance in [293], the larger dimensions and the magnitude of the applied forces are more challenging from the mechanical point of view. A structural stationary FEM analysis was carried out for evaluating the overall stress/deformation of the device in three different loading cases representing typical operative conditions. Three of them analyze the behavior of the device when a set of forces defined according to the model described in Section 7.3.2 are applied, while the fourth investigate the response of the device when the skin elasticity is saturated, i.e. when the end-effector is fixed. The analysis was performed with the 3D-CAD/CAE software, Fusion360 (Autodesk Inc.,US). The materials of the components used in these cases are ABS for all the components of the device except for the spring, realized in steel.

The behavior of the device was analyzed when the forces indicated with blue arrows in Figure 7.6 are applied on the three vertices of both platforms. A fixed constraint was set on the bottom part of the back hand's platform to simulate the contact with the hand. Six forces are applied to the fixed and mobile "Y" vertices, the directions of the forces are selected to simulate tendons' actions. Their magnitudes are chosen according to the overall interaction force direction to be simulated. Figure 7.6 shows the results of FEM analysis for the three-axis directions. All the subfigures on the top side report the results in terms of displacements while the subfigures on the bottom side show the results in terms of deformations. In Figure 7.6A and Figure 7.6D the results of the analysis
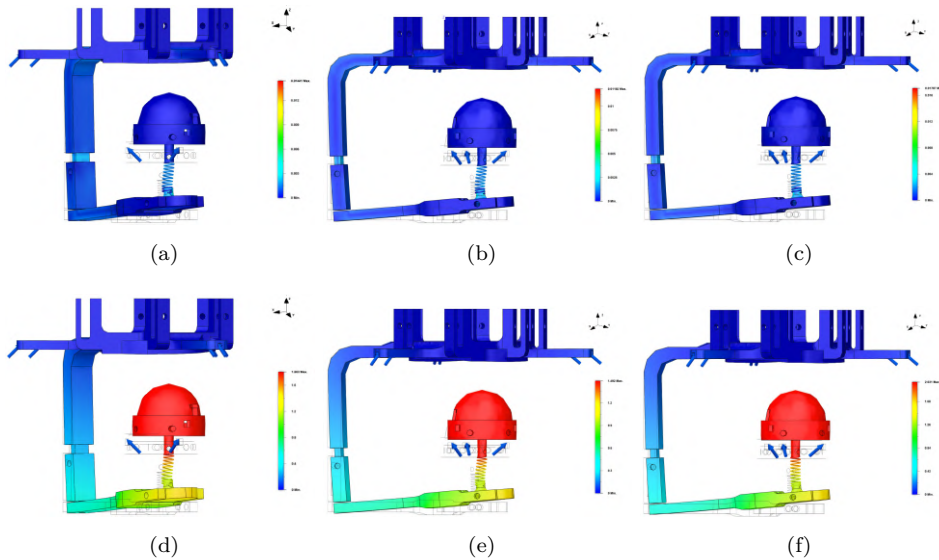
Figure 7.6: Results of the FEM structural analysis. The blue arrows indicate the forces applied in the simulations, the wireframe transparent CAD model represents the unde-formed model, while a 1X deformation of the device is represented in the colored sur-faces. (a) the displacements when a force with only z-component is applied, (b) and (c) show respectively the results of the displacements when a force with z-component and x-component or y-component is applied, subfigures (d), (e) and (f) on the right side report the results of the deformation for the same loading cases.

corresponding to an overall force acting along z direction are reported. In this case the forces' magnitudes are the same for all the simulated tendons and equal to 1 N. Concerning the corresponding displacement, Figure 7.6D shows that, as expected, it occurs mainly along the "z" axis. Figure 7.6B and Figure 7.6E show the results of the simulation of an overall force with components along z and y direction. For this simulation we have symmetrically modified four forces, by reducing their module to 0.5 N. In Figure 7.6C and Figure 7.6F finally we reported the results when an equivalent force with components along x and z directions is applied. As in the previous case, the forces have been modified symmetrically. Finally we verified the response of the device when the skin elasticity is saturated, to check the resistance of the platform on the back of the hand. The forces applied in this case are all with the same direction and intensity, i.e. 5N while the fixed constrains are two, one on the end-effector's module and the other on the bottom part of the back hand's platform (Figure 7.7). In general, results from the FEM analysis shows that the mechanical structure of the device can resist to the forces that are applied in haptics applications. The results of FEM analysis also show that, as expected, the main critical points of the structure are represented by the rigid link and the base of the spring. Moreover the choice of the spring is very another critical aspect to be considered to guarantee a suitable level of robustness and functionality of the device.

(a)   (b)
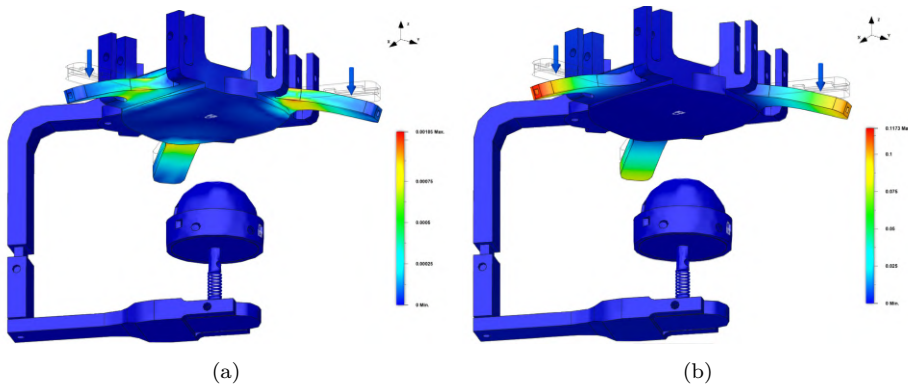
Figure 7.7: Results of the FEM analysis for the platform of the back of the hand under the action of an overall 15 N force (5N for each side of the "Y-shape"). Blue arrows indicate the forces applied while the transparent wireframe CAD model, is the reference undeformed model, while the colored surface corresponds to a 1X deformation of the haptic palm device. Subfigure (a) shows the displacement of the platform and the Subfigure (b) reports the deformation of the platform.

(a)   (b)   (c)
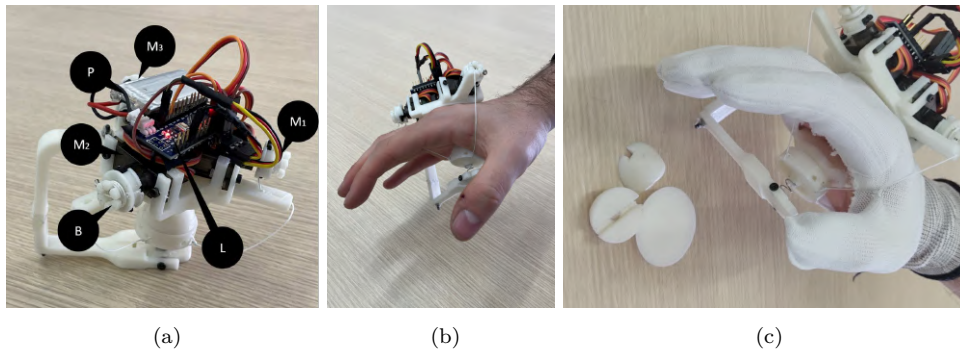
Figure 7.8: Prototype of the device presented in this work. In (a) shows the device hardware components. (b) report the "naked" device worn by a user. The figure (c) shows the final prototype worn by the user together with the different modules.

7.5 Prototype, hardware and components, control and application

Figure 7.8 shows the first prototype of the developed device for hand palm haptics stimulation. All the structural components are manufactured using an FDM (Fused Deposition Modeling) process with ABS material, except for the elastic element that is a standard off shelf steel spring.

For the transmission of forces, three MG-90S microserves were used (M_i in Figure 7.8B), powered by a 5V battery (P). Each of them has a stall torque of 20 Ncm. For the

	Technical specifics
Weight	$89.92g$
Dimensions $L \times l \times (h \pm \Delta h)$	$104 \times 81 \times (97 \pm 0.7)mm$
Degrees of freedom	3
Microprocessor	$ATmega328$
Clock speed of microcontroller	$16MHz$
Computer interface	$Serial\ COM$
Input Voltage	$5.0V$
Battery life	$\approx 5h$
Maximum speed	$9.5\frac{rad}{s}$
Maximum resisting force	$60.0N$
Maximum theoretical force on palm	$29.5N$
Minimum theoretical force on palm	$0.81N$
Maximum recall force	$30.5N$
Maximum contact surface	$\approx 7.06cm^2$
cost	$\approx \$50$

Table 7.2: Haptic palm device prototype main harware/software details and techincal specifications. The dimensions of device are measured without the glove, the value of Δh is equal the capability to extend and shorten the rigid link F respect G link.

control and data processing part, we used the Elegoo Nano V3+ microcontroller (ELE-GOO Inc.,CHN), (L), while the transmission with the virtual environment was carried out using serial communication. As previously introduced, the rendering of the force on the hand palm uses a tendon-based transmission. The tendons are anchored on one side to the pulleys of the motors fixed on the "Y-Shape" platform (A) of the back of the hand, on the other side to the "Y-arranged" connectors of the end-effector. The minimum size of each tendon is defined by the length of the thread needed, when it is under tension, to connect the platform of the end-effector to the" Y-shape" platform on the back of the hand. In order to adjust this length, the pulleys have been designed with an external part allowing to wrap the excess amount of tendon. A first version of the pulleys is shown in the CAD model (B in Figure 7.4) while an updated version is shown in the prototype in Figure 7.8B (B).

Figure 7.8C shows the first prototype worn by a user. From the first users' feedback we realized that the "naked" device was not easy and intuitive to wear it due to the uncertainties on the orientation caused by the symmetrical shape of the device. Then with the aim to avoid this ambiguity in the orientation and to help/guide the user's hand between the tendons when wearing the device, the device was embedded in a glove with a properly shaped hole in the center of the palm allowing the contact with the end-effector (Figure 7.8D).

As mentioned before, an elastic element was used in order to passively support the end-effector when it is not in contact with the palm. One side the spring should be enough stiff to keep the end-effector in an upright position even when the tendons are

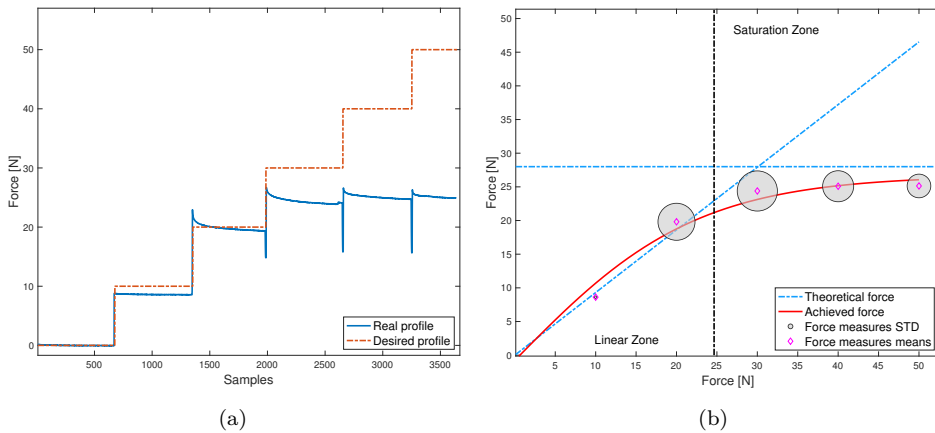(a)   (b)

Figure 7.9: Assessment of HapticPalm forces. (a) Results of force profile chase. (b) Characterization function of the device: red curve represents the device's real behavior, generated by interpolating the force measures means points at each step of 10N in the range [0, 50]N while in blue the theoretical behaviour obtained exploiting the formulation described in 7.3.2. The horizontal blue line corresponding to 28N, the maximum theoretical force while the black vertical line is the threshold between the linear zone and nonlinear zone of the real device characterization function.

not actuated. On the other side, the spring should be enough soft to avoid an overload to the motor, that should spend a part of their torque to apply the required haptic force and a part to deform the spring, as highlighted in Section 7.3.2. To meet this trade-off, we adopted a spring with a stiffness coefficient equal to 6.7 N/mm. Moreover, we decided to use a short spring, with a length of 7 mm, to keep the end-effector's size as compact as possible and with this choice, in the prototype, we observed a symmetric behavior of the spring both along the axial and radial directions.

Table 7.2 summarizes the main characteristics of the developed prototype. The maximum and minimum theoretical forces that can be applied on palm are evaluated according to the model presented in Section 7.3.2.

7.5.1   Experimental Force validation

The experimental force validation of the device consisted into a repeated recording of predefined forces exerted by the device and collected by high precision ATI force sensor Nano25 (ATI Industrial Automation Inc., US).

A user wears the HapticPalm with an ATI sensor inserted between the end effector plate module (H_2) and the hand palm using a textile pocket. The haptic device perform a step-wise force profile. For the sake of simplicity and without lack of generality direction of the resultant applied force is along the palm normal direction, each other force component value may be evaluated trivially from the trigonometric relationship between normal forces and oblique ones. The range of force is [0, 50]N with 10N steps.

The force measure was repeated 10 times and recorded in textual format. The results of one of the repetitions is depicted in Figure 7.9. The collection of all measure by ATI sensor were used to realize a lookup table of effective forces performed by HapticPalm and it is compared with the theoretical forces evaluated starting from statics formulation presented in 7.3.2. The Figure 7.9 reported the interpolating results of measure and the aforementioned theoretical evolution. According with the preliminary observation of achieved data, we tested several formulations of logistic function to interpolate curves for the force measures. The best interpolating curve was a an offset and scaled hyperbolic tangent function expressed as:

$$F_s = \alpha + \beta \tanh \left(\gamma \sum_{i=1}^{3} n_{f,i} \right)$$

With $\alpha = 27.46$, $\beta = -0.77$, and $\gamma = 0.044$, while $n_{f,i}$ indicates the normal force component due the tensions of *i-th* tendon.

In a range from 0 N to 25 N, the achieved force has a quite linear trend and the mean error committed on theoretical evaluation is equal to 0.87 ± 0.22N. Moreover in saturation zone the mean error accepted in stationary condition respect the theoretical limit value equal to 3.14 ± 0.95N. The steady state error in the saturation zone is approximately equal to 10% of the theoretical threshold, the resulting error, although not negligible, is to be understood as inclusive of the uncertainties on the dynamic mass-spring-friction model of the hand of the current user affecting the σ and k parameters, that actually are chosen such that $k = 500N/m$ and $\sigma \approx 0$, according to [233]. In addition the structural compliance of y-arranged guides for routing the tendons when the elasticity of the skin of the palm is saturated is an other source of errors in force saturation zone.

7.6 Usability Assessment

Given the device design specifications and functionality, usability was defined as a result of *i)* realism, *ii)* interchangeability of modules H_i, *iii)* carpal cluttering, and *iv)* general opinions about wearability. In order to collect an estimate for each of the four parameters, an experimentation campaign was conducted through user studies. Ten participants (4 females and 6 males) were therefore involved in the trial, all of them were right-handed, aged between 25-39 years. Each subject gave her/his written informed consent to participate and was able to discontinue participation at any time during experiments. The experimental evaluation protocols followed the declaration of Helsinki, and there was no risk of harmful effects on subjects' health. The experiments were carried out a virtual environment, shown in Figure 7.10, that consisted of three geometrically regular virtual objects (a cylinder, a cone, and a half sphere). A virtual hand avatar equipped with a three-axial force sensor in the palm (Figure 7.10) interacted with the objects, guided by the user's hand wearing the device. The haptic interaction between virtual objects and hand avatar is modeled similarly to the contact with a 3-DoF virtual spring and the rendered force is evaluated from the hand identation in the object according to a isotropic Hookonian model.

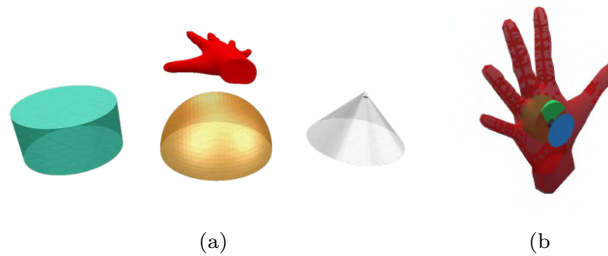(a)   (b

Figure 7.10: Virtual scene elements (a) consists into the three touchable object: the cone, the cylinder and the half sphere, and the virtual hand. (b)hand avatar details: hand (red), force sensor (green), contact area (blue).

The virtual environment was developed in CoppeliaSim v4.2 (Coppelia Robotics, Ltd., CHE), the interaction physics was solved by Bullet 2.78 physic engine with a simulation step of 10ms. The human hand movements were tracked with a LeapMotion controller (Ultraleap, Inc., US), and mapped into motions of human hand avatar, the participant observed the scene wearing an head mounted Display (HMD) to hide to the user view the modules currently instrumented. The communication between tracker system and virtual environment was provided by the Robotics Operating System (ROS). A experimental protocol was designed for the usability validation testing, composed of 14 steps:

S.0 Participant wears the HMD and s/he gets acquainted with tracker system and virtual scene;

S.1 The experimenter explain the protocol to the participant;

S.2 The participant wears the HapticPalm;

S.3 The experimenter chooses an EE-module on table and connects it;

S.4 The experimenter shows how to test the carpus cluttering state;

S.5 The participant mimes the experimenter to the best of her/his possibility;

S.6 The experimenter records the mobility score.

S.7 The participant interacts with one of three objects;

S.8 The experimenter submits the realism survey to the participant;

S.9 Experimenter and participant repeat S.8 and S.9 for each object in the scene;

S.10 Participant detaches the EE-module from device and put it in a box;

S.11 Experimenter and participant repeat all step since S.3, until all EE-modules are in the box;

S.12 Experimenter submits the surveys about interchangeability and records the participant statement;

S.13 Experimenter submits the surveys about general opinion to the participant and records the participant statement.

7.6.1 Cluttering testing (S.4-S.6)

At the beginning of each experiments the participants verified their residual carpal mobility as to verify the cluttering state of the palm. Wearing the current EE-module, they performed the Kapandji test for the mobility of the metacarpal carpal joint that, according to [303], consists in reaching with the thumb, in order, ten predefined sites: *i)* Radial side of the proximal phalanx of the index finger; *ii)* Radial side of the middle phalanx of the index finger; *iii)* Tip of the index finger; *iv)* Tip of the middle finger; *v)* Tip of the ring finger; *vi)* Tip of the little finger; *vii)* Distal interphalangeal joint crease of the little finger; *iix)* Proximal interphalangeal joint crease of the little finger; *ix)* Metacarpophalangeal joint crease of the little finger: *x)* Distal palmar crease. The test stopped at the first unreachable site and returns a score equal to the number of sites successfully reached.

7.6.2 Realism investigation (S.7-S.9)

In accordance with the device features, the realism investigation was based on the hypothesis that the more the surfaces with which one interacts and the surfaces of the tactors are similar the greater is the perceived realism. During the virtual object interaction users were not able to see their hand and know the module connected to the device that was changed after all three objects were inspected. In order to investigate this hypothesis, all the users were asked to inspect the 3 tangible virtual objects in sequence. At each single identification for 9 nine total identifications the participant was asked to express the perceived realism measured by mean opinion score (MOS) on a scale of 5 where 1 means "bad" while 5 "excellent". The MOS is a standardize policy to evaluate the quality of Experience according to [271].

7.6.3 Interchangeability Evaluation (S.12)

At the end of the experiment, each user was asked to evaluate the perceived load during the fulfillment of the task of changing the EE-modules. We used the two stages NASA task load index (NASA TLx) to measure the task load ([304, 251]). The questionnaire collects six factors, *i)* Mental Demand (MD), *ii)* Physical Demand (PD), *iii)* Temporal Demand (TD), *iv)* Performance (PR), *v)* Effort (EF) and *vi)* Frustration (FR), through the following questions:

MD :*"How mentally demanding was the task?"*
 PD :*"How physically demanding was the task?"*
 TD :*"How hurried or rushed was the pace of the task?"*
 PR :*"How successful were you in accomplishing what you were asked to do?"*
  EF :*"How hard did you have to work to accomplish your level of performance?"*
 FR :*"How insecure, discouraged, irritated, stressed, and annoyed were you?"*

Each of the six questions has a scale of 7 levels, considering 1 as "very low" and 7 as "very high" , except for the performance opinions where the scale is reversed (1 as "very high" and 7 as "very low"). Questions are reported in what follows: All load factors were pair-wised compared and the most relevant was chosen from time to time.

Index	Questions
	Emotion (e)
e1	*I feel worried and embarrassed.*
e2	*I feel tense.*
e3	*I would wear the device if it was invisible*
	Attachment (a)
a1	*feel the device on the body.*
a2	*I feel the device moving.*
a3	*I was not able to move as usual.*
a4	*I have difficult in putting on the device.*
	Harm (h)
h1	*The attached device causes me some kind of harm.*
	Perceived change (pc)
pc1	*I feel more bulky.*
pc2	*I feel change in the way people look at me.*
	Movement (m)
m1	*The device obstructs my movements.*
	Anxiety (an)
an1	*I do not feel secure with the device*
an2	*I feel that I do not have the device properly attached.*
an3	*I feel that the device is not working properly.*

Table 7.3: Questions for the CRSs evaluation.

7.6.4   General opinion survey (S.13)

Furthermore, the completion of the experiment was followed by the compilation of a survey based on the Comfort rating scales presented (CRSs) in [305] Through the CRSs questionns, reported in Table 7.3, we tryed to obtain a comprehensive assessment of the comfort in the use of the device by measuring *i)* Emotion (e) *ii)* Attachment (a)*iii)* Harm (h), *iv)* Perceived change (pc), *v)* Movement (m), and *vi)* Anxiety (an).

In particular, the harm is the physical sensation of conveying pain, and the movement is the awareness of modification to posture or movement due to direct impedance or inhibition by the device. The perceived change is the non-harmful indirect physical sensation making the wearer feel different overall with perceptions such as being awkward or uncoordinated, may result in making conscious compensations to movement or actions.

The CRSs uses for each questions a 21-point scale, from 0 to 20, anchored at each end with the labels "low" and "high",To calculate the average CRS score the scale of e3 was mirrored, making the e3 score homogeneous with all the other comfort values, where the lowest the value the better in terms of wearability.
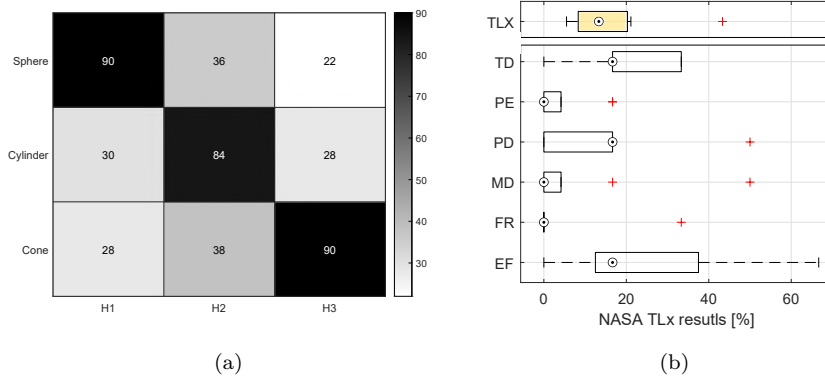
(a)

(b)

Figure 7.11: In (a) the perceived realism matrix, on principal diagonal are reported the results of most similar couple of virtual contact surface and modules.In (b) the evaluation of the participants' experience detaching and attaching the EE modules through NASA TLx in the form of a 7-point Likert scale.

7.6.5   Results and Discussion

First of all we analyzed the data about realism to asses our hypothesis about correlation between modularity and perceived realism. For the sake of clarity and completeness, the average users' opinions about realism are arranged into a 3×3 heat-map that compared touched objects versus end-effector modules. Although the average opinion score is generally above the *Poor* threshold, a clear increase is noticeable in correspondence with the largest diagonal of the heat-map in which the average perceived realism values are reported in correspondence with similarity between tactile modules and touched surfaces.

This result is consistent with the initial assumption that perceived realism grows as the similarity between real and virtual surfaces in contact with the palm grows, consequently the design of a haptic device in the palm must foresee, as in the case of the HapticPalm, a strategy of adaptation of the contact areas coherently with the virtual surfaces with which the user is called to interact to ensure the fidelity of the experience.

A possible strategy is therefore the interchangeability of the touch sensors, which must however avoid increasing the load of the user's task and / or making his experience temporally more expensive and emotionally more frustrating. In this regard, the analysis of the additional load due to the connection and disconnection of the modules using the NASA TLx questionnaire confirmed the adoptability of this strategy, demonstrating that the total additional load is less than 20%. As can be seen in Figure 7.11, the factors that most increase the total load of the task are the time requirement, which is inevitable given the need to interrupt the main task to replace the touch sensor, and the effort which instead is to be considered a time factor decreasing and inversely proportional to the experience gained by the user.

Furthermore, it was verified that the device did not significantly encumbered the palm, the Kapandji test, the results of which are reported in Figure 7.12, demonstrates that the average residual mobility with the device worn varies between 79% in case it is connected
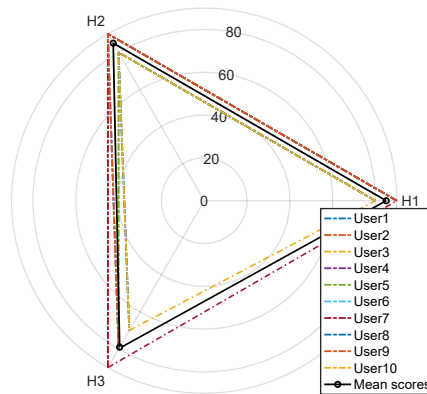
Figure 7.12: Results of Kapandji test for the three EE modules H_1 (half sphere), H_2 (flat), H_3 (cone), the dashed lines correspond to individual participant's result, while the continuous black one is the mean score.

the EE-module H_2 up to 85% with the other two modules.

The general opinions collected by CRSs survey are graphically reported for each questions in Figure 7.13. Generally the emotion load of experience is equal to $0,9 \pm 0,85$ while the attachment, mobility and perceived change are equal to $1,25 \pm 2,41$, $0,1 \pm 0,1$, and $0,9 \pm 1,8$, respectively. The harm is usually equal to $1,2 \pm 0,17$ and the score of anxiety is $0,3 \pm 0,2$. It's worth to notice that the attachment parameter is not very significant for the nature of the device itself whose purpose is to generate contact perception and must therefore be perceptible on the body.

7.6.6 An example of VR application

We have created a virtual reality scenario to demonstrate the functionality of the device in the case of different extended contacts. The scenario was developed in CoppeliaSim (Coppelia Robotics AG.,CHE) and it is a replica of a common office station. In the simulated environment, it is possible to interact with a series of objects on a desk and with the desk itself, in detail, each object is designed to test a specific haptic device end-effector. The module H2 is suitable for the exploration of laptop frames (Figure 7.14B), circular module H1 is intended for the interaction with the paperweight (Figure 7.14A), while the modules H3 and H4 are suitable for interacting with the desk plane and stacked books (Figure 7.14C and Figure 7.14D). Interaction with these objects is possible through a hand avatar sensorized in the palm and controllable by LeapMotion controller (Ultraleap.inc, US), a camera hand tracker system. As a further development of this work, an IMU-based tracking system will be integrated with the haptic device [306]. The forces, estimated by the triaxial virtual sensor, are the result of collisions with the dynamic model of the hand and objects, the collision forces are processed through
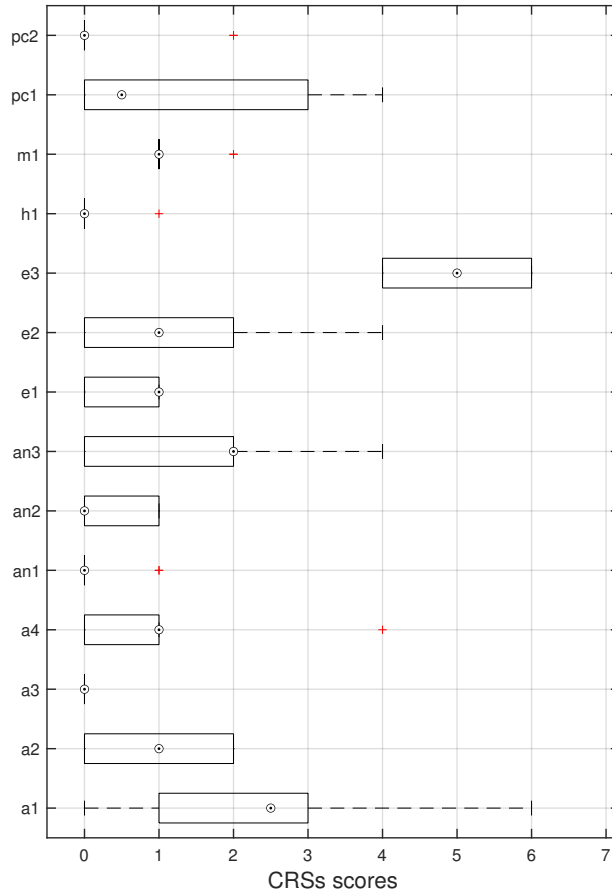
Figure 7.13: Evaluation of the participant's complete experience through CRSs Scores in the form of a 5-point Likert scale for each survey question.

Bullet 2.78 physical engine. The contact forces are then transmitted to the device during navigation, it is also possible to generate on-demand signal by from a recorded force profile from a previous exploration. The device and the virtual environment communicate via serial port.[1]

7.7 Conclusions

This work introduces a wearable haptic device for hand palm cutaneous stimulation, suitable to render the forces generated from palm/environment interactions in a virtual reality environment. As discussed in the initial part of the manuscript, due to the biomechanical structure and constraints of the palm and the need of wearability, the design of this device prototype is the result of different requirements including limited dimensions and

---

[1]A video demonstration is available at the following link: https://drive.google.com/file/d/15YgSfVR1ygYl6Do9mY12Ms9qyvuKcaSI/view?usp=sharing

Figure 7.14: The testing virtual scenario is composed of a rack and a plant in vase in background and a office station in the foreground. The interaction is provided by the red hand avatar of and the objects in foreground are chosen to use all modules: paperweight for H1 module, cover of book and surface of desk for H3 module and desk, laptop and book peaks for H2 module.

weight and capability to reproduce contact interactions and force components in a large surface as the palm. Ideally, the device should be very light, should not over constrain the hand, should not encumber palm, should apply forces suitable for accurately reproducing desired haptic simulations. The work proposes a tendon driven solution with a passive element that allows to disconnect the end-effector from the palm in absence of force to render.

The starting idea is a parallel tendon-driven mechanism actuated by three motors on the hand back. In the first part of the study the mechanism has been studied from the theoretical point of view by means of a simplified mathematical model. Then the idea has been detailed and an CAD model of the device has been realized, and a FEM analysis has been conducted to simulate the behavior of device in case of skin elasticity saturation. A first prototype of the device has been realized and some preliminary functional tests have been conducted. Three servomotors actuate the tendons and transmit symmetrically force from a "Y-shape" platform to an end-effector platform with a "Y-arrangement" of connection points. Several modules have been designed and 3D-printed to extend set of the reproducible surface sensations. The design of modules allows the easy connection and disconnection by means of a "T-shape" socket and a magnetic clip. According to the first experiences of the users in virtual environment and their opinions, the device was positioned and fixed on a shaped glove to guide the hand when wearing the device without covering the palm.

The subsequent study was performed to validate the performance and asses the usability of the Haptic Palm, a device providing a three dimensional force feedback to hand palm during experiences in virtual reality. According with the presentend results, the HapticPalm satisfied the usability criteria of realism, mobility, interchangeability and users' acceptance, using different standardized survey protocols (MOS, Likert scale), questionnaires (NASA TLx, CRSs) and tests (Kapandji mobility test). The results of realism investigation corroborate, also, our hypothesis that for a large contact surface as the palm the realism increase as higher is the similarity between virtual surface and tactile interfaces, while the interchangeability test asses that the modularity is a valid possible

solution to increase the similarity between real and virtual surfaces, avoiding the introduction of additional load to the virtual exploration task. In addition in our preliminary work we calculated the theoretical force and the maximum normal forces that can be applied by the device to a generic mean model of human hand skin in static condition; in this work we have experimentally validated them. The parametric uncertainties on human hand skin stiffness and damping and the deformation of back hand support generate a mean error of 10% in saturation zone of the HapticPalm. In future developments of this work we will realize a full tendon driven design. The employment of antagonistic tendons will avoid the need of the elastic component at the base of modules, recovering the reduction of force/torque generated by motor that actually is less over to 50% respect with the exert-able by motors. We will test this novel device comparing it with the actual HapticPalm for VR experience and its medical version proposed in [307]. Moreover we will conduct a study on the Just Notable Differences on modulus curvature to define the minimum number of modules for a realistic interaction.

Part III

Haptics for Medical Treatments

Haptics for Medical Treatments

I believe that this demonstration of the feasibility of a completely safe remotely performed surgical procedure - and notably the first trans-Atlantic operation - ushers in the third revolution we've seen in the field of surgery in the past ten years

Jacques Marescaux

Medicine and medical research have always been committed to exploring new tools and protocols to improve patients' health conditions and enhance healthcare professionals' performance. Every year, new technologies, drugs, and surgical instruments are introduced to the market to advance the quality of available therapies. Interestingly, even technologies originally developed for other purposes have proven to play an effective role in health care.

An excellent example is virtual reality, which was initially associated with the world of gaming. However, it has become a tool for immersive and detailed visualization of a patient's body [308, 309]. This technology is used for training surgeons on specific operations aimed at particular patients [310, 311]. Similarly, Computer-Aided Design (CAD) models, Finite Element Method (FEM) simulation, and Metabolic Pathway Modeling (MPM), widely used in the industry for the design, simulation of mechanical parts, and simulation of the cell life cycle, are now used to create virtual atlases of patients' organs, which facilitate intervention planning [312, 313].

As already discussed in Part I Chapter 3.2, haptics have also contributed to this process of reorientation of technologies. Exoskeletons, initially designed to increase work performance and for kinesthetic feedback [314, 67], have become rehabilitation tools [315, 316]; Devices for remote tactile communication, such as those presented in [163], can be used to guide people with visual impairment [176], or even for natural pace recovery in Parkinson's patients[177]; Technologies for tactile sensing and stimulation are re-purposed to set frameworks of tele-medicine[317]. Today, some of the most innovative applications of tactile devices for medical purposes are:

- **Rehabilitation by exoskeleton**, the same devices presented in Part I Chapter 2.1, used for kinesthetic rendering of digital interaction and remote display, may

be used to empower individuals with mobility impairments to experience a sense of touch, enhancing their control and coordination, and make their rehab task more engaging and captivating.

- **Pain Management and Manual Treatment** Haptic feedback is also emerging as a valuable tool in pain management and sensory analgesic treatment. Combining virtual reality environments with haptic sensations, allows patients to be distracted from the perceived pain. furthermore, specific haptic devices stimulate sensory pathways, promoting neural recovery and reintegration, providing an analgesic action of the painful limb similar to a manual treatment [2] (MT).

In the current part, some examples of these medical re-purposed haptic devices will be exposed. Chapter 8 and Chapter 10 will detail the design, prototyping, and validation of two novel devices: a gear-based exoskeleton for hand rehabilitation and a haptic pad for the treatment of chronic pain syndromes of the limb ends, respectively. On the other hand, Chapter 9 resumes the repurposing process and testing of the haptic devices proposed in Part II Chapter 7, tailoring this to exert MTs for hand diseases.

---

[2]Manual treatment refers to therapeutic interventions or procedures that involve the use of hands or physical touch by a healthcare professional to diagnose, prevent, or treat various physical conditions. Manual treatment techniques are often applied by practitioners such as physical therapists, chiropractors, osteopaths, massage therapists, and other healthcare professionals who use their hands to manipulate muscles, joints, and soft tissues.

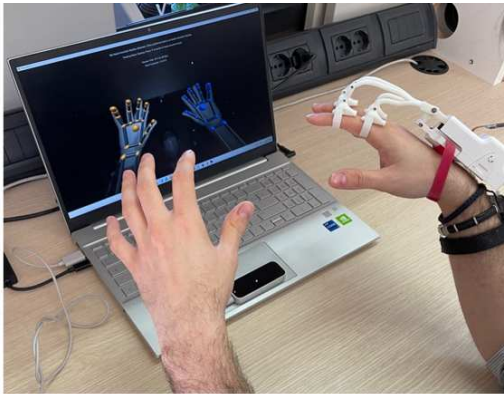# Rehabilitative Hand Exoskeleton with Gear-based Compliant Fingers

Figure 8.1: Prototype of the exoskeleton worn by the user during the compatibility test with optical MoCap system.

Exoskeletons and more in general wearable mechatronic devices represent a promising opportunity for rehabilitation and assistance to people presenting temporary and/or permanent diseases. However, there are still some limits in the diffusion of robotic technologies for neurorehabilitation, notwithstanding their technological developments and evidence of clinical effectiveness. One of the main bottlenecks that constrain the complexity, weight, and costs of exoskeletons is represented by the actuators. This problem is particularly evident in devices designed for the upper limb, and in particular for the hand, in which dimension limits and kinematics complexity are particularly challenging. This work presents the design and prototyping of a hand finger exoskeleton. In particular, we focus on the design of a gear-based differential mechanism aimed at coupling the motion of two adjacent fingers and limiting the complexity and costs of the system. The exoskeleton is able to actuate flexion/extension motion of the fingers and to apply bi-directional forces, i.e. it is able to both open and close the fingers. The kinematic structure of the finger actuation system has the peculiarity to present 3 DoFs when the exoskeleton is not worn and 1 DoF when it is worn, allowing better adaptability and higher wearability. The design of the gear-based differential is inspired by the mechanism widely employed in the automotive field, it allows to actuate two fingers with one actuator only, keeping their movements independent.

8.1   Motivation

Nowadays, the innovation in the rehabilitation processes and in assistive supports is guided by a twofold thrust. First, the overall social impact of chronic diseases related to the musculoskeletal and nervous system is becoming relevant, because the mean age of the population is increasing, thanks to a better quality of life. Indeed, recent statistics published by the World Health Organisation (WHO) shows that nearly one billion people worldwide are suffering due to the musculoskeletal and neurological diseases [318]. According to such statistics [319], in 2019, people were living more than 6 years longer than in 2000, but on average, only 5 of those additional years were lived in good health. Second, the spreading of technology in everyone's everyday life is becoming an important tool for preserving and guaranteeing a high-quality life also in the presence of temporary and/or permanent diseases. Technology advancements in the medical and assistive field constitute an important resource for people with disabilities, helping them in moving, performing manual tasks, communication and learning, providing autonomy in their Activities of Daily Living (ADLs), and globally in the whole process of integration. Innovations in technology are progressively changing the rehabilitation environment. The robot-mediated therapies is an emerging and promising field that incorporates robotics with neuroscience and rehabilitation to define new systems for supporting individuals with neurological diseases [320, 321, 322].

With the COVID-19 pandemic, that dramatically modified our habits, the request of innovative technological resources for rehabilitation have been significantly improved in order to be delivered remotely [323]. Therefore, in the immediate future, telerehabilitation could further spread and become more common, even necessary. Moreover, there are evident advantages in distance rehabilitation, whether synchronous (real-time) or asynchronous (store-and-forward). In fact, the availability of tools for autonomously performing physiotherapy exercises increases their intensity and efficiency, provides supplementary information about results and progress, reduces physiotherapists' efforts and the need of their physical presence during exercise sessions, and encourages autonomy and independence in people with disabilities. The research in this field is still in progress but suggests some health benefits in the use of exoskeletons in rehabilitation and assistive tasks, including improvements in gait function, body composition, aerobic capacity, bone density, and quality of life [324].

Concerning the hand, finger flexion and extension exercises, according to the disease of the subject, have an important effect on the recovery [325]. More in general, the execution of repetitive movements of the hand and the wrist with a controllable intensity, is an important part of the rehabilitation process [326]. In this context, we focus on the upper limbs and in particular on the hand and wrist. They play an important role in all ADLs and therefore significant research effort is focused on developing exoskeletons devices designed to retrain these parts of the human body [327, 328, 329]. The aim of hand exoskeletons is to emulate the physical effort of the therapist by producing the same movements able to maintain the physical abilities of the patient. Nonetheless, the presence of the physiotherapist is usually required and covers a supervisor role. The use of hand exoskeletons can be beneficial, as it requires a smaller workforce, allows a more

lasting and more intense therapy, reduce the need of long physical contacts and close personal distance between the therapist and the patient.

There are different types of hand exoskeletons, that have been developed on the basis of different criteria, i.e., size, weight, degrees of freedom (DoF), flexibility, wearability, modularity and actuation mechanism [330, 331, 332]. In [333, 334, 335, 336] the researchers focused on exoskeleton for the wrist. Hand exoskeleton design is a still open and challenging engineering and research topic, since the human hand has a quite complex kinematic structure. Broadly speaking, a fully actuated solution would require an actuator for each DoF, so, in theory, we would need four actuators for each actuated finger [314]. Rahman et al. [337] present a fifteen degrees of freedom (DoFs) hand exoskeleton, based on compliant mechanisms, that flex and extend the fingers by using bilateral movement training. In [338] a hand exoskeleton for rehabilitation purposes due to injuries is shown. It is actuated by using a Bowden cable setup driven by DC motors and it can be adjusted to various hand sizes thanks to the rack and pinion slide mechanism. The same cable mechanisms is used by Randazzo et al. [339] and by Marconi et al. [340]. In [341] the authors present a glove-type exoskeleton that actuates three fingers (excluding the little finger) and the thumb by using tendon cables routed in a glove while a different design approach are exploited for the hand exoskeletons based on rigid mechanical structure. This kind of devices use motors directly connected to the structure, that transmit the motion to the required joints. The most popular devices in this area are the ones based on remote center of rotation [342], four-bar linkage mechanisms [343], base-to-distal devices with mechanical links connected in series [344], and matched axis mechanical structure [345].

In this work we present the design and characterization of a modular hand finger exoskeleton, in which the number of actuators has been reduced by exploiting a gear-based miniaturized differential mechanism, in order to limit the weight, complexity and costs. One of the advantages of this kind of mechanism is that it is contained in a small box, while other solutions, such as tendon-based mechanisms, need a larger structure that could be uncomfortable for the user [346]. The developed hand exoskeleton is shown in Fig. 8.1. It is able to both flex and extend two adjacent fingers in an independent way, with an actuator only. If one of the coupled fingers finds an obstacle in its movement, the other one can still continue its motion. The second contribution presented in this work is an improvement of the mechanical transmission between the actuators and the phalanges, with respect to the hand exoskeleton previously developed and summarized in [347], that is a part of a wider modular system that also includes the wrist. The device has been designed to be adopted in rehabilitation and tele-rehabilitation applications and to be used by the patient both in collaboration with the therapist or autonomously. Concerning the design and prototyping of the differential mechanism for the coupling two adjacent finger modules, in particular, the work summarizes: (i) the mechanical, mechatronics and manufacturing aspects of the mechanism, including its structural analysis, hardware and control description; (ii) evaluate and compare the proposed solution with respect the previous ones [347], from the the actuation point of view; (iii) present a working prototype and its functional testing in operative conditions.
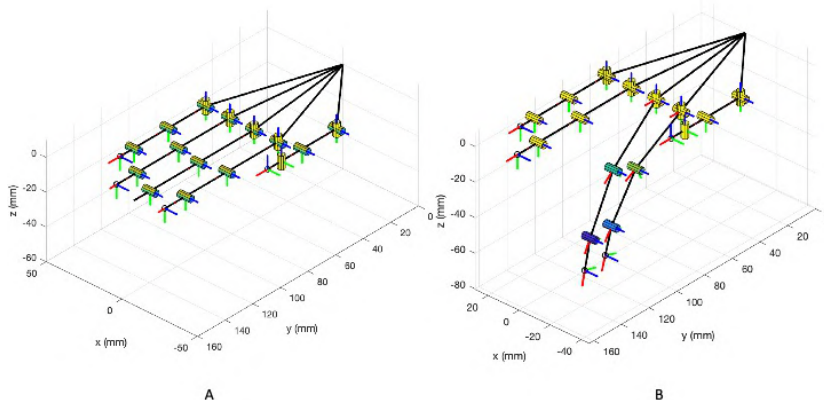
Figure 8.2: Schematic representation of the human hand 20 DoF model implemented in SynGrasp. **A** The hand in the reference open position. **B** Actuation of the first synergy for the index and middle flexion/extension motions.

8.2 Background and design requirements

8.2.1 Kinematic constraints: summary of human hand kinematics

The human hand has a quite complex kinematic structure, whose skeleton is composed of 27 bones, that can be divided in long bones and short bones. The carpus consists of eight short bones while the remaining 19 long bones constitute the metacarpus, the four fingers and the thumb. The bones lay the structural foundation for a complex mechanism with several DoFs (Degrees of Freedom). In [348] a 25 DoFs model of the human hand is presented, while in [349] the presented model has 30 DoFs. For the sake of simplicity in this work we refer to a simplified kinematic hand structure, in which we consider the carpus as unique rigid body while each finger as a planar kinematic chain, with two revolute joints in proximal interpahalngeal joint (PIP) and distal interphalangeal joint (DIP) and 2D hings in metacarpal joint (MCP). The thumb presents a different kinematics structure: a complete model of the the thumb has two DoFs in the trapeziometacarpal joint (TC), two in the metacarpophalangeal joint, and one in the interphalangeal joint (IP). However, given the reduced range of motion of abduction-adduction movement of thumb the model can be reduced to a 4 DoFs structure. Therefore, the reference hand model used in this work has 20 DoFs [350, 351].

The definition of the so-called postural synergies, result of the psychophysics research presented in [243] by Santello et al, has been exploited also in robotics to manage the complexity of actuation systems. In this work we used such definition in exoskeleton design, to reduce the number of actuated DoFs without compromising grip and manipulation capabilities of the hand. Postural synergies can be modelled as a mean for coordinating the large number of degrees of freedom of the human hand, expressed with the joint vari-

ables $\mathbf{q} \in \Re^{n_q}$, with a reduced number of variables $z \in \Re^{n_z}$, with $n_z << n_q$. Synergy constraint is typically expressed in terms of velocity as [350]:

$$\dot{\mathbf{q}} = \mathbf{S}\dot{\mathbf{z}} \tag{8.1}$$

where $\mathbf{S} \in \Re^{n_q \times n_z}$ is the so-called *synergy matrix*, $\dot{\mathbf{q}} \in \Re^{n_q}$ is a vector containing joint angular velocities and $\dot{\mathbf{z}}$ represents synergy velocities. Columns of the synergy matrix $\hat{\mathbf{S}}$ describes the so-called *postural synergies*. Postural synergies have been evaluated in [243] by processing a set of virtual grasp postures by means of the Principal Component Analysis. A set of users were asked to shape their hands imagining to grasp an object from a quite large set ($N = 57$), the corresponding postures were recorded using a CyberGlove system and the PCA was then applied to the obtained data. Results demonstrated that more than the 80% of the variance can be represented by the first 2 principal components, suggesting that, out of the 25 DoFs of a human hand, only two or three combinations can be used to shape the hand for basic grasps used in everyday life. This simplification principle has been investigated in the design of underactuated robotic hands [352].

In [353, 350] the postural synergies defined in [243] were adapted to the mathematical model of a human hand that was referred in those work as *paradigmatic* hand. The proposed model had 20 DoF, each finger had 4 DoF. Since the data in [243] were captured with a 15 DoFs CyberGlove system, the obtained synergy matrix $\mathbf{S}$ dimensions were 20×15. Such synergy matrix is available in SynGrasp Toolbox [351] or can be evaluated with the data available in [354].

Other studies available in the literature shows that the complexity of human hand kinematics can be simplified considering joint coordination. For instance, Cobos et al. in [355] showed that the interphalangeal distal joint of each finger moves with motion equal to and equal to a fixed fraction of the interphalangeal proximal joint.

The concept of postural synergies has been exploited also in this work in the design of the hand exoskeleton, to reduce the number of actuators. In particular, each module of exoskeleton has been designed to flex and extend two fingers so that in each finger joint rotation angles are coordinated according to the first postural synergy defined in [243], available in the data-set presented in [354].

In accordance with the above mentioned studies, the kinematic structure of the thumb is significantly different from the other fingers ones and it has not been exploited in this work. Furthermore, the device developed in this work is aimed at supporting the user in flexion/extension motion of the fingers, while adduction/abduction movements are not actuated. Consequently, the design of the exoskeleton modules will be synergy-based according to the following relationship:

$$\dot{\mathbf{q}}_i = \mathbf{S}_{1,i}\dot{z}_{1,i} \tag{8.2}$$

$$\dot{\mathbf{q}}_m = \mathbf{S}_{1,m}\dot{z}_{1,m} \tag{8.3}$$

Where $\mathbf{q}_i \in \Re^2$ and $\mathbf{q}_m \in \Re^2$ are the velocity vectors relative to MCP (MetaCarpo-Interphalangeal) and PIP (Proximal-Interphalangeal) flexion/extension joints of index and middle fingers, respectively. $\mathbf{S}_{1,i} \in \Re^2$, $\mathbf{S}_{1,m} \in \Re^2$ are extracted from $\mathbf{S}$ matrix, in particular $\mathbf{S}_{1,i}$ contains the elements of the 1-st column (first synergy), 6-th and 7-th rows

(MCP and PIP joints of the index finger), while $\mathbf{S}_{1,m}$ contains the elements of the 1-st column, 10-th and 11-th rows (MCP and PIP joints of the middle finger) [353, 350]. $\dot{z}_{1,i}$ and $\dot{z}_{1,m}$ are the synergy velocities for the index and middle fingers, respectively. If each finger is independently actuated, $\dot{z}_{1,i}$ and $\dot{z}_{1,m}$ are independent, while, if the fingers are coupled by means of a differential mechanism, the following relationship between synergy velocities can be set:

$$\dot{z}_1 = \frac{\dot{z}_{1,i} + \dot{z}_{1,m}}{2} \tag{8.4}$$

in which $\dot{z}_1$ represents the synergy velocity actuated by the motor. Fig. 8.2 reports the Syngrasp simplified graphical representation of the human hand 20 DoF model in the reference open configuration and with the activation of the first postural synergy for the index and middle flexion motions.

8.2.2 Independent and coupled actuation of fingers

Several actuating methods, active and passive, have been developed and implemented for hand exoskeletons. Among the active actuation methods, the most popular way of actuating hand exoskeletons is the one that exploits electric motors, i.e DC motors, brushless DC (BLDC) motors, servo motors and linear actuators [331]. Linear actuators are preferred in some applications because they can apply bi-directional forces and therefore can push or pull the mechanical linkage system to flex or extend the fingers [347]. Linear actuators that can be employed in this type of applications have quite small dimensions, so that one actuator per finger can be used. This kind of actuation has multiple advantages such as the possibility of making the exoskeleton's fingers independent, allowing a precise control in finger movements.

Linear actuators have a finite stroke, that limits the finger range of motion (ROM): the stroke that the actuator can realise is related to the ROM of the finger by means of exoskeleton kinematics relationships [314]. The linear actuator and the sizes of the linkages in the articulated transmission system have to be defined to allow the patient to fully flex and extend the finger, and this requirement could lead to a solution that is bulky and difficult to wear.

In this context, the miniaturized differential mechanism presented in this work allows to couple the actuation of two adjacent fingers, allowing to decrease the number of actuators, reducing the weight and the complexity of the system, and improving wearability. The differential mechanism does not rigidly connect the fingers, but maintains them independent, so if one of the two branches of the differential is blocked, the other one can still move. It's worth noticing that blocking one of the finger, the range of motion of the other finger is doubled. With the same mechanical linkage system used to flex and extend the finger, by using the differential mechanism finger ROM can be increased with respect to the one that can be obtained, without the differential mechanism, limited by actuator stroke.

Differential mechanisms are quite common in robotics, and in particular in robotic hands and fingers [356]. Planetary gear solutions have been presented for example in [357, 358, 359]. In tendon based systems, moving pulley differential mechanisms can be used [360]. In [359] a differential system based on gears is used for a novel architecture

of robotic hand and the properties of differential mechanisms arranged in cascade via parallel or serial connections is studied. In [361], an underactuated anthropomorphic gripper for prosthetic applications is presented, in which a mechanical lever inside the palm allowed to extend the grasping capabilities and improve the force transmission ratio of the gripper. This mechanism was further developed in [362], in which the differential mechanism included a set of locking buttons allowing the user to stop the motion of each finger.

8.2.3   Summary of the main exoskeleton requirements

The design of the exoskeleton was performed in close collaboration with a potential user, that continuously followed the development. The main requirements that guided the design of the exoskeleton for hand finger actuation, defined in accordance with the user, are reported in the following.

- **Wearability**: the exoskeleton should be easily worn by the user, possibly without the need of external assistance.

- **Encumbrance**: the encumbrance of the exoskeleton should be as contained as possible, the bottom surface of the fingers should not be constrained, to allow the user to grasp and manipulate objects.

- **Number of actuated DoF**: for each couple of adjacent fingers (e.g. index/middle, ring/little), only one actuator is employed, the motion of MCP, PIP and DIP of each finger should therefore be coupled by the mechanical structure of the exoskeleton transmission system, while the two fingers should be coupled through a differential system.

- **Type of motion**: the exoskeleton will actuate the flexion/extension motion of each finger only. The flexion/extension range for the MCP joint is $[0-90]$ deg.

- **Maximum force**: the developed exoskeleton will be able to apply a maximum equivalent force at the fingertip of 20 N both in flexion and extension.

8.3   Design and modeling

On the basis of the requirements described in Section 8.2, we designed and modeled the exoskeleton structure using the software Autodesk Fusion 360. The device is designed to ensure that the movements of the exoskeleton match the human hand ones and do not constrain or overload hand joints.

8.3.1   Differential mechanism

As previously introduced, a gear based differential mechanism is used to couple the motion between two adjacent fingers. The CAD model of the differential mechanism is shown in Fig. **??**. The size of the gear-based differential is reduced as much as possible, and
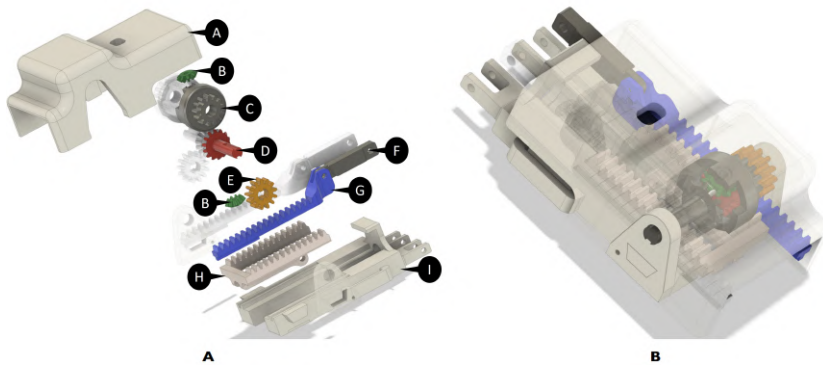
Figure 8.3: **A** Exploded CAD view of the differential mechanism. (A) differential mechanism cover box; (I) support for the linear actuator and for the differential mechanism parts. The differential mechanism is composed of: two satellite gears (B), two gears meshed with the shafts (D), two differential's branches (G,F), a rack (H), and two spur gears (E) meshed with two crowns (C). **B** Assembled differential mechanism.

the resulting dimensions are a trade-off between wearability, weight, motion smoothness, mechanical resistance and easy of manufacturing with FDM (Fused Deposition Modelling) and SLA (Stereo-Lithography) technologies available in our laboratory. The gear-based differential mechanism is actuated by one linear actuator only, fully contained in the mechanism box.

The differential mechanism is an epicyclic gear with 2 DoFs, composed of two main parts:

- **The differential gearing** consists of four bevel gears, i.e. two satellites (indicated with B in Fig. **??**A) gears and two gears joined to the shafts (D), that transmit the motion to the fingers of the exoskeleton by using the differential's branches (G,F).

- **The carrier** is actuated by a rack (H), which is powered by a linear actuator placed in a support base pocket (I). It contains two sites where the satellite gears of the differential gearing are mounted.

The carrier is designed to allow the connection between the differential box and the linear actuator. It is symmetrical and presents two spur gears on the side (E), joined to the crown (C in Fig. **??**A). The differential box contains the epicyclic gear. We choose a symmetric structure, in order to homogeneously distribute forces and torques, ensuring mechanical stability.

When the actuator is retracted, the hand is in the rest configuration (extended) pose. Instead, when the actuator is extended, it moves the rack, which is connected to the differential box, that is free to rotate. If no obstacle is encountered in the movement, the satellites of the differential mechanism do not rotate with respect to their own axes, so the shafts rotate jointly with the crown, with the same angular velocity. The transmission gears, that are keyed on the shafts, actuate the two terminal racks, connected to the fingers, allowing the flexion of the hand according to exoskeleton kinematics. If one finger
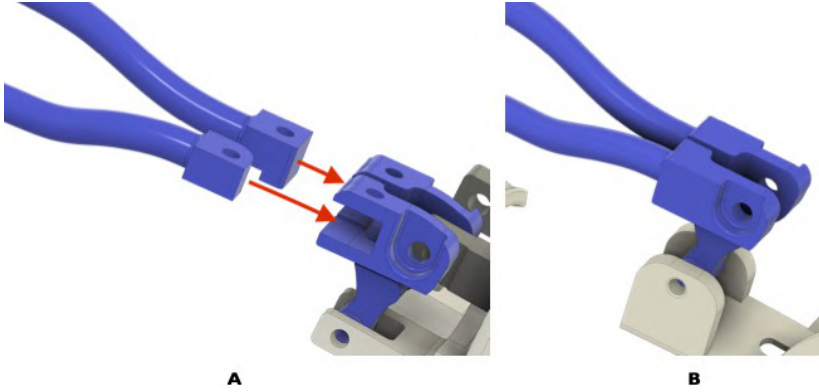
Figure 8.4: **A** new finger's module socket. **B** previous version of finger's module.

finds an obstacle, the adjacent finger keeps moving with a double velocity, according with the relation that describes the differential mechanism, that is:

$$\tau_{l,r} = \frac{\omega_r - \omega_c}{\omega_l - \omega_c} = -1 \Rightarrow \omega_c = \frac{\omega_l + \omega_r}{2} \tag{8.5}$$

where $\tau_{l,r}$ is the transmission ratio of the differential mechanism, according with the Willis equation, ω_r and ω_l are respectively the angular velocities of the right shaft and the left shaft, ω_c is the angular velocity of the carrier. Since the transmission ratio in a rack and pinion system is constant, the above relationship can be easily expressed as a function of linear actuator stroke s and differential output strokes for the index and middle fingers, indicated with s_i and s_m, as follows:

$$s = \frac{s_i + s_m}{2} \tag{8.6}$$

In this way the device can move two adjacent fingers with an actuator only and a power source, with the advantage of keeping independent the motion of fingers.

8.3.2   Finger actuation

As introduced in Section 8.2, user's comfort is an important requirement when we deal with wearable devices, especially if designed for rehabilitation. For this reason, the design of finger support is performed to increase the adaptability and wearability. The user should be able to wear/unwear the device easily and reasonably quickly, and the structure has to be easy adaptable to users with slightly different anthropometric measures.

It's worth to notice that the developed transmission system is underactuated when it is worn on the finger, i.e. the kinematic structure is "closed" by the finger, this feature allows a better wearability and a better adaptability to user's specific finger dimensions [347].

The finger module was previously presented and was developed to satisfy the above mentioned wearability and kinematic requirements. In the design proposed in this work, further improvements to the finger module have been implemented. In particular, the

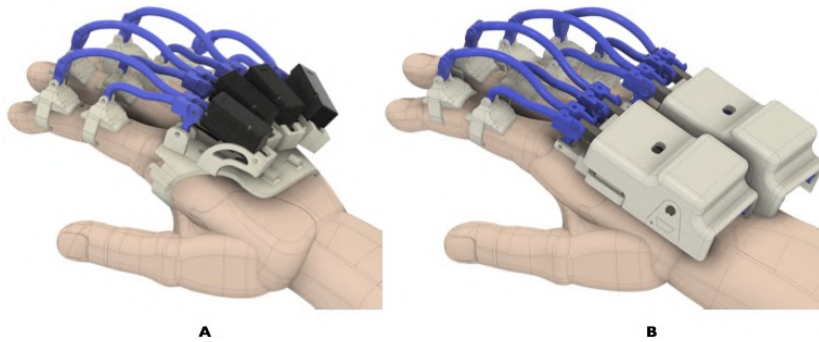Figure 8.5: **A** CAD model of the previous version of the exoskeleton worn on the hand. **B** CAD model of the proposed exoskeleton worn on the hand.

new version of the sockets, shown in Fig. 8.3 A, with respect to the version in Fig. 8.3 B allows to easy assembly/disassembly the finger modules to/from the actuator/differential without using any tool. The complete CAD model including the modules for the fingers and the differential mechanism is shown in Fig. 8.4. In particular, 8.4A shows the solution previously introduced in [347], in which each finger is independently actuated, while 8.4B shows an upgrade of that version that further simplify the assembly/deassembly of the device and further improve adaptability and wearability, in which fingers are coupled by two differentials and only two actuators are needed.

The mechanical transmission between differential outputs and finger phalanges has been developed to implement the concept of postural synergies, introduced by the neuroscientific studies summarized in the previous section. In particular, the position and dimension of the exoskeleton linkages have been defined to reproduce the first postural synergy on each finger. At the same time, the differential mechanism allows to maintain the fingers independent. In other words, for each finger the transmission mechanism is designed to replicate the same coordination between the proximal and intermediate interphalangeal joints observed in the first postural synergy, but each finger can be independently moved.

The finger actuation system has been developed so that, when actuated, the flexion/extension motion follows, with a suitable approximation, the first postural synergy, as previously introduced. A kinematic analysis was therefore carried out to show how the trajectory of the exoskeleton matches with the human one [363, 364]. The simplified kinematic scheme of the transmission is represented in Fig. 8.5 A. From the kinematics point of view, the finger actuation mechanism is composed of 5 rigid links: the actuator (a), represented by two rigid bodies, links 1 and 2, actuating the intermediate phalanx, and link 3 actuating the proximal phalanx. It's worth to notice that the element (a) represents the linear actuator for the device in which each finger is independently actuated, and the differential output when the fingers are coupled. The rigid bodies are connected by 5 revolute (R) joints and a prismatic (P) joint (the actuator, not represented in the scheme), resulting to have 3 DoF. When the exoskeleton is worn on the finger, the finger kinematics structure *closes* the mechanism. The resulting kinematic chain has 7 bodies
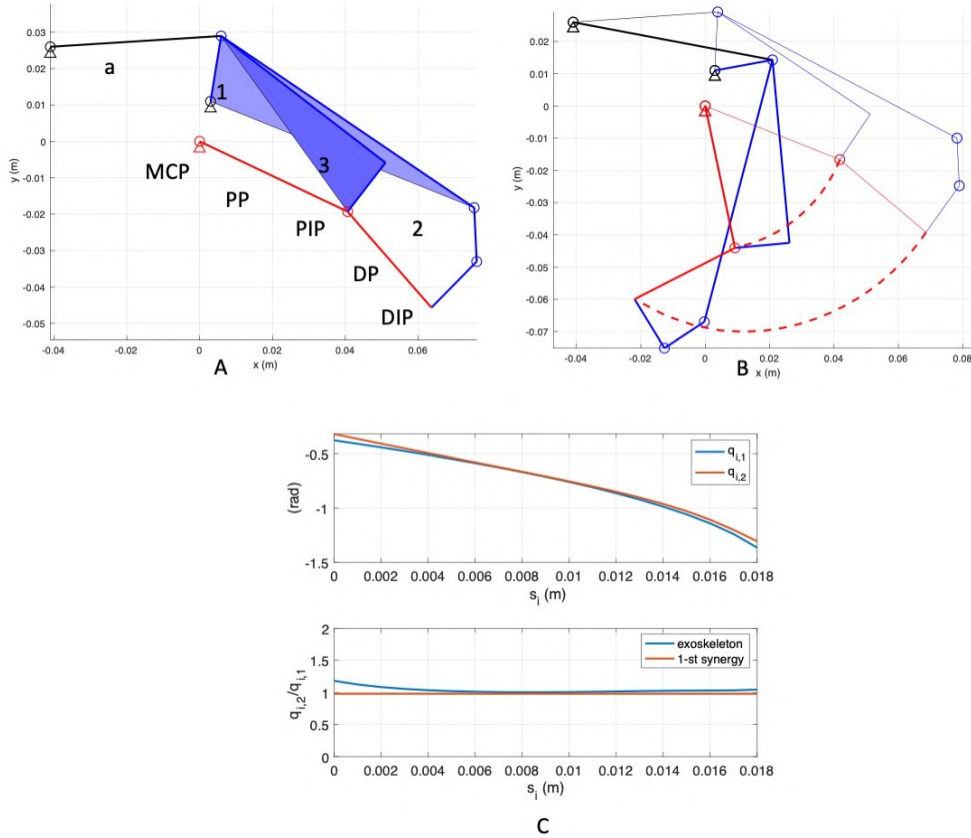
Figure 8.6: Kinematic scheme of the finger actuation system. **A** Kinematic scheme. The system is composed of an actuator (a), two links for intermediate phalange actuation, connected to the finger in correspondence with the DIP joint (elements 1 and 2), and a link for proximal phalanx actuation, connected to the finger in correspondence of the PIP joint. Red links represent the simplified f2-DoF finger structure. **B** Kinematic simulation. Thin lines represent the reference initial configuration, thick continuous lines represent the final close configuration, red dashed curves represent PIP and DIP point trajectories. **C** Results of kinematics analysis relative to the index finger module. Upper diagram: MPC and PIP joint rotation angles, $q_{1,i}$ and $q_{2,i}$ as a function of input (actuator or differential) stroke, indicated with z. Lower diagram: ratio between joint rotation angles, $q_{2,i}/q_{1,i}$ as a function of z, compared with the value obtained from the first postural synergy defined in [243].

(the above introduced links and finger proximal and intermediate phalanges), connected by 9 R-joints and 1 P-joint, with 1 residual DoF. A straightforward kinematic analysis allows to estimate finger motion as a function of the stroke applied by the element (a).

Fig. 8.5 B shows system initial (thin lines) and final (thick lines), and PIP and DIP
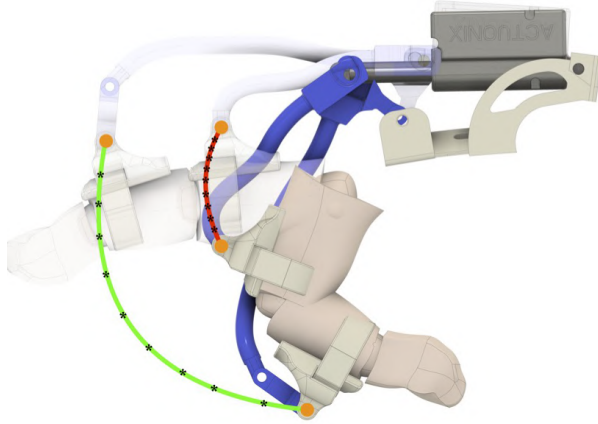
Figure 8.7: Multibody simulation of the finger exoskeleton worn on the index finger, performed to verify that during closure motion, exoskeleton elements do not interfere with the finger.

point trajectories. Fig. Fig. 8.5 C reports in the upper diagram the variation of index MPC and PIP angles, indicated with $q_{1,i}$ and $q_{2,i}$, respectively, as a function of element (a) stroke, indicated with s, while in the lower diagram the ratio $q_{2,i}/q_{1,i}$. It's interesting to notice that both $q_{1,i}$ and $q_{2,i}$ varies almost linearly with respect to s, and that therefore the ratio $q_{2,i}/q_{1,i}$ is almost constant. Such a ratio is very close to the value that can be obtained as $\tau = S_{1,7}/S_{1,6}$ (reported as a red horizontal line in the diagram). This result confirms that the exoskeleton finger actuation couples the MPC and PIP joints so that the finger follows the first postural synergy when its closure motion is guided by the exoskeleton.

Similar results can be obtained for the middle finger, From the above mentioned results, it is possible to directly correlate by means of a linear relationship the synergy inputs for the single fingers $z_{1,i}$ $z_{1,m}$ to differential output strokes s_i, s_m, i.e. it is possible to find four coefficients, a_i, b_i, a_m, b_m, such that

$$
\begin{aligned}
s_i &= a_i z_{1,i} + b_i, & (8.7) \\
s_m &= a_m z_{1,m} + b_m, & (8.8)
\end{aligned}
$$

and, finally, the input stroke provided by the linear actuator is related to s_i and s_m by the differential relationship introduced in eq. (8.6).

Future improvements of this work will be devoted to analyse the sensitivity of these results with respect to model uncertainties and user's personal anthropometric parameters. Such studies will consider not only finger movements but also other more complex and coordinated tasks, e.g. grasping. For this purpose, other types of simulation tools will be considered, as for instance the one proposed in [365].

The shape of the links have been designed to avoid interference with the finger during closure motion. Once the mechanism elements have been designed by means of a 3D CAD, a simple multibody configuration analysis was performed to verify that during the closure

Figure 8.8: Models of the index module used for FEM analyses. In all the subfigures the finger's support is made with ABS while the ring is composed by soft plastic material. **A** CAD model of the old index finer module solution, where the mechanism and the linear actuator's support are made in ABS. **B** is showing the CAD models of the new index finger module solution, where the finger mechanism and the differential mechanism support are made in aluminum. Blue arrows represent the applied forces while the area signed with a white padlock indicates the costrained parts.

motion the links do not interfere with subject phalanges. The results of this analysis is reported in Fig. 8.6, in which the finger in the final closed configuration and the PIP and DIP point trajectories are reported.

8.3.3   Structural Analysis

In this section we summarize the results of a set of basic structural analyses aimed at evaluating the structural resistance of the device and to select the materials to be used in the manufacturing phase. The structural analysis has been carried out on the finger actuation structure and on the differential mechanism components. Both the exoskeleton structures previously introduced have been considered.

The materials that have been considered for the mechanical structure of the finger and for the differential components were ABS, aluminum and steel. For the actuator and the differential mechanism support ABS has been considered. Finger supports for phalanges have been realised with ABS, while soft plastic has been used for the rings connecting the phalanges to the device. The studies have been realised with FEM analysis using 3D-CAD/CAE Autodesk® Fusion 360 software.

Finger actuation structure

The two exoskeleton solutions previously introduced can be used with the same linear actuator or with the differential, they only differ in the mechanical structure that allows to assembly/deassembly the module, then for all analysis we neglected the linear actuator and we focused on the mechanical structure study only.

To make a comparison under similar conditions, we investigated the module designed for the index finger for both the solutions. The analysis was conducted considering differ-
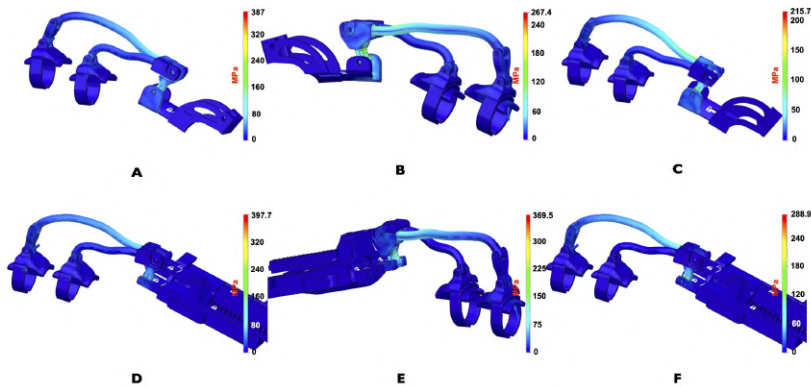
Figure 8.9: Results of the FEM structural analyses. Equivalent Von Mises stress distributions when a 20*N* magnitude force is applied on the distal part. The first row of subfigures reports the results for the previous finger module solution, when the materials used for the finger's links are ABS (**A**), aluminum (**B**) and steel (**C**). Subfigures **D**, **E** and **F** report the results for the new finger module solution when the materials used for the finger's mechanism are ABS, aluminum and steel, respectively.

Finger Module	Force	ABS		Aluminum		Steel	
		Von Mises	Displ.	Von Mises	Displ.	Von Mises	Displ.
	N	(MPa)	(mm)	(MPa)	(mm)	(MPa)	(mm)
Old	20	387.00	63.02	214.50	4.29	215.70	2.87
Old	-20	486.20	86.95	267.40	5.60	269.10	3.67
New	20	397.70	46.04	255.10	1.88	288.90	0.70
New	-20	763.8	74.14	369.50	3.16	429.40	1.28

Table 8.1: Synthesis of the FEM analysis results in terms of stress and displacement with 20N of applied force magnitude.

ent configurations, varying from the completely open to the completely closed one. The most critical loading condition corresponds to the completely open configuration. For the sake of conciseness, only the results relative to that configuration have been reported. In Fig. 8.7, the two finger actuation structure with two of the three materials previously defined are shown. The figure also shows the points where the forces are applied and the constrained parts by using a blue arrow and a white padlock, respectively. Forces are applied to the extremity of the structure as this part is considered to be the area involved the most in the hand rehabilitation process, aimed at reproducing the physiotherapist's force during finger flexion/extension exercise. The magnitude of the applied force is 20*N* both when the force points upward Fig. 8.7A, and when the force point downward (Fig. 8.7B). The materials considered are ABS, steel and aluminum.

A subset of the performed simulations are shown in the Fig. 8.8 and 8.9 while Table 8.1 lists the main results of all analysis. It's worth to observe that the maximum stress that can be sustained by a standard ABS is up to 60*MPa* and none of the models gives a
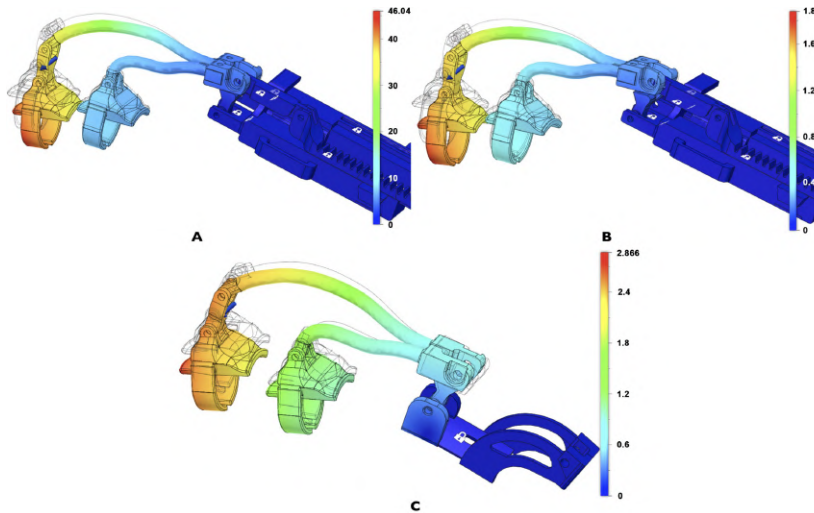
Figure 8.10: Results of the FEM structural analyses for the new (**A**,**B**) and old (**C**) index finger module in terms of displacements. The applied force has a magnitude of 20 N in all the cases, while the materials for the finger's mechanism used is ABS in **A**, aluminum in **B** and steel in **C**.

compatible result with this constraint by applying a force of magnitude $20N$. The results show that none of the two solutions can be realized with this material unless the forces we want to apply are reduced or the structure is modified (increasing the thickness and therefore realising a more bulky device). Regarding steel, the resistance coefficient is much higher, up to $500MPa$. In this case, the results show that in both the solutions have the maximum Von Mises equivalent stress is lower than that limit. Using aluminum, which has a maximum yield stress slightly lower than the steel, the maximum equivalent Von Mises stress values are compatible with material properties. However, since the two materials have different Young's modules, namely $210GPa$ for the steel and $75GPa$ for the aluminum, the maximum displacements are different, even if their values are still limited. On the basis of these analysis, aluminum results the best material, among the analysed ones, for the structural parts of the exoskeleton.

Differential mechanism

We have studied the two main assembled parts that compose the differential, i.e. *the differential gearing* and *the carrier*, to verify the overall stress and deformation level and define the best solution in terms of materials to be used for the realization of the proposed differential mechanism. In Fig. 8.10 the two main parts of the differential mechanism with three different combinations of materials are shown. The padlock indicates the parts of the model in which constraints are set, while the blue arrows indicate the forces that are applied. In all the structural analyses, the magnitude and direction of the applied forces are evaluated by analysing the statics of the whole device when a force with magnitude $20N$ is applied on the finger. For the carrier, Fig. 8.10A, the force is applied on the point
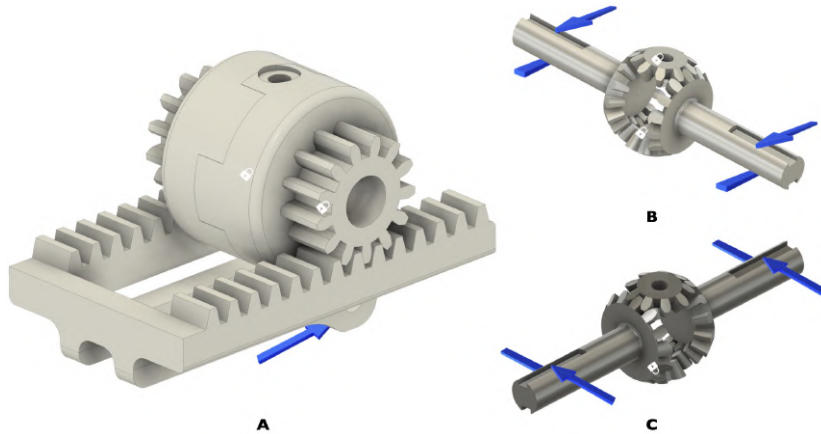
Figure 8.11: CAD model of the differential mechanism main parts used for FEM analyses. Blue arrows represent the applied forces while the area signed with a white padlock indicates the constrained parts for the structural analyses. Subfigure **A** shows the carrier made in ABS material while the other two subfigures show the differential gearing made in aluminum **B** and steel **C**.

in which the actuator connects to the rack and the constrained parts are inside the crown wheel. In order to study the critical points for the differential gears, forces and constraint are applied as shown in Fig. 8.10B and 8.10C, In particular, the constraints are applied to the satellite gears bases while the forces are applied to create a torque on the shafts.

In Fig. 8.11 simulation results are reported in terms of equivalent Von Mises stress, considering different materials. It can be observed that in all cases the FEM analyses return acceptable Von Mises equivalent stress values. All results are under the maximum stress value of the analysed materials. In this case, therefore, ABS could be a good solution because of its lightness, but on the other hand this material presents some drawbacks in terms of wear and friction, which reduces the effectiveness. Also in this case aluminum results to be the best solutions as it is lighter and more flexible than steel.

Table 8.2 summarizes the weights of both finger module solutions and the two main parts that compose the proposed differential mechanism, based on the material used. Form this table and from the above presented results the outcome is that the best solution, in terms of materials is aluminum for the structural elements of the proposed device.

8.4 Prototype

This section presents the exoskeleton prototypes developed with the finger structures and the differential mechanism previously described. The exoskeleton is developed to be worn on the back of the hand, facilitating the user in flexion and extension motions.

Even if from the analyses presented in the previous section it results that the optimal choice for the material composing structural parts is aluminum, in this phase of the development the first prototype was realised in ABS using manufacturing techniques
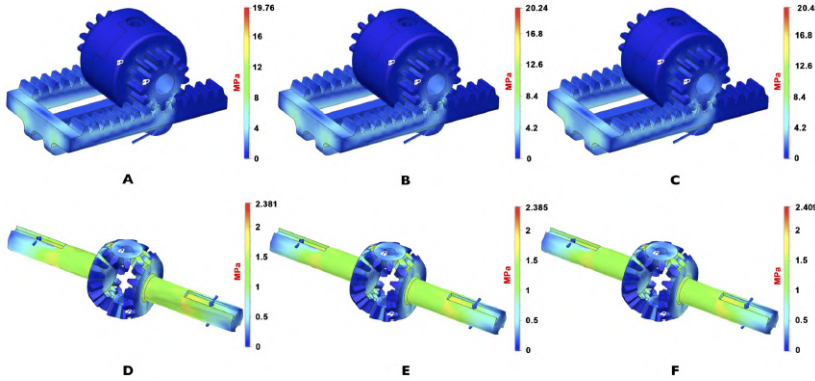
Figure 8.12: Results of the FEM structural analyses on the differential, equivalent Von Mises stress distributions. The first row of subfigures reports the results, for the carrier, of the FEM analysis when the materials used are ABS (**A** - max. Von Mises 19.76MPa), aluminum (**B** - max. Von Mises 20.24MPa) and steel (**C** - max. Von Mises 20.48MPa). Subfigures **D**, **E** and **F** report the results for the differential gearing when the materials are ABS (max. Von Mises 2.38MPa), aluminum (max. Von Mises 2.39MPa) and steel (max. Von Mises 2.41MPa).

	ABS weight (g)	**Steel** weight (g)	**Aluminum** weight (g)
Finger module	43.91	99.97	57.45
Differential	1.74	12.88	4.43
Carrier	9.07	67.13	23.09
Total	54.72	179.98	84.97

Table 8.2: Weights of the main parts of the exoskeleton.

which are commonly available.

In particular, FDM technique (Fused Deposition Modelling) was used to manufacture all the components. For the design and development of the exoskeleton we followed a specific procedure, as outlined in [366], that can be briefly summarized in: CAD modeling with Autodesk Fusion 360, conversion of the CAD model to STL, tranfer the STL file to the 3D-Printer. For the physical realization we used the 3D-printer *Stratasys F123*. The mechanical components were printed using the software GrabCAD Print. Components indicated with B, C, D, E, G, H in Fig.**??** were printed with a slicing height of 0.18 mm, while the other components, which did not need a high surface precision, were printed with a slicing height of 0.25 mm.

The device, is actuated by a linear actuator, that is sited between fingers, blocked in a pocket. The employed linear actuator is the Actuonix PQ-12. This actuator has a low weight, a stroke of $20mm$, that can exert a force suitable to allow the user to apply a maximum equivalent force at the fingertip of $20N$ both in flexion and extension. The force is generated by a DC motor that is connected with a worm gear, which makes the

Technical Features	
Max. Force (lifted)	45 N
Stroke	20 mm
Mass	15 g
Feedback Potentiometer	5 kΩ
Stall Current	550 mA @ 6V
Max Duty Cycle	20 %
Max Speed (no load)	15 mm/s

Table 8.3: Main Characteristics of the Actuonix PQ-12 linear actuator.

motion of the shaft possible. The main features of the linear actuator are summarized in Table 8.3. To control the motion of the linear actuator and to validate the prototype an Arduino Uno is used. Actuator position is controlled according to the scheme presented in Fig. 8.12 B. For a given desired posture, expressed in terms of index and middle joint rotation angles $\mathbf{q}_{des}$, an inverse kinematic procedure similar to the one presented in [244] is used to estimate the corresponding synergy value z_{des}, that is furthermore converted in actuator desired stroke s_{des}. A standard PID controller is then used to control the linear actuator. Control and electronics components are worn on the forearm with an armband as shown in Fig. 8.12. The device communicates via Bluetooth with a PC graphical user interface, that allows to manage and monitor exoskeleton motions [333].

Moreover, the hand exoskeleton is a module of a more complex device, which is designed for helping people with injuries of the upper limb [333]. This device includes a module specially designed for the rehabilitation of the wrist, that involves the implementation of a transmission based on tendons to actuate the wrist motions. It is made of thermoplastic material, such to be adapted to user's specific needs.

8.4.1 Experimental Validation

The prototypes of the exoskeleton presented in this work has been tested and compared with its previous versions. Six subjects aged 24-30 years, 4 males and 2 females, wore a CyberGlove3 (CyberGlove Systems.inc, US), a commercial hand tracking system with 22 joint angle sensors, and then they wore the previous version of exoskeleton described in [347], as shown in Fig. 8.12 and with each of these they completed 5 opening and closing repetitions. They repeated the task wearing the new exoskeleton and in addition, each participant completed a further cycle of five openings and closings with one side of differential mechanism mechanically blocked by the experimenter. Each subject took part in the entire experimental validation, gave her/his written informed consent to participate, and was able to interrupt participation at any time during experiments. The experiment protocols followed the declaration of Helsinki, and there was no risk of harmful effects on subjects' health.

Through the CyberGlove3 the joint values of the metacarpal and the proximal of the index and the middle of each participant were recorded. The range of the movement performed with the two versions of the exoskeleton was then evaluated as the absolute
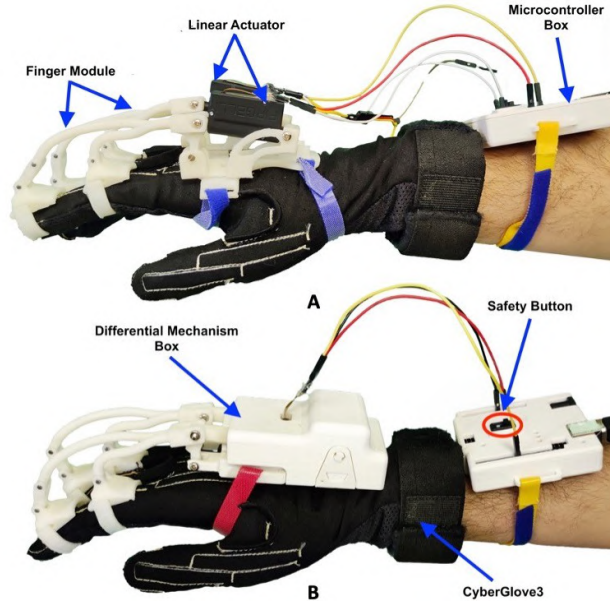
Figure 8.13: Experimental setup for the validation phases using the CyberGlove3. Subfigure **A** shows two previous finger modules while subfigure **B** shows the proposed device, both worn by the user.

difference of the mean values of each valley with the mean values of each peak immediately following.

The experimental results show that the new exoskeleton in free conditions extends the range of motion of the wearing hand by about 10% and just under 100% in the case of one side of the differential mechanism has been mechanically blocked. It has been observed that the metacarpal joints make a movement wider than 14,02±6.84% with the free differential mechanism and 90.02±8.34% with the blocked mechanism, while the proximal joints extend their mobility by 13.21±6,67 % in the first case and 69,61±27.03% in the other. One of the experimental trials is reported in Fig. 8.13.

8.4.2   Using the device with commercial tracking system

Further tests were conducted to demonstrate the usability of the proposed exoskeleton with a widely diffused and affordable commercial optical tracking systems. This aspect is important to let the device to be used in real rehabilitation contexts beyond research laboratories, in which sophisticated tracking system can not be adopted due to high costs and complexity. Specifically, the possibility of using the exoskeleton with the LeapMotion Controller (UltraLeap.inc, US) was tested as is shown in Fig. 8.14. The metrics used to evaluate if the device can be used with this type of connection system is the number of average disconnections during a bimanual task: results obtained with and without the exoskeleton were compared.

Six subjects aged between 24 and 30 years, 3 males and 3 females, participated in the
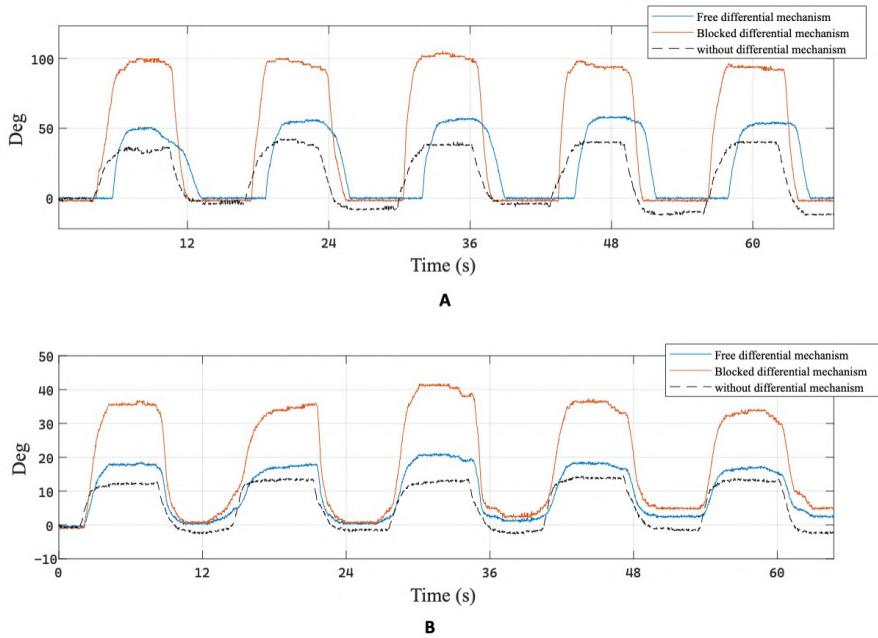
Figure 8.14: Joint rotation angles of the (A) metacarpo-phalangeal (MCP) and (B) proximal interphalangeal (PIP) joint of the middle finger recorded by the CyberGlove during a single repetition of the physiotherapy task. Blue curve represents joint angle obtained with the exoskeleton equipped with the differential mechanism, red curve represents the rotation of the same joint when the other finger is blocked, black curve represents joint rotation obtained with the previous version of the exoskeleton.

experimentation campaign, they were asked to complete three test cycle composed of five opening and closing movements performed simultaneously with both hands, the left one without exoskeleton while the right one assisted by the exoskeleton. Also for this other experimental campaign, each subject took part in the entire experimental validation, gave her/his written informed consent to participate, and was able to interrupt the participation at any time during experiments. The experiment protocols followed the declaration of Helsinki, and there was no risk of harmful effects on subjects health.

In particular, the subjects involved in the experiments were volunteer collaborators of our laboratory, with extensive experience in testing new wearable devices. General precautions and safety measures were implemented as far as possible to prevent risks for all the people involved in device development, including (i) supervision of all experiments with the developed devices by at least one technically skilled supervisor that is able to interrupt the device function immediately in case of technical dysfunction or discomfort of the subjects; (ii) software tools to detect malfunction and automatically inactivate the
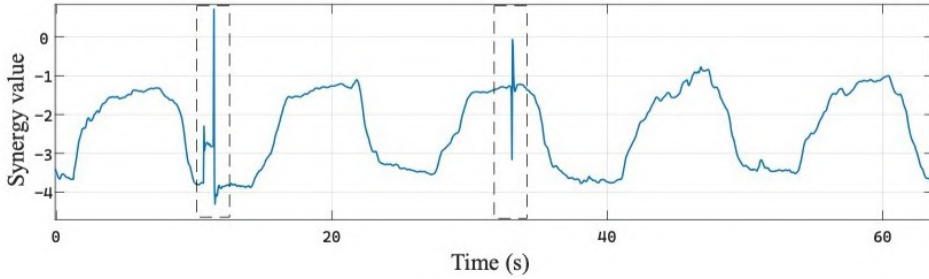
Figure 8.15: Use of the proposed exoskeleton with the LeapMotion Controller. First synergy activation value z estimated during the acquisition of the LeapMotion Controller during a the physiotherapy task. The dotted rectangles highlight the time interval in which the tracking system loose the hand in the frame.

devices if necessary; (iii) physical measures to detach the participants from the devices in case contact forces exceed a certain limit. Subjects involved in the project were not be exposed to unnecessary risk. Additional safety procedures were applied to comply with the COVID-19 pandemic-related issues. No personal data relative to the subjects were collected during the tests.

The movements were constantly acquired through LeapMotion and mapped joint-to-joint in the movements of two virtual hand avatars on the screen placed in front of the participants.

The number of hand-lost for both hands and the status of the Tracking system during the experimentation were recorded and the obtained results and reported in Table 8.4.

The results show an inevitable difference in the number of hand-lost between the free hand and the hand assisted by the exoskeleton, the free hand is always tracked better or equally than the hand assisted by the exoskeleton. The average number of hand-lost in a time interval of about $60s$ is equal to 1.44 ± 1.19 for the assisted hand and 0.78 ± 0.88 for the free hand. However, as can be seen from the graph shown in Fig. 8.14 B, the number of disconnections of the assisted hand and the duration of the same with respect to the length of the task is overall not excessive. These results allow to assert that the the tracking system and the assistive exoskeleton can be jointly used in rehabilitation exercises. The outcome of these tests, therefore, allows us to conclude that the physiotherapy exercises performed with the presented exoskeleton can be recorded and remotely monitored through commercial systems with low economic impact and wide diffusion.

8.5   Conclusions

In this work we presented an actuation system for a hand finger exoskeleton in which the motion of two adjacent fingers is coupled by a differential mechanism. The developed gear-based differential mechanism homogeneously distributes actuator's force, while keeping independent the motion of the coupled fingers, so that if one of them is blocked because

	1	2	3	4	5	6	7	8	9	10	11	12	13	14	15	16	17	18
Cl	B	B	G	G	G	G	G	G	G	G	G	G	G	B	B	G	G	G
Br	G	G	G	G	G	G	B	B	B	G	G	G	B	B	B	B	G	G
Ex	2	1	1	0	0	2	2	3	1	2	1	0	2	4	3	2	0	0
H	0	1	0	0	0	1	2	2	1	0	0	0	1	2	2	2	0	0

Table 8.4: Number of times the hand assisted by the exoskeleton was lost by the LeapMotion Controller tracking system for each individual trial depending on the quality of brightness and cleanliness of the sensor reported by the diagnostics software: "G" means good, "B" bad.

in contact with an obstacle, the other one is still able to move.

The reduction of the number of actuators is a significant advance for the device that is lighter, less complex, and with a lower energy consumption, therefore with a longer battery life cycle. In addition the updated transmission system allows to obtain a range of motion of the phalanges about 10% wider than the previous version, with the same actuator stroke. The device has also been tested in terms of compatibility with a simple and widely used tracking system with low economic impact, such as the LeapMotion Controller to demonstrate that with the presented version of the exoskeleton it is not only possible to carry out physiotherapy tasks but also to record and monitor them remotely, thus allowing to expand the rehabilitation possibilities and opportunities for patients, doctors and physiotherapists. The compatibility with widely diffused tracking systems also allows to increase the acceptance of physiotherapy allowing patients to interact with virtual worlds and scenarios making the therapy an interactive, playful and/or competitive act with themselves or with digital avatars and artificial intelligence.

The first impressions received from the user involved in the design phase turn out to be positive and optimistic, he considered the device lighter and more practical with respect to other devices as well as he considered natural the movement and. Overall the device was evaluated as comfortable both for wearability and functionality. A still open challenge is represented by the mechanical resistance, it has been verified from numerical simulations that ABS is not a suitable solution for the most involved components, in terms of maximum stress and friction, however this type of material has been employed in the first prototyping phase because manufacturing technologies for this material are widely available. Future developments of this study will include the realisation of prototypes with higher resistance materials (e.g. aluminum).

Chapter 9

Haptic Palm Redesign For Manual Therapy

In this chapter we present the redesign of HapticPalm, the wearable device based on a 3-DoF parallel robotic structure presented in Chapter 7, to make this suitable to exert manual treatment of specific hand diseases. The work focuses in particular on the design of the contact interfaces between the device end effector and the palm, that have to simulate the interaction with different surfaces.

9.1 Motivations

The use of robots or robotic devices in rehabilitation is rapidly increasing: as stated by *Mordor Intelligence*, rehabilitation robots market is expected to register a compounded annual growth rate of about 26% over the 2021 − 2026 period. The motivations of such an increasing trend are manifold. Medical rehabilitation required by people suffering from injuries are often complex, long-term, with psychological and physical dimensions, and outcomes are difficult to guarantee. Robot rehabilitation therapy can deliver high-intensity training, without the need of a continuous physical interaction with physiotherapists. However, one of the main concerns for the implementation of the rehabilitation is usually the cost and the technical complexity of the robotic devices. In this work we focus on hand rehabilitation.

Our primary tactile interactions with the world around us are provided thanks to our hands. According to Klatzky and Lederman tactile feelings in the palm impact hand-closing interactions [275]. Unfortunately, traumas, fractures, sprains, tissue pathologies, and illnesses that cause persistent pains or syndromes occurs frequently in the hand. Usually, hand issues can be treated by following two main different paths: conservative clinical therapy or, in severe cases, surgical treatment. Conservative clinical therapy basically consists in patient education to pain control, desensitization therapy, gradual exercises to increase the strength and flexibility of the affected hand and manual treatment (joint mobilizations, rhythmic stimulation, and force applications) . According to [367, 368], MT can reduce discomfort and enhance hand functionality while the preliminary studies presented by researchers in [369, 370, 371] assessed that MT has analgesic effects and can activates enzymatic anti-oxidative system, reducing the oxidative stress, which is responsible of an inflammatory event cascade, and alleviating the pain.

Nowadays different haptic technologies are combined with Virtual reality environments, games and robots for rehabilitation purposes [372, 373, 374]. Research in the haptic field for hand rehabilitation has produced practical tools and specific therapy for hand joint, ligament, skin issues and pain. In [375] by using a multi-finger device, Ferre
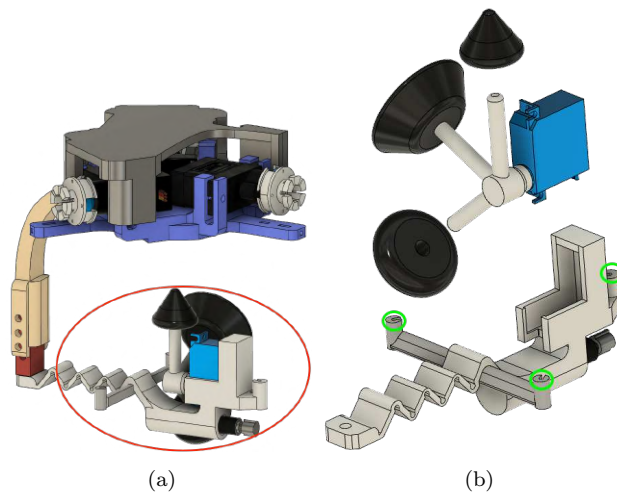
Figure 9.1: In (a) the HapticPalm redesigned to exert manual treatment. The palm part changed respect the version presented in Chapter 6 are red-circled and also magnified in (b)

et al., created a haptic framework that collects and replicates manual therapy techniques while Bouri et al. in [376] presents an innovative haptic device able to activate hand joint reproducing the MT for hemiplegic children rehabilitation.

In this chapter we present the improvements and the applicability of HapticPalm, the wearable haptic device based on a three-DoF parallel robotic structure, previously introduced in Part I Chapter 7 for rehabilitation application in virtual scenario as a motivational tool for people with hand pain/impairments. The system and the new wearable haptic device is shown in Fig. 10.1. In particular in this work we will: i) briefly describe the HapticPalm for hand palm stimulation based on tendons; ii) introduce the new improved version of HapticPalm end-effector and the design of new interchangeable modules able to provide compliant and vibrating stimulation on hand palm as it is suggested in [377, 378] iii) detail the new device parts from a mechanical and manufacturing point of view, including finite element method (FEM) and modal analysis, hardware and control description; v) present a working prototype of the device with a preliminary VR scenario.

9.2 Device Redesign for Manual Treatment

While The upper part of HapticPalm doesn't change, its end-effector has been redesigned:

- a "wave"shaped compliant link, inspired by [379], supports the modules,
- three elements for easy connection/disconnection of the tendons are included into the design,
- an autonomous interchanging mechanism of modules is added.

The resulting design of the medical version of HapticPalm is appreciable in Fig. 9.1). The first is connected directly to the part on the back by means of a "C"shaped rigid link

Figure 9.2: Modules of the new HapticPalm. M1 the plane-shaped module, M2 and M3 the spherical modules.

previously described while the remaining parts are connected to the actuation system through the tendons. With respect to the version presented in [264] the compliant mechanism allows the tip-palm disconnection when no contacts and forces have to be rendered on the palm. The connection points between tendons and the HapticPalm end-effector components have a triangular structure made up of three links with a *ad hoc* locking system for the cables (highlighted by the green circles in Fig. 9.1). The new end-effector consists of a shaft, directly connected to a micro servo, which is able to rotate to change module, since it hosts three different shafts on which different modules are connected. The modules are arranged in such a way to have a different contact shapes when a rotation of 65°, clockwise or counter-clockwise, of the micro-servo is applied, covering totally a range of 130°.

The new modules are very easily interchangeable, since they present just a hole in the bottom part, allowing to assemble/disassemble them without the use of any tool. In this way we maintained the old characteristic of the HapticPalm end-effector, i.e. the interchangeability of the modules (see Fig. 9.1), while the mobile element allows to feel different stimuli on the palm without the need of manual intervention. Three contact modules were realized (Fig. 9.2): a plane-shaped one (M1) that slightly modified with respect to the previous version, to introduce special edge reproducing the contact with edges and flat shapes respectively; two spherical modules with different curvature radii (M2 and M3) reproducing curved surfaces/corners and providing to the user different kind of pressure cues on the palm. The literature reports that pressure associated with vibrations provides different benefits depending on the select frequency. In particular, in a range of frequencies between (50 - 400) Hz the following benefits can be observed: muscle relaxation occurs at 50 Hz, spasticity is inhibited at 100 Hz, pain is relieved at 200 Hz, and muscles are trained up to 300 Hz [378]. HapticPalm end-effector has been therefore designed to to house a vibromotor, needed to provide vibrations to the palm corresponding to the above mentioned clinical requirements.

9.3   Structural analyses

The wearability and manufacturing constraints that guided the design process lead to a structure that could undergo to relatively high stationary and dynamic solicitations. In order to evaluate the mechanical resistance and the vibration characteristic of the mechanical structure of the device a set of Finite Element Analyses were carried out. The
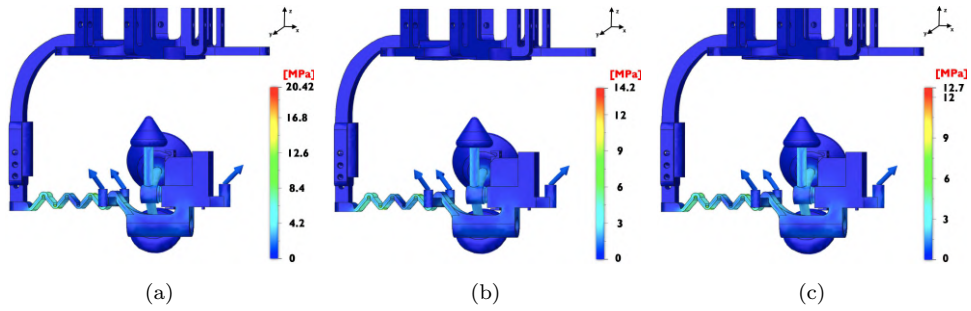
Figure 9.3: Results of the FEM structural analysis. The blue arrows indicate the forces applied in the simulations, corresponding to tendons. Equivalent stress values obtained when (a) a pure normal force, aligned with z-axis, (b) a force with components along y and z, and (c) a force with components along x and z, are applied to the palm

software that we used for this purpose is AutoDesk Fusion 360. We started with a static structural analysis and then we evaluated the response of the device to the vibrations induced by the vibromotor when vibration cues are applied.

9.3.1 Stationary Structural Analysis

The aim of the FEM analysis is to evaluate the stress response of the end-effector when it is constrained and/or loaded in different ways, reproducing the application of a specific pressure on the hand palm. The considered materials for the static structural analysis is ABS. The forces are applied in the three areas where the tendons are connected, in order to simulate their tension when they act on the end-effector. The constrain is applied at the top of the connection site of the end-effector (lower-left part of see Fig. **??**). The analyzed loading cases are:

Case 1 Three forces with the same magnitude F are applied along the z-axis (Fig. **??**).

Case 2 The tendon along the y-axis is exerting a force with magnitude F, while the other two with exert forces with magnitude $F/2$. This load configuration represent the case in which the device exerts a feedback force on the left/right part of the hand palm (Fig. **??**).

Case 3 The tendon along the x-axis pulls the end-effector with F force, while the tensions on the other two tendons are $F/2$. This time the configuration represents the case in which we want to move the end-effector on the upper/lower part of the hand (Fig. **??**).

Results relative to the numerical simulations in which $F = 1N$ are reported in Fig. **??**. It is evident that the most stressed zone of the end-effector in each case is in correspondence of the compliant wave link.

9.3.2 Modal Analysis

Since in this version of the end-effector a vibromotor was installed, we carried out a modal analysis that is coherent with the vibration frequencies that can be reproduced with it
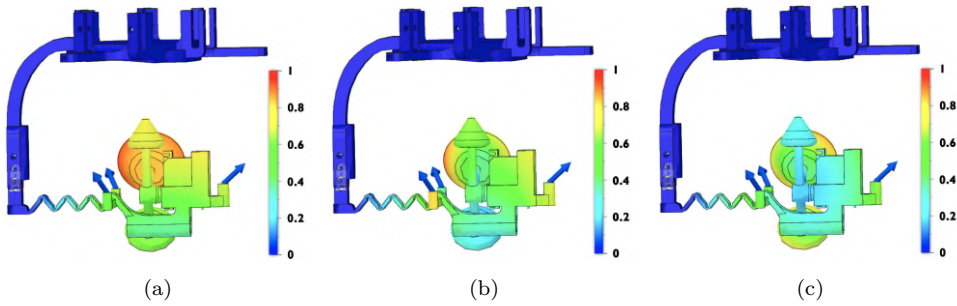
Figure 9.4: Results of the modal analysis. (a)110Hz (b) 215Hz (c) 375Hz

by taking into account the frequencies useful for physical benefits already described. We searched 8 modes of vibration in the frequency range of (50-400) Hz. We brief report three results of them Fig. 9.3, interesting in particular the end-effector. It is evidenced that in that cases Fig. 9.3 and Fig. 9.3, i.e. respectively 110 Hz and 215 Hz, the vibration is transmitted to the palm in a good way, especially in the first case.

9.4   Prototype

The prototype of the HapticPalm device for rehabilitation propose in virtual scenario is shown in Fig. 10.1. All structural components are produced using an FDM (Fused Deposition Modeling) technique with ABS material. Three MG-90S microservos with a 5V battery are employed to transmit forces to the HapticPalm end-effector. They have a 0.20 Nm stall torque. The Elegoo Nano V3+ microcontroller (ELEGOO Inc.,CHN), is employed for the control and data processing part while serial communication was used for transmission with the virtual environment.

As stated before, a 3-DoF, tendon-based, parallel transmission is used to produce the force on the hand palm. The cables are attached to the "Y-arranged"links of the end-effector on one side and on the other to the pulleys of the motors, located on the platform worn of the back of the hand. The thread length required to link the end-effector to the platform on the back of the hand when it is under tension determines the minimum size of each tendon. The pulleys contain an external part that enables the extra tendon to be wrapped in order to modify the cables length to adapt the device to different user hand sizes.

Moreover, the device is embedded in a glove with a suitably designed hole in the center of the palm allowing the direct contact with the end-effector. The glove is employed to avoid uncertainty in orientation and to assist or guide the user's hand between the tendons when wearing the device. The end-effector houses a BMS-303 Micro-Servo and a Micro 612 coreless vibration-motor in order to change the module in contact with the hand palm and to allow the user to have vibrations on the palm according to the previously mentioned clinical requirements. Finally the end-effector is passively supported by the 3D-printed compliant "wave"shaped link, as previously introduced, that allows to detach

the end-effector from the palm when no contact rendering is needed.

9.4.1 VR Application

To use the device exploiting the different types of contacts, we have developed a virtual reality scenario. The scenario was created in Unity, graphic engine, and each of the objects can interact with in the simulated environment. The two objects are made to test the end-effector modules. Specifically, the cube is for testing the M1 and M3 modules, while the sphere for M2 module. In particular, as soon as the user positions the avatar hand over one of the objects, with the HapticPalm worn, the appropriate module will be automatically selected. As soon as the avatar hand moves towards the object and virtually touches it, the user will start feeling the interaction through the device. It is also possible to activate the vibration during the interaction by selecting the check box highlighted. In this way, the device can be used both for enriching the navigation is VR environment through haptic feedback on the palm, and for making the physiotherapy exercises more interactive and therefore enhancing the rehabilitation process.

9.5 Conclusion and future works

We presented an upgrade in the design of HapticPalm, a wearable robotic device for hand palm. The new end-effector design was improved taking into account the opinion of users that tested the previous device. The new interchangeable modules and the replacement of the spring with a wave-joint shaped link improved wearability and easy of use. In the future, we plan to carry out a comparison between the previous version of the device and the current one in terms of exertable force, usability and immersivity of VR experience. In fact, the introduced vibromotor, allows the user to have a more immersive experience in VR, distracting, in this way, the user from the pain on the hand in case of rehabilitation use. Future improvements will be focused on the optimization of the general structure of the device, to reduce its dimension and therefore to improve its usability and adaptability. A more immersive virtual environment will be created, with new objects and a more user friendly GUI, and a set of user studies will be realized.

Chapter 10

Haptic Pad for CRPS-I Treatments

Figure 10.1: HAPP prototype testing in front of its graphic interfaces.

The aim of this chapter is to present HAPP, a new haptic portable device, designed to help patients suffering of Complex Regional Pain Syndrome type-1 disease, and more in general to investigate the effects of manual therapy for chronic pain illness of the carpus and metacarpus, by mimicking traditional mechanical and rhythmic stimuli characteristics of MTs. Its structure consists of a plate oriented by revolute-prismatic-spherical joints, with a rack-pinion mechanism that actuates the end-effector, stimulating the user's hand palm. We provide details about the device, such as the mechanical design, the mathematical model and a graphical user interface. Preliminary studies in order to evaluate the device force exerted at the user's palm were carried out.

10.1 Motivation

the CRPS-I is a chronic painful syndrome consisting of several alterations of perceived sensation as allodynia (pains for normally elicit pain stimulus), hyperalgesia (abnormal increase of sensitivity to pain), edema (the build-up of fluid in the body's tissue), vasomotor/sudomotor deregulation and tissue trophism modification. These symptoms spread from distal regions of the affected hand/arm to the opposite limb [380, 381, 382, 383]. Traditional clinical therapy for CRPS-I consists in patient education to pain management, desensitization therapy, manual therapy (MT) and progressive exercises to improve the strength and flexibility of the affected hand [384, 385, 386].

[387]. Regarding the effects on CRPS-I, the manual therapy allows to alleviate pains and improve hand functionality, according with [367, 368]. The literature about CRPS treatment with MT is still poor of information about pathophysiology of this syndrome. According with preliminary *in-vivo* investigation, presented in [381, 369, 370], this therapy has analgesic effects in mice, allowing the activation of inhibitors of neuroreceptors (adenosine, opioid, and cannabinoid).
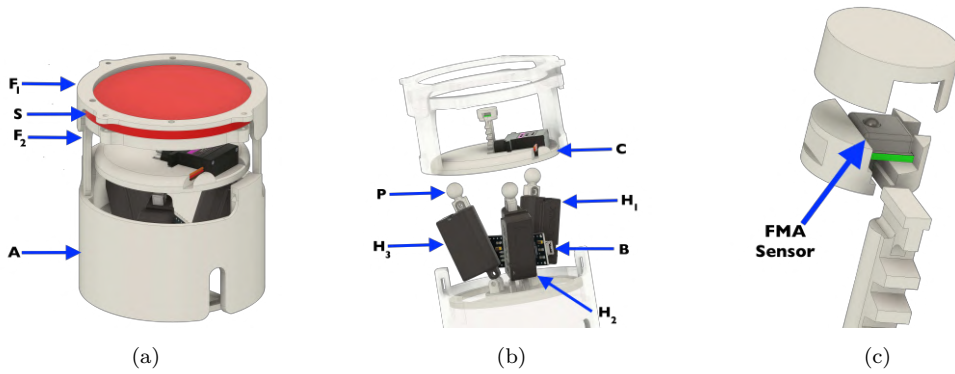
Figure 10.2: HAPP main features. (a), external CAD model. (b) and internal CAD model. (c) CAD model for the FMA sensor housing.

10.1.1   Related works

Haptic technologies are widely used in pre-clinical investigation and then in therapy. For example, it has been shown in [388] that the use of haptic technologies can simplify the transition of children with autism spectrum disorder during occupational therapies. In [179], the authors corroborated the feasibility hypothesis of a mechanical therapy for cardiovascular autonomic control in Parkinson's disease.

Research in the field of haptics has often provided clinical tools for the rehabilitation and specific treatment for joint, ligament and skin issues of hands. As reported in [389] by Choukou et al., different haptic technologies combined with robots ([372, 390, 391]), virtual reality environments and games ([392, 393, 374]) or both ([394, 373]) have been involved for the rehabilitation of the paretic upper limb of stroke patients. Bouri et al. in [376] presented an innovative haptic device designed specifically for the rehabilitation of hemiplegic children, which activates their hand joints, similarly to MT. In [395] and [396], the authors investigated about new haptic technologies to overall problems with handwriting or drawing due to graphomotor issues; they designed technologies and the protocol for the assessment and therapy for eye-hand coordination. Ferre et al., as reported in [375], realized a haptic framework that captures and mimics manual therapy techniques using a multifinger device.

In this work, we present HAPP(see Fig. 10.1), a haptic device for preclinical investigation on correlation between CRPS-I symptoms reduction and MT, and also for clinical treatment of CRPS-I and other diseases of carpus and metacarpus, by mimicking traditional mechanical and rhythmic stimulations proper of manual treatments. The haptic device design presented in Sec. 10.2 consists in parallel kinematic structure with 3-Degrees of Freedom (DoFs) that planarly moves and orients its interchangeable end-effector under the hand palm of the patient and provide locally a different mechanical stimulation according with needs and interests of the researcher; in the current version of the prototype, we designed an end-effector that exerts controlled force, which stimulates predefined contact area of the hand palm. A silicone rubber pad is inserted between patient palm and
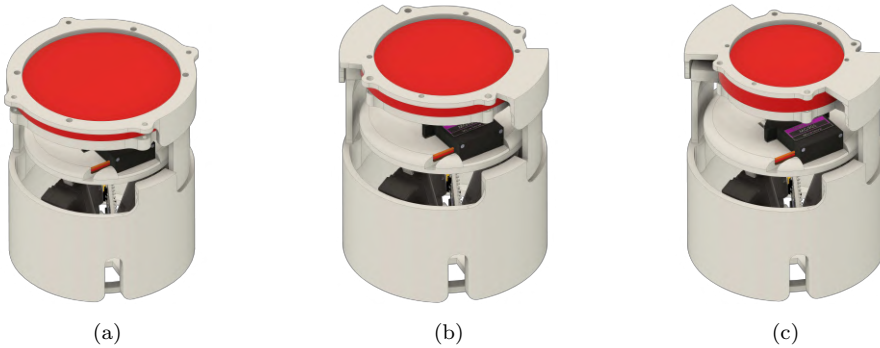
Figure 10.3: CAD model of the top part with different sizes, i.e. large (a), medium (b) and samll (c).

end-effector. This material was chosen to allow the sterilization of the device; however, since the presence of silicone alters the effects of the forces provided to patient, theoretical study and tests for actual device force are reported in Sec. 10.4. Conclusion and future studies are reported in Sec. 10.6.

10.2   Device Description

In this section, we will detail the design and the hardware components used for HAPP. The CAD model of the device is shown in Fig. 10.3: all its components were printed in Acrylonitrile Butadiene Styrene (ABS) using FDM (Fused Deposition Modeling) technique. It is made up of two main parts: a fixed one, called *bottom part* and an interchangeable one, called *top part*. The *bottom part* consists of the housing for the electronic part, the actuation module, and a circular plate that contains the end effector of the device, respectively **B**, **H**$_i$ and **C** in Fig. 10.2. The *top part* is in contact with the user's hand palm and it is designed in such a way to be easily assembled with the support base (**A** in Fig. 10.2) by making a twisting motion.

The device allows the interchangeability of different structures that support the human hand. Indeed, in order to adapt the device to the needs of users with different anthropometric dimension of the hand, the *top part* structure has been made in different sizes, i.e. small, medium, and large (see Fig. 10.3,10.3,10.3). Part **C** of the device constitute the end-effector of the device. This circular plate contains the housing for a servomotor, which is used to actuate the rack-pinion mechanism. The servomotor used is a Kuman MG90S (Kuman Trade Shenzhen Co., Ltd., US) with a stall torque of 25 Ncm at 6V. The shaft allows HAPPto exert the desired force on defined areas of the device that lie on the *top part*. With the aim to allow different types of stimuli at user's palm the shaft head has been made interchangeable.

In Fig. 10.2 the CAD model of the force sensor embodiment is shown. The sensor used is the FMA MicroForce Sensor FMAMSDXX025WCSC3 (Honeywell, North Carolina), a piezoresistive based force sensor that provides a digital output proportional to the force

applied on it. The FMA version with a force range of 25N and an accuracy of 0.5N was chosen and it is interfaced using SPI protocol. It has a maximum digital clock frequency of 800kHz and it is powered with an operating voltage of 3.3V. Furthermore, part **C** of the device plays a fundamental role in the orientation of the end-effector, since its lower part contains the spherical-shaped housings, which constitute the spherical joints between the actuation module $\mathbf{H}_i$ and the part **C**. These spherical housings are arranged in a particular shape, i.e. they are Y-shaped and consequently also the actuators are arranged in the same way. The actuators used are the Actuonix PQ12-P, which have a maximum stroke of 20 mm and exert a maximum force of 45N. The characteristics of these linear actuators are summarized in Tab. 10.1. Three actuators are used to move and orient the plate **C**, which is connected to them through a rigid-spherical link, indicated with **P**. Furthermore, the linear actuators are not positioned vertically with respect to the plate but are inclined by 45° each with the aim to ensure device stability, structural robustness and compactness. The device configuration is controlled with Arduino Nano 3.0.

In order to avoid direct contact of the shaft with the user's palm, the *top part* of the device is made up of two parts, i.e. **F1** and **F2**. They allow the insertion of a material **S**, which is soft to the touch and capable of being sterilized whenever the device is used. **F1** is connected to the *bottom part* of the device, while **F2** is fixed to **F1**. The material inserted between these two parts is made of silicone rubber. The cylindrical elastic pad is realized by molding and curing for four hours bi-component silicone rubber Eco-flex 00-30 (Smooth-On, inc. US) with platinum catalyst. The platinum catalyst allows the containment of the hardness of the silicone in a range of $[0 - 30]$ on the Shore A scale (ASTM D-412). The mold is fabricated by 3D-printing in ABS and coated with a mold releaser, the Easy Release 200 (Mann Release Technologies, inc. US), to ease extract the pad after the cure phase. The chemical properties of this silicone rubber, as we said, allow the sterilization of the pad that is in contact with the patient's palm both with chemical agent 70% ethanol (CH3CH2OH) cleaning reagent and autoclaving, since the silicone rubber hold its elastic proprieties up to 230°C, while the normal autoclaving temperature is about 180°C.

10.3 Mathematical model

10.3.1 Configuration analysis

From the kinematics point of view, HAPPis a 3-RPS (Revolute-Prismatic-Spherical), 3-DoF (Degrees of Freedom) parallel mechanism. Let us indicate with B_i, $i = 1, 2, 3$ the centers of the spherical joints on the *end effector* **C**, with O_1 the center of the circle passing through them, and with b its radius.

Let us also indicate with $S_1 = \langle O_1, x_1, y_1, z_1 \rangle$ a reference frame in which the x_1 axis is parallel to $\overrightarrow{O_1 B_1}$, z_1 is orthogonal to the plane defined by the B_i points, and y_1 is consequently defined. We assume that B_i points form an equilateral triangle, the coordinates of each vertex B_i, expressed in the S_1 reference frame are collected in the three-dimensional vectors $\mathbf{b}_i^1 = [b_{ix}^1, b_{iy}^1, b_{iz}^1]^{\mathrm{T}}$.

Table 10.1: Main characteristics of the PQ12-P linear actuator

Technical Features	
Mass	15 g
Max. Force (lifted)	45 N
Stroke	20 mm
Feedback Potentiometer	5 kΩ
Stall Current	550 mA @ 6V
Max Duty Cycle	20 %
Max Speed (no load)	15 mm/s

Each leg is composed of two links: the first is connected to the fixed base trough a revolute joint, the second one is connected to the end effector through a spherical joint. The links are connected to each other through a prismatic joint. Let us indicate with $\mathbf{u}_i$ the unit vector identifying, for each leg, the direction of the revolute joint axes. We can then define the plane π_i passing through B_i and perpendicular to $\mathbf{u}_i$. The revolute joint axes intersect this plane in A_i points

On the *bottom part*, we define O_0 as the center of the circle passing through A_i, and with a its radius. Let $S_0 = \langle O_0, x, y, z \rangle$ be a reference frame on the *bottom part*, with origin in O_0, x axis parallel to the $\overrightarrow{O_0 A_1}$ vector, z axis orthogonal to the plane defined by A_i points, and y consequently defined. Also in this case we assume that A_i points define a equilateral triangle.

The end effector will move w.r.t. the *bottom part* according to the displacement imposed by the linear actuators and to the kinematic constraints imposed by the mechanical structure. In particular the motion of each leg is plane, i.e. B_i points move on the planes previously introduced π_i.

Indicating with i_*, j_*, k_*, $* = x, y, z$, the unit vectors components corresponding to the axes x_1, y_1, and z_1, respectively, expressed w.r.t. S_0, we can define the corresponding rotation matrix $\mathbf{R}$ between S_1 and S_0. The coordinates of B_i w.r.t. S_0, collected in the three dimensional-vectors $\mathbf{b}_i = [b_{i,x}, b_{i,y}, b_{i,z}]^\mathrm{T}$, can be evaluated as

$$\mathbf{b}_i = \mathbf{p} + \mathbf{R}\mathbf{b}_i^1, \tag{10.1}$$

where $\mathbf{p} = [p_1, p_2, p_3]^\mathrm{T}$ is the three dimensional vector containing the coordinates of O_1 w.r.t. S_0.

Since B_i move on the three fixed planes π_i, the following constraint equations hold

$$b_{1,y} = 0, \quad b_{2,x} = \frac{1}{\sqrt{3}} b_{2,y}, \quad b_{3,x} = -\frac{1}{\sqrt{3}} b_{3,y}. \tag{10.2}$$

Eq. (10.2) introduces three constraints that limit the generic six–dimensional motion of the mobile platform. In particular, since three independent costraints have been introduced, the mobile platform has three DoF.

The position and orientation of the end effector can be defined by the position and orientation of O_1 w.r.t. S_0, described through its coordinates $\mathbf{p} = [p_x, p_y, p_z]^\mathrm{T}$ and Roll(α)–Pitch(β)–Yaw(ϕ) angles $\boldsymbol{\varphi} = [\alpha, \beta, \phi]^\mathrm{T}$, respectively. Since the platform has 3 DoF, we can
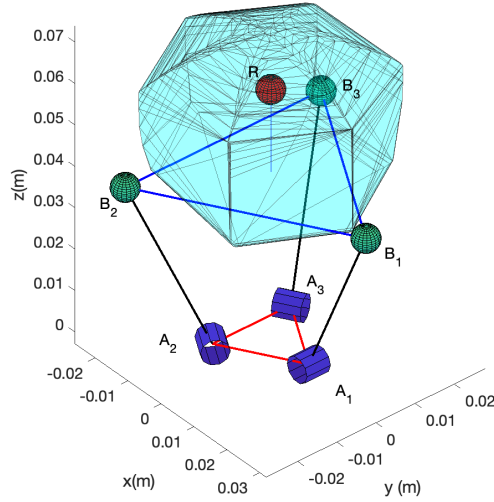
Figure 10.4: HAPP kinematic scheme and and workspace evaluation (cyan solid). The workspace is represented as the set of possible positions that R point can assume, considering actuators' strokes and device kinematic constraints.

select three of these six variables and evaluate the remaining ones. A convenient choice for the *independent* variables includes the displacement in the z direction, p_z, and the roll (α) and pitch (β) angles. Let us collect those variables in the vector $\boldsymbol{\xi} = [p_z, \alpha, \beta]^{\mathrm{T}}$. Recalling the rotation matrix expression as a function of RPY angles,

and the constraints in eq. (10.2), we can evaluate the other variables as

$$\phi = \arctan\left(\frac{\sin\beta\sin\alpha}{\cos\beta + \cos\alpha}\right), \tag{10.3}$$

$$p_x = \frac{b}{2}\left(\cos\phi\cos\beta - \sin\phi\sin\beta\sin\alpha - \cos\phi\cos\alpha\right), \tag{10.4}$$

$$p_y = -b\sin\phi\cos\beta. \tag{10.5}$$

To complete the preliminary analysis of the mechanism, let us analyse the position of the pin on the mobile platform, represented by point R. Its coordinates in S_1 frame are:

$$\mathbf{r}^1 = [0, 0, h]^{\mathrm{T}}, \tag{10.6}$$

using the above mentioned relationships, it is possible to evaluate its coordinates with respect to S_0 frame.

Finally, using the relationships in eq. (10.3),(10.4), and (10.5) it's possible to express pin position as a function of the independent variables, i.e. $\mathbf{r}(\boldsymbol{\xi})$.

Table 10.2: Joint extensions and relative orientation angles of end-effector to reach the four selected points for maximum net force distribution reconstruction.

Point	$p_{H1}(mm)$	$p_{H2}(mm)$	$p_{H3}(mm)$	α (deg)	β (deg)
1	20.0	0.0	20.0	-50.0	50.0
2	20.0	0.0	0.0	0.0	50.0
3	0.0	10.0	20.0	-25.6	25.6
4	20.0	20.0	20.0	0.0	0.0

10.3.2   Inverse kinematics

In the inverse kinematics problem, the independent variables $\boldsymbol{\xi} = [p_z, \alpha, \beta]^\mathrm{T}$ are defined, and we want to evaluate the corresponding displacements $\mathbf{q} = [q_1, q_2, q_3]^\mathrm{T}$ of the linear actuators.

For a given $\boldsymbol{\xi}$, eq. (10.3), (10.4), and (10.5) allow to define the vector $\mathbf{p}$ and the rotation matrix $\mathbf{R}$, completing the representation of the mobile platform configuration. Then, from eq. (10.1), it is possible to evaluate the coordinates of B_i w.r.t. S_0. The actuator displacements q_i can be then evaluated as

$$q_i = s_i - l_0, \tag{10.7}$$

where $s_i = |\mathbf{b}_i - \mathbf{a}_i|$ and l_0 is the actuator length in its reference configuration.

The above described relationships have been used to evaluate the device workspace, i.e. the set of positions that point R can reach, given device kinematic structure and actuator stroke. The obtained workspace, calculated by means of a Matlab script, is shown in Fig. 10.4.

To evaluate the force executable by HAPPon patient palm, a theoretical study and an experimental investigation were carried out. The net theoretical force $\boldsymbol{f}_n$ on the palm depends on the end-effector orientation angles α and β respect normal vector of the silicone rubber plane (in this evaluation, yaw angle ϕ has been neglected, since its value is limited in all the considered configurations).

$$\mathbf{f}_n(t) = |\mathbf{f}_b| \cos(\alpha) \cos(\beta), \tag{10.8}$$

where $|\boldsymbol{f}_b|$ is modulus of the normal force in *bottom part* reference frame evaluated as effect of the end-effector indentation in silicone rubber pad:

$$|\mathbf{f}_b| = \frac{l_2 - l_1}{l_1} \pi \rho_{EE}^2 E,$$

with $\frac{l_2-l_1}{l_1}$ is the material deformation (l_1 and l_2 are the thins of pad before and after indentation), ρ_{EE} is the radius of the end-effector contact area, and E is the approximated Young modulus of neo-Hookean material, evaluated starting from its hardness on Shore A scale σ_A, according to conversion function presented in [397]:

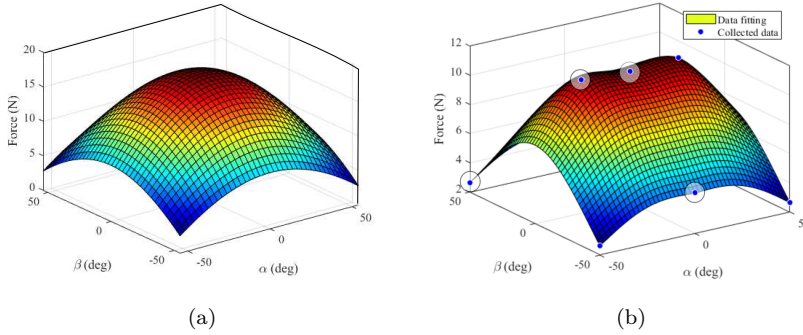$$log_{10}(E) = 0.0235\sigma_A - 0.6403.$$

Figure 10.5: In (a), the theoretical net force distribution through HAPP silicon pad depending on EE orientation angles α and β, in (b) the experimentally estimated net forces reconstructed for symmetry and interpolation by means of repeated force measures in four notable points (circled blue dots).

In accordance with eq. (10.8), the theoretical maximum forces is function of the end-effector orientation angles (Fig. 10.5) that can be evaluated starting from pin position:

$$\alpha = \arctan\left(\frac{r_z}{r_y}\right), \text{ and } \beta = \arctan\left(\frac{r_z}{r_x}\right).$$

10.4 Force Evaluation

On other hand several tests on four discrete points on pad were carried out to evaluate the real HAPPmaximum forces. The tests investigated force on four discretized points, reported in Tab. 10.2 and shown in Fig 10.5, inside a quarter of pad circumference, the results are extendable to complete pad for central symmetry of its geometry. The tests consisted of N end-effector indentation repetitions to apply the maximum forces on the hand of a user, with $N = 10$. The force values are collected by a high-precision ATI force sensor (ATI Industrial Automation Inc., US), placed between pad and human hand by means of glove pocket. Only one subject was involved into force testing, he gave his written informed consent to participate, and was able to discontinue participation at any time during experiments. The experiment protocols followed the declaration of Helsinki, and there was no risk of harmful effects on subjects' health. Data were acquired at frequency of 1kHz. Each pressure peaks were maintained and suspended for a time equal to $\delta t = 8.0$s. The recorded forces $\tilde{\boldsymbol{f}}(t)$ are analysed to extrapolate information about the net forces applied by HAPP, $\tilde{\boldsymbol{f}}_n$, as:

$$\tilde{\mathbf{f}}_n = \frac{1}{2N\delta t} \sum_{n=0}^{N} \left| \sum_{t=n\delta t}^{(n+1)\delta t} \tilde{\mathbf{f}}(t) - \sum_{t=(n+1)\delta t}^{(n+2)\delta t} \tilde{\mathbf{f}}(t) \right|.$$

To reconstruct the force distribution pad surface was conducted a interpolation on collected data, between several mathematical interpolating 3D functions we choose a Thin-plane

Table 10.3: ID signals and their values sent from graphic user interface to microcontroller for HAPP setting, regulation, actuation, and control.

Reference signal	ID	Values
Stimualtion type	s	$[s, v]$
Anthropometric dimensions	d	$[L, M, S]$
Stimulation 1	v	$[0 - 255]$
Stimulation 2	f	$[0 - 255]$
Desired position	p	$[1 - 9]$

spline model with a goodness of fit equal to $R^2 = 0.97$. The experimental results, graphically reported in Fig. 10.5 shown a general reduced maximum forces respect the theoretical estimation, in addition the tests shown that the user over 10 N started to detach the hand from the pad.

10.5   Demonstrative scenario

HAPPwas designed so that researchers and doctors can set up and control the device by using their laptop, in particular they can choose the desired position, force and other stimulus references as well as initial information about the discrete anthropometric dimensions that are then sent to the device via USB cable. For this purpose, the operator has a graphical user interface (GUI) that allows the easy setting of the stimuli through percentage bars and the placement of the piston in one of the nine discrete areas on the patient's palm (See Fig. 10.6). The graphical interface is easily expandable and is extremely modular, allowing the user to modify and increase the contact areas on the request of the researcher and integrate future end-effector modules for further kind of stimulation. The serial connection between laptop and device allows the exchange of data forward and potentially backward allowing the user to view the data provided by the device, such as the force measured by the force sensor, and record them for a retrospective investigation. The communication protocol is optimized to ensure good responsiveness, the references are transmitted forward only if these are modified by the user, the data sent is composed of two bytes, the first carries a modified reference ID and the second carries the value within a range as reported in Tab. 10.3. Fig. 10.7 shows the positions that HAPP can reach by using the before presented GUI.

10.6   Conclusion

In this work we presented HAPP, a haptic device for preclinical investigation of the mechanical therapy effects for pathologies/diseases of the hand, such as the complex regional pain syndrome type-I and stroke, and also for the systematic and remote control of the manual therapy exercises by exploiting its graphical user interface. In particular, with this work, we introduced the concept, detailed the mechanical design, and the mathematical model used, with preliminary studies, in order to evaluate the device force exerted
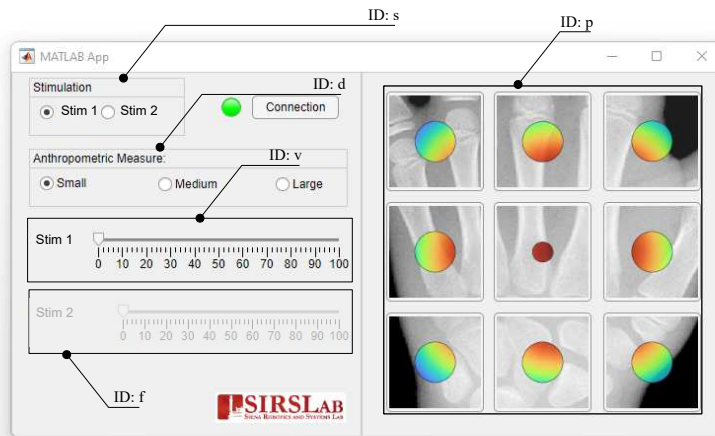
Figure 10.6: Graphical User Interface for HAPP.

Figure 10.7: From left to right, the nine discrete positions reached by the haptic device.

at the user's palm. The device uses a parallel 3-DoF structure position and orient its end-effector under the patient's hand palm and provide local force stimulation. HAPP's end-effector is interchangeable and in this work, a solution to exert the desired force in predefined areas of the user's palm was presented. Despite HAPP is in prototyping phase, it received positive opinions from experts of the rehabilitation field, which consider HAPPa promising device for mechanical therapy of the hand. Future works of this study will investigate the integration and control of the vibration stimulus on defined areas of the hand. Also, instead of controlling the device in position, we plan to implement a PID controller.

The CAD model of a proof of concept was designed. Its design is a trade-off between compactness, functionality, portability and capability of satisfying the initial requirements. The graphical user interface was arranged in advance with a bar that allows to set the vibration intensity. Other future works will include structural analysis, design optimization and studies on a control law that takes into account the force, vibration and additional stimulation to be transmitted to the user's palm. Moreover, a detailed comparison with other devices present in the literature will be done and integration with virtual reality environment systems for gaming, clinical propose, and human studies on device usability will be investigated.

Part IV

Haptics for Mechanobiological Research on Cancer

Haptics for Mechanobiological Research on Cancer

Many of us who conduct biomedical research do so with what could be described as a religious fervor. This would not have come as a surprise to Mary Lasker. She once told a reporter, "I am opposed to heart attacks and cancer the way one is opposed to sin." Amen.

Gregg L. Semenza

C ancer poses a significant threat globally, ranking as the second leading cause of death worldwide and imposing physical, emotional, and financial burdens on individuals, families, communities, and health systems [1].

Every day, 1500 lives are lost due to cancer-related deaths [398]. Local recurrence of cancer represents a significant unmet need, as it often precedes the metastatic dissemination of the disease that negatively impacts both long-term survival and the quality of life of patients [399, 400]. Commonly, cancer can attack any part of the human body. However, the heart is rarely affected by cancer. While it could be intuitive that cardiomyocyte-derived tumors are rare due to their low proliferative potential [401], it is less clear why other cell types that reside in the heart and can replicate are also rarely affected by cancer. Primary tumors of the myocardium are extremely uncommon, with a reported prevalence of around 0.0017% [402]. Additionally, cardiac metastases are also uncommon despite the heart being one of the most vascularized organs and blood constantly flowing through it. Metastasis to the heart often affects the pericardium or great vessels, and not the myocardium [403]. In addition, cancer cells ectopically implanted into the heart form small tumors, which are not vascularized, indicating that the cardiac environment disfavors the growth of both endothelial and cancer cells. However, mechanical unloading of the heart, as happens in patients implanted with a Left ventricular-assisted device (LVAD), results in cardiomyocyte (CM) division and cancer proliferations [404].

For these reasons, one of the most mesmerizing theories that may explain the inhibition of cell growth in the heart is based on the mechano-sensing capability of certain

---

[1]source: www.who.int/health-topics/cancer

cells, such as tumor cells, which activate signaling pathways when they perceive external forces. These pathways may lead to a metabolic stop or apoptosis [405, 406] of cells. **Mechanobiology**[2] has already demonstrated **oncogenesis and cellular Mechanics are related**, in fact:

- Changes in tissue stiffness and density are major drivers of tumor progression and are often exploited in cancer diagnosis by both palpation and imaging [407, 408].

- Mechanical properties (stiffness, elasticity) of the extracellular matrix affect cancer cell growth [409, 410].

However, the role of heartbeat (its pressure or strain) in the inhibition of cancer progression is still unknown, despite this may be exploited for a new kind of cancer therapy.

Current treatments are plagued with severe side effects and primarily rely on systemic therapy for metastatic disease, at a stage when a long-term cure is rarely achievable. These commonly consist of chemotherapy, radiotherapy, and more recently immunotherapy and targeted therapies. For many years, chemotherapy was the standard treatment for surgical cancer removal, but it has had limited success due to its off-target toxicity and the development of drug-resistant cancer cells. On the other hand, the combination of immunotherapy and targeted therapy (i.e. impacting only on cancer cells [411, 412]), has shown promising results in clinical trials for various types of cancer when used alone or in combination with traditional drugs[413], but not all patients respond and they can cause significant toxicity, particularly to the cardiovascular system[414]. Therefore, there is still a need for effective solutions to control local cancer recurrence and dissemination, as there are currently no available options for this. Mechanobiological treatments of cancer could face all challenges regarding local recurrences, exploiting a haptic-based non-invasive treatment of superficial tissues affected by tumors like melanoma.

In this contest, haptic interfaces become an essential tool to shed light on cancer biological mechanisms triggered by a mechanical load of the heart and, consequently, design new treatments for local recurrences. Furthermore, confirmation of this mechanobiological hypothesis would open a new and wide field of application for haptics involving it in the mechanobiological treatment of superficial tumors, such as melanoma and breast cancer. Additionally, existing haptic technologies could easily be re-purposed from tools for mixed reality and traditional medical protocols to devices for preventing tumor recurrences and freezing the clinical condition of a temporarily inoperable patient affected by cancer.

In what follows, two soft tactile interfaces for in-vitro e in-vivo mechanobiological investigations are proposed. The first is designed to replicate the dynamics of heartbeats on cultured cells (Chapter 11), while the latter consists of a soft anklet that provides a rhythmic mechanical cue on the limb of small animal models affected by tumors (Chapter 12).

---

[2]Mechanobiology is an emerging field of science at the interface of biology, engineering, and physics. It investigates how physical forces and changes in the mechanical properties of cells and tissues affect their life, contributing to development, cell differentiation, physiology, and disease

Chapter 11

Heart beat Simulation In-Vitro Model
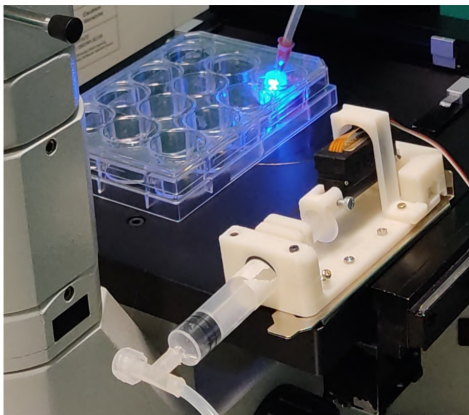
Figure 11.1: The prototype of the proposed device, used in a imaging procedure.

Mechanical stress plays a vital role in the regulation of several cellular processes. To reduce uncertainties in observations, biological research on cells is usually conducted *in-vitro*, i.e. on cells grown in highly-controlled lab environments. Although several devices able to reproduce proper stimuli on cells have been recently proposed, still there are several open challenges. Heart cells, for example, require millimetric wells to survive and grow *in-vitro*. Size of the culture wells for medium-throughput screening, integrability requirements with laboratory techniques, and biocompatibility with living organisms make the development of suitable end-effectors complex.

In this work, we present RobHeart, a modular soft robot with deformable end-effectors, fabricated by layering and molding bi-component silicone rubber, and specifically designed to seed and 3D stress heart cells (see Fig. 12.1).

11.1 Motivation

Mechanical stimulation of cells, indeed, alters their growth, proliferation and differentiation [415, 416, 417, 418]. In the human body, the heart is exposed to one of the highest mechanical stress [419]: Increased mechanical load halts regenerative properties even after birth [420], while cardiac unloading promotes heart cells proliferation and regeneration [421].

Yet, the mechanisms by which mechanical stimulations affect the proliferation of cardiac cells remain largely unknown. This is mainly due to the lack of suitable *in-vitro* and *ex-vivo* devices to reproduce the multiple mechanical stimuli acting on a living heart.

The development of devices to mimic the mechanical stimuli exerted *in-vivo* on cardiac cells is highly needed to define the molecular players controlling the proliferative potential of the heart in both physiological and pathological conditions.

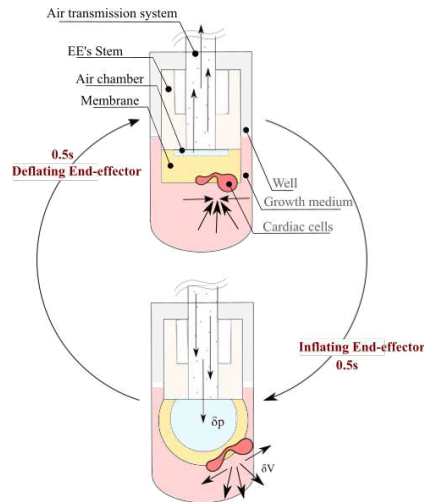Figure 11.2: RobHeart end-effector design and functioning: the end-effector consists of three parts, a stem (in light yellow) housing the air transmission system (in dotted white), an air chamber (in light blue) and a membrane (in yellow) with a flat surface to foster adhesion and equal redistribution of the cells (red). The cells are seeded on the membrane and, once adhered, the end-effector is immersed in growth medium (in pink) inside the well (in gray). A continuous cycle of inflation and deflation generates variations in pressure and volume of the membrane, stressing the cells. Pressure variation and cycle rate are chosen to mime a beating heart.

However, the medium-throughput screening (MTS) technique, that is usually exploited for this investigation, needs seeding sites smaller than two centimeters. On the other hand, most of the available technologies have sizes that are not compatible with standard laboratory glassware for research on cardiac cells. Hence, to pursue an effective stimulation millimetric devices have to be designed.

Research on applying mechanical stress to cells focused on mechanisms for monoaxial, biaxial, equibiaxal or three-axial stimuli [422, 423, 424] to exert tractions, compressions or sliding.

Several works propose pneumatic systems and Dielectric Elastomeric Actuators that exploit air chambers and piezoelectric effects to provide mechanical stress on cells grown in standard laboratory glassware. Dielectric elastomer actuators (DEA) and Micro Electro-Mechanical Systems (MEMS) are widely used as stimulators, since they can be miniaturized and parallelized. Moreover, they are compatible with interfaces for mono-layer culture of cells[425].

In [426, 427, 428, 429] several DEA- and MEMS-based devices are presented. The scalability to dimension suitable for heart cells is challenging and presents several technological issues on fabrication repeatability and instability phenomena[430].

Pneumatic devices are a valid alternative to DEA- and MEMS-based systems, allowing quick and simple development. Moreover, the air flow, as power supply, is intrinsically safer for the cells than the electrical signals required for MEMS and DEA devices, and do

not require wires and electronic components that get easily rusted in a humid environment (as the one of the incubator), contaminating the medium and the cellular culture. Some DEA devices as [431] could be used to study also the of mechano-electric coupling in cells. An extensive overview of devices can be found in [429]]. In all the pneumatic systems, one or more air chambers are used to deform elastic membranes, and different arrangements of the chambers generate tangential, normal or radial stretches. In [432], the authors presented a radial stimulator for a 90 mm Petri dish performing mechanical stimulation by means of an air chamber located underneath, while the same stimulation was provided by a circular air chamber with adiameter larger than 10mm in[433]. Mono-axial stimulation by linear strains are realized in [434] using antagonist air chambers under a squared membrane. Commercially available pneumatically-driven devices, as Flexcell (Flexcelling inc., US) and the STB series of StrexCell (STREX Inc. JP) consist of proprietary wells actuated linerally or radiarly by a electromechanical systems. However, all the mentioned devices are not compatible with standard multi-well plates and thus with MTS.

11.1.1   Contributions

In this work, leveraging our expertise in soft robotics and pneumatic systems

RobHeart consists of two main components: a soft end-effector (EE, shown in Fig. 11.2), and a pneumatic actuation system (shown in Fig. 11.5). The working principle is pictorially described in Fig. 11.2: The actuation inflates and deflates the soft and elastic EE air chamber, deforming its upper membrane, where cardiac cells grow and firmly adhere. In this way, the 3D mechanical stress leading to superficial and volumetric deformation of the membrane can be directly transmitted to the living organisms.

To meet dimensional requirements of MTS, the elastomeric membrane is integrated with the air chamber, creating an extremely compact deformable end-effector. The air flows from the actuation source to the soft EE by means of a transmission system consisting of tubes, connectors and splitters. Such a transmission system is designed to be easily scalable to multiple cellular cultures.

The design and fabrication of elastic and miniaturized EEs are the main challenges of this work, considering that the system has to mimic a living heart with a pressure up to 120mmHg and a cycle frequency between 1Hz and 1.5Hz. In addition, EEs have to satisfy requirements for cell manipulation concerning biocompatibility, optical transparency, and compliance to standard protocols on sterilization, immersion in the culture medium, and incubation, and to solve issues concerning scalability and uniform reproducibility.

Details on the RobHeart design, fabrication, validation and preliminary tests with cells are presented in Sec. **??**, 11.2, 11.3, and 11.4, respectively.

11.2   Materials and Methods

In this section, we describe the design of the RobHeart components: Sec.**??** details the end-effectors, while Sec.11.1.2 the pneumatic actuation system.
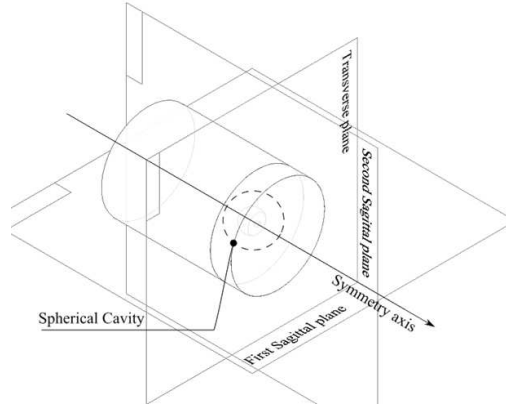
Figure 11.3: The design of the millimetric soft end-effector with its symmetry axis and the principal planes (first and second sagittal and transverse).

Table 11.1: FEA deformation related to probes. Results are expressed in millimeters (mm). In the case of lateral constraints, the values of probes ρ_2 and ρ_3 are null hence they are omitted.

| P_i | Free EEs | | | | | | | | | Constrained EEs | | |
| | ρ_1 | | | ρ_2 | | | ρ_3 | | | ρ_1 | | |
	δx	δy	δz	δx	δy	δz	δx	δy	δz	δx	δy	δz
16	$3e^{-5}$	$1e^{-5}$	0.46	$3e^{-5}$	0.05	0.13	0.05	$3e^{-5}$	0.13	$3e^{-5}$	$4e^{-5}$	0.13
32	$4e^{-6}$	$2e^{-6}$	0.92	$6e^{-5}$	0.09	0.26	0.09	$6e^{-5}$	0.26	$6e^{-4}$	$4e^{-6}$	0.29
64	$3e^{-5}$	$3e^{-5}$	1.81	$8e^{-6}$	0.19	0.55	0.19	$8e^{-6}$	0.55	$1e^{-5}$	$3e^{-8}$	0.53
128	$3e^{-5}$	$3e^{-5}$	3.66	$3e^{-4}$	0.39	1.05	0.39	$3e^{-4}$	1.05	$2e^{-6}$	$3e^{-4}$	1.13

11.2.1 Design of EEs

Each end-effector, as shown in Fig. 11.3, consists of two cylinders of 9mm diameter, fused together and realized in highly deformable elastic material. A 8mm high basal cylinder constitutes the stem, and a thinner cylinder plays the role of a deformable membrane thick 2mm. A spherical cavity, placed between the two elastic cylinders, realizes an air chamber.

The planar geometry of the membrane in deflated condition allows to seed homogeneously the heart cells on the EEs, while the chamber's spherical geometry was designed to reduce undesirable superficial asymmetry in inflated end-effectors.

A flat-headed needle is inserted in the stem and is in charge of introducing air from the actuation system to the air chamber.

Finite Element Analysis

Finite Element Analysis: A finite element analysis (FEA) was conducted to qualitatively and quantitatively inspect the deformations when increasing the pressure in the air cham-
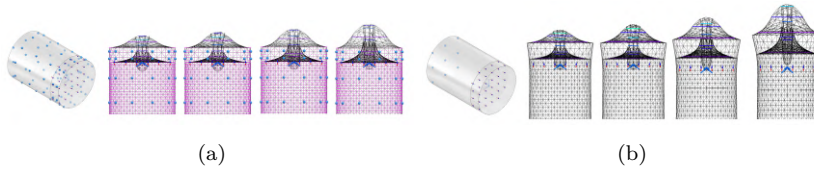
Figure 11.4: Results of the FEA with pressure equal to 16kPa, 32kPa, 64kPa, and 128kPa (from left to right). Blue dots mark the constrained surfaces. In (a) we show the results in case of "constrained EEs", while in (b) the results for "free EEs". Silicon rubber with Young modulus equal to 250 MPa was chosen for the material.

ber. More specifically, we wanted to observe the effects of the surface deformation in two particular conditions: *i)* EEs laterally constrained by the glass well ("constrained EEs"), and *ii)* EEs free to expand ("free EEs").

In the conducted analysis, the 3D-CAD/CAE Solid Edge® (Design Simulation Technologies, Inc.) software was used.

Stem and membrane of the end-effectors were assumed to be made of silicone material with elastic modulus chosen according to the experimental values of [435] based on theoretical results in [397].

All deformation analyses were carried out by constraining the base of the end-effectors and applying inside the air chamber four different pressures P_1=16kPa ($\approx$ 120mmHg), P_2=32kPa, P_3=64kPa, P_4=128kPa.

The analysis was conducted by inspecting the differential values of the position of three FEA probes placed on the upper surface of the membrane. The first probe ρ_1 is placed at the intersection of the upper surface of the membrane with the symmetry axis of the end effector, while probes ρ_2 and ρ_3 are placed at the intersection between the edge of the same membrane surface and the first sagittal plane and the second sagittal plane, respectively. The differential values of the probe positions are reported in Table 11.1.

In the case of "free EEs", as shown in Fig. 11.4, a deformation of the membrane is observed, as expected. However, the analysis also revealed a strangulation of the stem that contributes to the overall longitudinal deformation. Such a deformation is symmetric with respect to the EEs symmetry axis, therefore torsional phenomena are not generated after the inflation. On the other hand, in the "constrained EEs", at the same pressure, a lower longitudinal deformation and a zero radial deformation occur. In other words, the stem is not deformed either axially or radially (see Fig. 11.4).

11.2.2 Design of Actuation System

As shown in Fig. 11.5, the actuation system was designed according to approaches for rapid prototyping and laboratory replication. It consists of a multi-perforated plate (C) housing a linear actuator (B) and a commercial syringe (A) through appropriate supports. The connectors (G) fix the linear actuator, while the stopper (F) prevents the actuator from performing pitch movements that would lead to losing the contact with the syringe. Supports (D) and (H) hold and constrain the syringe system (shirt, plunger and tip).
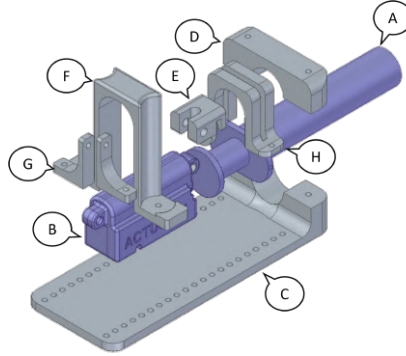
Figure 11.5: An exploded CAD view of the pneumatic actuation system. The syringe is indicated with (A), the linear actuator with (B), while (C) is the multi-holes base of the device. (D) connects the syringe with the base, (E) interlocks actuator with plunger, (F) and (G) hold the motor, and (H) avoids the motion of syringe shirt.

The plunger of the syringe system is propelled by means of the servo-motor, thanks to the one Degree of Freedom connector (E), designed for rigid connection, and for transmitting the motion from the actuator to the plunger, accommodating their relative movements.

The tip of the syringe is used as an interface between the actuation system and the EE flat-head needle. The air flows from the syringe tip to the needle, passing through a modular transmission system consisting of tubes, connectors and splitters, as shown in Fig. 11.2. The high modularity of the transmission system allows to easily and intuitively create an air recirculation network for exploiting several EEs in parallel.

A relevant issue is that the lengths, the widths of the pipes, as well as the number of branches, alter the behavior of the system, and change the pressure and deformation of EEs. In fact, in the hypothesis of air as perfect gas and according with Boyle law, we can write:

$$p_0 V_0 = pV$$

where p_0 and V_0 denote the system's pressure and volume in deflated condition of the plunger, respectively, and p and V are the pressure and volume in inflated condition. The pressure variation δp in the system depends on the volume variation δV but also on the volume V_0:

$$p_0 V_0 = (p_0 + \delta p)(V_0 - \delta V)$$

The relationship between volume and plunger motion δs is

$$\delta s = \frac{\delta p V_0}{p_0 + \delta p} \frac{1}{r_s^2 \pi}$$

where r_s is the internal radius of the syringe. However, the volume of the system in deflated condition V_0 is equal to the volume of the air into the syringe summed up with

the air volume in tubes and connectors (which are not neglectables). Hence:

$$\delta s = \frac{\delta p (s_0 r_s^2 \pi + \sum_{j=1}^{M} \upsilon_i + \sum_{i=1}^{N} \nu_i)}{r_s^2 \pi (p_0 + \delta p)} \tag{11.1}$$

where υ_i is the volume of each of the M connectors, ν_i is the volume of the i-th tube and N is the number of tubes used in the transmission system.

The topology of transmission impacts on the EEs internal pressure, and this alteration reflects on their deformation according to the Young law:

$$p_0 + \delta p = E \frac{\delta l}{l_0} \tag{11.2}$$

where E is the Young modulus of the end-effector material, while l_0 and δl are the EE length and linear deformation. Including Eq. 11.1 in the Young law (Eq. 11.2), it is possible to derive the expression of deformation as a function of the transmission system components:

$$\delta l = \frac{l_0 p_0 \left(s_0 r_s^2 \pi + \sum_{j=1}^{M} \upsilon_i + \sum_{i=1}^{N} \nu_i \right)}{E \left(s_0 r_s^2 \pi + \sum_{j=1}^{M} \upsilon_i + \sum_{i=1}^{N} \nu_i + r_s^2 \pi s_0 \right)}$$

11.3   RobHeart Fabrication

In this section, we will detail the fabrication procedure to realize a prototype of the proposed device.

11.3.1   Fabrication of EEs

The EEs are realized by pouring two layers of bi-component silicone rubber Ecoflex 00-30 (Smooth-On, inc. US). The chosen silicone rubber has a hardness 30 on the Shore 00 scale (ASTM D-412), and a translucent color.

During fabrication, the silicone was poured in subsequent steps into interlocking molds, fabricated in Acrylonitrile butadiene styrene (ABS) and exploited the Fused Deposition Modeling (FDM) technique.

The insertion of a tin sphere of radius 2mm between the membrane and the stem allows creating the air chamber. The tin sphere is the result of melting the raw material into an ABS mold, while a plate equipped with pins of diameter 1.5mm generates, during the stem care, a vertical guide for the flat-headed needle.

Needles with a tip having a diameter equal to 1.8mm and length of 10mm were chosen for inflating the EEs.

Each end-effector was equipped with a very thin silicone crown. This crown allows the EEs to adhere firmly to the well walls.

All molds have been sprayed with a mold release agent, the Easy Release 200 (Mann Release Technologies, inc. US), for quick and agile extraction of the fabricated soft EEs.

The manufacturing process is sequential, but highly parallelizable, alternating phases of silicone casting with phases of care and insertion. All care sub-phases took place at a

controlled temperature fixed to 23°C. The entire manufacturing cycle takes about 7hours and consists of four phases: *i)* membrane casting and care; *ii)* realization and introduction of the insert; *iii)* molding and care of the stem; *iv)* extraction of the silicone body and insertion of the needle-like connector. Details on EE molding are provided in Fig. 11.6.

Sterilization and Coating Procedure: Each end-effector has to undergo a three-step sterilization procedure and a subsequent coating treatment fostering the adhesion of the cardiac cells on the deformable membrane.

The end-effectors sterilization procedure consists in a manual removal of macroscopic corpuscles by means of adhesive work, followed by a soaking in 70% ethanol (CH_3CH_2OH) cleaning reagent for 900s. Then, to remove residual ethanol from the membrane, the EEs are washed with the Phosphate-Buffered Saline solution (PBS), a water-based salt solution commonly used in biological research.

Then, the membrane is coated with an adhesive glycoprotein, the fibronectin in solution with gelatin, a heterogeneous mixture of water soluble proteins present in collagen. The coating procedure is aimed at ensuring the attachment of cells on the membrane and requires a waiting time of 2 hours to be efficacious.

11.4 RobHeart Characterization

In this section, we will detail mathematical relations characterizing RobHeart components, and we will discuss experimental tests conducted to validate the retrieved mathematical models.

11.4.1 Characterization of the actuation system

First of all, the actuation system was validated by retrieving the experimental map between pressure and plunger displacement, and comparing this map with the theoretical profile related to Eq. 11.1. The pressure sensing and recording system consists of a pressure sensor MPX2200GP (Differential Pressure Range: 200kPa) connected to a micro-controller, and a differential amplification circuit realized with an AD623AN op-amp.

Fifteen trials were performed by applying pressures in the range of [0, 200]kPa and measuring the corresponding plunger displacements. Experimental data were interpolated, by parameterizing Eq. 11.1 and treating it as a fitting model:

$$\delta s = \alpha \frac{\delta p}{p_0 + \delta p} \tag{11.3}$$

Table 11.2: Recorded internal pressure of EEs just before the break point, expressed in kiloPascal (kPa).

ID	01_x	02_x	03_x	04_x	05_x	06_x	07_x	08_x	09_x	10_x	11_x
p_b	190.8	182.7	198.6	196.8	191.1	202.2	186.1	194.5	193.5	196.7	196.5
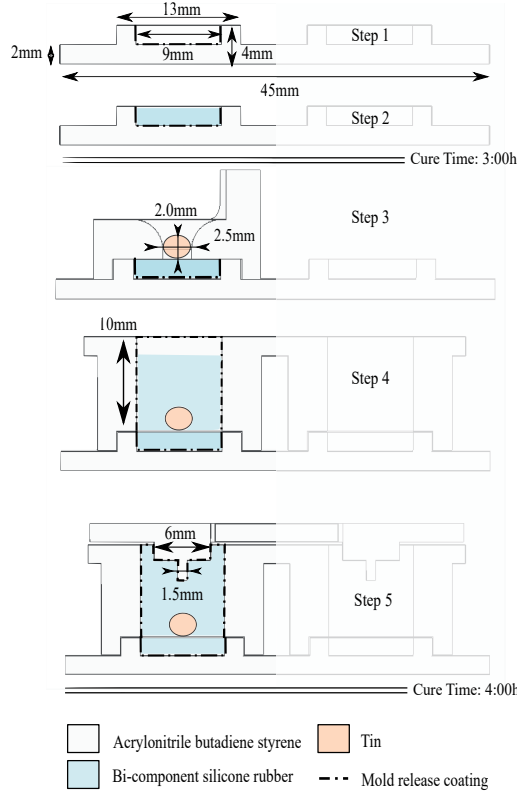
Figure 11.6: Fabrication steps of soft inflatable end-effectors. *Step 1*: The membrane mold is coated with released agents. *Step 2*: 1.27g of mixed bi-component silicon rubber is versed into the mold and cared for 3h at 23°C. *Step 3*: we insert the 3D printed guide for the tin ball centering the sphere. Removed the tin ball guide, the mold for the stem is stacked on the previous one and 4.1g of rubber is poured (*Step 4*). *Step 5*: The pinned plane is placed on the stem mold to generate the needle guide. A last cure phase of 4h is performed, before the needle insertion.

Table 11.3: Mean torsional angles (rad) w.r.t. first sagittal and transverse planes.

ID EE	01	02	03	04	05	06	07	08	09	10	11
$\overline{\delta\theta_s}$	0.02	0.02	0.011	0.02	0.01	0.02	0.01	0.02	0.01	0.02	0.02
$\overline{\delta\theta_t}$	0.02	0.02	0.03	0.02	0.01	0.01	0.02	0.01	0.02	0.02	0.02

where p_0 is the atmospheric pressure ($p_0 =$101.3kPa).

As it can be noticed in Fig. 11.7, the experimental curve fits the data with a quality factor equal to $R^2 = 0.986$ and deviates from the theoretical profile at most 0.41mm. The parameter α evaluated by data fitting is equal to $\hat{\alpha} = 31.83$, while the theoretical value, estimated using transmission system specs (see Sec. 11.2), is $\alpha_t = 32.45$ with and error equal to $\Delta\alpha = \|\hat{\alpha} - \alpha_t\| = 0.62$ ($\approx 1.9\%$ of α_t).
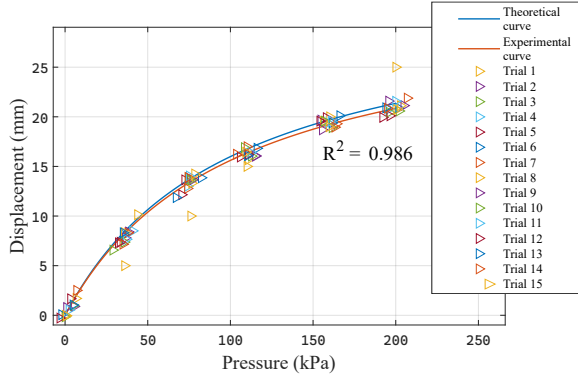
Figure 11.7: Plunger Pressure-Displacement curves: the red one is the fitting curve of experimental data, the blue one is the theoretical curve obtained from Boyle law and prototype specs. Interpolation quality factor R^2 is reported.
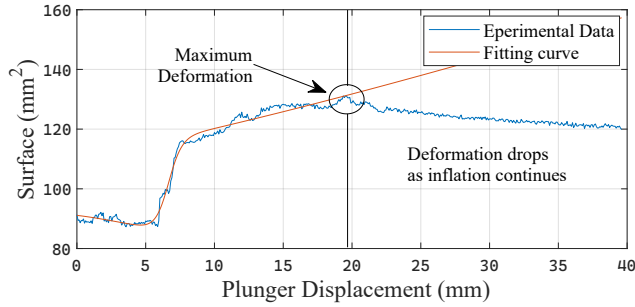
Figure 11.8: Example of EE behavior when increasing pressure is applied by moving the syringe plunger. The black vertical line cuts the plane in two parts, the behavior of unbroken EE is contained in the left half-plane, while in the right part there are data collected after the outbreak. The circle marks the blowing-up event.

11.4.2 Characterization of EEs

End-effectors breaking point, asymmetry and the deformability were evaluated by analyzing images acquired by a vision system composed of two cameras full HD 1MP with a frame rate equal to 30fps. The cameras were placed orthogonally to each other, one with the image plane parallel to the EE transverse plane, while the other was oriented to capture the projection of end-effector on the first sagittal plane. The image acquisition process took place in a brightness-controlled environment.

In each frame, the EEs were distinguished from the environment by performing region-based segmentation technique, and leading to a binary image with two regions: the first one $\Re_i$ is composed of the pixels $\wp(X, Y)$ containing a part of an EE, $\wp(X, Y) \in \Re_i \rightarrow \wp(X, Y) = 1$, and the remaining region $\bar{\Re}_i$ is such that $\wp(X, Y) = 0$.

We performed experiments using twenty-two EEs, the first eleven were involved in the

Figure 11.9: In (a) the binary image of the sagittal plane (left) and the transverse plane (right) are visually depicted, snapped in four pressure conditions: 19kPa, 48kPa, 90kPa, and 178kPa (from bottom to top). In (b) and (c) we show membrane Pressure-Volume and Pressure-Surface experimental data. The percentile standard deviation (std$_\%$) of EEs behaviors with respect to the mean (shown in black) is reported.

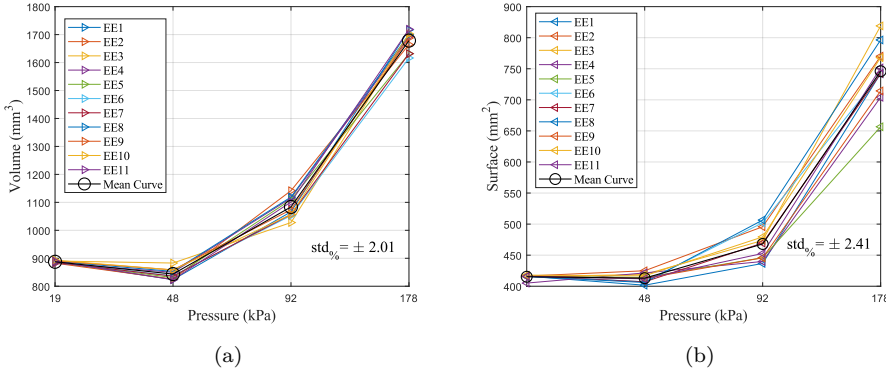investigation of breaking limit pressure, while the remaining were involved in *i)* EE symmetry analysis, *ii)* uniformity analysis among the fabricated EEs, and *iii)* characterization of EEs in the pressure-volume and pressure-membrane surface maps.

The first three moments of the image were calculated from the null order to the second-order to retrieve a numerical estimate of the projected surfaces, the position of the centroids, and the angle of torsions, respectively, according with image interpretation theory in [436].

The process of EE inflation is achieved by means of several back and forth movements of the syringe plunger, and when an EE breaks for excessive pressure, it does not emit audible sounds. Moreover, the subsequent deflation occurs slowly, and is really hard to detect by eye. Hence, we devised a method to estimate the breaking pressure by looking at the EE superficial deformation. The transverse and sagittal surfaces were estimated as normalization on the deflated state of the zero-order moment of the image:

$$S_i(p) = \frac{\sum_{X,Y \in \Re_i} \wp(X, Y)}{\left(\sum_{X,Y \in \Re_i} \wp(X, Y) \right)\big|_{\delta p = 0}} S_{0|i} \text{ with } \forall i \in \{s, t\};$$

The information about the projected surface deformation was used to estimate the breaking point of the EEs on the surface-plunger displacement plane. The pressure of break is evaluated by retrieving, according to Eq. **??**, the measured plunger displacement corresponding to the maximum sagittal deformation before depression line, as shown in Fig. 11.8. All eleven "x"-labeled of the twenty-two fabricated EEs were used to estimate the pressure breaking point: values are reported in Tab. 11.2, and the average result is equal to $p_{break} =$195.12±6.54kPa.

Concerning the actual symmetry of an EE, we computed torsional angles possibly arisen after the complete inflation. θ_s and θ_t denote such angles in the sagittal and

(a)

(b)
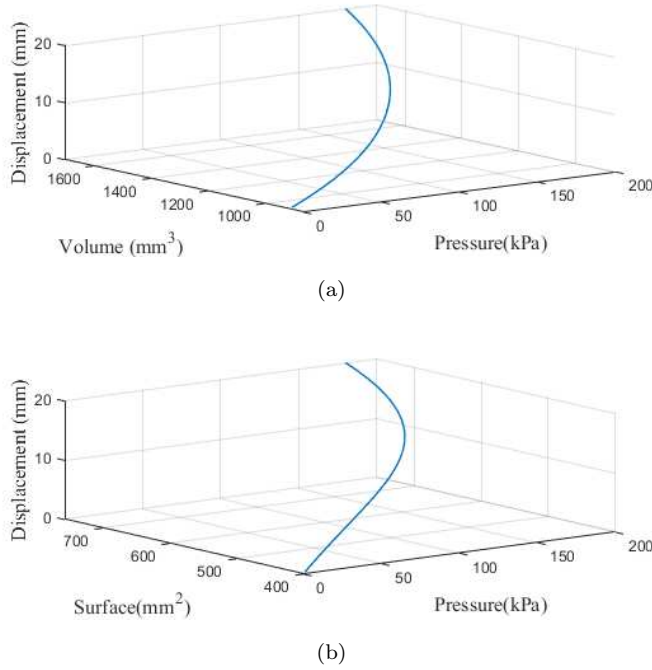
Figure 11.10: 3D maps of the pressure, the actuation motion and the volume or the surface of EEs in (a) and (b), respectively.

transverse planes, respectively. Symmetrical deformations (hence, no torsional angles) were expected according to the results of the FEAs presented in Sec. **??**.

$$\theta_i = \frac{1}{2} \arctan \left(\frac{2\mu_{1,1|i}}{\mu_{2,0|i} - \mu_{0,2|i}} \right) \text{ with } \forall i \in \{s, t\}$$

where $\mu_{2,0|i}$, $\mu_{0,2|i}$ are direct centered moments of the image projected on *i-th* plane and $\mu_{1,1|i}$ is mixed centered moment on the same plane:

$$\mu_{j,k|i} = \sum_{X,Y \in \Re_i} (X - \overline{x}_i)^j (Y - \overline{y}_i)^k \text{ with } \forall i \in \{s, t\};$$

where $(\overline{x}_s, \overline{y}_s)$ and $(\overline{x}_t, \overline{y}_t)$ are the centroid coordinates of the end-effectors' image projection on the sagittal and transverse plane, estimated as:

$$\overline{x}_i = \frac{\sum_{X,Y \in \Re_i} X}{\sum_{X,Y \in \Re_i} \wp(X,Y)}, \quad \overline{y}_i = \frac{\sum_{X,Y \in \Re_i} Y}{\sum_{X,Y \in \Re_i} \wp(X,Y)}.$$

To retrieve the desired estimates, we applied different pressures in the range [0, 180]kPa, corresponding to δs equal to 0.5mm, 1.0mm, 1.5mm and 2.0mm according to the experimental profile (see Sec. 11.3.1). The values of the mean variations of the angles with respect to the EE orientation in the deflated state, computed as $\overline{\delta\theta_i} = \|\theta_i - (\theta_i|_{\delta p=0})\|$, are reported in Table 11.3. The maximum angle of torsion is very small, equal to 0.024rad,

hence, it is possible to neglect torsional and asymmetric effects on the EEs, as expected by the FEAs.

The absence of significant asymmetry allowed to estimate the volume of the EEs as rotation of the sagittal surface about the normal axis at the center of the circular transverse surface:

$$V_{EE}(p) = 2 \int_0^{\frac{\pi}{2}} S_s(p) \frac{\sqrt{S_t(p)}}{\pi} \cos(\vartheta) \delta\vartheta$$

Starting from the estimate of the volume variation:

$$\delta V_{EE} = V_{EE}(p) - (V_{EE}(p)|_{\delta p=0}),$$

we estimated the surface of the membrane, under the hypothesis that the deformation generated by δp is geometrically approximated by the surface of a prolate semi-ellipsoid:

$$S(p) = \pi \left(\frac{S_t(p)}{\pi^2} + \frac{3\delta V_{EE}(p)\sqrt{S_t(p)}}{\pi 4 S_t(p)} \frac{\varepsilon}{n(\varepsilon)} \right) + (S(p)|_{\delta p=0})$$

with

$$\varepsilon = \arccos \left(\frac{4 S_t(p)\sqrt{S_t(p)}}{\pi 3 \delta V_{EE}(p)} \right)$$

Results about volume and contact area (Fig. 11.9) return information on the reproducibility of the manufacturing process. Thanks to the conducted analysis, indeed, we were able to estimate that the average dissimilarity among the manufactured EEs is about $\pm 2\%$ of the expected average behavior. Hence, we can assert that the fabricated EEs have a uniformity value of 97.99% and 97.59% concerning the volume and surface deformations, respectively.

Moreover, the analysis provides an estimate of the volumetric and superficial deformabilities, that were evaluated as the best interpolating functions given the pressure. We obtained that the best interpolation for both volume and surface trends follows an exponential law:

$$V_{EE} = 621.12 e^{0.0056p} + 290.71 e^{-0.0277p}$$

$$S = 27.56 e^{0.0148p} + 369.96 e^{-0.0002p}$$

The accuracy for volume-pressure and the surface-pressure interpolating curves are equal to $R^2 = 0.973$ and $R^2 = 0.957$, respectively. Within the safety margins, the soft EEs are able to increase the volume of the end-effector up to a maximum of 87.4% of the initial volume, while the membrane surface can be expanded up to a maximum of 83.8% with respect to the surface of the deflated end-effector. Such values refer to the average trends of the batch, shown in Fig. 11.10.

11.5   Tests with living cells

RobHeart is meant to be a device for *in-vitro* cell seeding and stimulation. Hence, we conducted a preliminary test to verify the appropriateness of the proposed device. We
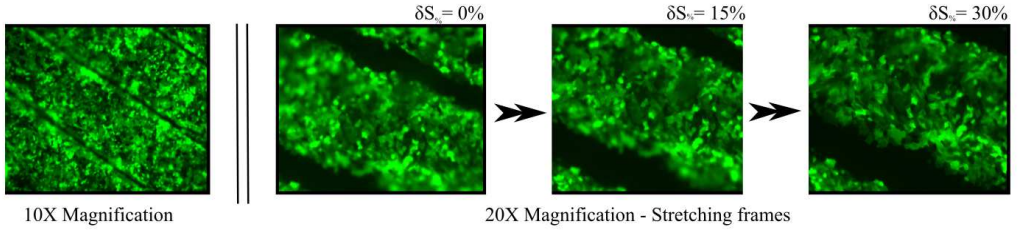
Figure 11.11: Cell imaging by Leica DM IL LED microscope (Leica Microsystems GmbH): 10x and 20x magnification. The last three frames show a deformation sequence of the cellular culture (green) achieved by inflating EEs. $\delta S_\%(p) = 0\%$, $\delta S_\%(p) = 15\%$, and $\delta S_\%(p) = 30\%$, (from left to right).The black strips are empty regions caused by texture transfer from the 3D printed mold to the silicone membrane. The larger the deformation, the larger the black regions, the cells are more distant from each other, and change their shape.

used adult cardiac muscle cell line HL-1 from mice to populate the surface of the end-effector membranes, with approximately 100.000 fibroblast per end-effector. The seeding lasted 2 hours. After that, RobHeart EEs have been transferred into a 12-well plate filled with basal medium Dulbecco's Modified Eagle Medium (DMEM) with high values of glucose ($C_6H_{12}O_6$), adding the 10% fetal bovine serum (FBS) and a mixture of penicillin G and streptomycin (Pen-Strep, $C_{39}H_{61}N_9O_{16}S$).

After 48 hours since seeding, a preliminary observation by fluorescence microscopy showed that the cells successfully adhered firmly to the surface of the EEs membrane, and that the deformation of the membrane, within the physiological limits, did not generate a cell detachment, but only a deformation, as it can be seen in Fig. 11.11.

11.6   Conclusion

In this work, we presented RobHeart, a novel soft robot to provide superficial and volumetric mechanical stimulation of cardiac cells. We detailed design and fabrication steps to satisfy the heart cell culture and medium-throughput screening requirements mentioned in Sec. 11.1.1.

Tests conducted on the actuation system and its end-effectors allowed to retrieve 3D laws mapping the actuation signal, the generated heart-like pressure and the superficial/-volumetric deformations. Moreover, results on experimental validation of end-effectors showed that the devised fabrication protocol allows uniform reproducibility. We also verified the limit condition of deformability before the EE break, which is higher than the deformation condition bearable before heart cells die ($\approx 30\%$), and preliminary tests were conducted on HL-1 cells grown on the top of RobHeart end-effectors to verify the appropriateness of the system.

Future work will focus on retrieving meaningful actuation patterns to investigate how the mechanical dynamics of the cardiac cycle acts on the heart cells. Pressure planning techniques will be integrated with visual servoing methods in a closed loop approach.

Chapter 12

Tibialis Stimulation of Cancer-Affected Mice

Figure 12.1: The prototype of the anklets used for an experimental trial.

Novel medical treatments require not only theoretical feasibility demonstration exploiting cellular models but also in vivo testing, evaluating the impact of the therapy in living organisms.

However, despite existing devices for simulating stimuli for cellular experimentation within in-vitro environments, a conspicuous lack persists in devices to perform mechanobiological investigations using animal models. Hence, our present work proposes a novel soft robotic device designed to exert low-frequency pressure and tensile stress on cancer cells implanted within the limbs of murine models. Using this device, we will investigate the feasibility of a prospective mechanotherapy for superficial cancer inhibition. The softness of the proposed wearable vet robot not only ensures the safety of the mice subjected to experimental trials but also distributes efficaciously the provided stimuli on the intricate anatomical contours of the animal's limb. To ensure the murine model's safety, collocate the actuation system, and parallelize the trials, we have implemented an air-based power supply mechanism, regulated by external switching signals to modulate applied tensile deformation. In addition to the presentation of our device's design and testing, we will summarize the findings gleaned from the first experiments conducted employing the aforesaid devices.

12.1 Motivation

One of the most significant challenges in dissecting the hypotheses stated at the beginning of Part III lies in the shortage of technologies capable of effectively stimulating cancerous tissues and cancer cells, particularly within living environments. While there are indeed devices designed for mechanically stimulating in vitro cultured cells as ones presented in Chapter 11, the exploration of tissue stimulation technologies in animal models has, to the best of our knowledge, been inadequately explored. Existing wearable technologies for animal use have primarily focused on veterinary [437, 438], or guidance [439], applications, predominantly tailored for medium and large animals. Remarkably, the design of haptic technologies for stimulating small laboratory animals, such as guinea pigs or

other mouse models commonly involved in medical and biological research, has remained largely unexplored.

To conduct haptic-enabled mechano-biological investigations exploiting small animal models, a new class of vet devices should be devised. These should be compact, effortlessly wearable around the rodent's limbs, and, most importantly, ensure the animal's safety to prevent any inadvertent harm or fatality during experimental procedures. Additionally, the interface between the device and the rodent must be biocompatible and non-toxic, accommodating the rodent's anatomical shapes.

12.1.1 Contributions

To address the stated requirements, the device here proposed consists of four soft anklets responsible for actively applying mechanical stress to the rodent's body, and a syringe-based pneumatic box that enables and controls the inflation of these. The stimulation reference is based on deformation exerted on the limb of the rodent, consequently, the control loop of the pneumatic box is closed on linear displacement of the syringe piston. Moreover, the pneumatic box is decentralized with respect to the anklets, to be compliant with a dynamic environment, such as an animal house of a biological research center. A network of pipes connects the actuation box with the anklets. The components of the device are chosen to exert a periodic stimulation with low frequency, akin to the mechanical load imposed by a human heartbeat, in alignment with the preliminary scientific evidence of our hypothesis. This work contributes to the haptic and mechanobiological research in the following ways:

Innovative Soft Wearable Robotic Device Design and Development: This device was engineered to facilitate mechanical stimulation within murine models, paving the way for several mechanobiological investigations, including the dissection of our hypothesis about cancer inhibition.

Protocol testing and Hypothesis Investigation: The vision of this work involved not only the realization of a functional prototype of the device but also the design of usage protocol. These were then put to the test, yielding valuable empirical data that bolsters the scientific foundation underpinning our hypothesis. Specifically, we aimed to substantiate the feasibility of mechanotherapy as a potent approach for impeding tumor proliferation.

12.2 Materials and Methods

In this section, we exploit the results of our work consisting of the design of the haptic interface and the outcome of the first tested experimental protocol.

12.2.1 Stimulation Device

In what follows, the tactile device consisting of parts is detailed.

(a)   (b)
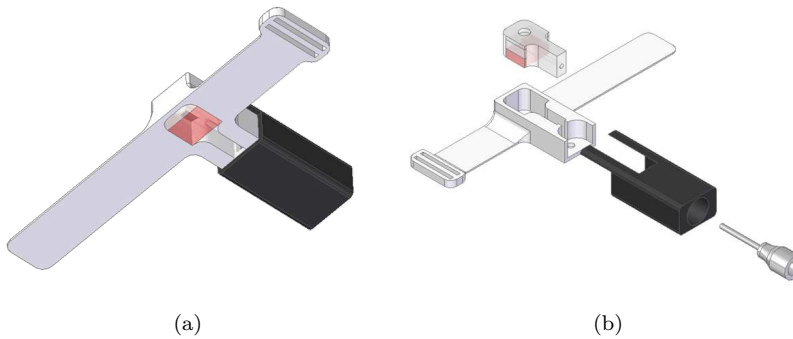
Figure 12.2: In (a) and (b), the isometric and exploded view of anklet. The transparent parts consist of the silcone rubber cube, the red one is the inflatable region of this. The white case wrapping the inflatable region is realized in TPU to be tied around the limb of mice while the black one is the plastic rigid case.
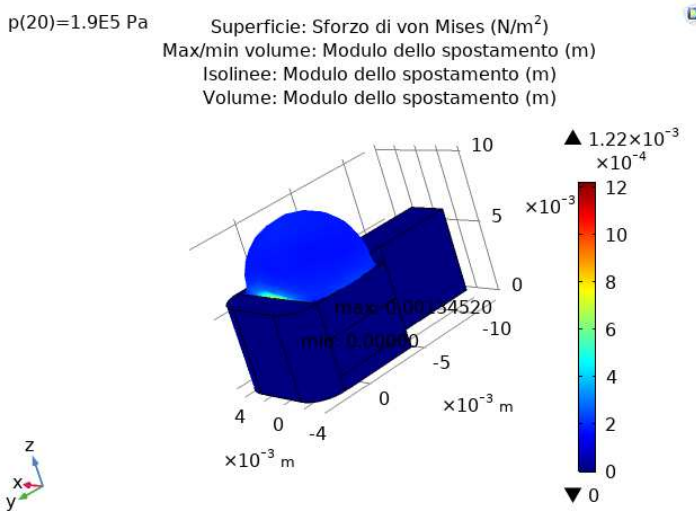
Figure 12.3: The visual outcome of EcoFlex 00-30 (Hardness 30 Shore 00) FEM simulation. The simulation is conducted with an input pressure in the hollow cavity of the anklet equal to 190 kPa. The material is model is exploited by Ogden formulation using the parameters proposed in [440].

Soft Anklets   The anklet design, as shown in Fig. 12.2.a consists of a deformable and inflatable hollow cube exerting pressure against the rodent's limb and a soft/rigid case wrapping it and fostering its wearability and attachment with the animal. The inflatable part of the device is realized from successive layers of deformable bi-component silicone rubber. The component measures 4 mm x 4 mm x 7 mm, to match the average dimensions of a guinea pig's extended tibial bone. The hollow inside the component has

(a) (b)
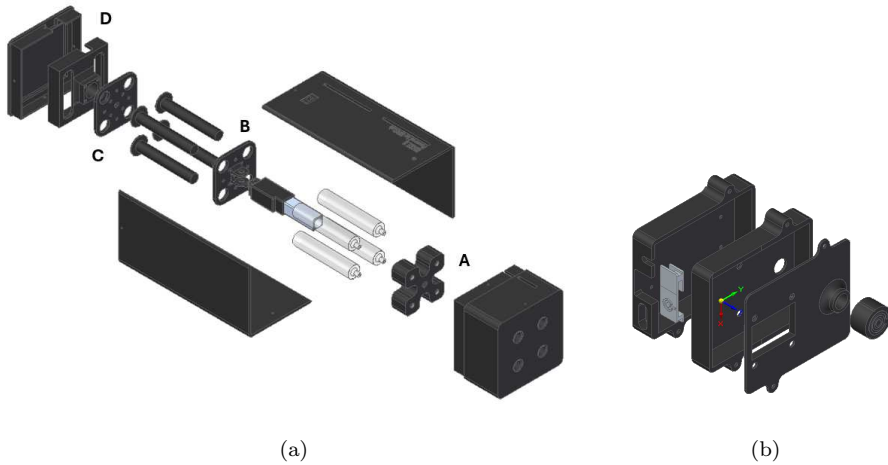
Figure 12.4: The pneumatic box and the control unit consisting the actuation system, in (a) and (b), respectively.

a cylindrical geometry and dimensions equal to 10 mm in length and 2 mm in diameter. It is asymmetrically positioned concerning the component's sagittal plane (as depicted in Fig. 12.2.b) with a distance of respect to the nearest face of the component equal to 2 mm, this arrangement ensures that the internal pressure escalation within the chamber prompts a deformation directed quite exclusively in one orientation. The material used to craft the components is a silicone rubber with hardness equal to 30 Shore 00, this is chosen, after several simulations conducted by FEM (see Fig. 12.3), to better simulate the ventricular wall dynamics.

The external socket is designed to encase the inflatable components, ensuring direct contact with the animal tissue. The socket envelopes the mouse limb and channels the stimulus directly toward the cancerous tissue providing a rigid constraint to deformation in the opposite direction. In practice, as the air chamber inflates along the path of least thickness and encounters the opposing rigid constraint, it projects a uniform and structurally robust region of the silicone rubber parallelepiped towards the murine limb. In addition, the soft/rigid case is instrumented with a soft belt fabricated using TPU material, to easily tighten the anklets around the mice limbs.

The airflow in and out of the air chamber is provided by the actuation system to which anklets are connected through pipes culminating with flat-head needles. A unidirectional valve, normally open in the deflation direction, is parallel to the inflatable component thanks to a bifurcation point along the pipe. This allows the long usage of anklets to recover the losses of air because of small leakage at the interface between the inflatable component and the needle.

Actuation System The actuation system encompasses the integrated system comprising actuators, controls, and sensors for the effectors. This consists of two main parts

a pneumatic box (PB) and a control unit (CU).

The core of the pneumatic box consists of an ad-hoc designed 2×2 syringe pump matrix activated by one only linear actuator. Referring to the Fig. 12.4.a, the linear actuator, normally extended, is directly interconnected with the sliding syringe air-chambers by means of connector **A**, while the pistons are grounded by **B** and **C** stoppers. The latter is constrained to the bottom part of the device composed of the external base of these (**D**) and the cover of the motor driver. The linear movements of the actuators are controlled thanks to an encoder instrumenting it and a PID controller. The resulting sliding of syringe cases along the pistons enables precise air injection and assumption towards and from the anklets. The whole pneumatic box is closed in a three-component case, internally coated with a phono-absorbent sponge to reduce the acoustic pollution of the functioning device.

On the other hand, the CU consists of an open-source microcontroller board, outfitted with a liquid crystal display and physical knobs for visualizing and intuitively adjusting both the frequency and intensity of the reference signal, respectively. The LCD offers to biological researchers a user-friendly graphic interface (GUI) for setting the stimulation and monitoring the device's operational status. All CU components are wrapped within an ABS case. The power supply plug of the CU is hidden by a compliant socket to avoid hardware damage due to liquid infiltration, while the interface with the pneumatic box is provided by a mag-safe connector to allow the fast disconnection and consequently stop the pneumatic box in case of emergencies such as animal injuries. The case of CU(see Fig. 12.4.b) is realized in ABS material by 3-D printing procedure.

12.2.2   Stimulation Protocol

A prototype of the presented device is realized by exploiting a fast prototype procedure to conduct some pioneering experiments about the cancer response to mechanical stimulation.

At the current stage of our research, the following investigations were aimed *i)* to test its efficacy on laboratory mice and *ii)* to delve into the hypothesis of inhibiting tumor proliferation through mechanical stimulation. Two mice are involved in the experimental campaign. In both tibialis anterior mice, 100k LG Cells were injected on the first day. In the following two days, one limb of each rodent is pieced two times per day. The stimulation sessions lasted 2 hours.

The stimulation is provided by the left hind mouse limb instrumented with the devised anklet, into which an identical quantity. This approach provided us with a control limb on the left, devoid of any stimulation, and a treated limb on the right. The mechanical stimulation reference for this study case consisted of a square wave, pulsating at a frequency of 1.00 Hz and boasting an amplitude of 30%. At the end of day 2, the tissue harvesting is conducted.

In the days following tissue harvesting, a staining protocol of the obtained biological material was conducted:

- The nuclei of the live cells contained in the tissue samples were identified using a marker per nucleus, 4',6-diamidin-2-phenyl (DAPI);
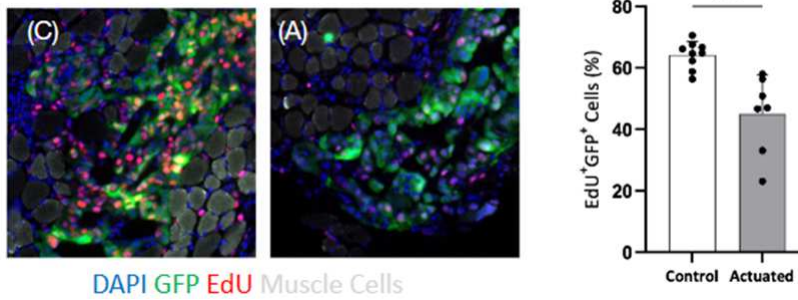
Figure 12.5: The results obtained from fluorescent microscopy analysis of two selected tissue slices, one from the control limb (C) and the other from the affected limb (A), showed cancer cells colored in green while reproducing, and living cells were marked in red and blue, respectively. The proportion of green area with or without a red marker was assessed to determine the percentage of replicating cancer cells. These values were compared statistically to establish a significant difference between samples C and A.
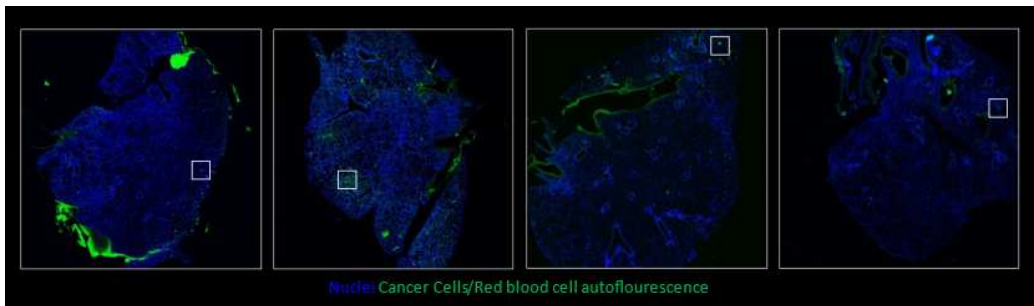
Figure 12.6: A representative imaging outcome of metastases and circulating cancer cell in a slice of mice lung.

- Cancer cells have been labeled with a green phosphorescent protein (GFP)

- The activity of cell proliferation has been immortalized through the absorption of 5-Ethynyl-2 -deoxyuridine (EdU), a marker of DNA synthesis in cell culture detecting cells undergone DNA synthesis

12.3 Results

Through fluorescence microscopy images and a region of interest (ROI) analysis, it was possible to quantify the percentage of replicating cancer cells as a percentile ratio of the EdU contained in areas marked with GFP. As noticeable in representative tissue slides reported in Fig. 12.5, a significant decrease in the proliferative capacity of tumor cells in the limb subjected to mechanical stimulation occurred. The right limb, the unstimulated one, exhibited a 60% proliferation rate among the tumor cells, while the treated limb

displayed a 40% proliferation rate.

In addition, a whole-body analysis was conducted to verify the absence of flowing cancer cells and metastases. To do this, we evaluate the levels of GFP in several organs through green ROI identification in the slices of mice's organs. This supplementary analysis failed to yield any evidence of tumor cells. Please refer to Fig. 12.6 for a visual representation of the results of the lung analysis, which is theoretically the primary site for any potential accumulation of the tumor cells employed in our study. Then, outcomes dispelled cancer vascularization effects and the dispersion of cells within the organism due to tissue compression.

These promising preliminary findings spurred us to embark on further tests, expanding our cohort to include a greater number of animal models. For instance, a parallel experimental test was executed involving four rodents, all subjected to a sinusoidal mechanical signal pulsing at a frequency of 0.5 Hz and showcasing an amplitude of 50%. The treatment protocol is the same as aforementioned and the outcomes remain coherent with the previous ones.

Part V

Conclusions

Conclusions

Computing is not about computers anymore.
It is about living

Nicholas Negroponte

At the conclusion of this document, it is appropriate to provide a comprehensive summary of the principal results and findings obtained from the documented scientific inquiry. The dissertation moved from basic principles to more complex practical uses. At its core, the primary focus of this document is to describe the outcomes achieved during our extensive research over the last three years. Our research has covered a wide range of topics including haptics, metaverses, medical treatments, and mechanobiology. As we bring this document to an epilogue, it is useful to summarize the acquired knowledge and look beyond it. The conclusions drawn from this document serve as a springboard for further investigations and exploration, providing a foundation upon which future research can be conducted. It is important to reflect on the implications of these findings and consider their potential impact on related fields.

Chapter 13

Final Remarks

In this thesis, three years of research about haptic display were resumed, mostly the focus on soft technologies. Starting with an overview of the human sense of touch and its significance in various fields, a detailed exploration of the state-of-the-art haptics technologies, including their advancements and limitations, and finally, an examination of their application across different industries with real-world examples, several new devices and methodologies were presented according to their application fields. The idea of repurposing haptic technology was introduced to expand the range of tactile display applications, drawing a comparison to the pharmaceutical process of repurposing drugs for different uses.

Pushing the boundaries of virtual and extended realities several new devices, proposed in Part I "Haptics for Metaverse Experiences", were presented as potential tools to enhance also a digital life in metaverses. Chapter 4 described a multi-channel display that combines a skin stretcher and textile-based wrist squeezer for rendering the stiffness of digital or remote objects in case of passive interaction with these. The conducted study demonstrates not only the efficacy of the proposed technology but also the feasibility of transmitting complex information like the stiffness decoupling the consisting signals and rendering each of them using a proper haptic cue. In Chapter 5 a novel approach based on the integration of haptics and pseudo-haptics methods was achieved to return kinesthesia on the user's hand interacting with digital objects: an imperceptible scaling of the movements of virtual hand concerning real ones allows that self-contact of the user finger pulp meanwhile the virtual digit touch the virtual object. Chapters 6 and 7 meticulously detailed the design and testing of two tendon-driven tactile interfaces, tailored to facilitate gestural communication between remote individuals and facilitate exploration within virtual environments, respectively.

In the pursuit of expanding the repertoire of medical applications for haptic technologies, Part II titled "Haptics for Medical Treatments"dissected three distinct technologies. These included an exoskeleton engineered to support hand rehabilitation tasks under remote supervision, leveraging a differential mechanism to ensure compliance. Additionally, portable pads with silicone rubber surfaces and a redesigned version of the tendon-driven display proposed in Chapter 7 were harnessed to administer manual treatments for trauma and syndromes like CRPS-I.

Venturing beyond the medical application, a repurposing of haptic is proposed in Part III "Haptics for Mechanobiological Research on Cancer"to foster the biological research of new therapeutic tools for fighting tumors. Starting from the scientific evidence about oncogenesis and mechanics correlation and rarity of cardiac cancer, two soft inflatable devices are developed to dissect the hypothesis that the rhythmic force cues, that the

heart exerts on its cells, inhibit the proliferation of cancer. In Chapter 10 a meso-scaled soft robot composed of a pneumatic syringe-based actuation and elastic end-effector is presented. The end-effector is tailored to host cells and stretches them, mimicking the mechanical loads of a beating heart in in-vitro cultures. On the other hand in Chapter 11 a soft anklet for small animal models, like rodents, is proposed as a tool to conduct mechanobiology investigation in-vivo, testing the feasibility of mechanical treatment of cancer in living organisms. All works reported in this thesis are revised versions of the works published as [441, 442, 264, 315, 443, 307, 444, 445, 307]. Instead of the work presented in Part III Chapter 11 that consists of a report of an early stage research.

13.1 Future Works and Perspective

All works presented here are intended to serve as a starting point for further in-depth research and exploration. For what regards tactile technologies for metaverses, it is essential to note that the several interfaces presented constitute a wide variety of devices designed to support different types of interactions that could occur in a digital world. Looking into the future, these diverse technological outcomes will be harnessed and integrated to develop unified haptic suits or tactile cloths with the aim of fully enhancing the user experience by combining multiple functions into one single device.

On the other hand, the tactile technologies presented in Part II may be included in a large framework for rehab and telemedicine. This integrated system could incorporate virtual reality environments, online data protocols for real-time transmission of tactile signals, as well as sensors for patient data collection. Consequently, this comprehensive framework could be utilized in clinical studies to assess treatment effectiveness and adapt hardware and software components based on user and clinician feedback.

Lastly, the extensive research conducted on cellular models and lab animals about cancer inhibition may pave the way for a new therapy to freeze the clinical state of a patient and fight tumor recurrences. Future research endeavors will not only contribute to advancing the fields of biology and mechanobiology but also catalyze the evolution of haptics into novel applications of cancer treatment. This groundbreaking work holds significant promise for transforming how we approach cancer treatment in the future.

Bibliography

[1] W. M. Bergmann Tiest and A. M. Kappers, "Haptic perception of gravitational and inertial mass," *Attention, perception, & psychophysics*, vol. 72, no. 4, pp. 1144–1154, 2010.

[2] J. A. McGrath, R. Eady, and F. Pope, "Anatomy and organization of human skin," *Rook's textbook of dermatology*, vol. 1, pp. 3–2, 2004.

[3] J. Dargahi and S. Najarian, "Human tactile perception as a standard for artificial tactile sensing—a review," *The international journal of medical robotics and computer assisted surgery*, vol. 1, no. 1, pp. 23–35, 2004.

[4] F. McGlone and D. Reilly, "The cutaneous sensory system," *Neuroscience & Biobehavioral Reviews*, vol. 34, no. 2, pp. 148–159, 2010.

[5] R. Cobo, J. García-Piqueras, J. Cobo, and J. A. Vega, "The human cutaneous sensory corpuscles: an update," *Journal of Clinical Medicine*, vol. 10, no. 2, p. 227, 2021.

[6] J. E. Hall and A. C. Guyton, "Textbook of medical physiology, saunders," *PA, USA*, 2011.

[7] J. D. Michelson and C. Hutchins, "Mechanoreceptors in human ankle ligaments," *The Journal of Bone & Joint Surgery British Volume*, vol. 77, no. 2, pp. 219–224, 1995.

[8] W. H. Talbot, I. Darian-Smith, H. H. Kornhuber, and V. B. Mountcastle, "The sense of flutter-vibration: comparison of the human capacity with response patterns of mechanoreceptive afferents from the monkey hand." *Journal of neurophysiology*, vol. 31, no. 2, pp. 301–334, 1968.

[9] K. O. Johnson and S. S. Hsiao, "Neural mechanisms of tactual form and texture perception," *Annual review of neuroscience*, vol. 15, no. 1, pp. 227–250, 1992.

[10] H. E. Torebjörk and J. L. Ochoa, "Specific sensations evoked by activity in single identified sensory units in man," *Acta Physiologica Scandinavica*, vol. 110, no. 4, pp. 445–447, 1980.

[11] J. Bell, S. Bolanowski, and M. H. Holmes, "The structure and function of pacinian corpuscles: a review," *Progress in neurobiology*, vol. 42, no. 1, pp. 79–128, 1994.

[12] J. Roelofsen, J. Klein-Nulend, and E. H. Burger, "Mechanical stimulation by intermittent hydrostatic compression promotes bone-specific gene expression in vitro," *Journal of biomechanics*, vol. 28, no. 12, pp. 1493–1503, 1995.

[13] I. Komuro and Y. Yazaki, "Control of cardiac gene expression by mechanical stress," *Annual review of physiology*, vol. 55, no. 1, pp. 55–75, 1993.

[14] L. Zentilin, U. Puligadda, V. Lionetti, S. Zacchigna, C. Collesi, L. Pattarini, G. Ruozi, S. Camporesi, G. Sinagra, M. Pepe *et al.*, "Cardiomyocyte vegfr-1 activation by vegf-b induces compensatory hypertrophy and preserves cardiac function after myocardial infarction," *The FASEB Journal*, vol. 24, no. 5, pp. 1467–1478, 2010.

[15] A. Di Matteo, E. Belloni, D. Pradella, A. Cappelletto, N. Volf, S. Zacchigna, and C. Ghigna, "Alternative splicing in endothelial cells: novel therapeutic opportunities in cancer angiogenesis," *Journal of Experimental & Clinical Cancer Research*, vol. 39, pp. 1–19, 2020.

[16] L. Ramage, G. Nuki, and D. Salter, "Signalling cascades in mechanotransduction: cell–matrix interactions and mechanical loading," *Scandinavian journal of medicine & science in sports*, vol. 19, no. 4, pp. 457–469, 2009.

[17] A. J. Ingram, H. Ly, K. Thai, M. Kang, and J. W. Scholey, "Activation of mesangial cell signaling cascades in response to mechanical strain," *Kidney international*, vol. 55, no. 2, pp. 476–485, 1999.

[18] D. V. Zhelev and R. M. Hochmuth, "Mechanically stimulated cytoskeleton rearrangement and cortical contraction in human neutrophils," *Biophysical journal*, vol. 68, no. 5, pp. 2004–2014, 1995.

[19] E. Celik, M. H. Abdulreda, D. Maiguel, J. Li, and V. T. Moy, "Rearrangement of microtubule network under biochemical and mechanical stimulations," *Methods*, vol. 60, no. 2, pp. 195–201, 2013.

[20] N. Shah, Y. Morsi, and R. Manasseh, "From mechanical stimulation to biological pathways in the regulation of stem cell fate," *Cell biochemistry and function*, vol. 32, no. 4, pp. 309–325, 2014.

[21] M. H. Hsieh and H. T. Nguyen, "Molecular mechanism of apoptosis induced by mechanical forces," *International review of cytology*, vol. 245, pp. 45–90, 2005.

[22] M. J. Ackerman and D. E. Clapham, "Ion channels—basic science and clinical disease," *New England Journal of Medicine*, vol. 336, no. 22, pp. 1575–1586, 1997.

[23] B. Martinac, "Mechanosensitive ion channels: molecules of mechanotransduction," *Journal of cell science*, vol. 117, no. 12, pp. 2449–2460, 2004.

[24] L. Volkers, Y. Mechioukhi, and B. Coste, "Piezo channels: from structure to function," *Pflügers Archiv-European Journal of Physiology*, vol. 467, pp. 95–99, 2015.

[25] J. Wu, A. H. Lewis, and J. Grandl, "Touch, tension, and transduction–the function and regulation of piezo ion channels," *Trends in biochemical sciences*, vol. 42, no. 1, pp. 57–71, 2017.

[26] K. M. Yamada and B. Geiger, "Molecular interactions in cell adhesion complexes," *Current opinion in cell biology*, vol. 9, no. 1, pp. 76–85, 1997.

[27] F. Kong, A. J. García, A. P. Mould, M. J. Humphries, and C. Zhu, "Demonstration of catch bonds between an integrin and its ligand," *Journal of Cell Biology*, vol. 185, no. 7, pp. 1275–1284, 2009.

[28] W. E. Thomas, V. Vogel, and E. Sokurenko, "Biophysics of catch bonds," *Annu. Rev. Biophys.*, vol. 37, pp. 399–416, 2008.

[29] A. Resnick and U. Hopfer, "Force-response considerations in ciliary mechanosensation," *Biophysical journal*, vol. 93, no. 4, pp. 1380–1390, 2007.

[30] A. R. Harris, P. Jreij, and D. A. Fletcher, "Mechanotransduction by the actin cytoskeleton: converting mechanical stimuli into biochemical signals," *Annual review of biophysics*, vol. 47, pp. 617–631, 2018.

[31] D. E. Ingber, "Mechanosensation through integrins: cells act locally but think globally," *Proceedings of the National Academy of Sciences*, vol. 100, no. 4, pp. 1472–1474, 2003.

[32] W. Chang and J. G. Gu, "Role of microtubules in piezo2 mechanotransduction of mouse merkel cells," *Journal of neurophysiology*, vol. 124, no. 6, pp. 1824–1831, 2020.

[33] M. Grunwald, *Human haptic perception: Basics and applications.* Springer Science & Business Media, 2008.

[34] T. A. Kern, "Biological basics of haptic perception," in *Engineering Haptic Devices: A Beginner's Guide for Engineers.* Springer, 2009, pp. 35–58.

[35] D. G. Caldwell, S. Lawther, and A. Wardle, "Tactile perception and its application to the design of multi-modal cutaneous feedback systems," in *Proceedings of IEEE International Conference on Robotics and Automation*, vol. 4. IEEE, 1996, pp. 3215–3221.

[36] J. C. Tuthill and E. Azim, "Proprioception," *Current Biology*, vol. 28, no. 5, pp. R194–R203, 2018.

[37] E. V. Evarts, "Sherrington's concept of proprioception," *Trends in Neurosciences*, vol. 4, pp. 44–46, 1981.

[38] U. Proske, "Kinesthesia: the role of muscle receptors," *Muscle & Nerve: Official Journal of the American Association of Electrodiagnostic Medicine*, vol. 34, no. 5, pp. 545–558, 2006.

[39] B. B. Edin and N. Johansson, "Skin strain patterns provide kinaesthetic information to the human central nervous system." *The Journal of physiology*, vol. 487, no. 1, pp. 243–251, 1995.

[40] P.-J. Lattanzio and R. J. Petrella, "Knee proprioception: a review of mechanisms, measurements, and implications of muscular fatigue," *Orthopedics*, vol. 21, no. 4, pp. 463–471, 1998.

[41] T. Kalisch, J.-C. Kattenstroth, R. Kowalewski, M. Tegenthoff, and H. R. Dinse, "Cognitive and tactile factors affecting human haptic performance in later life," *PLoS One*, vol. 7, no. 1, p. e30420, 2012.

[42] J.-L. Rodríguez, R. Velázquez, C. Del-Valle-Soto, S. Gutiérrez, J. Varona, and J. Enríquez-Zarate, "Active and passive haptic perception of shape: Passive haptics can support navigation," *Electronics*, vol. 8, no. 3, p. 355, 2019.

[43] K. R. Vaghela, A. Trockels, and M. Carobene, "Active vs passive haptic feedback technology in virtual reality arthroscopy simulation: Which is most realistic?" *Journal of Clinical Orthopaedics and Trauma*, vol. 16, pp. 249–256, 2021.

[44] M. Di Luca and A. Mahnan, "Perceptual limits of visual-haptic simultanety in virtual reality interactions," in *2019 IEEE World Haptics Conference (WHC)*. IEEE, 2019, pp. 67–72.

[45] J. E. Colgate, M. C. Stanley, and J. M. Brown, "Issues in the haptic display of tool use," in *Proceedings 1995 IEEE/RSJ international conference on intelligent robots and systems. Human robot interaction and cooperative robots*, vol. 3. IEEE, 1995, pp. 140–145.

[46] G. Ekman, "Weber's law and related functions," *The Journal of Psychology*, vol. 47, no. 2, pp. 343–352, 1959.

[47] U. Koçak, K. L. Palmerius, C. Forsell, A. Ynnerman, and M. Cooper, "Analysis of the jnd of stiffness in three modes of comparison," in *Haptic and Audio Interaction Design: 6th International Workshop, HAID 2011, Kusatsu, Japan, August 25-26, 2011. Proceedings 6.* Springer, 2011, pp. 22–31.

[48] O. Caldiran, H. Z. Tan, and C. Basdogan, "Visuo-haptic discrimination of viscoelastic materials," *IEEE Transactions on Haptics*, vol. 12, no. 4, pp. 438–450, 2019.

[49] A. M. Genecov, A. A. Stanley, and A. M. Okamura, "Perception of a haptic jamming display: Just noticeable differences in stiffness and geometry," in *2014 IEEE Haptics Symposium (HAPTICS)*. IEEE, 2014, pp. 333–338.

[50] B. Unger, R. Hollis, and R. Klatzky, "Jnd analysis of texture roughness perception using a magnetic levitation haptic device," in *Second Joint EuroHaptics Conference and Symposium on Haptic Interfaces for Virtual Environment and Teleoperator Systems (WHC'07)*. IEEE, 2007, pp. 9–14.

[51] T. Zeng, F. Giraud, B. Lemaire-Semail, and M. Amberg, "Haptic perception of curvature through active touch," in *2011 IEEE World Haptics Conference*. IEEE, 2011, pp. 533–538.

[52] J. Park, A. J. Doxon, W. R. Provancher, D. E. Johnson, and H. Z. Tan, "Haptic edge sharpness perception with a contact location display," *IEEE Transactions on Haptics*, vol. 5, no. 4, pp. 323–331, 2012.

[53] K. Drewing and M. O. Ernst, "Integration of force and position cues for shape perception through active touch," *Brain research*, vol. 1078, no. 1, pp. 92–100, 2006.

[54] Y. Lee, I. Jang, and D. Lee, "Enlarging just noticeable differences of visual-proprioceptive conflict in vr using haptic feedback," in *2015 IEEE World Haptics Conference (WHC)*. IEEE, 2015, pp. 19–24.

[55] A. Lécuyer, J.-M. Burkhardt, S. Coquillart, and P. Coiffet, ""boundary of illusion": an experiment of sensory integration with a pseudo-haptic system," in *Proceedings IEEE Virtual Reality 2001*. IEEE, 2001, pp. 115–122.

[56] Y. Ujitoko and Y. Ban, "Survey of pseudo-haptics: Haptic feedback design and application proposals," *IEEE Transactions on Haptics*, vol. 14, no. 4, pp. 699–711, 2021.

[57] F. Conti and O. Khatib, "Spanning large workspaces using small haptic devices," in *First Joint Eurohaptics Conference and Symposium on Haptic Interfaces for Virtual Environment and Teleoperator Systems. World Haptics Conference*. IEEE, 2005, pp. 183–188.

[58] J. K. Salisbury and M. A. Srinivasan, "Phantom-based haptic interaction with virtual objects," *IEEE Computer Graphics and Applications*, vol. 17, no. 5, pp. 6–10, 1997.

[59] T. Sansanayuth, I. Nilkhamhang, and K. Tungpimolrat, "Teleoperation with inverse dynamics control for phantom omni haptic device," in *2012 Proceedings of SICE Annual Conference (SICE)*. IEEE, 2012, pp. 2121–2126.

[60] C. Pacchierotti, M. Abayazid, S. Misra, and D. Prattichizzo, "Teleoperation of steerable flexible needles by combining kinesthetic and vibratory feedback," *IEEE transactions on haptics*, vol. 7, no. 4, pp. 551–556, 2014.

[61] T. Endo, H. Kawasaki, T. Mouri, Y. Ishigure, H. Shimomura, M. Matsumura, and K. Koketsu, "Five-fingered haptic interface robot: Hiro iii," *IEEE transactions on haptics*, vol. 4, no. 1, pp. 14–27, 2010.

[62] C. Pacchierotti, A. Tirmizi, and D. Prattichizzo, "Improving transparency in teleoperation by means of cutaneous tactile force feedback," *ACM Transactions on Applied Perception (TAP)*, vol. 11, no. 1, pp. 1–16, 2014.

[63] C. Pacchierotti, F. Chinello, M. Malvezzi, L. Meli, and D. Prattichizzo, "Two finger grasping simulation with cutaneous and kinesthetic force feedback," in *Proc. Int. Conf. on Human Haptic Sensing and Touch Enabled Computer Applications.* Springer, 2012, pp. 373–382.

[64] C. Pacchierotti, S. Sinclair, M. Solazzi, A. Frisoli, V. Hayward, and D. Prattichizzo, "Wearable haptic systems for the fingertip and the hand: taxonomy, review, and perspectives," *IEEE transactions on haptics*, vol. 10, no. 4, pp. 580–600, 2017.

[65] C. Carignan, J. Tang, and S. Roderick, "Development of an exoskeleton haptic interface for virtual task training," in *2009 IEEE/RSJ International Conference on Intelligent Robots and Systems.* IEEE, 2009, pp. 3697–3702.

[66] T. Koyama, I. Yamano, K. Takemura, and T. Maeno, "Multi-fingered exoskeleton haptic device using passive force feedback for dexterous teleoperation," in *IEEE/RSJ International Conference on Intelligent Robots and Systems*, vol. 3. IEEE, 2002, pp. 2905–2910.

[67] A. Frisoli, F. Rocchi, S. Marcheschi, A. Dettori, F. Salsedo, and M. Bergamasco, "A new force-feedback arm exoskeleton for haptic interaction in virtual environments," in *first joint eurohaptics conference and symposium on haptic interfaces for virtual environment and teleoperator systems. World haptics conference.* IEEE, 2005, pp. 195–201.

[68] F. Chinello, M. Malvezzi, D. Prattichizzo, and C. Pacchierotti, "A modular wearable finger interface for cutaneous and kinesthetic interaction: control and evaluation," *IEEE Transactions on Industrial Electronics*, vol. 67, no. 1, pp. 706–716, 2019.

[69] D. Prattichizzo, F. Chinello, C. Pacchierotti, and M. Malvezzi, "Towards wearability in fingertip haptics: a 3-dof wearable device for cutaneous force feedback," *IEEE Transactions on Haptics*, vol. 6, no. 4, pp. 506–516, 2013.

[70] F. Chinello, C. Pacchierotti, J. Bimbo, N. G. Tsagarakis, and D. Prattichizzo, "Design and evaluation of a wearable skin stretch device for haptic guidance," *IEEE Robotics and Automation Letters*, vol. 3, no. 1, pp. 524–531, 2017.

[71] L. Kuang, M. Ferro, M. Malvezzi, D. Prattichizzo, P. R. Giordano, F. Chinello, and C. Pacchierotti, "A wearable haptic device for the hand with interchangeable end-effectors," *IEEE Transactions on Haptics*, 2023.

[72] J. Bimbo, C. Pacchierotti, M. Aggravi, N. Tsagarakis, and D. Prattichizzo, "Teleoperation in cluttered environments using wearable haptic feedback," in *2017 IEEE/RSJ International Conference on Intelligent Robots and Systems (IROS).* IEEE, 2017, pp. 3401–3408.

[73] I. Hussain, L. Meli, C. Pacchierotti, G. Salvietti, D. Prattichizzo *et al.*, "Vibrotactile haptic feedback for intuitive control of robotic extra fingers." in *World Haptics*, 2015, pp. 394–399.

[74] S. Scheggi, F. Chinello, and D. Prattichizzo, "Vibrotactile haptic feedback for human-robot interaction in leader-follower tasks," in *Proceedings of the 5th International Conference on PErvasive Technologies Related to Assistive Environments*, 2012, pp. 1–4.

[75] S. Scheggi, L. Meli, C. Pacchierotti, and D. Prattichizzo, "Touch the virtual reality: using the leap motion controller for hand tracking and wearable tactile devices for immersive haptic rendering," in *ACM SIGGRAPH 2015 Posters*, 2015, pp. 1–1.

[76] I. Choi, E. W. Hawkes, D. L. Christensen, C. J. Ploch, and S. Follmer, "Wolverine: A wearable haptic interface for grasping in virtual reality," in *2016 IEEE/RSJ International Conference on Intelligent Robots and Systems (IROS).* IEEE, 2016, pp. 986–993.

[77] M. Gabardi, M. Solazzi, D. Leonardis, and A. Frisoli, "A new wearable fingertip haptic interface for the rendering of virtual shapes and surface features," in *2016 IEEE haptics symposium (HAPTICS)*. IEEE, 2016, pp. 140–146.

[78] D. Leonardis, M. Solazzi, I. Bortone, and A. Frisoli, "A wearable fingertip haptic device with 3 dof asymmetric 3-rsr kinematics," in *2015 IEEE world haptics conference (WHC)*. IEEE, 2015, pp. 388–393.

[79] S. B. Schorr and A. M. Okamura, "Three-dimensional skin deformation as force substitution: Wearable device design and performance during haptic exploration of virtual environments," *IEEE transactions on haptics*, vol. 10, no. 3, pp. 418–430, 2017.

[80] T. L. Baldi, N. d'Aurizio, and D. Prattichizzo, "Hand guidance using grasping metaphor and wearable haptics," in *2020 IEEE Haptics Symposium (HAPTICS)*. IEEE, 2020, pp. 961–967.

[81] H. Kim, H. Yi, H. Lee, and W. Lee, "Hapcube: A wearable tactile device to provide tangential and normal pseudo-force feedback on a fingertip," in *Proceedings of the 2018 CHI Conference on Human Factors in Computing Systems*, 2018, pp. 1–13.

[82] T. Maeda, R. Peiris, M. Nakatani, Y. Tanaka, and K. Minamizawa, "Wearable haptic augmentation system using skin vibration sensor," in *proceedings of the 2016 virtual reality international conference*, 2016, pp. 1–4.

[83] H. Kim, M. Kim, and W. Lee, "Hapthimble: A wearable haptic device towards usable virtual touch screen," in *Proceedings of the 2016 CHI Conference on Human Factors in Computing Systems*, 2016, pp. 3694–3705.

[84] M. Gabardi, D. Leonardis, M. Solazzi, and A. Frisoli, "Development of a miniaturized thermal module designed for integration in a wearable haptic device," in *2018 IEEE Haptics Symposium (HAPTICS)*. IEEE, 2018, pp. 100–105.

[85] Y. Osawa and S. Katsura, "Wearable thermal interface for sharing palm heat conduction," in *IECON 2018-44th Annual Conference of the IEEE Industrial Electronics Society*. IEEE, 2018, pp. 3310–3315.

[86] M. Zhu, S. Biswas, S. I. Dinulescu, N. Kastor, E. W. Hawkes, and Y. Visell, "Soft, wearable robotics and haptics: Technologies, trends, and emerging applications," *Proceedings of the IEEE*, vol. 110, no. 2, pp. 246–272, 2022.

[87] S. Jadhav, V. Kannanda, B. Kang, M. T. Tolley, and J. P. Schulze, "Soft robotic glove for kinesthetic haptic feedback in virtual reality environments," *electronic imaging*, vol. 29, pp. 19–24, 2017.

[88] T. Nakao, K. Kunze, M. Isogai, S. Shimizu, and Y. S. Pai, "Fingerflex: Shape memory alloy-based actuation on fingers for kinesthetic haptic feedback," in *Proceedings of the 19th International Conference on Mobile and Ubiquitous Multimedia*, 2020, pp. 240–244.

[89] P. Tran, S. Jeong, F. Lyu, K. Herrin, S. Bhatia, D. Elliott, S. Kozin, and J. P. Desai, "Flexotendon glove-iii: Voice-controlled soft robotic hand exoskeleton with novel fabrication method and admittance grasping control," *IEEE/ASME Transactions on Mechatronics*, vol. 27, no. 5, pp. 3920–3931, 2022.

[90] P. Tran, S. Jeong, S. L. Wolf, and J. P. Desai, "Patient-specific, voice-controlled, robotic flexotendon glove-ii system for spinal cord injury," *IEEE Robotics and Automation Letters*, vol. 5, no. 2, pp. 898–905, 2020.

[91] M. Hosseini, A. Sengül, Y. Pane, J. De Schutter, and H. Bruyninck, "Exoten-glove: A force-feedback haptic glove based on twisted string actuation system," in *2018 27th IEEE International Symposium on Robot and Human Interactive Communication (RO-MAN)*. IEEE, 2018, pp. 320–327.

[92] S. Baik, S. Park, and J. Park, "Haptic glove using tendon-driven soft robotic mechanism," *Frontiers in bioengineering and biotechnology*, vol. 8, p. 541105, 2020.

[93] R. Hinchet and H. Shea, "High force density textile electrostatic clutch," *Advanced Materials Technologies*, vol. 5, no. 4, p. 1900895, 2020.

[94] C. Suulker, A. Hassan, S. Skach, and K. Althoefer, "A comparison of silicone and fabric inflatable actuators for soft hand exoskeletons," in *2022 IEEE 5th International Conference on Soft Robotics (RoboSoft)*. IEEE, 2022, pp. 735–740.

[95] L. Liu, C. Yao, Y. Liu, P. Wang, Y. Chen, and F. Ying, "Flowglove: A liquid-based wearable device for haptic interaction in virtual reality," in *HCI International 2020–Late Breaking Papers: Digital Human Modeling and Ergonomics, Mobility and Intelligent Environments: 22nd HCI International Conference, HCII 2020, Copenhagen, Denmark, July 19–24, 2020, Proceedings 22*. Springer, 2020, pp. 316–331.

[96] V. Sanchez, C. J. Walsh, and R. J. Wood, "Textile technology for soft robotic and autonomous garments," *Advanced functional materials*, vol. 31, no. 6, p. 2008278, 2021.

[97] H. Xiong and X. Diao, "A review of cable-driven rehabilitation devices," *Disability and Rehabilitation: Assistive Technology*, vol. 15, no. 8, pp. 885–897, 2020.

[98] J. Sanjuan, A. D. Castillo, M. A. Padilla, M. C. Quintero, E. Gutierrez, I. P. Sampayo, J. R. Hernandez, and M. H. Rahman, "Cable driven exoskeleton for upper-limb rehabilitation: A design review," *Robotics and Autonomous Systems*, vol. 126, p. 103445, 2020.

[99] E. M. Young, A. H. Memar, P. Agarwal, and N. Colonnese, "Bellowband: A pneumatic wristband for delivering local pressure and vibration," in *2019 IEEE World Haptics Conference (WHC)*. IEEE, 2019, pp. 55–60.

[100] N. Agharese, T. Cloyd, L. H. Blumenschein, M. Raitor, E. W. Hawkes, H. Culbertson, and A. M. Okamura, "Hapwrap: Soft growing wearable haptic device," in *2018 IEEE International Conference on Robotics and Automation (ICRA)*. IEEE, 2018, pp. 5466–5472.

[101] W. Wu and H. Culbertson, "Wearable haptic pneumatic device for creating the illusion of lateral motion on the arm," in *2019 IEEE World Haptics Conference (WHC)*. IEEE, 2019, pp. 193–198.

[102] M. Zhu, A. H. Memar, A. Gupta, M. Samad, P. Agarwal, Y. Visell, S. J. Keller, and N. Colonnese, "Pneusleeve: In-fabric multimodal actuation and sensing in a soft, compact, and expressive haptic sleeve," in *Proceedings of the 2020 CHI conference on human factors in computing systems*, 2020, pp. 1–12.

[103] E. Pezent, P. Agarwal, J. Hartcher-O'Brien, N. Colonnese, and M. K. O'Malley, "Design, control, and psychophysics of tasbi: A force-controlled multimodal haptic bracelet," *IEEE Transactions on Robotics*, vol. 38, no. 5, pp. 2962–2978, 2022.

[104] M. Aggravi, F. Pausé, P. R. Giordano, and C. Pacchierotti, "Design and evaluation of a wearable haptic device for skin stretch, pressure, and vibrotactile stimuli," *IEEE Robotics and Automation Letters*, vol. 3, no. 3, pp. 2166–2173, 2018.

[105] F. Chinello, C. Pacchierotti, N. G. Tsagarakis, and D. Prattichizzo, "Design of a wearable skin stretch cutaneous device for the upper limb," in *2016 IEEE Haptics Symposium (HAPTICS)*. IEEE, 2016, pp. 14–20.

[106] A. Gupta, A. A. R. Irudayaraj, and R. Balakrishnan, "Hapticclench: Investigating squeeze sensations using memory alloys," in *Proceedings of the 30th Annual ACM Symposium on User Interface Software and Technology*, 2017, pp. 109–117.

[107] C. Pacchierotti, G. Salvietti, I. Hussain, L. Meli, and D. Prattichizzo, "The hring: A wearable haptic device to avoid occlusions in hand tracking," in *2016 IEEE haptics symposium (HAPTICS)*. IEEE, 2016, pp. 134–139.

[108] T. Aoki, H. Mitake, S. Hasegawa, and M. Sato, "Haptic ring: touching virtual creatures in mixed reality environments," in *SIGGRAPH'09: Posters*, 2009, pp. 1–1.

[109] S. B. Schorr and A. M. Okamura, "Fingertip tactile devices for virtual object manipulation and exploration," in *Proceedings of the 2017 CHI conference on human factors in computing systems*, 2017, pp. 3115–3119.

[110] T. Kurogi, Y. Yonehara, R. L. Peiris, T. Fujiwara, and K. Minamizawa, "Haptic plaster: soft, thin, light and flexible haptic display using dea composed of slide-ring material for daily life," in *ACM SIGGRAPH 2019 Emerging Technologies*, 2019, pp. 1–2.

[111] A. Talhan, H. Kim, and S. Jeon, "Tactile ring: Multi-mode finger-worn soft actuator for rich haptic feedback," *IEEE Access*, vol. 8, pp. 957–966, 2019.

[112] A. Talhan, H. Kim, and S. Jeon, "Wearable soft pneumatic ring with multi-mode controlling for rich haptic effects," in *ACM SIGGRAPH 2019 Posters*, 2019, pp. 1–2.

[113] D. Hwang, J. Lee, and K. Kim, "On the design of a miniature haptic ring for cutaneous force feedback using shape memory alloy actuators," *Smart Materials and Structures*, vol. 26, no. 10, p. 105002, 2017.

[114] J. Saint-Aubert, J. Manson, I. Bonan, Y. Launey, A. Lécuyer, and M. Cogné, "Effect of vibrations on impression of walking and embodiment with first- and third-person avatar," *IEEE Transactions on Visualization and Computer Graphics*, vol. 29, no. 12, pp. 5579–5585, 2023.

[115] X. de Tinguy, C. Pacchierotti, M. Marchal, and A. Lécuyer, "Enhancing the stiffness perception of tangible objects in mixed reality using wearable haptics," in *2018 IEEE Conference on Virtual Reality and 3D User Interfaces (VR)*, 2018, pp. 81–90.

[116] S. V. Salazar, C. Pacchierotti, X. de Tinguy, A. Maciel, and M. Marchal, "Altering the stiffness, friction, and shape perception of tangible objects in virtual reality using wearable haptics," *IEEE Transactions on Haptics*, vol. 13, no. 1, pp. 167–174, 2020.

[117] X. de Tinguy, C. Pacchierotti, M. Marchal, and A. Lécuyer, "Toward universal tangible objects: Optimizing haptic pinching sensations in 3d interaction," in *2019 IEEE Conference on Virtual Reality and 3D User Interfaces (VR)*, 2019, pp. 321–330.

[118] R. Nordahl, S. Serafin, N. C. Nilsson, and L. Turchet, "Enhancing realism in virtual environments by simulating the audio-haptic sensation of walking on ground surfaces," in *2012 IEEE Virtual Reality Workshops (VRW)*, 2012, pp. 73–74.

[119] N. Ouarti, A. Lécuyer, and A. Berthoz, "Haptic motion: Improving sensation of self-motion in virtual worlds with force feedback," in *2014 IEEE Haptics Symposium (HAPTICS)*, 2014, pp. 167–174.

[120] K. M. A. Aziz, H. Luo, L. Asma, W. Xu, Y. Zhang, and D. Wang, "Haptic handshank – a handheld multimodal haptic feedback controller for virtual reality," in *2020 IEEE International Symposium on Mixed and Augmented Reality (ISMAR)*, 2020, pp. 239–250.

[121] W. Park, S. Park, L. Kim, and S. Shin, "Haptic mouse interface actuated by an electromagnet," in *2011 International Conference on Complex, Intelligent, and Software Intensive Systems*, 2011, pp. 643–646.

[122] S.-M. Cho and S.-Y. Kim, "Shake it: A portable haptic mouse and shaking application," in *2009 ICCAS-SICE*, 2009, pp. 3788–3791.

[123] C.-M. Wu, C.-W. Hsu, T.-K. Lee, and S. Smith, "A virtual reality keyboard with realistic haptic feedback in a fully immersive virtual environment," *Virtual Reality*, vol. 21, pp. 19–29, 2017.

[124] J. Perret and E. Vander Poorten, "Touching virtual reality: a review of haptic gloves," in *ACTUATOR 2018; 16th International Conference on New Actuators*. VDE, 2018, pp. 1–5.

[125] J. Perret and E. Vander Poorten, "Commercial haptic gloves," in *Proceedings of the 15th Annual EuroVR Conference*. VTT Technology, 2018, pp. 39–48.

[126] M. Giordano, I. Hattwick, I. Franco, D. Egloff, E. Frid, V. Lamontagne, C. TeZ, C. Salter, and M. Wanderley, "Design and implementation of a whole-body haptic suit for "ilinx", a multisensory art installation," in *12th International Conference on Sound and Music Computing (SMC-15), Ireland, July 30, 31 & August 1, 2015*, vol. 1. Maynooth University, 2015, pp. 169–175.

[127] D. Kang, C.-G. Lee, and O. Kwon, "Pneumatic and acoustic suit: multimodal haptic suit for enhanced virtual reality simulation," *Virtual Reality*, vol. 27, no. 3, pp. 1647–1669, 2023.

[128] A. Al Maimani and A. Roudaut, "Frozen suit: designing a changeable stiffness suit and its application to haptic games," in *Proceedings of the 2017 CHI Conference on Human Factors in Computing Systems*, 2017, pp. 2440–2448.

[129] G. Spagnoletti, L. Meli, T. L. Baldi, G. Gioioso, C. Pacchierotti, and D. Prattichizzo, "Rendering of pressure and textures using wearable haptics in immersive vr environments," in *2018 IEEE Conference on Virtual Reality and 3D User Interfaces (VR)*. IEEE, 2018, pp. 691–692.

[130] E. Strasnick, C. Holz, E. Ofek, M. Sinclair, and H. Benko, "Haptic links: Bimanual haptics for virtual reality using variable stiffness actuation," in *Proceedings of the 2018 CHI Conference on Human Factors in Computing Systems*, 2018, pp. 1–12.

[131] W. Dangxiao, G. Yuan, L. Shiyi, Y. Zhang, X. Weiliang, and X. Jing, "Haptic display for virtual reality: progress and challenges," *Virtual Reality & Intelligent Hardware*, vol. 1, no. 2, pp. 136–162, 2019.

[132] R. J. Stone, "Haptic feedback: A brief history from telepresence to virtual reality," in *International Workshop on Haptic Human-Computer Interaction*. Springer, 2000, pp. 1–16.

[133] E. Normand, C. Pacchierotti, E. Marchand, and M. Marchal, "Visuo-haptic rendering of the hand during 3d manipulation in augmented reality," *IEEE Transactions on Haptics*, 2024.

[134] M. Maisto, C. Pacchierotti, F. Chinello, G. Salvietti, A. De Luca, and D. Prattichizzo, "Evaluation of wearable haptic systems for the fingers in augmented reality applications," *IEEE transactions on haptics*, vol. 10, no. 4, pp. 511–522, 2017.

[135] L. Meli, C. Pacchierotti, G. Salvietti, F. Chinello, M. Maisto, A. De Luca, and D. Prattichizzo, "Combining wearable finger haptics and augmented reality: User evaluation using an external camera and the microsoft hololens," *IEEE Robotics and Automation Letters*, vol. 3, no. 4, pp. 4297–4304, 2018.

[136] H. Bai, S. Li, and R. F. Shepherd, "Elastomeric haptic devices for virtual and augmented reality," *Advanced Functional Materials*, vol. 31, no. 39, p. 2009364, 2021.

[137] G. V. A. G. Asanka Perera and A. M. H. S. Abeykoon, "Review on bilateral teleoperation with force, position, power and impedance scaling," in *7th International Conference on Information and Automation for Sustainability*, 2014, pp. 1–7.

[138] A. Bolopion and S. Régnier, "A review of haptic feedback teleoperation systems for micromanipulation and microassembly," *IEEE Transactions on Automation Science and Engineering*, vol. 10, no. 3, pp. 496–502, 2013.

[139] K. Darvish, L. Penco, J. Ramos, R. Cisneros, J. Pratt, E. Yoshida, S. Ivaldi, and D. Pucci, "Teleoperation of humanoid robots: A survey," *IEEE Transactions on Robotics*, vol. 39, no. 3, pp. 1706–1727, 2023.

[140] A. Tirmizi, C. Pacchierotti, and D. Prattichizzo, "On the role of cutaneous force in teleoperation: subtracting kinesthesia from complete haptic feedback," in *2013 World Haptics Conference (WHC)*, 2013, pp. 371–376.

[141] C. Pacchierotti, A. Tirmizi, G. Bianchini, and D. Prattichizzo, "Enhancing the performance of passive teleoperation systems via cutaneous feedback," *IEEE Transactions on Haptics*, vol. 8, no. 4, pp. 397–409, 2015.

[142] S. McAmis and K. B. Reed, "Application of haptic feedback to a combot," in *2012 IEEE Haptics Symposium (HAPTICS)*, 2012, pp. 553–557.

[143] A. Casalino, C. Messeri, M. Pozzi, A. M. Zanchettin, P. Rocco, and D. Prattichizzo, "Operator awareness in human–robot collaboration through wearable vibrotactile feedback," *IEEE Robotics and Automation Letters*, vol. 3, no. 4, pp. 4289–4296, 2018.

[144] R. Luz, J. Corujeira, J. L. Silva, and R. Ventura, "Traction awareness through haptic feedback for the teleoperation of ugvs," in *2018 27th IEEE International Symposium on Robot and Human Interactive Communication (RO-MAN)*, 2018, pp. 313–319.

[145] A. Ghosh, J. Penders, P. E. Jones, and H. Reed, "Experience of using a haptic interface to follow a robot without visual feedback," in *The 23rd IEEE International Symposium on Robot and Human Interactive Communication*, 2014, pp. 329–334.

[146] A. Gani, O. Pickering, C. Ellis, O. Sabri, and P. Pucher, "Impact of haptic feedback on surgical training outcomes: A randomised controlled trial of haptic versus non-haptic immersive virtual reality training," *Annals of Medicine and Surgery*, vol. 83, p. 104734, 2022. [Online]. Available: https://www.sciencedirect.com/science/article/pii/S2049080122014947

[147] C. Basdogan, S. De, J. Kim, M. Muniyandi, H. Kim, and M. Srinivasan, "Haptics in minimally invasive surgical simulation and training," *IEEE Computer Graphics and Applications*, vol. 24, no. 2, pp. 56–64, 2004.

[148] M. Tavakoli, R. Patel, and M. Moallem, "A haptic interface for computer-integrated endo-scopic surgery and training," *Virtual Reality*, vol. 9, pp. 160–176, 03 2006.

[149] J. Guo and S. Guo, "A haptic interface design for a vr-based unskilled doctor training system in vascular interventional surgery," in *2014 IEEE International Conference on Mechatronics and Automation*, 2014, pp. 1259–1263.

[150] M. Guiatni, V. Riboulet, and A. Kheddar, "Design and evaluation of a haptic interface for interactive simulation of minimally-invasive surgeries," in *2009 IEEE/ASME International Conference on Advanced Intelligent Mechatronics*, 2009, pp. 1336–1341.

[151] D. Escobar-Castillejos, J. Noguez, L. Neri, A. Magana, and B. Benes, "A review of simulators with haptic devices for medical training," *Journal of Medical Systems*, vol. 40, 02 2016.

[152] E. Abdi, D. Kulić, and E. Croft, "Haptics in teleoperated medical interventions: Force measurement, haptic interfaces and their influence on user's performance," *IEEE Transactions on Biomedical Engineering*, vol. 67, no. 12, pp. 3438–3451, 2020.

[153] C. Gaudeni, T. Lisini, G. Achilli, M. Mandalà, and D. Prattichizzo, *Instrumenting Hand-Held Surgical Drills with a Pneumatic Sensing Cover for Haptic Feedback*, 09 2020, pp. 398–406.

[154] Y. Zheng, M. Ershad, and A. M. Fey, "Toward correcting anxious movements using haptic cues on the da vinci surgical robot," in *2022 9th IEEE RAS/EMBS International Conference for Biomedical Robotics and Biomechatronics (BioRob)*, 2022, pp. 1–8.

[155] E. Lopez, L. Zollo, and E. Guglielmelli, "Teleoperated control based on virtual fixtures for a redundant surgical system," in *2013 IEEE/RSJ International Conference on Intelligent Robots and Systems*, 2013, pp. 450–455.

[156] A. M. Okamura, "Methods for haptic feedback in teleoperated robot-assisted surgery," *Industrial Robot: An International Journal*, vol. 31, no. 6, pp. 499–508, 2004.

[157] A. A. Syed, X. guang Duan, X. Kong, M. Li, Yonggui-Wang, and Q. Huang, "6-dof maxillofacial surgical robotic manipulator controlled by haptic device," in *2012 9th International Conference on Ubiquitous Robots and Ambient Intelligence (URAI)*, 2012, pp. 71–74.

[158] N. Enayati, E. De Momi, and G. Ferrigno, "Haptics in robot-assisted surgery: Challenges and benefits," *IEEE Reviews in Biomedical Engineering*, vol. 9, pp. 49–65, 2016.

[159] C. Wagner, N. Stylopoulos, and R. Howe, "The role of force feedback in surgery: analysis of blunt dissection," in *Proceedings 10th Symposium on Haptic Interfaces for Virtual Environment and Teleoperator Systems. HAPTICS 2002*, 2002, pp. 68–74.

[160] I. Bortone, D. Leonardis, N. Mastronicola, A. Crecchi, L. Bonfiglio, C. Procopio, M. Solazzi, and A. Frisoli, "Wearable haptics and immersive virtual reality rehabilitation training in children with neuromotor impairments," *IEEE Transactions on Neural Systems and Rehabilitation Engineering*, vol. 26, no. 7, pp. 1469–1478, 2018.

[161] M. L. Gordon and S. Zhai, "Touchscreen haptic augmentation effects on tapping, drag and drop, and path following," in *Proceedings of the 2019 CHI Conference on Human Factors in Computing Systems*, 2019, pp. 1–12.

[162] G. Huisman, T. Lisini Baldi, N. D'Aurizio, and D. Prattichizzo, "Feedback of head gestures in audio-haptic remote communication," in *Proceedings of the 2021 ACM International Symposium on Wearable Computers*, 2021, pp. 135–137.

[163] T. L. Baldi, G. Paolocci, D. Barcelli, and D. Prattichizzo, "Wearable haptics for remote social walking," *IEEE transactions on haptics*, vol. 13, no. 4, pp. 761–776, 2020.

[164] J. Smith and K. MacLean, "Communicating emotion through a haptic link: Design space and methodology," *International Journal of Human-Computer Studies*, vol. 65, no. 4, pp. 376–387, 2007.

[165] N. D'Aurizio, T. Ramundo, T. L. Baldi, A. Moscatelli, and D. Prattichizzo, "On the correlation between tactile stimulation and pleasantness," *IEEE Transactions on Haptics*, 2023.

[166] A. Papadopoulou, J. Berry, T. Knight, and R. Picard, "Affective sleeve: Wearable materials with haptic action for promoting calmness," in *Distributed, Ambient and Pervasive Interactions: 7th International Conference, DAPI 2019, Held as Part of the 21st HCI International Conference, HCII 2019, Orlando, FL, USA, July 26–31, 2019, Proceedings 21.* Springer, 2019, pp. 304–319.

[167] C. Kelling, D. Pitaro, and J. Rantala, "Good vibes: the impact of haptic patterns on stress levels," in *Proceedings of the 20th International Academic Mindtrek Conference*, 2016, pp. 130–136.

[168] O. Ozioko, W. Taube, M. Hersh, and R. Dahiya, "Smartfingerbraille: A tactile sensing and actuation based communication glove for deafblind people," in *2017 IEEE 26th International Symposium on Industrial Electronics (ISIE)*. IEEE, 2017, pp. 2014–2018.

[169] H. P. Savindu, K. Iroshan, C. D. Panangala, W. Perera, and A. C. De Silva, "Brailleband: Blind support haptic wearable band for communication using braille language," in *2017 IEEE International Conference on Systems, Man, and Cybernetics (SMC)*. IEEE, 2017, pp. 1381–1386.

[170] J. P. Fritz, T. P. Way, and K. E. Barner, "Haptic representation of scientific data for visually impaired or blind persons," in *Proceedings of the CSUN Conference on Technology and Disability*. Citeseer, 1996.

[171] U. Gollner, T. Bieling, and G. Joost, "Mobile lorm glove: introducing a communication device for deaf-blind people," in *Proceedings of the sixth international conference on tangible, embedded and embodied interaction*, 2012, pp. 127–130.

[172] C. Colwell, H. Petrie, D. Kornbrot, A. Hardwick, and S. Furner, "Haptic virtual reality for blind computer users," in *Proceedings of the third international ACM conference on Assistive technologies*, 1998, pp. 92–99.

[173] O. Lahav and D. Mioduser, "Haptic-feedback support for cognitive mapping of unknown spaces by people who are blind," *International Journal of Human-Computer Studies*, vol. 66, no. 1, pp. 23–35, 2008.

[174] J. Kilian, A. Neugebauer, L. Scherffig, and S. Wahl, "The unfolding space glove: A wearable spatio-visual to haptic sensory substitution device for blind people," *Sensors*, vol. 22, no. 5, p. 1859, 2022.

[175] S. Kammoun, C. Jouffrais, T. Guerreiro, H. Nicolau, and J. Jorge, "Guiding blind people with haptic feedback," *Frontiers in Accessibility for Pervasive Computing (Pervasive 2012)*, vol. 3, 2012.

[176] S. Scheggi, A. Talarico, and D. Prattichizzo, "A remote guidance system for blind and visually impaired people via vibrotactile haptic feedback," in *22nd Mediterranean conference on control and automation*. IEEE, 2014, pp. 20–23.

[177] S. Rossi, T. Lisini Baldi, M. Aggravi, M. Ulivelli, D. Cioncoloni, V. Niccolini, L. Donati, and D. Prattichizzo, "Wearable haptic anklets for gait and freezing improvement in parkinson's disease: a proof-of-concept study," *Neurological sciences*, vol. 41, pp. 3643–3651, 2020.

[178] E. Rabin, J. Chen, L. Muratori, J. DiFrancisco-Donoghue, and W. G. Werner, "Haptic feedback from manual contact improves balance control in people with parkinson's disease," *Gait & posture*, vol. 38, no. 3, pp. 373–379, 2013.

[179] F. Barbic, M. Galli, L. Dalla Vecchia, M. Canesi, V. Cimolin, A. Porta, V. Bari, G. Cerri, F. Dipaola, T. Bassani *et al.*, "Effects of mechanical stimulation of the feet on gait and cardiovascular autonomic control in parkinson's disease," *Journal of Applied Physiology*, vol. 116, no. 5, pp. 495–503, 2014.

[180] B. I. Edwards, K. S. Bielawski, R. Prada, and A. D. Cheok, "Haptic virtual reality and immersive learning for enhanced organic chemistry instruction," *Virtual Reality*, vol. 23, no. 4, pp. 363–373, 2019.

[181] S. Madangopal, S. Jagannath, and B. Madapur, "Haptic teaching-learning practices in architecture education," *Journal of Advanced Research in Civil Engineering and Architecture*, vol. 2, no. 1, pp. 1–16, 2020.

[182] M. E. O'Neill, "Corporeal experience: A haptic way of knowing," *Journal of Architectural Education*, vol. 55, no. 1, pp. 3–12, 2001.

[183] S. Marullo, T. L. Baldi, G. Paolocci, N. D'Aurizio, and D. Prattichizzo, "No face-touch: Exploiting wearable devices and machine learning for gesture detection," in *2021 IEEE International Conference on Robotics and Automation (ICRA)*. IEEE, 2021, pp. 4187–4193.

[184] F. Visser, "Haptic feedback in a posture correcting wearable," B.S. thesis, University of Twente, 2018.

[185] E. Rabin, S. B. Bortolami, P. DiZio, and J. R. Lackner, "Haptic stabilization of posture: changes in arm proprioception and cutaneous feedback for different arm orientations," *Journal of neurophysiology*, vol. 82, no. 6, pp. 3541–3549, 1999.

[186] E. S. Ege, F. Cetin, and C. Basdogan, "Vibrotactile feedback in steering wheel reduces navigation errors during gps-guided car driving," in *2011 IEEE World Haptics Conference*. IEEE, 2011, pp. 345–348.

[187] F. Beruscha, K. Augsburg, and D. Manstetten, "Haptic warning signals at the steering wheel: A literature survey regarding lane departure warning systems (short paper)," 2011.

[188] S. M. Petermeijer, D. A. Abbink, M. Mulder, and J. C. De Winter, "The effect of haptic support systems on driver performance: A literature survey," *IEEE transactions on haptics*, vol. 8, no. 4, pp. 467–479, 2015.

[189] J. Morrell and K. Wasilewski, "Design and evaluation of a vibrotactile seat to improve spatial awareness while driving," in *2010 IEEE Haptics Symposium*. IEEE, 2010, pp. 281–288.

[190] V. Girbes, L. Armesto, J. Dols, and J. Tornero, "Haptic feedback to assist bus drivers for pedestrian safety at low speed," *IEEE transactions on haptics*, vol. 9, no. 3, pp. 345–357, 2016.

[191] L. M. Stanley, "Haptic and auditory cues for lane departure warnings," in *Proceedings of the human factors and ergonomics society annual meeting*, vol. 50, no. 22. SAGE Publications Sage CA: Los Angeles, CA, 2006, pp. 2405–2408.

[192] G. M. Fitch, J. M. Hankey, B. M. Kleiner, and T. A. Dingus, "Driver comprehension of multiple haptic seat alerts intended for use in an integrated collision avoidance system," *Transportation research part F: traffic psychology and behaviour*, vol. 14, no. 4, pp. 278–290, 2011.

[193] M. Hirokawa, N. Uesugi, S. Furugori, T. Kitagawa, and K. Suzuki, "Effect of haptic assistance on learning vehicle reverse parking skills," *IEEE transactions on haptics*, vol. 7, no. 3, pp. 334–344, 2014.

[194] C. Wang, F. Li, Y. Wang, and J. R. Wagner, "Haptic assistive control with learning-based driver intent recognition for semi-autonomous vehicles," *IEEE Transactions on Intelligent Vehicles*, vol. 8, no. 1, pp. 425–437, 2021.

[195] P. Di Campli San Vito, E. Brown, S. Brewster, F. Pollick, S. Thompson, L. Skrypchuk, and A. Mouzakitis, "Haptic feedback for the transfer of control in autonomous vehicles," in *12th International Conference on Automotive User Interfaces and Interactive Vehicular Applications*, 2020, pp. 34–37.

[196] S. Pushpakom, F. Iorio, P. A. Eyers, K. J. Escott, S. Hopper, A. Wells, A. Doig, T. Guilliams, J. Latimer, C. McNamee *et al.*, "Drug repurposing: progress, challenges and recommendations," *Nature reviews Drug discovery*, vol. 18, no. 1, pp. 41–58, 2019.

[197] G. Paolocci, T. Lisini Baldi, and D. Prattichizzo, "Human rendezvous via haptic suggestion," in *International AsiaHaptics conference*.   Springer, 2018, pp. 262–267.

[198] R. V. Kozinets, "Immersive netnography: a novel method for service experience research in virtual reality, augmented reality and metaverse contexts," *Journal of Service Management*, 2022.

[199] C. Helman. Defining The Metaverse Today. [Online]. Available: https://www.forbes.com/sites/cathyhackl/2021/05/02/defining-the-metaverse-today/

[200] D. Prattichizzo, F. Chinello, C. Pacchierotti, and K. Minamizawa, "Remotouch: A system for remote touch experience," in *19th International Symposium in Robot and Human Interactive Communication*.   IEEE, 2010, pp. 676–679.

[201] T. Lisini Baldi, S. Scheggi, L. Meli, M. Mohammadi, and D. Prattichizzo, "GESTO: A glove for enhanced sensing and touching based on inertial and magnetic sensors for hand tracking and cutaneous feedback," vol. 47, no. 6, pp. 1066–1076, 2017.

[202] S. A. Hossain, A. S. M. M. Rahman, and A. El Saddik, "Measurements of multimodal approach to haptic interaction in second life interpersonal communication system," *IEEE Transactions on Instrumentation and Measurement*, vol. 60, no. 11, pp. 3547–3558, 2011.

[203] F. Sanfilippo, L. I. Hatledal, and K. Pettersen, "A fully–immersive hapto–audio–visual framework for remote touch," in *Proc. of the 11th IEEE International Conference on Innovations in Information Technology (IIT'15), Dubai, United Arab Emirates*, 2015.

[204] C. Eckert and J.-F. Boujut, "The role of objects in design co-operation: communication through physical or virtual objects," *Computer Supported Cooperative Work*, vol. 12, no. 2, pp. 145–151, 2003.

[205] M. Brereton and B. McGarry, "An observational study of how objects support engineering design thinking and communication: implications for the design of tangible media," in *Proceedings of the SIGCHI conference on Human Factors in Computing Systems*, 2000, pp. 217–224.

[206] D. Nicolini, J. Mengis, and J. Swan, "Understanding the role of objects in cross-disciplinary collaboration," *Organization science*, vol. 23, no. 3, pp. 612–629, 2012.

[207] C. Bueger and J. Stockbruegger, "Actor-network theory: objects and actants, networks and narratives," in *Technology and World Politics*. Routledge, 2017, pp. 42–59.

[208] D.-I. D. Han, Y. Bergs, and N. Moorhouse, "Virtual reality consumer experience escapes: preparing for the metaverse," *Virtual Reality*, pp. 1–16, 2022.

[209] M. Lombard and T. Ditton, "At the heart of it all: The concept of presence," *Journal of computer-mediated communication*, vol. 3, no. 2, p. JCMC321, 1997.

[210] C. Youngblut, "Experience of presence in virtual environments," Institute for Defense Analyses, Alexandria VA, Tech. Rep., 2003.

[211] F. Biocca, "The cyborg's dilemma: Progressive embodiment in virtual environments," *Journal of computer-mediated communication*, vol. 3, no. 2, p. JCMC324, 1997.

[212] H. T. Regenbrecht, T. W. Schubert, and F. Friedmann, "Measuring the sense of presence and its relations to fear of heights in virtual environments," *International Journal of Human-Computer Interaction*, vol. 10, no. 3, pp. 233–249, 1998.

[213] G. Riva, F. Mantovani, C. S. Capideville, A. Preziosa, F. Morganti, D. Villani, A. Gaggioli, C. Botella, and M. Alcañiz, "Affective interactions using virtual reality: the link between presence and emotions," *Cyberpsychology & behavior*, vol. 10, no. 1, pp. 45–56, 2007.

[214] M. Slater, D.-P. Pertaub, and A. Steed, "Public speaking in virtual reality: Facing an audience of avatars," *IEEE Computer Graphics and Applications*, vol. 19, no. 2, pp. 6–9, 1999.

[215] W. M. B. Tiest and A. M. Kappers, "Cues for haptic perception of compliance," *IEEE transactions on haptics*, vol. 2, no. 4, pp. 189–199, 2009.

[216] M. A. Srinivasan and R. H. LaMotte, "Tactual discrimination of softness," *Journal of neurophysiology*, vol. 73, no. 1, pp. 88–101, 1995.

[217] J. J. Gibson, "Observations on active touch," *Psychological review*, vol. 69, no. 6, pp. 477–491, 1962.

[218] R. Harper and S. Stevens, "Subjective hardness of compliant materials," *Quarterly Journal of Experimental Psychology*, vol. 16, no. 3, pp. 204–215, 1964.

[219] M. Singhala and J. D. Brown, "Prefatory study of the effects of exploration dynamics on stiffness perception," in *2020 IEEE Haptics Symposium (HAPTICS)*. IEEE, 2020, pp. 128–133.

[220] H. Z. Tan, N. I. Durlach, G. L. Beauregard, and M. A. Srinivasan, "Manual discrimination of compliance using active pinch grasp: The roles of force and work cues," *Perception & psychophysics*, vol. 57, no. 4, pp. 495–510, 1995.

[221] F. Sorgini, L. Massari, J. D'Abbraccio, E. Palermo, A. Menciassi, P. B. Petrovic, A. Mazzoni, M. C. Carrozza, F. N. Newell, and C. M. Oddo, "Neuromorphic vibrotactile stimulation of fingertips for encoding object stiffness in telepresence sensory substitution and augmentation applications," *Sensors*, vol. 18, no. 1, p. 261, 2018.

[222] Y. Visell, "Tactile sensory substitution: Models for enaction in hci," *Interacting with Computers*, vol. 21, no. 1-2, pp. 38–53, 2009.

[223] R. Raisamo, I. Rakkolainen, P. Majaranta, K. Salminen, J. Rantala, and A. Farooq, "Human augmentation: Past, present and future," *International Journal of Human-Computer Studies*, vol. 131, pp. 131–143, 2019.

[224] J. Craig and V. Petterson, "Introduction to the practice of telemedicine," *Journal of telemedicine and telecare*, vol. 11, no. 1, pp. 3–9, 2005.

[225] S. J. Sirintrapun and A. M. Lopez, "Telemedicine in cancer care," *American Society of Clinical Oncology Educational Book*, vol. 38, pp. 540–545, 2018.

[226] V. Villani, F. Pini, F. Leali, and C. Secchi, "Survey on human–robot collaboration in industrial settings: Safety, intuitive interfaces and applications," *Mechatronics*, vol. 55, pp. 248–266, 2018.

[227] J. Wessberg, H. Olausson, K. W. Fernstrom, and A. B. Vallbo, "Receptive field properties of unmyelinated tactile afferents in the human skin," *Journal of neurophysiology*, vol. 89, no. 3, pp. 1567–1575, 2003.

[228] R. Ackerley, H. B. Wasling, J. Liljencrantz, H. Olausson, R. D. Johnson, and J. Wessberg, "Human c-tactile afferents are tuned to the temperature of a skin-stroking caress," *Journal of Neuroscience*, vol. 34, no. 8, pp. 2879–2883, 2014.

[229] Å. Vallbo, H. Olausson, and J. Wessberg, "Unmyelinated afferents constitute a second system coding tactile stimuli of the human hairy skin," *Journal of neurophysiology*, vol. 81, no. 6, pp. 2753–2763, 1999.

[230] K. S. Severson, D. Xu, M. Van de Loo, L. Bai, D. D. Ginty, and D. H. O'Connor, "Active touch and self-motion encoding by merkel cell-associated afferents," *Neuron*, vol. 94, no. 3, pp. 666–676, 2017.

[231] R. D. Luce and W. Edwards, "The derivation of subjective scales from just noticeable differences." *Psychological review*, vol. 65, no. 4, p. 222, 1958.

[232] M. Morioka and M. J. Griffin, "Dependence of vibrotactile thresholds on the psychophysical measurement method," *International Archives of Occupational and Environmental Health*, vol. 75, no. 1, pp. 78–84, 2002.

[233] H. Alexander and T. Cook, "Variations with age in the mechanical properties of human skin in vivo," in *Bed sore biomechanics.* Springer, 1976, pp. 109–117.

[234] Q. H. Van and M. Harders, "Augmenting contact stiffness in passive haptics—preliminary results with twisted string actuation," in *2017 IEEE World Haptics Conference (WHC)*. IEEE, 2017, pp. 148–153.

[235] E. P. Scilingo, M. Bianchi, G. Grioli, and A. Bicchi, "Rendering softness: Integration of kinesthetic and cutaneous information in a haptic device," *IEEE Transactions on Haptics*, vol. 3, no. 2, pp. 109–118, 2010.

[236] E. Richard, A. Tijou, P. Richard, and J.-L. Ferrier, "Multi-modal virtual environments for education with haptic and olfactory feedback," *Virtual Reality*, vol. 10, no. 3-4, pp. 207–225, 2006.

[237] A. Lecuyer, S. Coquillart, A. Kheddar, P. Richard, and P. Coiffet, "Pseudo-haptic feedback: can isometric input devices simulate force feedback?" IEEE, 2000, pp. 83–90.

[238] A. Lécuyer, "Simulating haptic feedback using vision: A survey of research and applications of pseudo-haptic feedback," *Presence: Teleoperators and Virtual Environments*, vol. 18, no. 1, pp. 39–53, 2009.

[239] Y. Ban, T. Kajinami, T. Narumi, T. Tanikawa, and M. Hirose, "Modifying an identified curved surface shape using pseudo-haptic effect." IEEE, 2012, pp. 211–216.

[240] F. Argelaguet, D. A. G. Jáuregui, M. Marchal, and A. Lécuyer, "Elastic images: Perceiving local elasticity of images through a novel pseudo-haptic deformation effect," *ACM Trans. on Applied Perception (TAP)*, vol. 10, no. 3, pp. 1–14, 2013.

[241] Y. Taima, Y. Ban, T. Narumi, T. Tanikawa, and M. Hirose, "Controlling fatigue while lifting objects using pseudo-haptics in a mixed reality space." IEEE, 2014, pp. 175–180.

[242] A. Lécuyer, J.-M. Burkhardt, and L. Etienne, "Feeling bumps and holes without a haptic interface: the perception of pseudo-haptic textures," 2004, pp. 239–246.

[243] M. Santello, M. Flanders, and J. F. Soechting, "Postural hand synergies for tool use," *Journal of neuroscience*, vol. 18, no. 23, pp. 10 105–10 115, 1998.

[244] S. Mulatto, A. Formaglio, M. Malvezzi, and D. Prattichizzo, "Using postural synergies to animate a low-dimensional hand avatar in haptic simulation," vol. 6, no. 1, pp. 106–116, 2012.

[245] A. Bicchi, M. Gabiccini, and M. Santello, "Modelling natural and artificial hands with synergies," *Philosophical Trans. of the Royal Society B: Biological Sciences*, vol. 366, no. 1581, pp. 3153–3161, 2011.

[246] F. Ficuciello, D. Zaccara, and B. Siciliano, "Synergy-based policy improvement with path integrals for anthropomorphic hands." IEEE, 2016, pp. 1940–1945.

[247] H. Z. Tan, M. A. Srinivasan, C. M. Reed, and N. I. Durlach, "Discrimination and identification of finger joint-angle position using active motion," *ACM Trans. on Applied Perception*, vol. 4, no. 2, p. 10, 2007.

[248] K. Stroud, L. Pickett, and B. Tillman, "Nasa human integration design handbook (hidh): Revitalization of space-related human factors, environmental, and habitability data and design guidance," 2008.

[249] T. N. Cornsweet, "The staircase-method in psychophysics," *The American Journal of Psychology*, vol. 75, no. 3, pp. 485–491, 1962.

[250] K. A. Akins, "Neurophilosophy: Toward a unified theory of the mind/brain," *The Journal of Philosophy*, vol. 87, no. 2, pp. 93–102, 1990.

[251] S. G. Hart, "Nasa-task load index (nasa-tlx); 20 years later," in *Proceedings of the human factors and ergonomics society annual meeting*, vol. 50, no. 9. Sage publications Sage CA: Los Angeles, CA, 2006, pp. 904–908.

[252] B. Oxlund, "An anthropology of the handshake," *Anthropology Now*, vol. 12, no. 1, pp. 39–44, 2020.

[253] P. M. Hall and D. A. Spencer Hall, "The handshake as interaction," 1983.

[254] I. Sigley, "It has touched us all: Commentary on the social implications of touch during the covid-19 pandemic," *Social Sciences & Humanities Open*, vol. 2, no. 1, p. 100051, 2020.

[255] D. Prattichizzo, "Haptics and pandemic," *IEEE Transactions on Haptics*, vol. 14, no. 1, pp. 1–1, 2021.

[256] A. Jain, A. Shaikh, and K. Malhotra, "Handshake habit amongst medical practitioners, need to abandon and embrace an alternative: analytical study in view of covid-19 pandemic," *International Journal of Community Medicine and Public Health*, vol. 7, no. 6, p. 2352, 2020.

[257] H. Cai, B. Tu, J. Ma, L. Chen, L. Fu, Y. Jiang, and Q. Zhuang, "Psychological impact and coping strategies of frontline medical staff in hunan between january and march 2020 during the outbreak of coronavirus disease 2019 (covid-19) in hubei, china," *Medical science monitor: international medical journal of experimental and clinical research*, vol. 26, pp. e924 171–1, 2020.

[258] C. K. T. Lima, P. M. de Medeiros Carvalho, I. d. A. S. Lima, J. V. A. de Oliveira Nunes, J. S. Saraiva, R. I. de Souza, C. G. L. da Silva, and M. L. R. Neto, "The emotional impact of coronavirus 2019-ncov (new coronavirus disease)," *Psychiatry research*, p. 112915, 2020.

[259] S. Joshi, S. Collins, W. Kamino, R. Gomez, and S. Šabanović, "Social robots for socio-physical distancing," in *International Conference on Social Robotics*. Springer, 2020, pp. 440–452.

[260] V. Prasad, R. Stock-Homburg, and J. Peters, "Human-robot handshaking: A review," *International Journal of Social Robotics*, pp. 1–17, 2021.

[261] M. Ammi, V. Demulier, S. Caillou, Y. Gaffary, Y. Tsalamlal, J.-C. Martin, and A. Tapus, "Haptic human-robot affective interaction in a handshaking social protocol," in *Proceedings of the Tenth Annual ACM/IEEE International Conference on Human-Robot Interaction*, 2015, pp. 263–270.

[262] J. Beaudoin, T. Laliberté, and C. Gosselin, "Haptic interface for handshake emulation," *IEEE Robotics and Automation Letters*, vol. 4, no. 4, pp. 4124–4130, 2019.

[263] F. Vigni, E. Knoop, D. Prattichizzo, and M. Malvezzi, "The role of closed-loop hand control in handshaking interactions," *IEEE Robotics and Automation Letters*, vol. 4, no. 2, pp. 878–885, 2019.

[264] M. Dragusanu, A. Villani, D. Prattichizzo, and M. Malvezzi, "Design of a wearable haptic device for hand palm cutaneous feedback," *Frontiers in Robotics and AI*, vol. 8, p. 706627, 2021.

[265] L. Meli, I. Hussain, M. Aurilio, M. Malvezzi, M. K. O'Malley, and D. Prattichizzo, "The hbracelet: a wearable haptic device for the distributed mechanotactile stimulation of the upper limb," *IEEE Robotics and Automation Letters*, vol. 3, no. 3, pp. 2198–2205, 2018.

[266] E. Knoop, M. Bächer, V. Wall, R. Deimel, O. Brock, and P. Beardsley, "Handshakiness: Benchmarking for human-robot hand interactions," in *2017 IEEE/RSJ International Conference on Intelligent Robots and Systems (IROS)*. IEEE, 2017, pp. 4982–4989.

[267] A. Melnyk, P. Henaff, V. Khomenko, and V. Borysenko, "Sensor network architecture to measure characteristics of a handshake between humans," in *2014 IEEE 34th International Scientific Conference on Electronics and Nanotechnology (ELNANO)*. IEEE, 2014, pp. 264–268.

[268] A. Pérez-González, M. Vergara, and J. L. Sancho-Bru, "Stiffness map of the grasping contact areas of the human hand," *Journal of biomechanics*, vol. 46, no. 15, pp. 2644–2650, 2013.

[269] Y. Gao, H. Li, and Y. Luo, "An empirical study of wearable technology acceptance in healthcare," *Industrial Management & Data Systems*, 2015.

[270] Y. Lee, K. A. Kozar, and K. R. Larsen, "The technology acceptance model: Past, present, and future," *Communications of the Association for information systems*, vol. 12, no. 1, p. 50, 2003.

[271] T. Hoßfeld, P. E. Heegaard, M. Varela, and S. Möller, "Qoe beyond the mos: an in-depth look at qoe via better metrics and their relation to mos," *Quality and User Experience*, vol. 1, no. 1, pp. 1–23, 2016.

[272] W. F. Chaplin, J. B. Phillips, J. D. Brown, N. R. Clanton, and J. L. Stein, "Handshaking, gender, personality, and first impressions." *Journal of personality and social psychology*, vol. 79, no. 1, p. 110, 2000.

[273] J. J. Abbott, P. Marayong, and A. M. Okamura, "Haptic virtual fixtures for robot-assisted manipulation," in *Robotics research*. Springer, 2007, pp. 49–64.

[274] P. W. Battaglia, D. Kersten, and P. R. Schrater, "How haptic size sensations improve distance perception," *PLoS Comput Biol*, vol. 7, no. 6, p. e1002080, 2011.

[275] S. J. Lederman and R. L. Klatzky, "Hand movements: A window into haptic object recognition," *Cognitive psychology*, vol. 19, no. 3, pp. 342–368, 1987.

[276] H. Iwata, H. Yano, F. Nakaizumi, and R. Kawamura, "Project feelex: adding haptic surface to graphics," in *Proceedings of the 28th annual conference on Computer graphics and interactive techniques*, 2001, pp. 469–476.

[277] C. W. Borst and C. D. Cavanaugh, "Haptic controller design and palm-sized vibrotactile array," *technical report*, 2004.

[278] J. Martinez, D. Griffiths, V. Biscione, O. Georgiou, and T. Carter, "Touchless haptic feedback for supernatural vr experiences," in *2018 IEEE Conference on Virtual Reality and 3D User Interfaces (VR)*. IEEE, 2018, pp. 629–630.

[279] C. Pacchierotti, S. Sinclair, M. Solazzi, A. Frisoli, V. Hayward, and D. Prattichizzo, "Wearable haptic systems for the fingertip and the hand: taxonomy, review, and perspectives," *IEEE Transactions on Haptics*, vol. 10, no. 4, pp. 580–600, 2017.

[280] K. Minamizawa, S. Kamuro, S. Fukamachi, N. Kawakami, and S. Tachi, "Ghostglove: Haptic existence of the virtual world," in *ACM SIGGRAPH 2008 new tech demos*, 2008, pp. 1–1.

[281] K. Minamizawa, S. Kamuro, N. Kawakami, and S. Tachi, "A palm-worn haptic display for bimanual operations in virtual environments," in *International Conference on Human Haptic Sensing and Touch Enabled Computer Applications*. Springer, 2008, pp. 458–463.

[282] M. Achibet, A. Girard, A. Talvas, M. Marchal, and A. Lécuyer, "Elastic-arm: Human-scale passive haptic feedback for augmenting interaction and perception in virtual environments," in *2015 IEEE Virtual Reality (VR)*. IEEE, 2015, pp. 63–68.

[283] B. Son and J. Park, "Haptic feedback to the palm and fingers for improved tactile perception of large objects," in *Proceedings of the 31st Annual ACM Symposium on User Interface Software and Technology*, 2018, pp. 757–763.

[284] B. Son and J. Park, "Tactile sensitivity to distributed patterns in a palm," in *Proceedings of the 20th ACM International Conference on Multimodal Interaction*, 2018, pp. 486–491.

[285] J. Martínez, A. García, M. Oliver, J. P. Molina, and P. González, "Identifying virtual 3d geometric shapes with a vibrotactile glove," *IEEE computer graphics and applications*, vol. 36, no. 1, pp. 42–51, 2014.

[286] E. F. Borja, D. A. Lara, W. X. Quevedo, and V. H. Andaluz, "Haptic stimulation glove for fine motor rehabilitation in virtual reality environments," in *International Conference on Augmented Reality, Virtual Reality and Computer Graphics*. Springer, 2018, pp. 211–229.

[287] R. Kovacs, E. Ofek, M. Gonzalez Franco, A. F. Siu, S. Marwecki, C. Holz, and M. Sinclair, "Haptic pivot: On-demand handhelds in vr," in *Proceedings of the 33rd Annual ACM Symposium on User Interface Software and Technology*, 2020, pp. 1046–1059.

[288] H. Kajimoto, "Design of cylindrical whole-hand haptic interface using electrocutaneous display," in *International Conference on Human Haptic Sensing and Touch Enabled Computer Applications*. Springer, 2012, pp. 67–72.

[289] I. Zubrycki and G. Granosik, "Novel haptic device using jamming principle for providing kinaesthetic feedback in glove-based control interface," *Journal of Intelligent & Robotic Systems*, vol. 85, no. 3-4, pp. 413–429, 2017.

[290] X. de Tinguy, T. Howard, C. Pacchierotti, M. Marchal, and A. Lécuyer, "Weatavix: Wearable actuated tangibles for virtual reality experiences," in *Haptics: Science, Technology, Applications*, I. Nisky, J. Hartcher-O'Brien, M. Wiertlewski, and J. Smeets, Eds. Cham: Springer International Publishing, 2020, pp. 262–270.

[291] D. Trinitatova, D. Tsetserukou, and A. Fedoseev, "Touchvr: a wearable haptic interface for vr aimed at delivering multi-modal stimuli at the user's palm," in *SIGGRAPH Asia 2019 XR*, 2019, pp. 42–43.

[292] D. Trinitatova and D. Tsetserukou, "Deltatouch: a 3d haptic display for delivering multimodal tactile stimuli at the palm," in *2019 IEEE World Haptics Conference (WHC)*. IEEE, 2019, pp. 73–78.

[293] F. Chinello, C. Pacchierotti, M. Malvezzi, and D. Prattichizzo, "A three revolute-revolute-spherical wearable fingertip cutaneous device for stiffness rendering," *IEEE Transactions on Haptics*, vol. 11, no. 1, pp. 39–50, 2018.

[294] M. H. Swartz, *Physical diagnosis: History and examination*. WB Saunders, 2002.

[295] O. A. Van Nierop, A. van der Helm, K. J. Overbeeke, and T. J. Djajadiningrat, "A natural human hand model," *The Visual Computer*, vol. 24, no. 1, pp. 31–44, 2008.

[296] K. Kubo, Y.-S. Cheng, B. Zhou, K.-N. An, S. L. Moran, P. C. Amadio, X. Zhang, and C. Zhao, "The quantitative evaluation of the relationship between the forces applied to the palm and carpal tunnel pressure," *Journal of biomechanics*, vol. 66, pp. 170–174, 2018.

[297] A. Berti, J.-P. Merlet, and M. Carricato, "Solving the direct geometrico-static problem of 3-3 cable-driven parallel robots by interval analysis: Preliminary results," in *Cable-Driven Parallel Robots*. Springer, 2013, pp. 251–268.

[298] M. Carricato and G. Abbasnejad, "Direct geometrico-static analysis of under-constrained cable-driven parallel robots with 4 cables," in *Cable-Driven Parallel Robots*. Springer, 2013, pp. 269–285.

[299] P. Miermeister, W. Kraus, and A. Pott, "Differential kinematics for calibration, system investigation, and force based forward kinematics of cable-driven parallel robots," in *Cable-Driven Parallel Robots*. Springer, 2013, pp. 319–333.

[300] M. A. Khosravi and H. D. Taghirad, "Experimental performance of robust pid controller on a planar cable robot," in *Cable-Driven Parallel Robots*. Springer, 2013, pp. 337–352.

[301] R. Yao, H. Li, and X. Zhang, "A modeling method of the cable driven parallel manipulator for fast," in *Cable-Driven Parallel Robots*. Springer, 2013, pp. 423–436.

[302] M. Malvezzi, F. Chinello, D. Prattichizzo, and C. Pacchierotti, "Design of personalized wearable haptic interfaces to account for fingertip size and shape," *IEEE Transactions on Haptics*, pp. 1–1, 2021.

[303] A. Kapandji, "Clinical test of apposition and counter-apposition of the thumb," *Annales de chirurgie de la main: organe officiel des societes de chirurgie de la main*, vol. 5, no. 1, pp. 67–73, 1986.

[304] S. G. Hart and L. E. Staveland, "Development of nasa-tlx (task load index): Results of empirical and theoretical research," in *Advances in psychology*. Elsevier, 1988, vol. 52, pp. 139–183.

[305] J. F. Knight and C. Baber, "A tool to assess the comfort of wearable computers," *Human factors*, vol. 47, no. 1, pp. 77–91, 2005.

[306] T. Lisini Baldi, S. Scheggi, L. Meli, M. Mohammadi, and D. Prattichizzo, "GESTO: A Glove for Enhanced Sensing and Touching Based on Inertial and Magnetic Sensors for Hand Tracking and Cutaneous Feedback," vol. 47, no. 6, pp. 1066–1076, Dec 2017.

[307] D. Troisi, M. Dragusanu, A. Villani, D. Prattichizzo, and M. Malvezzi, "Hapticpalm: A wearable robotic device for haptics and rehabilitative hand treatments," in *International Conference on Social Robotics*. Springer Nature Switzerland Cham, 2022, pp. 402–411.

[308] S. De Buck, F. Maes, J. Ector, J. Bogaert, S. Dymarkowski, H. Heidbuchel, and P. Suetens, "An augmented reality system for patient-specific guidance of cardiac catheter ablation procedures," *IEEE Transactions on Medical Imaging*, vol. 24, no. 11, pp. 1512–1524, 2005.

[309] S. Nicolau, X. Pennec, L. Soler, X. Buy, A. Gangi, N. Ayache, and J. Marescaux, "An augmented reality system for liver thermal ablation: design and evaluation on clinical cases," *Medical image analysis*, vol. 13, no. 3, pp. 494–506, 2009.

[310] F. Aïm, G. Lonjon, D. Hannouche, and R. Nizard, "Effectiveness of virtual reality training in orthopaedic surgery," *Arthroscopy: the journal of arthroscopic & related surgery*, vol. 32, no. 1, pp. 224–232, 2016.

[311] J. D. Bric, D. C. Lumbard, M. J. Frelich, and J. C. Gould, "Current state of virtual reality simulation in robotic surgery training: a review," *Surgical endoscopy*, vol. 30, pp. 2169–2178, 2016.

[312] T. Erol, A. F. Mendi, and D. Doğan, "The digital twin revolution in healthcare," in *2020 4th international symposium on multidisciplinary studies and innovative technologies (ISMSIT)*. IEEE, 2020, pp. 1–7.

[313] M. Cellina, M. Cè, M. Alì, G. Irmici, S. Ibba, E. Caloro, D. Fazzini, G. Oliva, and S. Papa, "Digital twins: The new frontier for personalized medicine?" *Applied Sciences*, vol. 13, no. 13, p. 7940, 2023.

[314] M. Malvezzi, T. L. Baldi, A. Villani, F. Ciccarese, and D. Prattichizzo, "Design, development, and preliminary evaluation of a highly wearable exoskeleton," in *2020 29th IEEE International Conference on Robot and Human Interactive Communication (RO-MAN)*. IEEE, 2020, pp. 1055–1062.

[315] M. Dragusanu, D. Troisi, A. Villani, D. Prattichizzo, and M. Malvezzi, "Design and prototyping of an underactuated hand exoskeleton with fingers coupled by a gear-based differential," *Frontiers in Robotics and AI*, vol. 9, p. 862340, 2022.

[316] A. Gupta and M. K. O'Malley, "Design of a haptic arm exoskeleton for training and rehabilitation," *IEEE/ASME Transactions on mechatronics*, vol. 11, no. 3, pp. 280–289, 2006.

[317] M. Pompilio, N. D'Aurizio, T. L. Baldi, L. Franco, G. Gabriele, and D. Prattichizzo, "A novel wearable sensing device enabling remote palpation," in *2024 IEEE Haptics Symposium (HAPTICS)*. IEEE, 2024, pp. 149–156.

[318] W. H. Organization, *World health statistics 2016: monitoring health for the SDGs sustainable development goals.* World Health Organization, 2016.

[319] W. H. Organization, *World health statistics 2021: monitoring health for the SDGs sustainable development goals.* World Health Organization, 2021.

[320] A. Peretti, F. Amenta, S. K. Tayebati, G. Nittari, and S. S. Mahdi, "Telerehabilitation: review of the state-of-the-art and areas of application," *JMIR rehabilitation and assistive technologies*, vol. 4, no. 2, p. e7, 2017.

[321] E. Martinez-Martin and M. Cazorla, "Rehabilitation technology: assistance from hospital to home," *Computational intelligence and neuroscience*, vol. 2019, 2019.

[322] I. Díaz, J. M. Catalan, F. J. Badesa, X. Justo, L. D. Lledo, A. Ugartemendia, J. J. Gil, J. Díez, and N. García-Aracil, "Development of a robotic device for post-stroke home telerehabilitation," *Advances in Mechanical Engineering*, vol. 10, no. 1, p. 1687814017752302, 2018.

[323] M. Anthonius Lim and R. Pranata, "Letter to the editor regarding 'the challenging battle of mankind against covid-19 outbreak: Is this global international biological catastrophe the beginning of a new era?'–is telehealth the future of orthopaedic and rehabilitation in post-covid-19 era?" 2020.

[324] A. S. Gorgey, R. Sumrell, and L. L. Goetz, "Exoskeletal assisted rehabilitation after spinal cord injury," *Atlas of Orthoses and Assistive Devices*, pp. 440–447, 2019.

[325] P. S. Lum, C. G. Burgar, P. C. Shor, M. Majmundar, and M. Van der Loos, "Robot-assisted movement training compared with conventional therapy techniques for the rehabilitation of upper-limb motor function after stroke," *Archives of physical medicine and rehabilitation*, vol. 83, no. 7, pp. 952–959, 2002.

[326] M. Dragusanu, T. L. Baldi, Z. Iqbal, D. Prattichizzo, and M. Malvezzi, "Development of a wearable exoskeleton for hand/wrist rehabilitation and training."

[327] R. Gopura, D. Bandara, K. Kiguchi, and G. K. Mann, "Developments in hardware systems of active upper-limb exoskeleton robots: A review," *Robotics and Autonomous Systems*, vol. 75, pp. 203–220, 2016.

[328] S. Hesse, H. Schmidt, C. Werner, and A. Bardeleben, "Upper and lower extremity robotic devices for rehabilitation and for studying motor control," *Current opinion in neurology*, vol. 16, no. 6, pp. 705–710, 2003.

[329] N. Rehmat, J. Zuo, W. Meng, Q. Liu, S. Q. Xie, and H. Liang, "Upper limb rehabilitation using robotic exoskeleton systems: a systematic review," *International Journal of Intelligent Robotics and Applications*, vol. 2, no. 3, pp. 283–295, 2018.

[330] V. Moreno-SanJuan, A. Cisnal, J.-C. Fraile, J. Pérez-Turiel, and E. de-la Fuente, "Design and characterization of a lightweight underactuated raca hand exoskeleton for neurorehabilitation," *Robotics and Autonomous Systems*, p. 103828, 2021.

[331] T. du Plessis, K. Djouani, and C. Oosthuizen, "A review of active hand exoskeletons for rehabilitation and assistance," *Robotics*, vol. 10, no. 1, p. 40, 2021.

[332] T. Shahid, D. Gouwanda, S. G. Nurzaman *et al.*, "Moving toward soft robotics: A decade review of the design of hand exoskeletons," *Biomimetics*, vol. 3, no. 3, p. 17, 2018.

[333] M. Dragusanu, T. Lisini Baldi, Z. Iqbal, D. Prattichizzo, and M. Malvezzi, "Design, development and control of a tendon-actuated exoskeleton for wrist rehabilitation and training," in *Proc. IEEE Int. Conf. on Robotics and Automation*, Paris, FR, June 2020.

[334] N. W. Bartlett, V. Lyau, W. A. Raiford, D. Holland, J. B. Gafford, T. D. Ellis, and C. J. Walsh, "A soft robotic orthosis for wrist rehabilitation," *Journal of Medical Devices*, vol. 9, no. 3, 2015.

[335] A. Gupta, M. K. O'Malley, V. Patoglu, and C. Burgar, "Design, control and performance of ricewrist: a force feedback wrist exoskeleton for rehabilitation and training," *The International Journal of Robotics Research*, vol. 27, no. 2, pp. 233–251, 2008.

[336] H. I. Krebs, B. T. Volpe, D. Williams, J. Celestino, S. K. Charles, D. Lynch, and N. Hogan, "Robot-aided neurorehabilitation: a robot for wrist rehabilitation," *IEEE transactions on neural systems and rehabilitation engineering*, vol. 15, no. 3, pp. 327–335, 2007.

[337] M. A. Rahman and A. Al-Jumaily, "Design and development of a hand exoskeleton for rehabilitation following stroke," *Procedia Engineering*, vol. 41, pp. 1028–1034, 2012.

[338] F. Zhang, L. Hua, Y. Fu, H. Chen, and S. Wang, "Design and development of a hand exoskeleton for rehabilitation of hand injuries," *Mechanism and Machine Theory*, vol. 73, pp. 103–116, 2014.

[339] L. Randazzo, I. Iturrate, S. Perdikis, and J. d. R. Millán, "mano: A wearable hand exoskeleton for activities of daily living and neurorehabilitation," *IEEE Robotics and Automation Letters*, vol. 3, no. 1, pp. 500–507, 2017.

[340] D. Marconi, A. Baldoni, Z. McKinney, M. Cempini, S. Crea, and N. Vitiello, "A novel hand exoskeleton with series elastic actuation for modulated torque transfer," *Mechatronics*, vol. 61, pp. 69–82, 2019.

[341] D. Popov, I. Gaponov, and J.-H. Ryu, "Portable exoskeleton glove with soft structure for hand assistance in activities of daily living," *IEEE/ASME Transactions on Mechatronics*, vol. 22, no. 2, pp. 865–875, 2016.

[342] D. Wang, Q. Meng, Q. Meng, X. Li, and H. Yu, "Design and development of a portable exoskeleton for hand rehabilitation," *IEEE Transactions on Neural Systems and Rehabilitation Engineering*, vol. 26, no. 12, pp. 2376–2386, 2018.

[343] M. Bianchi, M. Cempini, R. Conti, E. Meli, A. Ridolfi, N. Vitiello, and B. Allotta, "Design of a series elastic transmission for hand exoskeletons," *Mechatronics*, vol. 51, pp. 8–18, 2018.

[344] I. Jo, Y. Park, J. Lee, and J. Bae, "A portable and spring-guided hand exoskeleton for exercising flexion/extension of the fingers," *Mechanism and Machine Theory*, vol. 135, pp. 176–191, 2019.

[345] A. Bataller, J. Cabrera, M. Clavijo, and J. Castillo, "Evolutionary synthesis of mechanisms applied to the design of an exoskeleton for finger rehabilitation," *Mechanism and Machine Theory*, vol. 105, pp. 31–43, 2016.

[346] H. In, B. B. Kang, M. Sin, and K.-J. Cho, "Exo-glove: A wearable robot for the hand with a soft tendon routing system," *IEEE Robotics & Automation Magazine*, vol. 22, no. 1, pp. 97–105, 2015.

[347] M. Dragusanu, Z. Iqbal, D. Prattichizzo, and M. Malvezzi, "Synthesis and design of a modular hand exoskeleton for rehabilitation and training," in *ASME 2021 IMECE, International Mechanical Engineering Congress and Exposition*, November 1-5 2021.

[348] R. Tubiana, "Architecture and functions of the hand," *The Hand 1*, pp. 19–93, 1981.

[349] J. Lee and T. L. Kunii, "Model-based analysis of hand posture," *IEEE Computer Graphics and applications*, vol. 15, no. 5, pp. 77–86, 1995.

[350] D. Prattichizzo, M. Malvezzi, M. Gabiccini, and A. Bicchi, "On motion and force controllability of precision grasps with hands actuated by soft synergies," *IEEE transactions on robotics*, vol. 29, no. 6, pp. 1440–1456, 2013.

[351] M. Malvezzi, G. Gioioso, G. Salvietti, and D. Prattichizzo, "Syngrasp: A matlab toolbox for underactuated and compliant hands," *IEEE Robotics & Automation Magazine*, vol. 22, no. 4, pp. 52–68, 2015.

[352] M. G. Catalano, G. Grioli, E. Farnioli, A. Serio, C. Piazza, and A. Bicchi, "Adaptive synergies for the design and control of the pisa/iit softhand," *The International Journal of Robotics Research*, vol. 33, no. 5, pp. 768–782, 2014.

[353] M. Gabiccini, A. Bicchi, D. Prattichizzo, and M. Malvezzi, "On the role of hand synergies in the optimal choice of grasping forces," *Autonomous Robots*, vol. 31, no. 2, pp. 235–252, 2011.

[354] M. Bianchi and M. V. Liarokapis, "Handcorpus, a new open-access repository for sharing experimental data and results on human and artificial hands," in *IEEE World Haptics Conference (WHC)*, 2013.

[355] S. Cobos, M. Ferre, M. A. Sánchez-Urán, and J. Ortego, "Constraints for realistic hand manipulation," *Proc. Presence*, pp. 369–370, 2007.

[356] L. Birglen and C. M. Gosselin, "Force analysis of connected differential mechanisms: Application to grasping," *The International Journal of Robotics Research*, vol. 25, no. 10, pp. 1033–1046, 2006.

[357] L. Birglen and C. M. Gosselin, "On the force capability of underactuated fingers," in *2003 IEEE International Conference on Robotics and Automation (Cat. No. 03CH37422)*, vol. 1. IEEE, 2003, pp. 1139–1145.

[358] N. Fukaya, S. Toyama, T. Asfour, and R. Dillmann, "Design of the tuat/karlsruhe humanoid hand," in *Proceedings. 2000 IEEE/RSJ International Conference on Intelligent Robots and Systems (IROS 2000)(Cat. No. 00CH37113)*, vol. 3. IEEE, 2000, pp. 1754–1759.

[359] G. A. Zappatore, G. Reina, and A. Messina, "Analysis of a highly underactuated robotic hand," *Int. J. Mech. Control*, vol. 18, no. 4, pp. 17–23, 2017.

[360] B. Massa, S. Roccella, M. C. Carrozza, and P. Dario, "Design and development of an underactuated prosthetic hand," in *Proceedings 2002 IEEE international conference on robotics and automation (Cat. No. 02CH37292)*, vol. 4. IEEE, 2002, pp. 3374–3379.

[361] M. Baril, T. Laliberté, C. Gosselin, and F. Routhier, "On the design of a mechanically programmable underactuated anthropomorphic prosthetic gripper," *Journal of Mechanical Design*, vol. 135, no. 12, p. 121008, 2013.

[362] G. P. Kontoudis, M. V. Liarokapis, A. G. Zisimatos, C. I. Mavrogiannis, and K. J. Kyriakopoulos, "Open-source, anthropomorphic, underactuated robot hands with a selectively lockable differential mechanism: Towards affordable prostheses," in *2015 IEEE/RSJ international conference on intelligent robots and systems (IROS)*. IEEE, 2015, pp. 5857–5862.

[363] G. Carbone, E. C. Gerding, B. Corves, D. Cafolla, M. Russo, and M. Ceccarelli, "Design of a two-dofs driving mechanism for a motion-assisted finger exoskeleton," *Applied Sciences*, vol. 10, no. 7, 2020. [Online]. Available: https://www.mdpi.com/2076-3417/10/7/2619

[364] D. Cafolla and G. Carbone, "A study of feasibility of a human finger exoskeleton," in *Service Orientation in Holonic and Multi-Agent Manufacturing and Robotics*. Springer, 2014, pp. 355–364.

[365] G. A. Zappatore, G. Reina, and A. Messina, "A toolbox for the analysis of the grasp stability of underactuated fingers," *Robotics*, vol. 8, no. 2, p. 26, 2019.

[366] D. Cafolla, M. Ceccarelli, M. Wang, and G. Carbone, "3d printing for feasibility check of mechanism design," *Int. J. Mech. Control*, vol. 17, no. 1, pp. 3–12, 2016.

[367] J. E. Bialosky, M. D. Bishop, D. D. Price, M. E. Robinson, and S. Z. George, "The mechanisms of manual therapy in the treatment of musculoskeletal pain: a comprehensive model," *Manual therapy*, vol. 14, no. 5, pp. 531–538, 2009.

[368] J. Camarinos and L. Marinko, "Effectiveness of manual physical therapy for painful shoulder conditions: a systematic review," *Journal of Manual & Manipulative Therapy*, vol. 17, no. 4, pp. 206–215, 2009.

[369] D. F. Martins, F. Bobinski, L. Mazzardo-Martins, F. J. Cidral-Filho, F. P. Nascimento, V. M. Gadotti, and A. R. Santos, "Ankle joint mobilization decreases hypersensitivity by activation of peripheral opioid receptors in a mouse model of postoperative pain," *Pain Medicine*, vol. 13, no. 8, pp. 1049–1058, 2012.

[370] D. Martins, L. Mazzardo-Martins, F. Cidral-Filho, V. Gadotti, and A. Santos, "Peripheral and spinal activation of cannabinoid receptors by joint mobilization alleviates postoperative pain in mice," *Neuroscience*, vol. 255, pp. 110–121, 2013.

[371] A. S. Salgado, J. Stramosk, D. D. Ludtke, A. C. Kuci, D. C. Salm, L. A. Ceci, F. Petronilho, D. Florentino, L. G. Danielski, A. Gassenferth *et al.*, "Manual therapy reduces pain behavior and oxidative stress in a murine model of complex regional pain syndrome type i," *Brain sciences*, vol. 9, no. 8, p. 197, 2019.

[372] H.-C. Wu, Y.-C. Liao, Y.-H. Cheng, P.-C. Shih, C.-M. Tsai, and C.-Y. Lin, "The potential effect of a vibrotactile glove rehabilitation system on motor recovery in chronic post-stroke hemiparesis," *Technology and Health Care*, vol. 25, no. 6, pp. 1183–1187, 2017.

[373] X. Huang, F. Naghdy, G. Naghdy, and H. Du, "Clinical effectiveness of combined virtual reality and robot assisted fine hand motion rehabilitation in subacute stroke patients," in *2017 International Conference on Rehabilitation Robotics (ICORR)*. IEEE, 2017, pp. 511–515.

[374] A. Maris, K. Coninx, H. Seelen, V. Truyens, T. De Weyer, R. Geers, M. Lemmens, J. Coolen, S. Stupar, I. Lamers *et al.*, "The impact of robot-mediated adaptive i-travle training on impaired upper limb function in chronic stroke and multiple sclerosis," *Disability and Rehabilitation: Assistive Technology*, vol. 13, no. 1, pp. 1–9, 2018.

[375] M. Ferre, I. Galiana, R. Wirz, and N. Tuttle, "Haptic device for capturing and simulating hand manipulation rehabilitation," *IEEE/ASME Transactions on Mechatronics*, vol. 16, no. 5, pp. 808–815, 2011.

[376] M. Bouri, C. Baur, R. Clavel, C. Newman, and M. Zedka, "Handreha": a new hand and wrist haptic device for hemiplegic children," in *ACHI 2013, The Sixth International Conference on Advances in Computer-Human Interactions*, 2013, pp. 286–292.

[377] M. Cardinale and J. Wakeling, "Whole body vibration exercise: are vibrations good for you?" *British journal of sports medicine*, vol. 39, no. 9, pp. 585–589, 2005.

[378] R. Saggini, S. M. Carmignano, T. Palermo, R. G. Bellomo *et al.*, "Mechanical vibration in rehabilitation: state of the art," *Journal of novel physiotherapies*, vol. 6, no. 06, 2016.

[379] M. Dragusanu, G. M. Achilli, M. C. Valigi, D. Prattichizzo, M. Malvezzi, and G. Salvietti, "The wavejoints: a novel methodology to design soft-rigid grippers made by monolithic

3d printed fingers with adjustable joint stiffness," in *2022 International Conference on Robotics and Automation (ICRA)*. IEEE, 2022, pp. 6173–6179.

[380] T. J. Coderre, D. N. Xanthos, L. Francis, and G. J. Bennett, "Chronic post-ischemia pain (cpip): a novel animal model of complex regional pain syndrome-type i (crps-i; reflex sympathetic dystrophy) produced by prolonged hindpaw ischemia and reperfusion in the rat," *Pain*, vol. 112, no. 1-2, pp. 94–105, 2004.

[381] F. Birklein and M. Schmelz, "Neuropeptides, neurogenic inflammation and complex regional pain syndrome (crps)," *Neuroscience letters*, vol. 437, no. 3, pp. 199–202, 2008.

[382] W. S. Kingery, "Role of neuropeptide, cytokine, and growth factor signaling in complex regional pain syndrome," *Pain medicine*, vol. 11, no. 8, pp. 1239–1250, 2010.

[383] C. Maihöfner, F. Seifert, and K. Markovic, "Complex regional pain syndromes: new pathophysiological concepts and therapies," *European Journal of Neurology*, vol. 17, no. 5, pp. 649–660, 2010.

[384] H. M. Oerlemans, R. J. A. Goris, T. De Boo, and R. A. Oostendorp, "Do physical therapy and occupational therapy reduce the impairment percentage in reflex sympathetic dystrophy? 1," *American journal of physical medicine rehabilitation*, vol. 78, no. 6, pp. 533–539, 1999.

[385] T. O. Smith, "How effective is physiotherapy in the treatment of complex regional pain syndrome type 1? a review of the literature," *Musculoskeletal Care*, vol. 3, no. 4, pp. 181–200, 2005.

[386] H. van de Meent, M. Oerlemans, A. Bruggeman, F. Klomp, R. van Dongen, R. Oostendorp, and J. P. Frölke, "Safety of "pain exposure" physical therapy in patients with complex regional pain syndrome type 1," *Pain*, vol. 152, no. 6, pp. 1431–1438, 2011.

[387] P. Moss, K. Sluka, and A. Wright, "The initial effects of knee joint mobilization on osteoarthritic hyperalgesia," *Manual therapy*, vol. 12, no. 2, pp. 109–118, 2007.

[388] A. J. Beaudoin, F. Pedneault, M. Houle, C. Bilodeau, M.-P. Gauvin, D. Groleau, P. Brochu, and M. Couture, "Case study assessing the feasibility of using a wearable haptic device or humanoid robot to facilitate transitions in occupational therapy sessions for children with autism spectrum disorder," *Journal of Rehabilitation and Assistive Technologies Engineering*, vol. 8, p. 20556683211049041, 2021.

[389] M.-A. Choukou, S. Mbabaali, J. Bani Hani, and C. Cooke, "Haptic-enabled hand rehabilitation in stroke patients: a scoping review," *Applied Sciences*, vol. 11, no. 8, p. 3712, 2021.

[390] E. B. Brokaw, T. M. Murray, T. Nef, P. S. Lum, D. Nichols, and R. J. Holley, "Time independent functional task training: a case study on the effect of inter-joint coordination driven haptic guidance in stroke therapy," in *2011 IEEE International Conference on Rehabilitation Robotics*. IEEE, 2011, pp. 1–6.

[391] A. A. Timmermans, R. J. Lemmens, M. Monfrance, R. P. Geers, W. Bakx, R. J. Smeets, and H. A. Seelen, "Effects of task-oriented robot training on arm function, activity, and quality of life in chronic stroke patients: a randomized controlled trial," *Journal of neuroengineering and rehabilitation*, vol. 11, no. 1, pp. 1–12, 2014.

[392] G. G. Fluet, A. S. Merians, Q. Qiu, A. Davidow, and S. V. Adamovich, "Comparing integrated training of the hand and arm with isolated training of the same effectors in persons with stroke using haptically rendered virtual environments, a randomized clinical trial," *Journal of neuroengineering and rehabilitation*, vol. 11, no. 1, pp. 1–11, 2014.

[393] R. C. Loureiro, W. S. Harwin, R. Lamperd, and C. Collin, "Evaluation of reach and grasp robot-assisted therapy suggests similar functional recovery patterns on proximal and distal arm segments in sub-acute hemiplegia," *IEEE Transactions on Neural Systems and Rehabilitation Engineering*, vol. 22, no. 3, pp. 593–602, 2013.

[394] J. Broeren, M. Rydmark, A. Björkdahl, and K. S. Sunnerhagen, "Assessment and training in a 3-dimensional virtual environment with haptics: a report on 5 cases of motor rehabilitation in the chronic stage after stroke," *Neurorehabilitation and neural repair*, vol. 21, no. 2, pp. 180–189, 2007.

[395] N. Pernalete, S. Edwards, R. Gottipati, J. Tipple, V. Kolipakam, and R. V. Dubey, "Eye-hand coordination assessment/therapy using a robotic haptic device," in *9th International Conference on Rehabilitation Robotics, 2005. ICORR 2005.* IEEE, 2005, pp. 25–28.

[396] N. Pernalete, R. Gottipati, J. Grantner, S. Edwards, D. Janiak, J. Haskin, and R. Dubey, "Integration of an intelligent decision support system and a robotic haptic device for eye-hand coordination therapy," in *2007 IEEE 10th International Conference on Rehabilitation Robotics.* IEEE, 2007, pp. 283–291.

[397] K. Larson, "Can you estimate modulus from durometer hardness for silicones," *Dow Corning Corporation*, pp. 1–6, 2016.

[398] P. S. Steeg, "Targeting metastasis," *Nature reviews cancer*, vol. 16, no. 4, pp. 201–218, 2016.

[399] X. Wu, A. Baig, G. Kasymjanova, K. Kafi, C. Holcroft, H. Mekouar, A. Carbonneau, B. Bahoric, K. Sultanem, and T. Muanza, "Pattern of local recurrence and distant metastasis in breast cancer by molecular subtype," *Cureus*, vol. 8, no. 12, 2016.

[400] D. E. Rowe, R. J. Carroll, and C. L. Day Jr, "Prognostic factors for local recurrence, metastasis, and survival rates in squamous cell carcinoma of the skin, ear, and lip: implications for treatment modality selection," *Journal of the American Academy of Dermatology*, vol. 26, no. 6, pp. 976–990, 1992.

[401] M. Bettencourt-Dias, S. Mittnacht, and J. P. Brockes, "Heterogeneous proliferative potential in regenerative adult newt cardiomyocytes," *Journal of cell science*, vol. 116, no. 19, pp. 4001–4009, 2003.

[402] J. M. Sarjeant, J. Butany, and R. J. Cusimano, "Cancer of the heart: epidemiology and management of primary tumors and metastases," *American Journal of Cardiovascular Drugs*, vol. 3, pp. 407–421, 2003.

[403] A. D. Goldberg, R. Blankstein, and R. F. Padera, "Tumors metastatic to the heart," *Circulation*, vol. 128, no. 16, pp. 1790–1794, 2013.

[404] R. Y. Loyaga-Rendon, C. Inampudi, J. A. Tallaj, D. Acharya, and S. V. Pamboukian, "Cancer in end-stage heart failure patients supported by left ventricular assist devices," *ASAIO Journal*, vol. 60, no. 5, pp. 609–612, 2014.

[405] G. Cheng, J. Tse, R. K. Jain, and L. L. Munn, "Micro-environmental mechanical stress controls tumor spheroid size and morphology by suppressing proliferation and inducing apoptosis in cancer cells," *PLoS one*, vol. 4, no. 2, p. e4632, 2009.

[406] J. Shu, H. Deng, Y. Zhang, F. Wu, and J. He, "Cancer cell response to extrinsic and intrinsic mechanical cue: Opportunities for tumor apoptosis strategies," *Regenerative Biomaterials*, p. rbae016, 2024.

[407] L. Mahoney and A. Csima, "Efficiency of palpation in clinical detection of breast cancer." *Canadian Medical Association Journal*, vol. 127, no. 8, p. 729, 1982.

[408] H. van Overhagen, K. Brakel, M. W. Heijenbrok, J. H. van Kasteren, C. N. van de Moosdijk, A. C. Roldaan, A. P. van Gils, and B. E. Hansen, "Metastases in supraclavicular lymph nodes in lung cancer: assessment with palpation, us, and ct," *Radiology*, vol. 232, no. 1, pp. 75–80, 2004.

[409] M. Najafi, B. Farhood, and K. Mortezaee, "Extracellular matrix (ecm) stiffness and degradation as cancer drivers," *Journal of cellular biochemistry*, vol. 120, no. 3, pp. 2782–2790, 2019.

[410] S. Ishihara and H. Haga, "Matrix stiffness contributes to cancer progression by regulating transcription factors," *Cancers*, vol. 14, no. 4, p. 1049, 2022.

[411] D. E. Gerber, "Targeted therapies: a new generation of cancer treatments," *American family physician*, vol. 77, no. 3, pp. 311–319, 2008.

[412] J. S. Ross, D. P. Schenkein, R. Pietrusko, M. Rolfe, G. P. Linette, J. Stec, N. E. Stagliano, G. S. Ginsburg, W. F. Symmans, L. Pusztai *et al.*, "Targeted therapies for cancer 2004," *American journal of clinical pathology*, vol. 122, no. 4, pp. 598–609, 2004.

[413] M. Vanneman and G. Dranoff, "Combining immunotherapy and targeted therapies in cancer treatment," *Nature reviews cancer*, vol. 12, no. 4, pp. 237–251, 2012.

[414] T. A. Agunbiade, R. Y. Zaghlol, and A. Barac, "Heart failure in relation to tumor-targeted therapies and immunotherapies," *Methodist DeBakey Cardiovascular Journal*, vol. 15, no. 4, p. 250, 2019.

[415] J. H.-C. Wang and B. P. Thampatty, "An introductory review of cell mechanobiology," *Biomechanics and modeling in mechanobiology*, vol. 5, no. 1, pp. 1–16, 2006.

[416] K. S. Kang, S.-J. Lee, H. Lee, W. Moon, and D.-W. Cho, "Effects of combined mechanical stimulation on the proliferation and differentiation of pre-osteoblasts," *Experimental & molecular medicine*, vol. 43, no. 6, pp. 367–373, 2011.

[417] N. Fahy, M. Alini, and M. J. Stoddart, "Mechanical stimulation of mesenchymal stem cells: Implications for cartilage tissue engineering," *Journal of Orthopaedic Research®*, vol. 36, no. 1, pp. 52–63, 2018.

[418] C. Rinoldi, M. Costantini, E. Kijeńska-Gawrońska, S. Testa, E. Fornetti, M. Heljak, M. Ćwiklińska, R. Buda, J. Baldi, S. Cannata *et al.*, "Tendon tissue engineering: effects of mechanical and biochemical stimulation on stem cell alignment on cell-laden hydrogel yarns," *Advanced healthcare materials*, vol. 8, no. 7, p. 1801218, 2019.

[419] R. Chabiniok, V. Y. Wang, M. Hadjicharalambous, L. Asner, J. Lee, M. Sermesant, E. Kuhl, A. A. Young, P. Moireau, M. P. Nash *et al.*, "Multiphysics and multiscale modelling, data–model fusion and integration of organ physiology in the clinic: ventricular cardiac mechanics," *Interface focus*, vol. 6, no. 2, p. 20150083, 2016.

[420] I. Shadrin, A. Khodabukus, and N. Bursac, "Striated muscle function, regeneration, and repair," *Cellular and molecular life sciences*, vol. 73, no. 22, pp. 4175–4202, 2016.

[421] D. C. Canseco, W. Kimura, S. Garg, S. Mukherjee, S. Bhattacharya, S. Abdisalaam, S. Das, A. Asaithamby, P. P. Mammen, and H. A. Sadek, "Human ventricular unloading induces cardiomyocyte proliferation," *Journal of the American College of Cardiology*, vol. 65, no. 9, pp. 892–900, 2015.

[422] J. Bleuel, F. Zaucke, G.-P. Brüggemann, and A. Niehoff, "Effects of cyclic tensile strain on chondrocyte metabolism: a systematic review," *PLoS One*, vol. 10, no. 3, p. e0119816, 2015.

[423] N. Rosa, R. Simoes, F. D. Magalhães, and A. T. Marques, "From mechanical stimulus to bone formation: a review," *Medical engineering & physics*, vol. 37, no. 8, pp. 719–728, 2015.

[424] A. Sabine, Y. Agalarov, H. Maby-El Hajjami, M. Jaquet, R. Hägerling, C. Pollmann, D. Bebber, A. Pfenniger, N. Miura, O. Dormond *et al.*, "Mechanotransduction, prox1, and foxc2 cooperate to control connexin37 and calcineurin during lymphatic-valve formation," *Developmental cell*, vol. 22, no. 2, pp. 430–445, 2012.

[425] A. Poulin, C. S. Demir, S. Rosset, T. V. Petrova, and H. Shea, "Dielectric elastomer actuator for mechanical loading of 2d cell cultures," *Lab on a Chip*, vol. 16, no. 19, pp. 3788–3794, 2016.

[426] A. Poulin, S. Rosset, and H. Shea, "Fabrication and characterization of silicone-based dielectric elastomer actuators for mechanical stimulation of living cells," in *Electroactive Polymer Actuators and Devices (EAPAD) XX*, vol. 10594. International Society for Optics and Photonics, 2018, p. 105940V.

[427] D. Cei, J. Costa, G. Gori, G. Frediani, C. Domenici, F. Carpi, and A. Ahluwalia, "A bioreactor with an electro-responsive elastomeric membrane for mimicking intestinal peristalsis," *Bioinspiration & biomimetics*, vol. 12, no. 1, p. 016001, 2016.

[428] J. H.-C. Wang, G. Yang, and Z. Li, "Controlling cell responses to cyclic mechanical stretching," *Annals of biomedical engineering*, vol. 33, no. 3, pp. 337–342, 2005.

[429] R. Yang, J. A. Broussard, K. J. Green, and H. D. Espinosa, "Techniques to stimulate and interrogate cell–cell adhesion mechanics," *Extreme Mechanics Letters*, vol. 20, pp. 125–139, 2018.

[430] S. J. A. Koh, T. Li, J. Zhou, X. Zhao, W. Hong, J. Zhu, and Z. Suo, "Mechanisms of large actuation strain in dielectric elastomers," *Journal of Polymer Science Part B: Polymer Physics*, vol. 49, no. 7, pp. 504–515, 2011.

[431] M. Imboden, E. de Coulon, A. Poulin, C. Dellenbach, S. Rosset, H. Shea, and S. Rohr, "High-speed mechano-active multielectrode array for investigating rapid stretch effects on cardiac tissue," *Nature communications*, vol. 10, no. 1, pp. 1–10, 2019.

[432] C. Simmons, J. Sim, P. Baechtold, A. Gonzalez, C. Chung, N. Borghi, and B. Pruitt, "Integrated strain array for cellular mechanobiology studies," *Journal of Micromechanics and Microengineering*, vol. 21, no. 5, p. 054016, 2011.

[433] J. Kreutzer, L. Ikonen, J. Hirvonen, M. Pekkanen-Mattila, K. Aalto-Setälä, and P. Kallio, "Pneumatic cell stretching system for cardiac differentiation and culture," *Medical engineering & physics*, vol. 36, no. 4, pp. 496–501, 2014.

[434] Y. Huang and N.-T. Nguyen, "A polymeric cell stretching device for real-time imaging with optical microscopy," *Biomedical microdevices*, vol. 15, no. 6, pp. 1043–1054, 2013.

[435] T. Still, M. Oudich, G. Auerhammer, D. Vlassopoulos, B. Djafari-Rouhani, G. Fytas, and P. Sheng, "Soft silicone rubber in phononic structures: Correct elastic moduli," *Physical Review B*, vol. 88, no. 9, p. 094102, 2013.

[436] F. Chaumette, S. Hutchinson, and P. Corke, "Visual servoing," in *Springer Handbook of Robotics*. Springer, 2016, pp. 841–866.

[437] J. M. Florez, M. Shah, E. M. Moraud, S. Wurth, L. Baud, J. Von Zitzewitz, R. Van Den Brand, S. Micera, G. Courtine, and J. Paik, "Rehabilitative soft exoskeleton for rodents," *IEEE Transactions on Neural Systems and Rehabilitation Engineering*, vol. 25, no. 2, pp. 107–118, 2016.

[438] D. Na, "A flexible external skeleton robot for rehabilitation exercise of rats with paralysis of lower limbs," *Revista Científica de la Facultad de Ciencias Veterinarias*, vol. 29, no. 5, pp. 1170–1180, 2019.

[439] C. Mancini, "Animal-computer interaction (aci) changing perspective on hci, participation and sustainability," in *CHI'13 Extended Abstracts on Human Factors in Computing Systems*, 2013, pp. 2227–2236.

[440] L. Marechal, P. Balland, L. Lindenroth, F. Petrou, C. Kontovounisios, and F. Bello, "Toward a common framework and database of materials for soft robotics," *Soft robotics*, vol. 8, no. 3, pp. 284–297, 2021.

[441] T. L. Baldi, N. D'Aurizio, A. Villani, and D. Prattichizzo, "Generating kinesthetic feedback using self contact and velocity scaling," in *2021 IEEE World Haptics Conference (WHC)*. IEEE, 2021, pp. 619–624.

[442] N. D'Aurizio, T. L. Baldi, A. Villani, K. Minamizawa, Y. Tanaka, and D. Prattichizzo, "Wearable haptics for object compliance discrimination through passive touch," in *2021 IEEE World Haptics Conference (WHC)*. IEEE, 2021, pp. 894–899.

[443] M. Dragusanu, D. Troisi, A. Villani, D. Prattichizzo, and M. Malvezzi, "Happ: A haptic portable pad for hand disease manual treatment," in *2022 31st IEEE International Conference on Robot and Human Interactive Communication (RO-MAN)*. IEEE, 2022, pp. 345–350.

[444] M. Dragusanu, Z. Iqbal, A. Villani, N. D'Aurizio, D. Prattichizzo, and M. Malvezzi, "Hans: a haptic system for human-to-human remote handshake," in *2022 9th IEEE RAS/EMBS International Conference for Biomedical Robotics and Biomechatronics (BioRob)*. IEEE, 2022, pp. 1–8.

[445] A. Villani, G. Ciucci, A. Colliva, S. Marullo, S. Zacchigna, and D. Prattichizzo, "Robheart: Soft robot for heart-like volumetric stress on seeded cardiac cells," in *2022 9th IEEE RAS/EMBS International Conference for Biomedical Robotics and Biomechatronics (BioRob)*. IEEE, 2022, pp. 01–08.

Novel Devices for Haptics Repurposing

From Metaverses Towards a Mechanobiological Cancer Treatment

A L B E R T O
V I L L A N I

2020-2024

REPURPOSING word refers to the practice of testing the effects of an already assessed drug and its molecules on pathologies different from the one for which the medicine was created. Sometimes, repurposing allows researchers to discover new ways to treat serious pathologies and diseases. Thalidomide, initially marketed as a sedative, was later found to be effective in treating multiple myeloma, a type of cancer. Similarly, AZT (Zidovudine), originally developed as a cancer drug, became the first approved treatment for HIV/AIDS.

In this thesis, the **HAPTICS** repurposing will be proposed to open new application fields, drawing from a study of state-of-the-art haptics towards examples of novel or renewed tactile displays for various and unconventional applications such as metaverses, medical pain management, and mechano-biological research on cancer.

MEDICINE

METAVERSE

BIOLOGY

UNIVERSITÀ
DISIENA
1240

Department of information engineering and mathematics (DIISM)

In collaboration with
International Center for Genetic Engineering and
Biotechnology (ICGEB)